JYU DISSERTATIONS 646

Topi Löytäinen

Exclusive Photoproduction of Heavy Vector Mesons in Ultraperipheral Nuclear Collisions

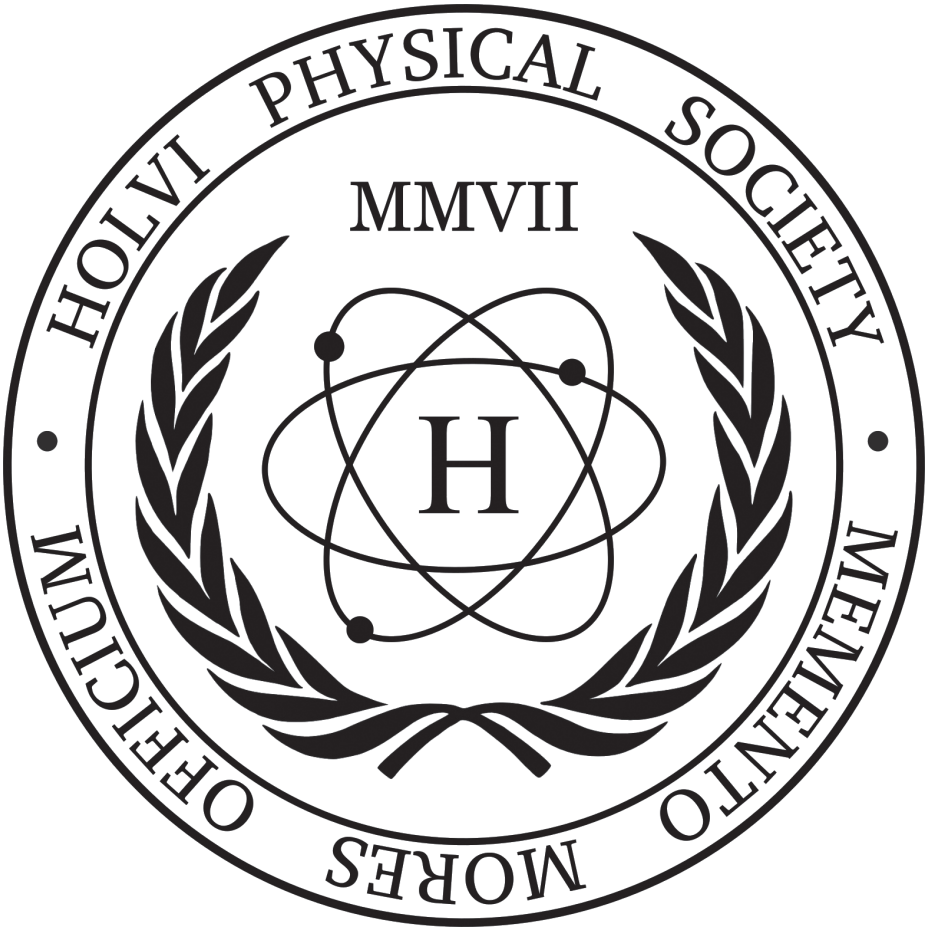

UNIVERSITY OF JYVÄSKYLÄ
FACULTY OF MATHEMATICS
AND SCIENCE

JYU DISSERTATIONS 646

Topi Löytäinen

Exclusive Photoproduction of Heavy Vector Mesons in Ultraperipheral Nuclear Collisions

Esitetään Jyväskylän yliopiston matemaattis-luonnontieteellisen tiedekunnan suostumuksella
julkisesti tarkastettavaksi yliopiston Ylistönrinteen salissa FYS1
kesäkuun 2. päivänä 2023 kello 12.

Academic dissertation to be publicly discussed, by permission of
the Faculty of Mathematics and Science of the University of Jyväskylä,
in Ylistönrinne, auditorium FYS1, on June 2, 2023 at 12 o'clock noon.

JYVÄSKYLÄN YLIOPISTO
UNIVERSITY OF JYVÄSKYLÄ

JYVÄSKYLÄ 2023

Editors
Ilari Maasilta
Department of Physics, University of Jyväskylä
Ville Korkiakangas
Open Science Centre, University of Jyväskylä

Cover picture by Holvi Physical Society.

ISBN 978-951-39-9577-5 (PDF)
URN:ISBN:978-951-39-9577-5
ISSN 2489-9003

Permanent link to the online version of this publication: http://urn.fi/URN:ISBN:978-951-39-9577-5

Jyväskylä University Printing House, Jyväskylä 2023

ABSTRACT

Löytäinen, Topi
Exclusive Photoproduction of Heavy Vector Mesons in Ultraperipheral Nuclear Collisions

This thesis investigates the possibility of describing coherent exclusive photoproduction of heavy-vector mesons in ultraperipheral heavy-ion collisions (UPCs) by using inclusive collinearly factorizable parton distribution functions (PDFs). The aim is to chart the scale dependence and the PDF-originated uncertainties of such photoproduction cross sections, arising in the approximation where the generalized parton distributions (GPDs) are simply approximated by their forward limit counter parts, i.e., the PDFs. The introductory part presents the PDFs and GPDs in their physics contexts, their connection to each other and to the nuclear ones, shows the full leading order (LO) calculation of the photoproduction amplitude in perturbative quantum chromodynamics (pQCD) and describes the way the quark contribution arises at next-to-leading order (NLO). Furthermore, details of the required modeling of the form factors and photon fluxes are described before finally collecting everything together for the nucleus-nucleus UPCs.

The described framework is the basis on which most of the results of the papers [PI, PII, PIII] rely. Article [PI] was the very first NLO pQCD study of rapidity differential cross sections of coherent exclusive photoproduction of J/ψ mesons in lead-lead UPCs. Article [PII] extended the results to the case of oxygen-oxygen collisions and studied the possibility of constraining the strong scale dependence of the results of article [PI] through suitably chosen ratios of cross sections. Then finally in article [PIII] the framework was extended to the case of Υ mesons with the addition of the skewing correction through the Shuvaev transform.

The results show the importance of the ERBL region for a strongly growing gluon PDF but other than that no tight constraints for the gluons were found. Surprisingly, sensitivity to the quark PDFs was discovered in the J/ψ case, due to which the studied process may be a probe of the elusive strangeness content of bound nucleons. The sensitivity originates from the cancelling nature of the LO and NLO gluon contributions in the scattering amplitude. This thesis paves the way towards including the studied exclusive processes as constraints in the global analysis of PDFs and their nuclear counterparts.

Keywords: Particle interactions, particle phenomena, particle production, quantum chromodynamics, relativistic heavy-ion collisions, strong interaction

TIIVISTELMÄ (ABSTRACT IN FINNISH)

Löytäinen, Topi
Raskaiden vektorimesonien eksklusiivinen fototuotto ultraperifeerisissä ydintörmäyksissä

Tässä väitöskirjassa tutkitaan mahdollisuutta kuvata prosesseja, joissa syntyy raskas vektorimesoni fototuoton kautta koherentisti ja eksklusiivisesti raskaiden ionien ultraperifeerisissä törmäyksissä (UPC) käyttämällä inklusiivisia kollineaarisesti faktoroitavissa olevia partonijakaumia (PDF). Tavoitteena on kartoittaa laskettujen vaikutusalojen skaalariippuvuus ja PDF-epävarmuudet approksimaatiossa, jossa yleistetyt partonijakaumat (GPD) korvataan niiden etusuunnan vastineilla eli PDF:llä. Väitöskirjan johdannossa esitetään PDF:t ja GPD:t niiden fysikaalisissa konteksteissa sekä niiden yhteys toisiinsa ja niiden vastineisiin ytimissä. Johdanto käy läpi fototuottoamplitudin alimman kertaluvun (LO) laskun kvanttiväridynamiikan häiriöteoriassa (pQCD) ja kuvaa kuinka kvarkkikontribuutio syntyy alinta seuraavassa kertaluvussa (NLO). Tämän lisäksi johdannossa kuvataan ne yksityiskohdat, joita tarvitaan muototekijöiden sekä fotonivuon laskemiseen ennen kuin kaikki nämä tekijät yhdistetään ydin-ydin-UPC:lle.

Kuvattu viitekehys on se, jolla suurin osa artikkeleiden [PI, PII, PIII] tuloksista on saatu. Artikkeli [PI] oli ensimmäinen NLO-pQCD-tutkimus rapiditeetin suhteen differentioiduista vaikutusaloista J/ψ:n koherentille eksklusiiviselle fototuotolle lyijy-lyijy-UPC:ssä. Artikkeli [PII] laajensi tulokset happi-happi-törmäyksiin ja tutki mahdollisuutta rajoittaa artikkelissa [PI] havaittua vahvaa skaalariippuvuutta sopivasti valituilla vaikutusalasuhteilla. Artikkelissa [PIII] viitekehys laajennettiin Υ-mesoneihin sekä lisättiin ns. skewness-korjaus Shuvaev-muunnoksen kautta.

Tulokset näyttävät ERBL-alueen tärkeyden voimakkaasti kasvavalle gluoni-PDF:lle, mutta tämän lisäksi tutkimuksessa ei löydetty tiukkoja rajoitteita gluoneille. Tuloksissa nähtiin yllättävä herkkyys kvarkkikontribuutioille J/ψ:n tapauksessa, jonka vuoksi tarkasteltu prosessi saattaa tarjota mahdollisuuden tutkia vaikeasti havaittavaa outokvarkkikontribuutiota sidotuissa ytimissä. Tämä herkkyys johtuu sironta-amplitudin LO- sekä NLO-gluonikontribuutioiden tavasta kumota toisensa. Tutkimus valaa toivoa sille, että tässä työssä käsiteltyjä prosesseja voitaisiin mahdollisesti käyttää tulevaisuudessa datarajoitteina PDF:lle sekä niiden vastineille ytimissä.

Author

Topi Löytäinen
Department of Physics
University of Jyväskylä
Finland

Supervisors

Senior Lecturer Hannu Paukkunen
Department of Physics
University of Jyväskylä
Finland

Professor Kari J. Eskola
Department of Physics
University of Jyväskylä
Finland

Reviewers

Professor Joakim Nystrand
Department of Physics and Technology
University of Bergen
Norway

Dr. François Arleo
SUBATECH, IMT Atlantique
Université de Nantes, IN2P3/CNRS
France

Opponent

Professor Emeritus Paul Hoyer
Department of Physics
University of Helsinki
Finland

PREFACE

"Hope is the thing with feathers - that perches in the soul" – Emily Dickinson. This errand of mine started in the spring of 2018 and now the train has at long last reached its final destination in the first half of the Lord's year 2023. Now, at the final station, it surely looks like the past five years have been but an uphill battle which I could not have completed alone.

I am very thankful for the guidance and the enthusiasm of my supervisors Dr. Hannu Paukkunen and Prof. Kari J. Eskola whose patience I must have tested on more than one occasion. So thank you for bearing with me! Moreover, I would not be where I am today without the help of my collaborators Dr. Vadim Guzey and Dr. Chris Flett on whose expertise I confided on multiple occasion. I would also like to extend my gratitude to the Magnus Ehrnrooth foundation for the financial support I received over the years. This thesis work was done at the Department of Physics of the University of Jyväskylä and in the QCD-theory project at the Helsinki Institute of Physics, and as a part of the Center of Excellence in Quark Matter of the Academy of Finland. It was funded also by the Academy of Finland project 330448. I thank Prof. Joakim Nystrand and Dr. Francois Arleo for reviewing the original version of this thesis and Prof. Emer. Paul Hoyer for promising to act as my opponent at the public examination.

Nothing exists by itself in a vacuum. And for that fact of life I am grateful since without the help of my family and friends, I do not think I could have continued to march onwards. I would like to thank my brothers, Niko and Jere, and my parents, Mom and Dad, for all their love and support. As to my academic peers; I would like to thank the Holvi community for every second I got to spend in the office (not forgetting the immemorable conference cruises): Petja, Lotta, Henri, Mikko, Oskari, Jani, Mikko, Miha and all the alumni as well. Thanks to the whole QCD group – Heikki, Ilkka and Tuomas in particular – for the supportive and stimulating working environment.

I would like to thank all my past and present friends for their support and the time outside of the department where I spent most of my working days: Matti, Marco, Valtteri and Pauliina, Teemu, Giovanni, Sauli, Anni and the Gang; Jyrki, Marvin, Tiia, Sami, Adrian, Pablo and the Ramnath sisters. The downstair physicists, with their pint's of science, did also carry me onward in times of need: Janne, Kofi, Daniel, George, Joonas, Andy and the rest of the Liverpool crew. Lastly, and do forgive me if I forgot to mention your name, the people of RT – especially in Jyväskylä and in Stockholm – deserve my gratitude as well.

I have made countless mistakes, both personal and professional, and should I have been the wiser, I might have learned faster from them. I am not sure how the ending of this chapter of my life would have been without the love and support of Candice whose refuge I sought across the sea. Words cannot even begin to describe how thankful I am but let me try anyway: Thank you!

– Topi Löytäinen, March 2023, Jyväskylä

LIST OF INCLUDED ARTICLES

[PI] Kari J. Eskola, Christopher A. Flett, Vadim Guzey, Topi Löytäinen and Hannu Paukkunen, *Exclusive J/ψ photoproduction in ultraperipheral Pb+Pb collisions at the CERN Large Hadron Collider calculated at next-to-leading order perturbative QCD*, Phys. Rev. C. 106 **no.3**, 035202, arXiv: 2203.11613 [hep-ph] (Mar. 2022).

[PII] Kari J. Eskola, Christopher A. Flett, Vadim Guzey, Topi Löytäinen and Hannu Paukkunen, *Next-to-leading order perturbative QCD predictions for exclusive J/ψ photoproduction in oxygen-oxygen and lead-lead collisions at the LHC*, Phys. Rev. C. 107 **no.4**, 044912, arXiv: 2210.16048 [hep-ph] (Oct. 2022).

[PIII] Kari J. Eskola, Christopher A. Flett, Vadim Guzey, Topi Löytäinen and Hannu Paukkunen, *Predictions for exclusive* Υ *photoproduction in ultraperipheral Pb+Pb collisions at the LHC at next-to-leading order in perturbative QCD*, submitted to Eur. Phys. J. C, arXiv: 2303.03007 [hep-ph] (Mar. 2023).

Author's contribution

The author developed the framework, the code, performed all numerical calculations, produced all the figures and wrote the first drafts for articles [PI] and [PII]. For article [PIII] the author wrote the first draft, performed a significant part of the calculations and produced all the figures.

CONTENTS

1 INTRODUCTION

Without justifying to the reader why quantum field theories (QFTs) are the best way to describe the world around us, as is done in many excellent books on the subject [1–11], we will just start with the assumption that such a framework is needed for the description of the data available from modern-day particle accelerators. Moreover, the physical world with its wonderful, bizarre and beautiful phenomena, more often than not, can be described through the framework of some given symmetry. With the choice of the symmetry group being `SU(3)`, we arrive at the theory of Quantum Chromodynamics (QCD) which is currently the best known theory to describe the strong nuclear force, one of the four fundamental forces seen in nature. The application of this theory to one particular example – out of a class of scattering processes called exclusive processes – is the subject matter of this thesis.

1.1 Quantum dynamics

For a physicist the easiest way to define a given QFT is to state the underlying Lagrangian density $\mathcal{L}$ describing the system. For QCD it is given by

$$\mathcal{L}_{\mathrm{QCD}} = \sum_q \bar{\psi}_q^j (i\not{D})_{jk} \psi_q^k - m_q \bar{\psi}_q^j \psi_q^j - \frac{1}{4} F_{\mu\nu}^a F^{a,\mu\nu}, \tag{1}$$

where the sum over q runs over all possible quark and antiquark flavors, we use the well known Einstein summation convention for the Lorentz indices μ and ν, the indices j, k, a label color, ψ_q denotes the quark fields, $F_{\mu\nu}^a$ is the field strength tensor for gluons. For the QCD covariant derivative D_μ we used the Feynman slashed notation $\not{D} = D_\mu \gamma^\mu$ where γ^μ are the Dirac gamma matrices. The covariant derivative in QCD is given by

$$(D_\mu)_{jk} = \delta_{jk} \partial_\mu - i g_s t_{jk}^a A_\mu^a, \tag{2}$$

where g_s is the strong coupling constant, $A_\mu = A_\mu^a t^a$ is the gluon field and t^a are the generators of the SU(3) symmetry group. The field strength tensor is then given by

$$F_{\mu\nu} = \frac{i}{g_s}[D_\mu, D_\nu] = \partial_\mu A_\nu - \partial_\nu A_\mu - i g_s [A_\mu, A_\nu], \tag{3}$$

where $[\cdots, \cdot\cdot]$ denotes the commutator. For details on the SU(3) invariance, the (anti)commutation relations and the Feynman rules for the free, non-interacting fields, we will refer the interested reader to a few appropriate references [12–17].

In the studied photoproduction processes, we will also deal with a theory describing electromagnetic interactions called Quantum Electrodynamics (QED). Historically, QED was discovered before QCD and it is the simpler theory – due to the simpler gauge symmetry group of U(1) – out of the two. Similarly as with QCD, QED is defined through the underlying Lagrangian density

$$\mathcal{L}_{\text{QED}} = \sum_f \bar{\psi}_f (i \not{D}) \psi_f - m_f \bar{\psi}_f \psi_f - \frac{1}{4} F_{\mu\nu} F^{\mu\nu}, \tag{4}$$

where f runs over all fermion fields which interact electromagnetically, ψ_f labels a fermion field, m_f is the mass of the fermion and the covariant derivative D_μ is now given by

$$D_\mu = \partial_\mu - ieA_\mu \,, \tag{5}$$

where now with this sign choice the coupling constant e is positive definite i.e. $e > 0$. The photon field strength tensor $F_{\mu\nu}$ is then given by

$$F_{\mu\nu} = \partial_\mu A_\nu - \partial_\nu A_\mu. \tag{6}$$

Note that in the above we are lacking the term proportional to the commutator of the photon field A due to its Abelian nature and that both in the QCD and the QED Lagrangians we have deliberately left undefined the possible gauge-fixing terms. It is these two theories which we would like to apply to the process of coherent exclusive photoproduction of heavy-vector mesons V in ultra-peripheral collisions (UPCs) of two heavy ions A, i.e. the process $A + A \to A + V + A$. By ultraperipheral one means that the scattering between the two heavy ions happens at a distance which is greater than the sum of the radii of the nucleus A such that we can think of the scattering to happen between the photon field of one of the ions with the other ion.

1.2 Tools of choice

In addition to defining the QCD and QED Lagrangians we also need some tools how to calculate predictions out of our theory. Due to the complexity of the problems associated with high-energy particle physics, computer driven methods and tools have become ever more attractive over the years. In the context of this thesis, the symbolic manipulation software FORM [18], programs generating Feynman diagrams like QGRAF [19], programs reducing Feynman integrals to master integrals like

REDUZE [20], Mathematica [21], and in particular the FeynCalc package of it [22], deserve to be pointed out as well.

We will not dive too much into detail of the above tools even though some aspects of all of them have been used in one form or another in this thesis or in the results used by this thesis. The main tools adopted are those of *pen and paper* and the programming languages C++ [23] and Python [24]. In addition to the results presented in the articles [PI, PII, PIII], the main utility of this thesis comes from the attempt to bridge the gap between the theoretical description – or maybe more aptly the phenomenology of it – of the non-perturbative part of inclusive processes (parton distribution functions, PDFs) and the theoretical description of the non-perturbative part of exclusive processes (generalized parton distribution functions, GPDs) in the context of heavy-ion collisions.

This thesis consists of an introductory part divided into six chapters and the three articles [PI, PII, PIII]. First in chapter 2, we will present the QFT definitions of the PDFs and GPDs and discuss the main motivation behind this work: nuclear corrections to PDFs – namely nuclear PDFs (nPDFs). Then in chapter 3 we move on to tackle the forward limit photoproduction calculation for the $\gamma + p \to V + p$ scattering process which will be sketched at leading order (LO) perturbative QCD. We will also say a few words about the next-to-leading order (NLO) calculation [25] with the quark contribution particularly in mind. The application of this calculation to the heavy-nucleus case is then essentially just a matter of replacing the underlying GPDs with their nuclear counterparts nPDFs, combined with a relatively straightforward calculation of the form factor and of the photon flux which we will outline in chapter 4. The main results of the papers [PI, PII, PIII], in addition to some extra analysis which was left out of the original articles, is then presented in chapter 5. Finally, in chapter 6 we will summarize the main results of this thesis with possible future developments that could be carried out.

2 PDFs, nPDFs AND GPDs

It was aptly noted in the preface of [12] that "true tests of perturbative QCD often turn out merely as tests of the author's cleverness in parametrizing the nonperturbative uncalculable part of the problem and not as actual tests of QCD" which alludes to the challenges with which we are faced when working with PDFs, GPDs and nPDFs. In this chapter we outline the theoretical basis on which the PDFs, GPDs and nPDFs rely and how they are interconnected with each other. We will denote both the PDFs and the GPDs with the capital letter F^i where the upper index i defines the type of the parton and distinction between the two comes from the fact that PDFs take only one light-cone momentum fraction as an input, i.e. $F^i(x)$ is a PDF, while GPDs take two light-cone momentum fractions and one Mandelstam variable, i.e. $F^i(x, \xi, t)$ is a GPD. The dependence on the factorization scale μ is then always left as implicit and, unless explicitly specified, the PDFs and the GPDs always refer to that of a proton.

2.1 Factorization theorems

If you want the probability of one thing happening, which depends on the probabilities of two non-correlated events, just multiply the two probabilities together! At its heart, this is the whole idea behind the collinear factorization theorem in particle collisions where we factor a process of interest, say a lepton-hadron collision, into a perturbatively calculable part, which we call the hard-scattering part, and into a perturbatively non-calculable part, which we call the soft-scattering part. To state this explicitly, the factorization theorem in an inclusive process between a lepton l and a hadron h, where we produce some final state $l' + X$ – we need to tag the outgoing lepton l' in order to know the exchanged momenta – of interest, i.e. $l + h \to l' + X$, is usually given at the differential cross section level $d\sigma$ where we write [13, 26–28]

$$d\sigma^{l+h\to l'+X}(p, q) = \sum_{i,X} F_h^i \otimes d\hat{\sigma}^{l+i\to l'+X}(p, q) + \mathcal{O}\left(Q^{-2}\right), \tag{7}$$

where p is the momentum of the hadron h, q is the momentum transferred by the lepton, i.e. $q = l - l'$ such that $-q^2 = Q^2$ and i labels the parton which takes part in the hard-scattering process. The symbol $\otimes$ denotes a convolution between the PDF F_h^i and the perturbatively calculable hard-scattering cross section $d\hat{\sigma}$, and it is taken over x which is the fractional momentum of the hadron h as carried by the parton i. The term $\mathcal{O}(Q^{-2})$ denotes the order at which we truncate our expansion in powers of Q [9, ch. 32.4], and if such terms are neglected it is good to keep in mind that we are technically dealing with an approximation.

The use of the theorem described by equation 7 is that through it we do not need to be able to calculate the full process but only the hard-scattering part $d\hat{\sigma}$ and deduce the rest – the soft-scattering part F_h^i – from the experimentally measured $d\sigma$. Then as long as the soft-scattering part stays the same, we can use those results in combination of a hard-scattering calculation to predict some other process of interest. All of this relies on the assumption that there is no *a priori* reason to believe that, at least on average, the distributions of partons within e.g. protons differ from one proton to another.

The above is the way factorization is traditionally formulated for PDFs which historically have been determined only from inclusive scatterings. The situation is slightly different for GPDs which arise in exclusive scatterings where we need to take extra care to specify the process in which we are interested. The easiest process for us might be the Deeply Virtual Compton Scattering (DVCS), i.e. $\gamma^*(q) + p(p) \to \gamma(q') + p(p')$. There are differences in how the factorization theorem is presented for GPDs, i.e. whether it is given through the invariant amplitude $\mathcal{M}$ or in terms of the hadronic tensor $T^{\mu\nu}$ but when one takes into account all appropriate factors of i, 2π and the occasional delta functions, these formulations obviously agree with each other [29–31]. We can write,

$$\mathcal{M}(\gamma^* + p \to \gamma + p) = \sum_i T^i(x, \xi, Q^2) \otimes F^i(x, \xi, t) + \mathcal{O}(Q^{-1}), \tag{8}$$

where i is the flavor of the parton inside the proton, x is the light-cone momentum fraction over which the convolution is taken, ξ, known as the skewness variable, parametrizes the momentum transfer, the square of the momentum is $Q^2 = -q^2$ and t is now the Mandelstam variable [32]. Moreover, T^i labels the hard scattering part and F^i is the soft scattering, i.e. the GPD, part. Note that sometimes $\mathcal{O}(Q^{-1})$ is replaced by $\mathcal{O}(Q'^{-1})$ where $Q'^2 = q'^2$ but this depends on the exact context [31].

The modification of equation 8 to the case where we produce a vector meson in the final state from an on shell photon is the one which we need in this work. This means that the amplitude for the process $\gamma + p \to V + p'$ is then factored into three parts [31, 33],

$$\mathcal{M}(\gamma + p \to V + p') = \sum_i F^i(x, \xi, t) \otimes T_{ij}(x, \xi, z, Q^2) \otimes \phi_V^j(z) + \mathcal{O}(Q^{-1}), \tag{9}$$

where F^i is the GPD for flavor i inside the proton p, T_{ij} is the hard-scattering function as initiated by the flavor i and ϕ_V^j is the vector meson vertex which ties two outgoing quarks of flavor j into the vector meson V. This factor ϕ is sometimes

called the light-cone wavefunction because it is typically calculated in the context of the leading approximation of the non-relativistic QCD (NRQCD) expansion [34]. The factors x, ξ and t are as in equation 8 and z can be interpreted in the scaling limit as the minus-momentum fraction of the quark j inside the vector meson. Note that the convolutions are taken over the variables x and z. Strictly speaking, the factorization theorem for an exclusive production of a vector meson, as shown by equation 9, has only been proven in the leptoproduction case [33, 35] but it is our hope, as proposed in [25], that the photoproduction process can be factorized in a similar manner due to the high mass of the produced heavy quark pair such that we can simply replace Q by a scale which is of the order of the heavy quark mass.

2.2 Definition of the distributions

Deriving the QFT definitions of the PDFs and the GPDs in their full length goes beyond the scope of this thesis but it is still of interest to us to give a rough sketch of how they arise in the historical context in which they were discovered. For the PDFs this discovery was made in the context of deep inelastic scattering (DIS) between an electron and a proton i.e. $e + p \to e' + X$ [36, 37]. The challenge in defining the GPDs is that they emerge in the context of exclusive scattering where we have to define carefully the process which we are studying i.e. what are the exact initial and final states, what kinematical limits do we take, do we allow for the flip of the helicity, do we consider spin dependent GPDs and so on. For the interested reader there exists several good summaries on the vast theory of GPDs, see e.g. Refs. [31, 38–43]. This then raises the question: what GPDs will we eventually need in the process of interest to us?

In the most general case there are altogether 16 quark and gluon leading twist GPDs, each one depending on four variables [31, 44] and for example, in the Virtual Compton Scattering (VCS) off a proton, $\gamma^* + p \to \gamma + p'$, we still find twelve distinct helicity amplitudes requiring twelve different GPDs for a complete description [45, 46]. The DVCS is a special case of VCS where we impose the Bjorken limit where the proton of momentum p^μ absorbs a photon of momentum q^μ such that $Q^2 = -q^2 \to \infty$, $p \cdot q \to \infty$ and $Q^2/p \cdot q$ finite [47]. In this limit we are left with only four GPDs: the vector current conserving the proton helicity and the one flipping it and then the vector-tensor current conserving proton helicity and the one flipping it. We will eventually be interested in the so called helicity-preserving forward limit, the exact definition we will give later, in which we are left only with one helicity conserving vector current. For the derivation of the GPDs from the DVCS amplitude the reader is directed to the literature [33, 47–50].

2.2.1 PDFs from DIS

The theoretical and the experimental work around DIS are cornerstones of particle physics and have been textbook material for many decades [4, 5, 9, 51–55]. The

QFT definitions of the quark PDF F^q, and the gluon PDF F^g, in the $A^+ = 0$ gauge, A being the gluon field, are given by [4, p.466-467]

$$\begin{aligned} F^q(x) &= \frac{1}{2}\sum_\sigma \frac{1}{2}\int_{-\infty}^{\infty}\frac{d\lambda}{2\pi}e^{ix(p\cdot z)}\langle p_\sigma|\bar{\psi}_q\left(-\frac{1}{2}z\right)\not{n}_-\psi_q\left(\frac{1}{2}z\right)|p_\sigma\rangle\Big|_{z=\lambda n_-,A^+=0} \\ F^g(x) &= \frac{1}{2}\sum_\sigma \frac{1}{xp^+}\int_{-\infty}^{\infty}\frac{d\lambda}{2\pi}e^{ix(p\cdot z)}\langle p_\sigma|G^{+\mu}\left(-\frac{1}{2}z\right)G_\mu{}^+\left(\frac{1}{2}z\right)|p_\sigma\rangle\Big|_{z=\lambda n_-,A^+=0}, \end{aligned} \tag{10}$$

where we have adopted the more contemporary notation of [25]. In equation 10 the spin, note that we have explicitly written out the spin average, of the proton $|p_\sigma\rangle$, with momentum p, is labeled by σ, x is the fractional momentum of the parton, ψ_q is the quark field of flavor q and n_-^ν is a light-like 4-vector pointing opposite to the direction of the proton's momentum. Moreover, the definition has an implicit sum over colors, $G^{+\mu}$ is the gluon field strength tensor and we have left out the explicit factorization scale dependence. Strictly speaking at LO we would only find the quark PDF and not the gluon one because of the lack of direct coupling between a photon and a gluon. The gluon distribution would then arise in a similar manner in NLO.

For our purposes we will be satisfied with the general statement of the factorization in inclusive processes as given in equation 7, the definition of PDFs as given in equation 10 and the less rigorous presentation of Ref. [9, ch. 32.5] where it is argued that since the PDFs are interpreted as probabilities we should – given the context of quantum mechanics – be able to write

$$F^q(x) = \sum_X \int d\Pi_X |\langle X|\psi_q(0)|p(P)\rangle|^2 \delta(xn\cdot P - n\cdot p), \tag{11}$$

where we have left color and spin averaging implicit, P is the momentum of the proton, p is the momentum of the parton inside the proton and n is the lightlike vector to the direction opposite to the proton momentum. If we consider DIS in the Breit frame (sometimes called the brick wall frame due to the electron simply flipping its momentum in the collision) we could take $n = (1,0,0,1)$. The proton is then moving in the direction $\bar{n} = (1,0,0,-1)$. The above equation describes the overlap that the proton state has, when we operate to it with a quark field operator ψ, over all the possible states X such that the proton momentum P is split up to the parton momenta p and the X state momenta p_X i.e. $P = p + p_X$. We can then insert the factor $1 = \int d^4p\delta(P - p - p_X)$ to force the condition of momentum conservation and write the delta function of equation 11 in a different manner

$$F^q(x) = \sum_X \int d\Pi_X \int \frac{dt}{2\pi} e^{-itn\cdot(xP - P + p_X)} |\langle X|\psi_q(0)|p(P)\rangle|^2. \tag{12}$$

We can then open up the square, use the well known result of how the fields behave under translations, $\psi(x) = e^{ix\cdot\hat{\mathcal{P}}}\psi(0)e^{-ix\cdot\hat{\mathcal{P}}}$, where $\hat{\mathcal{P}}$ is the momentum operator, and sum over the final states – assuming completeness – to eventually find

$$F^q(x) = \int \frac{dt}{2\pi} e^{-itx(n\cdot P)}\langle p(P)|\psi_q^\dagger(tn/2)\psi_q(-tn/2)|p(P)\rangle. \tag{13}$$

We can insert $\bar{\psi}$ in the above by noting that $\bar{\psi} = \psi^\dagger\gamma^0$ and $1 = \gamma^0\gamma^0$. Additionally, for a massless quark, we know from the momentum space Dirac equation that $\not{p}\psi = 0$ which we can write as $\not{\bar{n}}\psi \approx 0$ if we first introduce a type of Sudakov decomposition for p

$$p^\mu = \frac{1}{2}(p\cdot\bar{n})n^\mu + \frac{1}{2}(p\cdot n)\bar{n}^\mu + p_\perp^\mu, \tag{14}$$

where $p_\perp \cdot n = p_\perp \cdot \bar{n} = 0$ and $n^2 = \bar{n}^2 = 0$. Now $\not{\bar{n}}\psi = 0$ implies $2\gamma^0\psi = \not{n}\psi$ which gives us our final form

$$F^q(x) = \frac{1}{2}\int \frac{dt}{2\pi} e^{-itx(n\cdot P)}\langle p(P)|\bar{\psi}_q(tn/2)\not{n}\psi_q(-tn/2)|p(P)\rangle, \tag{15}$$

agreeing with equation 10 after one change of variables. This then completes our rough sketch of how the PDFs arise in a given process. The principal idea being that inclusive cross sections are linearly proportional to the PDFs.

2.2.2 GPDs from DVCS

The GPDs have been "discovered and rediscovered over the decades" ever since the 1970's starting with the Compton Scattering (CS) i.e. $\gamma + p \to \gamma + p$, see e.g. Ref. [31, ch. 1] and similarly to DIS, the Compton amplitude – mostly off an electron – is an extremely well-known process in the literature [2, 4, 5, 9, 11, 53, 56]. As such our only hope is to offer a context as to how GPDs arise in a given process. In the electron case we naturally do not see how GPDs arise but it is the CS process – in a suitable kinematical limit – off a proton where we find the GPDs of interest to us. For us the easiest way to see the emergence of the GPDs is through DVCS, i.e. $\gamma^*(q) + p(p) \to \gamma(q-\Delta) + p(p+\Delta)$, which is also a well known process in the literature [29, 47, 50, 57–59]. The first obvious difference is that this is an exclusive process which means that we cannot sum over the complete final states which was essential in the derivation of the PDFs.

The definitions of the quark GPD F^q and the gluon GPD F^g are given by

$$\begin{aligned}
F^q(x,\xi,t) &= \frac{1}{2}\int_{-\infty}^{\infty}\frac{d\lambda}{2\pi}e^{ix(Pz)}\langle p'|\bar{q}\left(-\frac{1}{2}z\right)\not{n}_- q\left(\frac{1}{2}z\right)|p\rangle\Big|_{z=\lambda n_-},\\
F^g(x,\xi,t) &= \frac{1}{Pn_-}\int_{-\infty}^{\infty}\frac{d\lambda}{2\pi}e^{ix(Pz)}\langle p'|G^{+\mu}\left(-\frac{1}{2}z\right)G_\mu^{\ +}\left(\frac{1}{2}z\right)|p\rangle\Big|_{z=\lambda n_-},
\end{aligned} \tag{16}$$

where we have again used the notation of [25]. Note that the GPDs have support only in the range $x \in [-1,1]$ such that the parameter x can be interpreted as a fractional momenta of the parton. The region $|x| \in [\xi, 1]$ is known as the DGLAP region and $|x| \in [0,\xi]$ is known as the ERBL region. In the DGLAP region the GPDs can be thought of as the generalizations of the more traditional PDFs and in the ERBL region they should be thought of as generalizations of the meson distribution amplitudes [31].

Since we are not interested in the DVCS process itself but only in the way that the GPDs can be understood to arise at the amplitude level of an exclusive process,

we will leave this process here and not develop it any further. The reader should now have a rudimentary understanding of how PDFs and GPDs of a proton arise in inclusive and exclusive processes. Our final goal is to apply all this formalism to the case of nucleus-nucleus collisions where we need to take into account non-trivial nuclear corrections.

2.2.3 Connection between PDFs and GPDs

Comparing then equations 10 and 16 we see that the link between a PDF and GPD is such that we would need to set the initial momenta p and the final momenta p' equal and average (sum) over the initial (final) state spins. The easiest way to think about this is to Lorentz decompose the QFT definition of the GPDs $F^j(x,\xi,t)$ into a vector part and a tensor-vector part

$$F^j(x,\xi,t) = \frac{1}{2(Pn_-)}\Bigg[\mathcal{H}^j(x,\xi,t)\bar{u}(p')\not{n}_- u(p) + \mathcal{E}^j(x,\xi,t)\bar{u}(p')\frac{i\sigma^{\alpha\beta}n_{-\alpha}\Delta_\beta}{2m_p}u(p)\Bigg], \tag{17}$$

where the index $j = q, g$ refers to quarks or gluons, the momentum P is the average of the incoming and outgoing momenta, i.e. $(p+p')/2$, u is the Dirac spinor solution for a proton, $i\sigma^{\alpha\beta}$ is given by $(-1/2)[\gamma^\alpha, \gamma^\beta]$ and $\mathcal{H}^j(x,\xi,t)$ and $\mathcal{E}^j(x,\xi,t)$ are some scalar functions also collectively referred to as GPDs [31]. In the limit which we will be working in, we ignore contributions arising from $\mathcal{E}^j(x,\xi,t)$ since it is multiplied by the exchanged momenta $\Delta = p' - p$. We also assume no helicity flip – i.e. incoming and outgoing spins are the same – with which we get, using the well known spin projections, the relation between the quark and the gluon distributions to be

$$F^q(x,0,0) = F^q(x) \text{ and } F^g(x,0,0) = xF^g(x) \text{ for } x > 0. \tag{18}$$

In Ji's parametrization [47] the fractional momentum x can also take negative values but GPDs can be related back to the positive x region through the following symmetry properties:

$$F^q(x,0,0) = -F^{\bar{q}}(-x) \text{ and } F^g(x,0,0) = F^g(-x) \text{ for } x < 0. \tag{19}$$

Equations 18 and 19 hold for the free proton PDFs and GPDs but we will assume that such a limit holds equally for the nuclear distributions as well. In this way it is good to keep in mind that any nuclear modifications that we apply will be applied only onto the $\mathcal{H}^j(x,\xi,t)$ GPDs. Next, let us look at the nuclear corrections in more detail.

2.3 Nuclear corrections to PDFs/GPDs

One additional and quite fundamental difference between PDFs and GPDs is that whereas the PDFs can be thought of as particle densities – due to the fact that they

appear at the cross section level – this interpretation is not equally clear for the GPDs. The GPDs appear at the amplitude level and as such should be thought of as probability amplitudes of finding a specified parton pair sandwiched between a given initial and a final state. In this way the GPDs can be thought of as four point functions. This fact in addition to the larger domain of the GPDs means that the GPDs offer a more detailed image of the internal structure of the hadrons as has been extensively discussed in the literature [31, 38, 40, 41, 60].

For the case of heavier elements, one is naturally lead to ask the question: how does the environment of heavier nuclei affect the parton distributions? On a superficial level the change from a PDF to a nPDF is not huge: instead of a proton colliding with a proton we might have two nuclear beams – labeled by their mass number A – colliding with each other, i.e., $A + A \to X$, which would mean that equation 10 would be minimally modified to

$$\begin{aligned} F_A^q(x) &= \frac{1}{2}\int_{-\infty}^{\infty}\frac{d\lambda}{2\pi}e^{ix(P\cdot z)}\langle A|\bar{\psi}_q\left(-\frac{1}{2}z\right)\not{n}_-\psi_q\left(\frac{1}{2}z\right)|A\rangle\Big|_{z=\lambda n_-,A^+=0} \\ F_A^g(x) &= \frac{1}{xP^+}\int_{-\infty}^{\infty}\frac{d\lambda}{2\pi}e^{ix(P\cdot z)}\langle A|G^{+\mu}\left(-\frac{1}{2}z\right)G_y{}^+\left(\frac{1}{2}z\right)|A\rangle\Big|_{z=\lambda n_-,A^+=0}, \end{aligned} \tag{20}$$

where the proton state $|p\rangle$ has been swapped for a nucleus state $|A\rangle$ and we have left the average over the spin σ implicit. More precisely, in the framework of collinear factorization we imagine that the collision process takes place between two nucleons that represent somehow an average nucleon inside the nucleus so that a more precise labeling of the states might be $|p_A\rangle$. This being said, one could imagine that there is some spatial dependence to the way the partons are distributed within this larger nucleus – for this avenue of research the reader is directed towards Refs. [61–66] – but in our framework we will consider such corrections to be unimportant and work only with spatially averaged distributions.

A lot of effort has been put to pin down the nuclear effects within a heavy nucleus, see e.g. Refs. [67–77], and what has been discovered so far is that the nucleus receives non-trivial corrections over the full range of the fractional parton momentum x. The scale dependence of the distributions, free and bound proton alike, is considered to be completely determined by the Dokshitzer-Gribov-Lipatov-Altarelli-Parisi (DGLAP) evolution equation [78–81]. In short the corrections over x are as follows: starting from zero and going all the way up to $x \lesssim 0.03$ we have a suppression in the nPDFs as compared to their free counterparts and this effect is known as *shadowing* of the distributions. Moving between x values of $0.03 \lesssim x \lesssim 0.3$ we are in the so called *antishadowing* region where the nPDFs are enhanced as compared to the PDFs. The nPDFs get suppressed again in the EMC (short for European Muon Collaboration) region at $0.3 \lesssim x \lesssim 0.8$ after which the nPDFs are enhanced again due to the *Fermi motion* for x values approximately greater than 0.8. See [82] for a detailed summary of this.

In this work we will be interested especially in the EPPS16 [73] and EPPS21 [76] parametrizations of the nPDFs where the bound PDFs are calculated from the free proton PDFs after multiplying them with appropriate nuclear correction factors R.

Moreover, in the EPPS framework the partonic content of neutrons is acquired from protons through the approximate isospin symmetry and as such the nPDF for a nucleus of mass number A and an atomic number Z is obtained from

$$F_A^i(x) = \frac{Z}{A}F_{p/A}^i(x) + \frac{A-Z}{A}F_{n/A}^i(x), \text{ where } F_{p/A}^i(x) = R_A^i(x)F_p^i(x). \quad (21)$$

Here i labels the parton in question, $F_{p/A}^i$ is the bound proton PDF, $F_{n/A}^i$ is the bound neutron PDF and R_A^i is the nuclear correction to the flavor i in the nucleus A. The values of F_p^i are determined from free proton collisions and the values of R_A^i from heavier nucleus collisions via global analyses.

Nuclear effects on GPDs – unpolarized or polarized – have not attracted much of main stream attention but the field might become more important in the future as experimental setups become better and better. For a few references discussing GPDs and nuclear corrections to them, see e.g. Refs. [60, 83–87]. For our purposes, we will be working mostly with the unpolarized, spatially averaged distributions in the kinematical limit of $t \approx 0$ and $\xi \approx 0$ such that the limits given by equations 18 and 19 are taken exactly and that the nuclear corrections are added e.g. like in Eq. 21. Note that this also means that we will be ignoring any corrections arising from the ERBL region and effectively we approximate the nGPDs arising in this process exactly by their nPDF counterparts assuming that they follow the DGLAP evolution equations. For literature developing the GPD modeling, see e.g. Refs. [42, 88–90].

3 PHOTOPRODUCTION BASELINE

Before continuing to the actual process of interest in this thesis we still need to tackle the sub-process of it, namely the coherent exclusive photoproduction of heavy-vector mesons: $\gamma + p \to V + p$. As we know now, in exclusive scatterings we are probing the GPDs but the interest in this process in the high-energy particle physics community started some thirty years ago when Ryskin proposed that the cross section of diffractive J/ψ electroproduction in the Leading Log Approximation (LLA) can be written to be proportional to the square of the gluon PDF [91]. It was later pointed out how in the LLA the distributions which we find in this process indeed reduce to the usual gluon PDF at the kinematical point $t = 0$; for a nice summary, see [31, ch. 8.1]. In what follows we will sketch the photoproduction calculation in the forward limit $t = 0$ at LO perturbative QCD (pQCD).

The exclusive production of a vector meson contains an additional experimental challenge which is not present in DIS or DVCS: we never actually see the produced vector meson in our detectors but instead we see a spike in the production of two back-to-back leptons, i.e. l^+l^-, at an invariant mass which matches that of the vector meson. This means that we need to somehow tie the observed final state to the intermediate heavy-vector meson state and the way this is usually done is through the decay width of the meson. For a detailed account on the LO pQCD calculation of $J/\psi \to l^+l^-$ decay widths and the helicity-basis approach – which we will employ in the calculation below – see Ref. [92].

In our approach, in papers [PI] and [PII], we will take the high-energy forward limit in which the GPDs reduce to their PDF counterparts such that over the full range of the x domain they follow the DGLAP evolution of parton densities [78–81]. So to be absolutely clear, we will then neglect the ERBL region where the GPDs follow the evolution of meson distribution amplitudes [93, 94]. On the soft part of the calculation we will also ignore any non-forward contributions but it should be pointed out that people have considered examples where this constraint has been relaxed to see how much the off-forwardness contributes, see e.g. [84, 95, 96].

Before continuing on to the LO calculation let us explicitly state the kinematical variables of the process $\gamma(q) + p(p) \to V(K) + p(p')$. We will follow closely the presentation given in Ref. [25] but the process has also been considered in detail in

Ref. [97] and in a more general kinematical setting in Refs. [98, 99]. The momentum of the incoming nucleon is labeled by p, the momentum of the incoming photon by q, the momentum of the outgoing nucleon by p' and the momentum of the heavy vector meson by K. We will explicitly set all particles on their mass shell $p^2 = p'^2 = m_N^2$, $q^2 = 0$ and $K^2 = M^2$ where m_N is the nucleon mass and M is the mass of the vector meson. This means that the calculation is done in the approximation where the spin states of the outgoing vector meson will match exactly those of the incoming photon. Furthermore, in the calculation of the vector meson vertex we will explicitly assume that the mass of the meson is two times the mass of the heavy quark m_Q, i.e. $M = 2m_Q$. We can use these to define kinematical variables of interest

$$s = (p+q)^2 = W^2;\ p' - p = \Delta;\ t = \Delta^2;\ P = \frac{p+p'}{2};\ \zeta = \frac{M^2}{W^2}. \tag{22}$$

Note that ζ is now the Bjorken-x equivalent of this exclusive process. Additionally, in order to use the Sudakov decomposition, we introduce the light-cone vectors n_+ and n_-, which obey $n_+^2 = n_-^2 = 0$ and $n_+ \cdot n_- = 1$, such that any four-vector l can be written as

$$l^\mu = l^+ n_+^\mu + l^- n_-^\mu + l_\perp,\ l^2 = 2l^+l^- - \boldsymbol{l}^2, \tag{23}$$

where $l_\perp = (0, 0, \boldsymbol{l})$, $\boldsymbol{l}$ is a two dimensional vector and for defining other light-cone vectors we use the Kogut-Soper convention [100–103]. With the help of these ligh-cone vectors, the momenta can be decomposed in a similar manner to Ji's notation

$$\begin{aligned}
p &= (1+\xi)Wn_+ + \frac{m_N^2}{2(1+\xi)W}n_-,\ q = \frac{W^2 - m_N^2}{2(1+\xi)W}n_-, \\
p' &= (1-\xi)Wn_+ + \frac{m_N^2 + \boldsymbol{\Delta}^2}{2(1-\xi)W}n_- + \Delta_\perp, \\
\Delta &= -2\xi Wn_+ + \left(\frac{\xi m_N^2}{(1-\xi)(1+\xi)W} + \frac{\boldsymbol{\Delta}^2}{2(1-\xi)W}\right)n_- + \Delta_\perp,
\end{aligned} \tag{24}$$

where we have introduced the skewness parameter ξ which in the scaling limit of $s \to \infty$ quantifies the momentum transfer in the plus direction n_+. This is easily seen as follows:

$$\begin{aligned}
&p \to (1+\xi)Wn_+;\ p' \to (1-\xi)Wn_+;\ \Delta \to -2\xi Wn_+ \\
&\Rightarrow \xi = \frac{p_+ - p'_+}{p_+ + p'_+}.
\end{aligned} \tag{25}$$

The numerical value can be found from

$$\begin{aligned}
W^2 &= (K+p')^2 = M^2 + 2K\cdot p' + m_N^2 \\
&= M^2 + 2m_N^2 - t + \frac{1-\xi}{1+\xi}(W^2 - m_N^2) - 2m_N^2 + m_N^2 \\
&= M^2 - t + \frac{1-\xi}{1+\xi}(W^2 - m_N^2) + m_N^2 \\
\Leftrightarrow \xi &= \frac{\frac{M^2}{W^2} - \frac{t}{W^2}}{2 - \frac{M^2}{W^2} - \frac{2m_N^2}{W^2} + \frac{t}{W^2}},
\end{aligned} \tag{26}$$

where from going from the first line to the second line we used $K = p + q - p'$, then from the second line to the third line we just plugged in our decomposition of momenta as given in equation 24 and then solved for ξ. The scaling limit is given when we ignore the terms t/W^2 and m_N^2/W^2 which gives us

$$\xi = \frac{\zeta}{2-\zeta} \Leftrightarrow \zeta = \frac{2\xi}{1+\xi}. \tag{27}$$

3.1 Leading order calculation

The desired scattering matrix element S_{fi} is acquired by sandwiching the scattering matrix operator S, as defined by

$$S = T \exp\left[i \int d^4x \mathcal{L}_I(x) \right], \tag{28}$$

in between the initial state $|i\rangle$ and the final state $|f\rangle$. In equation 28 the term $\mathcal{L}_I(x)$ gives the interaction Lagrangian density and the way to derive this expression for S is quite nicely summarized in [8]. For our particular process of interest, at this order of the perturbation theory, the initial state $|i\rangle$, the final state $|f\rangle$ and the interaction Lagrangian density $\mathcal{L}_I$ are given by

$$|i\rangle = |\gamma(q)p(p)\rangle;\ |f\rangle = |V(K)p(p')\rangle;\ \mathcal{L}_I = \mathcal{L}_{I,\mathrm{QCD}} + \mathcal{L}_{I,\mathrm{QED}}, \tag{29}$$

where $\mathcal{L}_{I,\mathrm{QCD}} = \bar{\psi}_Q^j (i\not{A})_{jk} \psi_Q^k$ is the QCD interaction term, $\mathcal{L}_{I,\mathrm{QED}} = \bar{\psi}_Q (i\not{A}_\gamma) \psi_Q$ is the QED interaction term and Q labels a heavy quark. To be explicit about what we mean here is that we consider up, down and strange quarks to be massless and charm and beauty to be the heavy quarks, and that the light quark flavors enter the calculation only at $\mathcal{O}(g_s^3)$ at the amplitude level. Note also that the coupling constants e and g_s are now implicitly in the definition of the gauge fields A and A_γ.

We do not have terms coming from the full QCD Lagrangian from the $F^a_{\mu\nu} F^{a,\mu\nu}$ term – which are proportional to g_s or g_s^2 – because of color constraints or due to the fact that they are higher up in the expansion in the strong coupling g_s. That is, the terms proportional to $\mathcal{O}(g_s)$ would always end up being proportional to f^{abb} and terms proportional to $\mathcal{O}(g_s^2)$ would need two additional interaction terms in order to produce a connected graph i.e. the amplitude would end up being proportional to g_s^4. Notice also that terms giving the free theory are disregarded due to our formulation of the S-matrix. Hence we expand the S-matrix up to the third term in $\mathcal{L}_I$,

$$\begin{aligned} S_{fi} = \langle V(K)P(p')|T\Bigg(1 + i\int d^4x \mathcal{L}_I(x) + \frac{i^2}{2!}\int d^4x \mathcal{L}_I(x) \int d^4y \mathcal{L}_I(y) \\ + \frac{i^3}{3!}\int d^4x \mathcal{L}_I(x) \int d^4y \mathcal{L}_I(y) \int d^4z \mathcal{L}_I(z) + \mathcal{O}(e^2, g_s^3)\Bigg)|\gamma(q)P(p)\rangle. \end{aligned} \tag{30}$$

The term proportional to one does not contribute at all since there is no way of making a vector meson out of a photon without interactions. Terms proportional

to $\mathcal{O}(e^2, g_s^3)$ we disregard as being small due to the high number of the coupling constants. The term $\mathcal{O}(\mathcal{L}_I)$ does not produce connected diagrams and thus gets ignored. The last term on the first line has terms proportional to e^2, eg_s and g_s^2 where the first one is disregarded as being too small. The term with g_s^2 does not have QED interaction and thus we would not be able to connect the incoming photon to the rest of the process. The mixing term proportional to eg_s also does not contribute as it has only one gluon field and as such we cannot find the needed definitions for the GPDs or the meson vertex as required by the factorization theorem [33]. That leaves us with the term on the second line with three Lagrangians $\mathcal{L}_I$ which has terms proportional to e^3, $e^2 g_s$, eg_s^2 and g_s^3. We ignore all the other terms except for eg_s^2 being too high in the powers of the coupling. This means that we can write the matrix element as

$$\begin{aligned} S_{fi} &\approx \langle V(K)P(p')|T\left(\frac{i^3}{3!}\int d^4x\mathcal{L}_I(x)\int d^4y\mathcal{L}_I(y)\int d^4z\mathcal{L}_I(z)\right)|\gamma(q)p(P)\rangle \\ &\approx \langle V(K)P(p')|T\Bigg(\frac{i^3}{3!}\cdot 3\int d^4xd^4yd^4z \\ &\qquad (\bar{\psi}^a_Q(i\not{A}_\gamma)\psi^a_Q)_x(\bar{\psi}^b_Q(i\not{A})_{bc}\psi^c_Q)_y(\bar{\psi}^d_Q(i\not{A})_{de}\psi^e_Q)_z\Bigg)|\gamma(q)P(p)\rangle \end{aligned} \tag{31}$$

after some relabeling of the integration variables. Note that now a, b, c, d and e label color indices. For the color factors we know that each interaction term with a gluon provides us with a t^a and that the quark fields will be sandwiched between the vacuum and the vector meson state and the gluon fields are sandwiched between the hadron states – which force the color to be the same – which gives for each term the color factor $T_R = Tr[t^a t^b] = (1/2)\delta^{ab}$.

By Wick's theorem [104] the time ordered product can be expressed as a sum of all possible contractions which in this case means a sum of zero, one, two, three or four contractions. From these possibilities only the ones where we have two contractions of quark fields contribute leaving two quark fields, the photon field and the two gluon fields uncontracted. The two quark fields will be used to define the vector meson vertex, the photon field operates to the incoming photon and the two gluon fields will be used to define the GPD. We can move the time ordering operator inside the integrals and consider only the product of operators which we are left with after applying Wick's theorem

$$\begin{aligned} \mathcal{T}(x,y,z) &= T\left((\bar{\psi}(i\not{A}_\gamma)\psi)_x(\bar{\psi}(i\not{A})\psi)_y(\bar{\psi}(i\not{A})\psi)_z\right) \\ &= N\Big((\bar{\psi}\not{A})_z S_F(z-x)\not{A}_\gamma(x)S_F(x-y)(\not{A}\psi)_y \\ &+ (\bar{\psi}\not{A})_y S_F(y-x)\not{A}_\gamma(x)S_F(x-z)(\not{A}\psi)_z \\ &+ (\bar{\psi}\not{A}_\gamma)_x S_F(x-y)\not{A}(y)S_F(y-z)(\not{A}\psi)_z \\ &+ (\bar{\psi}\not{A})_z S_F(z-y)\not{A}(y)S_F(y-x)(\not{A}_\gamma\psi)_x \\ &+ (\bar{\psi}\not{A})_y S_F(y-z)\not{A}(z)S_F(z-x)(\not{A}_\gamma\psi)_x \\ &+ (\bar{\psi}\not{A}_\gamma)_x S_F(x-z)\not{A}(z)S_F(z-y)(\not{A}\psi)_y\Big) \end{aligned} \tag{32}$$

where the two first lines correspond to the term where both quark fields in the interaction term evaluated at x have been contracted, the second two to the one

where both quark fields at y have been contracted and last two to the one where both fields at z have been contracted. We have also dropped the color indices and the heavy quark label Q for readability and used the well known result that a contraction between two fermion fields is the position space propagator

$$\begin{aligned}\overbrace{\psi^a_\alpha(x)\bar{\psi}^b_\beta}(y) &= \langle 0|T(\psi^a_\alpha(x)\bar{\psi}^b_\beta(y))|0\rangle = S_F^{ab}(x-y)_{\alpha\beta} \\ &= \delta^{ab}\int \frac{d^4l}{(2\pi)^2}e^{-il(x-y)}\frac{i(\not{l}+m)_{\alpha\beta}}{l^2-m^2+i\epsilon} = -\overbrace{\bar{\psi}^b_\beta(y)\psi^a_\alpha}(x),\end{aligned} \tag{33}$$

where $|0\rangle$ labels the vacuum state. As argued in the proof of the factorization theorem, we know that the gluon fields will be used for the definition of the gluon GPD and the quark fields will be used in the vector meson vertex [33]. This means that the matrix element can be factored as

$$S_{fi} \sim N\left[Tr\left[\langle V(K)|\psi\bar{\psi}A^\mu_\gamma|\gamma\rangle P(\cdots)_{\mu\nu\eta}\right]\langle P(p')|A^\nu A^\eta|P(p)\rangle\right] \tag{34}$$

where the trace is taken over the Dirac indices, $P(\dots)_{\mu\nu\eta}$ denotes the product of the remaining gamma matrices and propagators and for simplicity we have left out all extra labels. Given the photon field operator

$$A^\mu_\gamma(x) = \int \frac{d^3\vec{k}}{(2\pi)^3\sqrt{2E_{\vec{k}}}}\sum_{\lambda=1}^{2}\left(a(k,\lambda)\varepsilon^\mu(k,\lambda)e^{-ik\cdot x} + a^\dagger(k,\lambda)\varepsilon^{*\mu}(k,\lambda)e^{ik\cdot x}\right), \tag{35}$$

where a is the annihilation operator and $a^\dagger$ is the creation operator obeying the standard boson commutation relations, i.e. $[a(\vec{k},\lambda), a^\dagger(\vec{k}',\lambda')] = \delta_{\lambda\lambda'}(2\pi)^3\delta^3(\vec{k}-\vec{k}')$ and zero otherwise. Moreover, ε and ε^* are the photon polarization vectors. We can then operate to the photon state $|\gamma\rangle$ which gives us

$$A^\mu_\gamma(x)|\gamma(q,\lambda)\rangle = \varepsilon^\mu_\gamma(q,\lambda)e^{-iqx}|0\rangle, \tag{36}$$

where λ labels the helicity state of the photon. Note that the photon field operator contains also a creation operator which also operates to this state but such terms do not contribute here.

Each term in equation 32 has two uncontracted gluon fields and two uncontracted fermion fields evaluated at one of the space-time points x, y or z. For the first two rows in the normal ordered product in equation 32 we can use integration over x to fix the two propagator loop momenta together with the photon momentum. Similarly, we fix the next two through y integration and the last two through z integration. For the remaining integration variables, e.g. y and z on the first two rows, it is helpful to do a change of variables to the "center-of-mass" frame i.e. $y = R - r/2$ and $z = R + r/2$ (Jacobian is 1) which allows us – after a few translations of the fields – to identify the overall momentum conserving delta function $\delta^4(p+q-K-p')$ through the R integral. This means that we have two four-dimensional integrals left: the integral over r and the integral over the loop momenta introduced by one of the propagators.

To be explicit, after the change of variables, the first term of $P(\cdots)_{\nu\eta} = \varepsilon^\mu P(\cdots)_{\mu\nu\eta}$ in equation 34 would be

$$\gamma_\nu S_F(z-x)\not{\varepsilon}_\gamma S_F(x-y)\gamma_\eta, \tag{37}$$

and so on for the remaining five. The proof that this can indeed be done – i.e. that equation 34 holds – would amount to the actual proof of factorization which we will just take as given in the literature. From the three terms in equation 34, let us first deal with the piece with the vector meson in the final state. In a general Fock-state expansion the V state can be written as

$$|V\rangle = \psi_1|\bar{Q}Q\rangle + \psi_2|\bar{Q}Qg\rangle + \cdots , \tag{38}$$

where Q labels a heavy-quark state and g labels a gluon state. We will take this state in the non-relativistic (NR) limit and at the lowest Fock-state for the vector meson [105–107] which means that for us the vector meson state is composed of a pair of on-shell quarks, i.e. $k_1^2 = k_2^2 = m_Q^2$, such that $k_1 + k_2 = K$ [25, 33, 97, 98]. Moreover, the states $|\bar{Q}_a\rangle$ and $|Q_b\rangle$ have to have the same color index $a = b$ since we only consider the state $|\bar{Q}Q\rangle$ and neglect all higher-order terms i.e. terms with $\psi_{i\neq 1}$.

The typical way of relating the produced vector meson state to the experimentally observable lepton state is to relate the desired matrix element to the decay width calculation where a similar matrix element arises. In order to do this, we need the following spinor products [92]:

$$\begin{aligned} &v(\uparrow)\bar{u}(\uparrow) = -\frac{1}{\sqrt{2}}\not{\varepsilon}_V^*(\uparrow)\left(\frac{\not{K}+M}{2}\right);\ v(\downarrow)\bar{u}(\downarrow) = -\frac{1}{\sqrt{2}}\not{\varepsilon}_V^*(\downarrow)\left(\frac{\not{K}+M}{2}\right) \\ &\frac{1}{\sqrt{2}}[v(\uparrow)\bar{u}(\downarrow) + v(\downarrow)\bar{u}(\uparrow)] = -\frac{1}{\sqrt{2}}\not{\varepsilon}_V^*(0)\left(\frac{\not{K}+M}{2}\right), \end{aligned} \tag{39}$$

where u and v refer to the free heavy quark spinors, ε_V is the vector meson polarization vector and the arrows denote the helicity eigenstates. Note that equations 39 are derived for a vector meson in the final state and the relation for the initial state, used in the decay width calculation, one would need to take the complex conjugate equation 39. With that in mind, we should point out that it is the Fourier transform of the matrix element $\langle V(K)|\psi\bar{\psi}|0\rangle$ – note the meson in the final state – which is sometimes referred to as the wavefunction of the meson state and it quantifies our ignorance of the soft QCD dynamics [41].

The problem of not being able to calculate the QCD dynamics in full has been considered in the literature on multiple occasions [34, 108–111] and for our purposes we will quantify our ignorance through the factor B as

$$\langle V|\psi\bar{\psi}|0\rangle = \frac{B}{\sqrt{3}}\left(\frac{-1}{\sqrt{2}}\right)\not{\varepsilon}_V^*\left(\frac{\not{K}+M}{2}\right), \tag{40}$$

where $\sqrt{3}$ is the color state normalization factor and the minus sign originates from our spinor sign convention. This factor relates back to the decay width calculation and the NRQCD element $\langle O_1\rangle_V$ through

$$B^2 = \frac{M\Gamma^{V\to l^+l^-}}{8\pi\alpha_{QED}^2 e_Q^2},\ B^2 = \frac{1}{3}\frac{\langle O_1\rangle_V}{M} \tag{41}$$

where e_Q is the fractional charge of the heavy quark and $\Gamma^{V\to l^+l^-}$ is the decay width of the vector meson to the l^+l^- lepton channel. This is a good place to point out

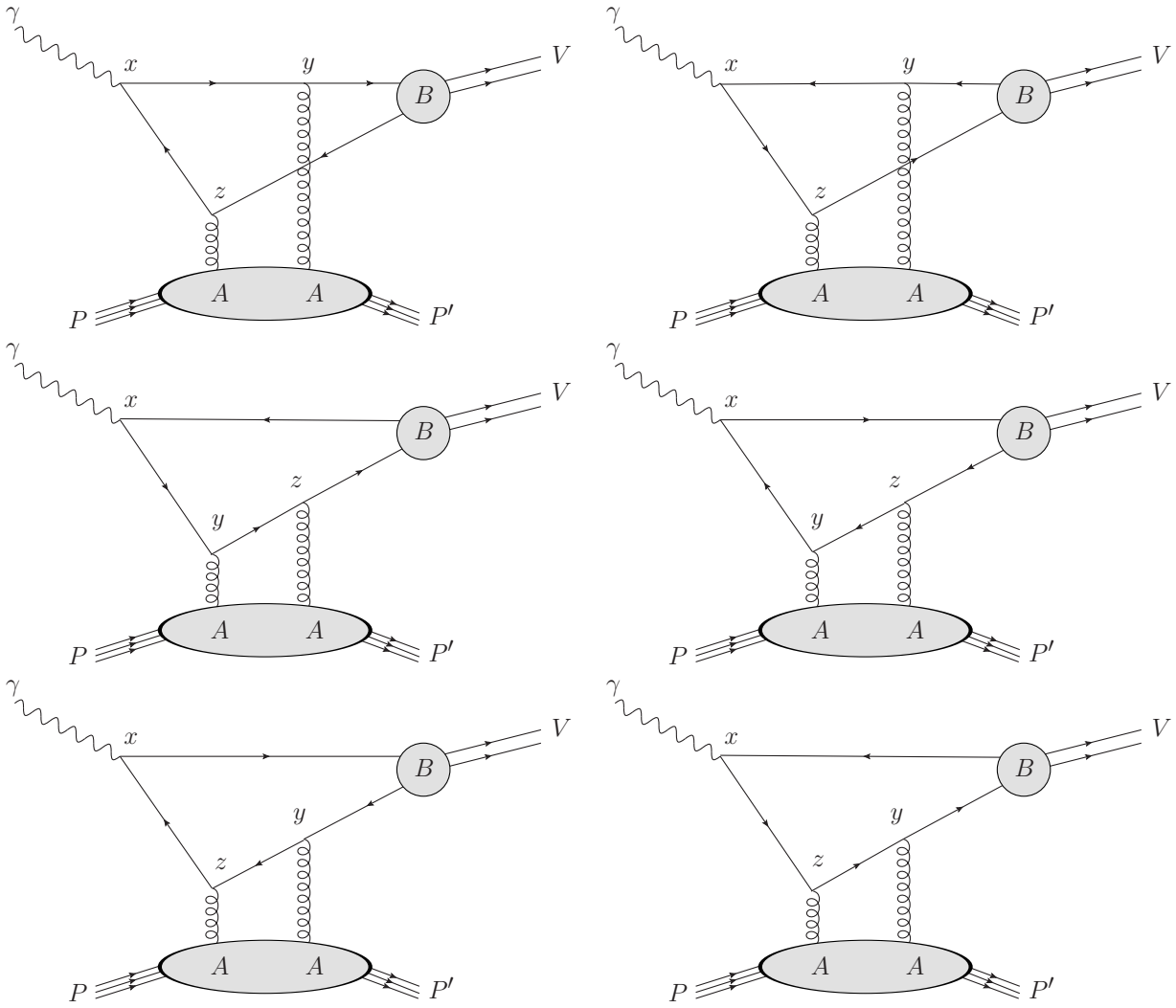

FIGURE 1 Diagrammatical presentations of the six different contributions in the LO calculation of the coherent photoproduction amplitude. The first row corresponds to the first two terms in equation 32, the second row to the third and the fourth and the last row to the fifth and the sixth terms.

to the reader how the development so far, i.e. equations 32, 34 and 40, can be interpreted diagrammactically as shown in Fig. 1.

Before turning our attention to the product of the gluon fields in equation 34, we need to consider what happens to the trace over the vector meson vertex and hard scattering part $P(\cdots)_{\nu\eta}$. One can either do it by hand by expanding the gamma matrices in a manner similar to the Sudakov decomposition or use the Feyncalc package of Mathematica or the symbolic manipulation program FORM to calculate the traces but the end result with all methods is

$$Tr\left[\not{\varepsilon}_V^*\left(\frac{\not{V}+M}{2}\right)P(\cdots)_{\nu\eta}\right]=\frac{16}{m_Q}g_{\nu\eta}(\varepsilon_V^*\cdot\varepsilon_\gamma). \tag{42}$$

This is actually a quite nice result as the product ends up being independent of the momenta introduced by the propagators or the external momentum vectors. Because of this, as the product of the gluon fields operates to hadron states on the light-cone, we can use the loop momenta to identify a few delta functions, i.e. $\delta(r^+)$ and $\delta^2(r_\perp^2)$, which leaves us only with an integral over r^- and an integral over the loop momenta l^+. Putting all this together we find that S_{fi} is now given by

$$\begin{aligned}S_{fi}=&i(2\pi)^4\delta^4(p+q-K-p')\frac{B}{\sqrt{3}}\left(\frac{-1}{\sqrt{2}}\right)\frac{16}{m_Q}g_{\nu\eta}(\varepsilon_V^*\cdot\varepsilon_\gamma)\pi e_Q e\alpha_s T_R\\&\int dr^-\int\frac{dl^+}{2\pi}e^{ir^-(l^++\Delta^+/2)}\langle p'|A^\nu\left(\frac{-r}{2}\right)A^\eta\left(\frac{r}{2}\right)|p\rangle,\end{aligned} \tag{43}$$

where e is the QED coupling constant and α_s is related to the strong coupling constant by $4\pi\alpha_s=g_s^2$. Note that the above equation is not yet in Ji's symmetric notation, i.e. we have not yet explicitly applied the decomposition introduced in Eq. 24, as often given in the literature, and in order to do this we need to do one additional change of variables. Now instead of integrating over l we will integrate over x such that $l=(x+\xi)\bar{p}$ where $\bar{p}=(p+p')/2$. In this way the momenta are given in terms of the light-like vectors $\bar{p}$ and n, for which $\bar{p}^2=n^2=0$ and $\bar{p}\cdot n=1$, as

$$p=(1+\xi)\bar{p};\ q=\frac{s}{2(1+\xi)}n;\ p'=(1-\xi)\bar{p}, \tag{44}$$

from which we immediately see $\Delta=-2\xi\bar{p}$ and we think of $\bar{p}$ to be on the plus lightcone and n to be on the minus lightcone. Note how the above is the strict forward limit of the decomposition presented in equation 24. In this basis we see that the integration range for x will be $[-1,1]$ since the matrix element with the product of the gluon fields inside is zero for partons with momenta greater than that of the incoming parent hadron. Moreover, since the integration variable r is pointing only in the minus direction we can do one additional change of variable, i.e. $r^-=\lambda n^-$, and integrate over λ to get

$$\begin{aligned}S_{fi}=&i(2\pi)^4\delta^4(p+q-K-p')\frac{B}{\sqrt{3}}\left(\frac{-1}{\sqrt{2}}\right)\frac{16}{m_Q}g_{\nu\eta}(\varepsilon_V^*\cdot\varepsilon_\gamma)\pi e_Q e\alpha_s T_R\\&\int_{-1}^{1}dx(\bar{p}\cdot n)\int\frac{d\lambda}{2\pi}e^{ix(r\cdot\bar{p})}\langle p'|A^\nu\left(\frac{-r}{2}\right)A^\eta\left(\frac{r}{2}\right)|p\rangle\Big|_{r=\lambda n}.\end{aligned} \tag{45}$$

It was shown in [29, 112] that the gluon field $A_\mu(x)$ in the light-cone gauge $n \cdot A = 0$ can be expressed in terms of the gluon field strength tensor $G_{\mu\nu}$ as

$$A_\mu(x) = \int dt n^\nu e^{-\epsilon t} G_{\mu\nu}(x + nt), \tag{46}$$

where ϵ is an infinitesimal parameter i.e. the above relation is to be thought in the limit $\epsilon \to 0$. By substituting this in for the gluon fields, translating the field strength tensors, using the Schwinger parameter trick

$$\frac{i}{A} = \int_0^\infty ds\, e^{isA}, \text{ when } \mathrm{Im}(A) > 0, \tag{47}$$

to do the t integral, we find that the invariant matrix element can be written as

$$\mathcal{M}_{fi} = \left(\frac{-B}{\sqrt{3}\sqrt{2}}\right) \frac{8\pi}{m_Q} (\varepsilon_V^* \cdot \varepsilon_\gamma) e e_Q \alpha_s \int_{-1}^{1} dx \frac{F^g(x, \xi, t)}{(x + \xi - i\epsilon)(x - \xi + i\epsilon)}, \tag{48}$$

in accordance with our sign choice of

$$S_{fi} = \delta_{fi} + i(2\pi)^4 \delta^4(p_f - p_i) \mathcal{M}_{fi}. \tag{49}$$

Note that the derivation of equation 48 is the proof of the factorization theorem as presented in equation 9.

The expression of equation 48 agrees with the result presented in [25] with the exception of the sign originating from a different spinor sign convention. The next step would be to square this to get an expression for the t-differential cross section

$$\frac{d\sigma(p + \gamma \to V + p')}{dt} = \frac{\overline{|\mathcal{M}(p + \gamma \to V + p')|^2}}{16\pi\lambda(s, 0, 0)}, \tag{50}$$

where λ is the Källén function given by $\lambda(x, y, z) = (x - y - z)^2 - 4yz$. In order to do this, we need to be mindful of the spin sums, i.e. we are interested in unpolarized scatterings so we average over initial states and sum over final state spins such that the square of the product of the polarization vectors gives

$$\frac{1}{2}\frac{1}{2} \sum_{i,j=\pm 1} |\varepsilon_V^{*i} \cdot \varepsilon_\gamma^j|^2 = \frac{1}{2}, \tag{51}$$

where one factor of $1/2$ is for the incoming proton and the other is for the incoming photon. The effect of the spin sums of the incoming and outgoing hadrons over the GPD is nothing because of the forward limit that we enforce i.e. the Lorentz decomposition of the amplitude defining the GPD gives us only the vector current that is proportional to $\bar{u}(p, s')\gamma^\mu u(p, s) = 2\delta^{ss'} p^\mu$. This allows us to write the square of the averaged matrix element as

$$\overline{|\mathcal{M}(\gamma + p \to V + p')|^2} = \frac{B^2}{3 \cdot 2} \frac{(8\pi)^2}{m_Q^2} \cdot e^2 e_Q^2 \alpha_s^2 |I(\xi, t = 0)|^2, \tag{52}$$

where

$$I(\xi, t=0) = \int_{-1}^{1} dx \frac{F^g(x,\xi,t)}{(x+\xi-i\epsilon)(x-\xi+i\epsilon)}. \tag{53}$$

Substituting the expression for B^2 we find

$$\overline{|\mathcal{M}(p+q\to K+p')|^2} = \frac{16\pi}{3\cdot 2}\frac{8\pi\Gamma^{V\to l^+l^-}}{M}\frac{\alpha_s^2}{\alpha_{QED}}|I(\xi,t=0)|^2, \tag{54}$$

and further to the expression for the t-differential cross section

$$\left.\frac{d\sigma(\gamma+p\to V+p')}{dt}\right|_{t=0} = \frac{1}{s^2}\frac{8\pi}{3\cdot 2}\frac{\Gamma^{V\to l^+l^-}}{M}\frac{\alpha_s^2}{\alpha_{QED}}|I(\xi,t=0)|^2, \tag{55}$$

where s is the Mandelstam variable. We are working in the limit $s\to\infty$ and in this limit the amplitude is argued to be mainly imaginary [31, 91]. We see that the amplitude is composed of real numbers except for the values of the integral I. We can then use the symmetry property of the gluon GPD, $F^g(x,\xi,t) = F^g(-x,\xi,t)$, and the Cauchy principal value prescription to find

$$\begin{aligned} I(\xi,t=0) &= 2\int_0^1 dx \frac{F^g(x,\xi,t)}{(x+\xi-i\epsilon)(x-\xi+i\epsilon)} \\ &= 2\left[\mathcal{P}\left(\int_0^1 dx \frac{F^g(x,\xi,t)}{(x+\xi)(x-\xi)}\right) - i\pi\frac{F^g(\xi,\xi,t)}{2\xi}\right]. \end{aligned} \tag{56}$$

We will then take the GPD in its forward limit and ignore the real part given by $\mathcal{P}(\cdots)$ to get

$$\left.\frac{d\sigma(\gamma+P\to V+P')}{dt}\right|_{t=0} \approx \frac{1}{s^2}\frac{8\pi^3}{3\cdot 2}\frac{\Gamma^{V\to l^+l^-}}{M}\frac{\alpha_s^2}{\alpha_{QED}}[F^g(\xi)]^2. \tag{57}$$

Approximating $2\xi\approx\zeta$ we find

$$\left.\frac{d\sigma(\gamma+P\to V+P')}{dt}\right|_{t=0} \approx \frac{16\pi^3}{3}\frac{\Gamma^{V\to l^+l^-}}{M^5}\frac{\alpha_s^2}{\alpha_{QED}}[\xi F^g(\xi)]^2, \tag{58}$$

which agrees with the expression in [91] for the exception that the gluon PDF here gets evaluated at ξ instead of 2ξ. This difference arises because of our replacement of the GPDs by $F^g(x,0,0) = xF^g(x)$. The term $F^g(\xi,\xi,t)$ corresponds to the most asymmetric situation where incoming gluon carries 2ξ momentum and the outgoing gluon carries zero. One may ask: does the GPD at this value probe the PDF at the value of the skewness parameter like we have approximated or does it probe the PDF closer to the Bjorken-x analog ζ? In our forward limit approximation we have taken the former. The result in [91] is then recovered by making the substitution $F^g(\xi,\xi,t)\to 2\xi F^g(2\xi)$.

3.2 Quarks at next-to-leading order

For the full NLO calculation we refer the reader to the literature [25, 97–99] but it is still of interest to us to say a few words especially about the quark part which ends up having a rather important contribution to this process. We will follow closely the notation of [25] and try to give a transparent description of what kind of terms are neglected when the factorization theorem is applied to this process. In NLO the calculational procedure itself stays exactly the same as for LO i.e. we just keep on expanding the interaction Lagrangian and calculate the ever more complex time-ordered products. The challenge comes from the fact that the interaction Lagrangian has to be upgraded now to contain also the gluon self-interactions and the light quark currents as well

$$\begin{aligned} \mathcal{L}_{I,QCD} &= \bar{\psi}_Q^j (i\not{A})_{jk} \psi_Q^k + \mathcal{L}_{I,g} + \bar{\psi}_q^j (i\not{A})_{jk} \psi_q^k, \\ \mathcal{L}_{I,QED} &= \bar{\psi}_Q (i\not{A}_\gamma) \psi_Q + \bar{\psi}_q (i\not{A}_\gamma) \psi_q \end{aligned} \tag{59}$$

where ψ_q now labels the light quark flavors and $\mathcal{L}_{I,g}$ gives the self-interaction terms for the gluons

$$\mathcal{L}_{I,g} = -\frac{g_s}{4} \left(f^{abc} \left\{ \partial_\mu A_\nu^a - \partial_\nu A_\mu^a, A^{\mu,b} A^{\nu,c} \right\} + g_s f^{abc} f^{ade} A_\mu^b A_\nu^c A^{\mu,d} A^{\nu,e} \right), \tag{60}$$

where $\{\cdot\cdot\,,\cdot\cdot\}$ denotes the anti-commutator and f^{abc} are the completely antisymmetric `SU(3)` structure constants. One can clearly see that there will be a myriad of gluon terms spawning for this process, see e.g. Refs. [25, 98] for Feynman diagrams, and working them out by hand is most likely not the best course of action. We will not develope the gluon initiated NLO part any further than this and turn our attention now to the quark-current terms.

The reason why we keep the light and heavy quark currents separate like this is that the quarks which we find inside the proton are assumed to be so light so that we can treat them as being massless. We could also just forget about the light-quark current for the QED Lagrangian since based on the factorization theorem we will eventually neglect such contributions [33] i.e. the photon enters only the hard scattering part of the process. However, this relies on the argument that the scale of the process is big enough so that power counting arguments are valid. If this is not the case, factorization starts to break down and there is no guarantee what the results will be like. We will later demonstrate the strong scale dependence of the amplitude so it is good to keep in mind these possible terms which need to be considered if one starts to investigate possible ways of mitigating the scale dependence.

In any case, we can then expand the S-matrix to higher-order terms in coupling constants e and g_s. We will still neglect terms proportional to $\mathcal{O}(e^2)$ at the amplitude level and we must have one QED coupling present so the terms that we end up

neglecting in QCD coupling constant are $\mathcal{O}(g_s^5)$. This gives us

$$\begin{aligned} S_{fi} = \langle V(K)P(p')|T\Bigg(&\frac{i^4}{4!}\int d^4x\mathcal{L}_I(x)\int d^4y\mathcal{L}_I(y)\int d^4z\mathcal{L}_I(z)\int d^4w\mathcal{L}_I(w) \\ &+ \frac{i^5}{5!}\int d^4x\mathcal{L}_I(x)\int d^4y\mathcal{L}_I(y)\int d^4z\mathcal{L}_I(z)\int d^4w\mathcal{L}_I(w)\int d^4v\mathcal{L}_I(v) \\ &+ \mathcal{O}(e^2, g_s^5)\Bigg)|\gamma(q)P(p)\rangle \end{aligned} \tag{61}$$

for the NLO contribution with only quark current present. The term $\mathcal{O}(\mathcal{L}^4)$ does not contribute here since we cannot leave the gluon fields uncontracted (otherwise factorization theorem does not hold) and there would always be at least one gluon field uncontracted. This is because one of the interaction terms always has to include the QED interaction vertex since otherwise we are unable to have our final state. This means that to a good approximation the NLO quark contribution is given by what is left of

$$\int d^4x\mathcal{L}_I(x)\int d^4y\mathcal{L}_I(y)\int d^4z\mathcal{L}_I(z)\int d^4w\mathcal{L}_I(w)\int d^4v\mathcal{L}_I(v), \tag{62}$$

after sandwiching it between the intial and final states. Note that this product will still produce gluon iniatiated processes i.e. terms which are propotional to the gluon GPD but since we are interested in the quark initiated process we will require that all gluon fields are contracted. Additionally, we require that one of the heavy currents is a QED current, two of the remaining currents are heavy QCD currents and two are light QCD currents. Any other choice would violate the factorization theorem. This being said, there are five ways of choosing the QED interaction term and $3 \cdot 2 = 6$ ways of choosing pair of light flavors multiplied by pair of heavy flavors. After some relabeling of the indices we find the expression

$$\begin{aligned} S_{fi} = \langle V(K)P(p')|T\Bigg(&\frac{i^5}{5!}5\cdot 3\cdot 2\int d^4xd^4yd^4zd^4wd^4v(\bar{\psi}_Q(i\not{A}_\gamma)\psi_Q)_x \\ &\times(\bar{\psi}_Q(i\not{A})\psi_Q)_y(\bar{\psi}_Q(i\not{A})\psi_Q)_z(\bar{\psi}_q(i\not{A})\psi_q)_w(\bar{\psi}_q(i\not{A})\psi_q)_v\Bigg)|\gamma(q)P(p)\rangle. \end{aligned} \tag{63}$$

Comparing this expression to the equivalent LO one given in equation 31 we see that it is essentially the same with the additional two light quark currents. The next step in the process is to express the time ordered product as the sum of the normal ordered products. We must have only one contraction between the light quarks and this can happen in two ways: either $\psi_q(w)$ contracts with $\bar{\psi}_q(v)$ or then $\bar{\psi}_q(w)$ contracts with $\psi_q(v)$ which gives us either a quark propagator or an antiquark propagator.

The gluon fields that accompany the light flavor quarks have to be contracted with the gluon fields with the heavy flavor currents because otherwise we would again produce disconnected graphs. Then assuming that factorization holds in NLO – i.e. as given by equation 9 – we find an expression which is similar to the one in LO

– i.e. equation 34 – but now instead of the gluon fields we have a pair of the light quark fields between the proton states. The quark initiated process can be visualized diagrammatically as shown in Fig. 2 [98].

For the rest of the details of the NLO calculation we refer the reader to the literature on it [25, 97–99] but we should still point out that at NLO one needs to apply the tools of renormalization theory i.e. renormalization of the mass, the quark fields and the strong coupling in addition to the scheme-dependent definitions of the GPDs. After all the dust has settled, the invariant amplitude for this process – with the GPDs taken in the modified minimal-subtraction ($\overline{\text{MS}}$) scheme – can be written as [25]

$$\mathcal{M}_{\text{NLO}}^{\gamma+P\to V+P'} = \frac{4\pi\sqrt{4\pi\alpha_{\text{QED}}}e_Q(\varepsilon_V^*\cdot\varepsilon_\gamma)}{3\pi}\sqrt{\frac{\langle O_1\rangle_V}{m_Q^3}}I(\xi,t). \tag{64}$$

At NLO the integral $I(\xi,t)$, in addition to a more complex gluon channel, receives contributions also from the quark sector,

$$I(\xi,t) = \int_{-1}^{1} dx[F^g(x,\xi,t)T_g(x,\xi) + F^{q,S}(x,\xi,t)T_q(x,\xi)], \tag{65}$$

where we have intentionally suppressed the dependence on the factorization scale μ_F and the renormalization scale μ_R from the hard scattering functions T_i. Here, F^g is the gluon GPD, $F^{q,S}$ is the quark singlet GPD given in terms of the quark GPDs F^q as

$$F^{q,S}(x,\xi,t) = \sum_{q=u,d,s,c} F^q(x,\xi,t). \tag{66}$$

Note that in our framework, we simply add the charm quark in as a massless particle inside the nucleon – justifying this with the fact that we always consider factorization scales above the mass threshold of the charm – but a rigorous treatment of this would require a more indepth analysis of the effects of using different flavour-number schemes [113, 114].

The hard-scattering coefficient functions $T_g(x,\xi)$ and $T_q(x,\xi)$ in equation 65 are given by

$$\begin{aligned} T_g(x,\xi) &= \frac{\xi}{(x-\xi+i\epsilon)(x+\xi-i\epsilon)}\left[\alpha_s(\mu_R) + \frac{\alpha_s^2(\mu_R)}{4\pi}f_g\left(\frac{x-\xi+i\epsilon}{2\xi}\right)\right], \\ T_q(q,\xi) &= \frac{2\alpha_s^2(\mu_R)}{3\pi}f_q\left(\frac{x-\xi+i\epsilon}{2\xi}\right), \end{aligned} \tag{67}$$

where strictly speaking there are two kinds of ϵ's in T_g. The one given as an argument for f_g arises when (in using the dispersion relation technique for solving the amplitude) one continues the Mandelstam s to the complex plane and the ones in the front appear from the gluon field to gluon field strength tensor connection as was given in Eq. 46. For the exact forms of the functions f_g and f_q we will use those

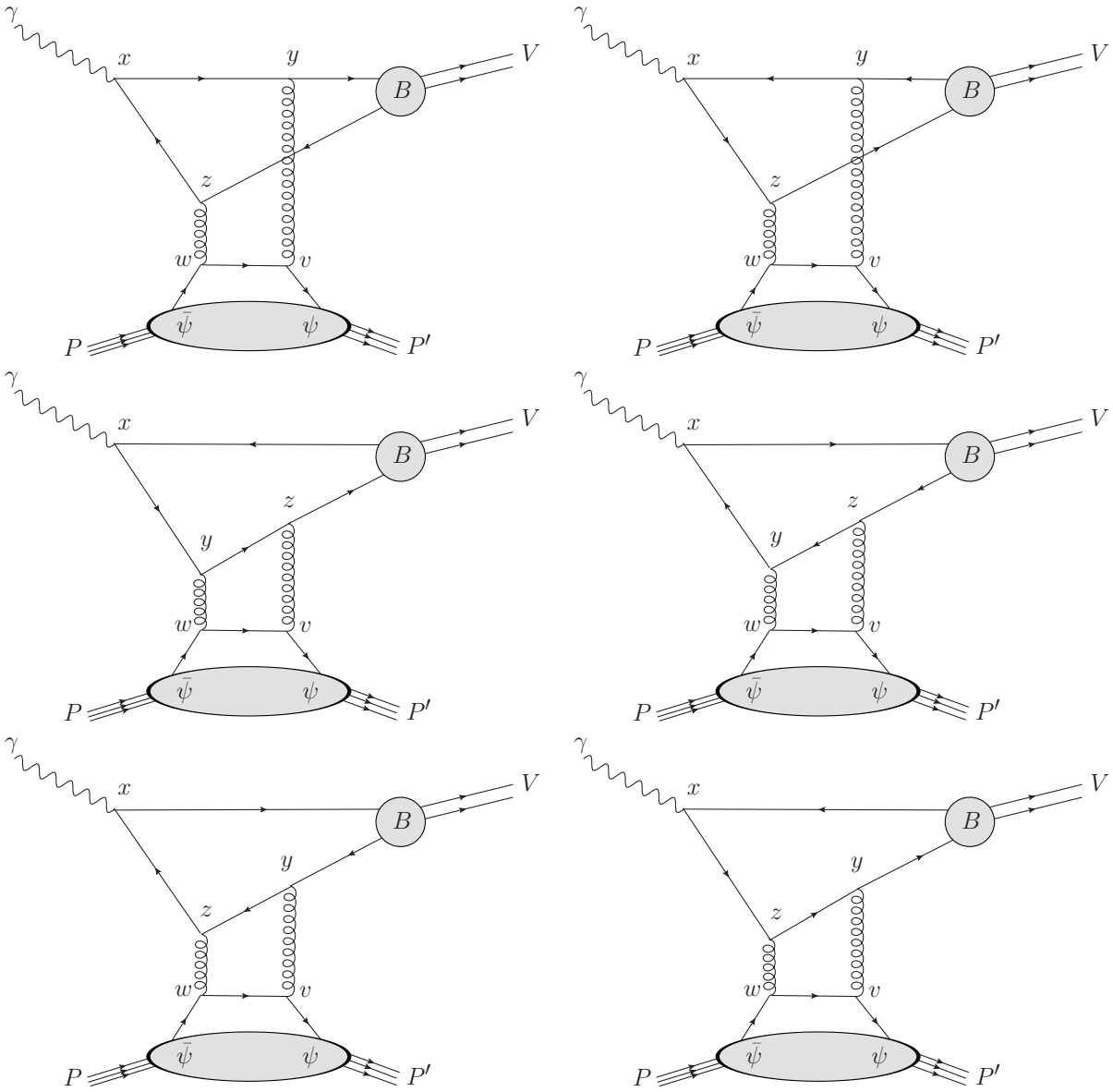

FIGURE 2 Diagrammatical presentations of the six different quark initiated contributions in the NLO calculation of the coherent photoproduction amplitude. The diagrams arise in the same manner as the corresponding LO ones (see equation 32) after applying the Wick's theorem and the factorization theorem to equation 63. The antiquark initiated ones are acquired by flipping the spacetime points w and v.

presented in [25]. The quark contribution is given by

$$\begin{aligned} f_q(z) = &\left(\ln\left(\frac{4m_Q^2}{\mu_F^2}\right)\right)(1+2z)\left(\frac{\ln(-z)}{1+z} - \frac{\ln(1+z)}{z}\right) - \pi^2\frac{13(1+2z)}{48z(1+z)} \\ &+ \frac{2\ln(2)}{1+2z} + \frac{\ln(-z)+\ln(1+z)}{1+2z} + (1+2z)\left(\frac{\ln^2(-z)}{1+z} - \frac{\ln^2(1+z)}{z}\right) \\ &+ \frac{3-4z+16z(1+z)}{4z(1+z)}\mathrm{Li}_2(1+2z) - \frac{7+4z+16z(1+z)}{4z(1+z)}\mathrm{Li}_2(-1-2z), \end{aligned} \tag{68}$$

where $\mathrm{Li}_2(z)$ is the dilogatrithm function and z is to be thought of as a complex number. For the gluon contribution we need to first define a few shorthands, the first of which are the constants c_1 and c_2 as given by

$$c_1 = C_F = \frac{N_c^2-1}{2N_c};\ c_2 = C_F - \frac{C_A}{2} = -\frac{1}{2N_c}, \tag{69}$$

where N_c is the number of colors, C_F is the quadratic Casimir for the fundamental presentation of `SU(N)` and C_A is the quadratic Casimir for the adjoint presentation. Then we also need the QCD beta function

$$\beta_0 = \frac{11N_c}{3} - \frac{2n_f}{3}, \tag{70}$$

where n_f is the number of active light quark flavors, alongside with the auxiliary functions $a_1(z)$ and $a_2(z)$

$$\begin{aligned} a_1(z) = &\frac{c_1}{4}\left(5+16z-\frac{6}{1+z}+\frac{1}{(1+2z)^2}-\frac{5}{1+2z}\right) \\ &-\frac{c_2}{2}\left(2+\frac{3}{z}+8z-\frac{1}{1+z}\right), \\ a_2(z) = &\frac{c_1}{8}\left(12+\frac{9}{z}+64z-\frac{2}{(1+z)^2}+\frac{21}{1+z}-\frac{4}{1+2z}\right) \\ &-\frac{c_2}{4}\left(8+\frac{3}{z^2}+\frac{11}{z}+32z-\frac{2}{(1+z)^2}+\frac{9}{1+z}\right). \end{aligned} \tag{71}$$

With these one can write the gluon contribution as

$$
\begin{aligned}
f_g(z) &= 4(c_1-c_2)(1+2z(1+z))\left(\frac{\ln(-z)}{1+z}-\frac{\ln(1+z)}{z}\right)\left(\ln\left(\frac{4m_Q^2}{\mu_F^2}\right)-1\right)\\
&+\beta_0\ln\left(\frac{\mu_R^2}{\mu_F^2}\right)+4(c_1-c_2)(1+2z(1+z))\left(\frac{\ln^2(-z)}{1+z}-\frac{\ln^2(1+z)}{z}\right)-8c_1\\
&-\pi^2\left(\frac{2+z(1+z)(25+88z(1+z))}{48z^2(1+z)^2}c_1+\frac{10+z(1+z)(7-52z(1+z))}{24z^2(1+z)^2}c_2\right)\\
&-\ln(2)\left(\frac{1+6z(1+z)(1+2z(1+z))}{z(1+z)(1+2z)^2}c_1+\frac{(1+2z)^2}{z(1+z)}c_2\right)\\
&+\pi\frac{\sqrt{-z(1+z)}}{z(1+z)}\left(\frac{7}{2}c_1-3c_2\right)\\
&+2c_2\frac{\sqrt{-z(1+z)}}{z(1+z)}\left(\frac{1+4z}{1+z}\arctan\left(\sqrt{\frac{-z}{1+z}}\right)+\frac{3+4z}{z}\arctan\left(\sqrt{\frac{1+z}{-z}}\right)\right)\\
&-\frac{\arctan^2\left(\sqrt{\frac{-z}{1+z}}\right)}{2z(1+z)}\left((7+4z)c_1-2\frac{1+2z-2z^2}{1+z}c_2\right)\\
&-\frac{\arctan^2\left(\sqrt{\frac{1+z}{-z}}\right)}{2z(1+z)}\left((3-4z)c_1-2\frac{3+6z+2z^2}{z}c_2\right)+2a_1(z)\ln(-z)\\
&+2a_1(-1-z)\ln(1+z)+2a_2(z)\mathrm{Li}_2(1+2z)+2a_2(-1-z)\mathrm{Li}_2(-1-2z).
\end{aligned}
\tag{72}
$$

Note that for $f_g(z)$ the input variable z is to be thought of as a complex number just like for f_q. Given these definitions we should still point out that the full NLO expressions, as given in equation 67, obey the symmetry properties $T_g(x,\xi) = T_g(-x,\xi)$ and $T_q(x,\xi) = -T_q(-x,\xi)$ which will be helpful when we implement the results numerically.

In addition to the more complex hard scattering function, in NLO the NRQCD element receives higher order contributions [25, 34, 109, 115]

$$
\Gamma^{V\to l^+l^-} = \frac{2e_Q^2\pi\alpha_{\mathrm{QED}}^2}{3}\frac{\langle O_1\rangle_V}{m_Q^2}\left[1-\frac{3\alpha_s(\mu_R)}{3\pi}\right]^2. \tag{73}
$$

We point out that the pQCD expansion of the decay width is somewhat questionable as the NNLO correction is actually larger than the NLO one [115] but as we are working in the NLO accuracy we are satisfied with the above equation. The squaring of the NLO amplitude proceeds exactly as in the LO case with the exception that the NLO integral $I(\xi,t)$ is now considerably more complicated. This has also the effect that the Cauchy principal value prescription, as shown in Eq. 56, for the integral becomes difficult to handle.

4 UPCs IN NUCLEUS-NUCLEUS COLLISIONS

Next, we would like to apply the results of the previous section to the scattering process which we set out to study, i.e., the case of nucleus-nucleus collisions $A_1 + A_2 \to A_1 + V + A_2$ where A_1 and A_2 denote some colliding nuclei and V is a produced heavy vector meson. For example in [PI] we were interested in colliding lead nuclei producing a J/ψ in the final state and it is the presentation therein which we will follow closely here. Since in the final state we observe only the heavy vector meson, it is very likely that the process was initiated by a quasi-real photon and that the collision of the two nuclei was ultraperipheral. In particular we are considering unpolarized beams, assume no spatial dependence of the partons inside the bound nucleons and require that there are no hadron-hadron interactions [116–118].

4.1 Cross sections

We still need a few last ingredients – the photon flux, the form factor and an expression for the photoproduction cross section – in order to put everything together and start making predictions. In regards to the photon flux, the framework which we will be working in is called the equivalent-photon approximation (EPA) (also known as Weizsäcker-Williams approximation [119, 120]) where the total cross section for the process $\sigma^{A_1A_2\to A_1VA_2}$ is expressed as the following sum of two convolutions [116, 121, 122],

$$\begin{aligned}\sigma^{A_1A_2\to A_1VA_2} = &\int dk^- \frac{dN_\gamma^{A_2}(k^-)}{dk^-}\sigma^{A_1\gamma(k^-)\to A_1V} \\ &+ \int dk^+ \frac{dN_\gamma^{A_1}(k^+)}{dk^+}\sigma^{\gamma(k^+)A_2\to VA_2},\end{aligned} \tag{74}$$

where $\sigma^{A_1\gamma\to A_1V}$ and $\sigma^{\gamma A_2\to VA_2}$ are the photoproduction cross sections – which we sketched in LO in chapter 3 – and $dN_\gamma^{A_i}(k^\pm)/dk^\pm$ are the impact-parameter integrated photon fluxes. One should note how this way of writing the cross section is another example of factorization in the sense that we say that the full process can

be divided into two parts: first the photon gets emitted from a nucleus and then it collides with the target. The full result is then the product of these two integrated over all possible values of energy. In this way we also neglect any interference between the amplitudes where the photons are emitted by different nuclei which is an important effect at smallest values of t but has negligible effect on the t-integrated cross sections [123, 124].

The photon momentum in EPA is taken collinear with the colliding nuclei such that the energies $k^{\pm}$ are given by $k^{\pm} = |\vec{k}_{1,2}|$ i.e. k^{+} is the energy in the plus direction as defined by the direction of A_1 and k^{-} is the energy in the minus direction as defined by the direction of A_2. Since we are interested in the process in which $p_T^2 \ll M_V^2$ – i.e. the meson gets produced essentially parallel to the incoming photon – we can express the photon momentum in terms of kinematical variables of the process by setting everything collinear along the z-axis and expanding the Mandelstam variable t as

$$t = (k - p_V)^2 = -2k \cdot p_V + M_V^2 = -2M_V k^{\pm}(\cosh y \mp \sinh y) + M_V^2, \tag{75}$$

where k is the photon momentum, p_V is the heavy-vector meson momentum, M_V is the mass of the meson and y is the rapidity of the meson. We are interested in the case where $|t| \ll M_V^2$ (see [125] for a physical justification) so that we can shuffle the above expression to find

$$2k^{\pm} \approx M_V e^{\pm y}. \tag{76}$$

The experimental data available for nucleus-nucleus collisions from the large hadron collider (LHC) [126–129] are given for rapidity differential cross sections so we still need to differentiate the total cross section with respect to the vector meson rapidity y. Since we know how the photon energy and the rapidity are related, i.e. equation 76, we can simply use chain rule to write

$$\begin{aligned}\frac{d\sigma^{A_1A_2\to A_1VA_2}}{dy} = &\left[k\frac{dN_\gamma^{A_2}(k)}{dk}\sigma^{A_1\gamma(k)\to A_1V}\right]_{k=k^-} \\ &+ \left[k\frac{dN_\gamma^{A_2}(k)}{dk}\sigma^{A_1\gamma(k)\to A_1V}\right]_{k=k^+},\end{aligned} \tag{77}$$

for the rapidity-differential cross section.

4.1.1 Form factor and the photon flux

We assume that the invariant scattering amplitude $\mathcal{M}^{\gamma A\to VA}$ can be factored into the product of $\mathcal{M}$ being evaluated at $t = 0$ and multiplied by a nuclear form factor $F_A(t)$ (also known as the two-gluon form factor [91]) which in the case of photon-nucleus collisions gives [130]

$$\mathcal{M}^{\gamma A\to VA}(t, W) = F_A(t)\mathcal{M}_A^{\gamma N\to VN}(0, W), \tag{78}$$

where W is the center of mass (c.m.s.) energy for the photon-nucleon collision and N indicates the per-nucleon amplitude in the nucleus A. We can then write the

photoproduction cross section as an integral over t – where t is always negative and we integrate from minus infinity to some non-zero small value – of the t-differetial cross section such that

$$\begin{aligned} \sigma^{\gamma A\to VA}(W) &= \left.\frac{d\sigma_A^{\gamma N\to VN}}{dt}\right|_{t=0} \int\limits_{t_{\min}}^{\infty} dt' |F_A(-t')|^2, \\ \frac{d\sigma_A^{\gamma N\to VN}}{dt} &= \frac{\overline{|\mathcal{M}_A^{\gamma N\to VN}(t,W)|^2}}{16\pi W^4}, \end{aligned} \tag{79}$$

after flipping the integration limits and doing the change of variables $t = -t'$. Note that the square of the invariant amplitude $\mathcal{M}_A^{\gamma N\to VN}$ has been first squared and then averaged (summed) over the initial-state (final-state) spins. For the minimum value of t we can derive that [131]

$$t_{\min} \approx \left(\frac{M_V^2}{4k\gamma_L}\right)^2, \tag{80}$$

which is acquired by keeping the incoming hadron mass non-zero, expanding to terms up to $\mathcal{O}(s^{-4})$ and disregarding higher terms. In the above γ_L is the Lorentz factor – i.e. giving the nucleon energy E_N in terms of the nucleon mass m_N as $E_N = \gamma_L m_N$ – which e.g. in the center of mass frame for LHC Run1 energy of $\sqrt{s_{NN}} = 2.76$ TeV is approximately 1500.

At any given fixed W, equation 78 does not seem that shocking but if we let both t and W vary then *ab initio* there is no guarantee that this type of a factorization would work. This then raises the question of how to model the form factor $F_A(t)$? For the case of the photon colliding with a free proton we simply replace the the square of the form factor with an experimentally determined exponential factor – i.e. $|F_A(-t')|^2 = e^{-bt'}$ in which case it is also typical to set $t_{min} = 0$ – which seems to work rather reasonably with the available experimental data [132]. Sometimes the slope parameter is taken to be constant, like in [25], but we apply the following parametrization [98, 133],

$$b\ \text{GeV}^2 = b_{0,V} + 4\alpha'_P \ln\left(\frac{W}{W_0}\right), \tag{81}$$

where $b_{0,V} = 4.63$ for $V = J/\psi$, $b_{0,V} = 4.9$ for $V = \Upsilon$, $\alpha'_P = 0.06$ and $W_0 = 90$ GeV. Then how about the case of a bound nucleon?

What the form factor should tell us is, roughly speaking, how momentum is distributed – and by this token how it is transferred in the scattering process – within the colliding nucleus. Our approach is the same as what has been in the literature [134–136] where the form factor is described by a Fourier transform of the underlying nuclear density distribution $\rho_A(r)$,

$$F_A(t) = \int d^3r \rho_A(r) e^{i\vec{q}\cdot\vec{r}}, \tag{82}$$

where $|\vec{q}| = \sqrt{|t|}$. This then changes the question to: how do we know the underlying nuclear density distribution? Well, strictly speaking we do not know this either but

a good approximation can be thought to be given by the charge density distribution which historically has been measured from elastic electron-nucleus scatterings. There exists a wide variety of different density distributions – e.g. Harmonic-oscillator, Fourier-Bessel expansion, two-parameter Fermi (2pF), three-parameter Fermi (3pF), three-parameter Gaussian etc – which have been fitted to the data for a wide variety of different nuclei [137, 138]. In the context of this thesis we are mainly interested in initial states where we have only lead or only oxygen nuclei colliding with each other i.e. Pb+Pb or O+O collisions. For lead the distribution is 2pF (also know as Woods-Saxon distribution [139]) and for oxygen the distribution is 3pF:

$$\rho_{\mathrm{A}}(r,d,R_A) = \frac{\rho_0}{1+e^{\frac{r-R_A}{d}}}; \qquad \rho_{\mathrm{A}}(r,d,R_A,w) = \frac{\rho_0\left(1+w\left(\frac{r}{R_A}\right)^2\right)}{1+e^{\frac{r-R_A}{d}}} \tag{83}$$

where d is the skin-depth parameter, R_A is the radius of the nucleus and w (sometimes called the wine-bottle parameter [137]) is the one additional parameter introduced when changing from 2pF to 3pF. All these parameter values can be checked from the literature [137, 138] but the radius R_A we will model with

$$R_A/\mathrm{fm} = 1.12\cdot A^{1/3} - 0.86\cdot A^{-1/3}, \tag{84}$$

as can be derived from the 2pF-distribution with the choices $\rho_0 = 0.17$ fm^{-3} and $d = 0.54$ fm [140].

For the photon flux kdN/dk for a nucleus with mass number A and an atomic number Z we need two ingredients: number of equivalent photons of energy k at some transverse distance $b = |\vec{b}|$, i.e. $N_\gamma^A(k,\vec{b})$, and a factor ensuring that no hadronic interaction takes place, which we denote by $\Gamma_{AA}(\vec{b})$. The former we will calculate from [116, 141–143]

$$N_\gamma^A(k,\vec{b}) = \frac{Z^2\alpha_{QED}}{\pi^2}\left|\int_0^\infty dl_\perp J_1(bl_\perp)\frac{l_\perp^2 F(l_\perp^2+k^2/\gamma_L^2)}{l_\perp^2+k^2/\gamma_L^2}\right|^2, \tag{85}$$

where J_1 is the modified cylindrical Bessel function of the first kind, γ_L is the Lorentz gamma factor and F is the form factor but now normalized to one i.e. $F(t) = F_A(t)/A$. We can model the hadronic interactions with a Poisson distribution f – i.e. a Glauber-type probability [144] – in which case the factor Γ will correspond to the case of $n = 0$ hadronic interactions

$$f(n;\bar{n}_{NN}(\vec{b})) = \frac{\bar{n}_{NN}(\vec{b})^n}{n!}e^{-\bar{n}_{NN}(b)} \Rightarrow \Gamma_{AA}(\vec{b}) = f(0;\bar{n}_{NN}(\vec{b})) = e^{-\bar{n}_{NN}(b)}, \tag{86}$$

where the average number of nucleon-nucleon collisions $\bar{n}_{NN}(\vec{b})$ is given as a product of the total nucleon-nucleon cross section $\sigma_{NN}(s)$ and the overlap function $T_{AA}(\vec{b})$,

$$\bar{n}_{NN}(\vec{b}) = \sigma_{NN}(s)T_{AA}(\vec{b}) = \sigma_{NN}(s)\int d^2b_1 T_A(\vec{b})T_A(\vec{b}-\vec{b}_1), \tag{87}$$

where T_A in turn is known as the nuclear optical density and it is given by the integral of the underlying nucleon density distribution,

$$T_A(\vec{b}) = \int_{-\infty}^{\infty} dz\rho_A(\sqrt{z^2+\vec{b}^2}). \tag{88}$$

For the energy dependence of the total nucleon-nucleon cross section we use the PDG parametrization [145]

$$\sigma_{NN}(s) = H \log\left(\frac{s}{s_M^{ab}}\right) + P^{ab} + R_1^{ab}\left(\frac{s}{s_M^{ab}}\right)^{-\eta_1} - R_2^{ab}\left(\frac{s}{s_M^{ab}}\right)^{-\eta_2}, \tag{89}$$

where $s_M^{ab} = (2m_p + M)^2$, m_p being the mass of the proton, and the other parameter values are given by

$$\begin{aligned} &M = 2.1206 \text{ GeV}; H = 0.272 \text{ mb}; \; P^{ab} = 34.41 \text{ mb} \\ &R_1^{ab} = 13.08 \text{ mb}; \; R_2^{ab} = 7.394 \text{ mb}; \; \eta_1 = 0.4473; \; \eta_2 = 0.5486. \end{aligned} \tag{90}$$

Putting these terms together the photon flux can then be calculated from

$$k\frac{dN_\gamma^A(k)}{dk} = \int d^2\vec{b} N_\gamma^A(k,\vec{b})\Gamma_{AA}(\vec{b}). \tag{91}$$

Because the impact-parameter dependent flux contains the Bessel function, the integrand of equation 91 oscillates at large values of b which makes the numerical evaluation of the flux challenging. The way to mitigate this problem is to take advantage of the fact that at large enough distances anything looks like a point like particle. That is, we take the impact-parameter dependent flux for a point-like (pl) particle [119, 146]

$$N_{\gamma/Z}^{\text{pl}}(k,\vec{b}) = \frac{Z^2\alpha_{\text{QED}}}{\pi^2}\frac{k^2}{\gamma_L^2}\left(K_1^2(\zeta_R) + \frac{1}{\gamma_L^2}K_0^2(\zeta_R)\right), \tag{92}$$

where K_0 and K_1 are modified Bessel functions of the second kind and the ζ_R parameter is given by

$$\zeta_R = \frac{kb}{\gamma_L}. \tag{93}$$

The trick is then to divide the integration region in equation 91 into two parts: first in the range $[0, b_{\text{min}}]$ and the second in $[b_{\text{min}}, \infty]$. The first part we can do numerically quite fast but the latter part is more challenging. To this end we will add and subtract the transverse distance dependent flux for a point-like particle inside the integral going from b_{min} to ∞, since we know that $N_\gamma^A(k,\vec{b})\Gamma_{AA}(\vec{b})$ and $N_{\gamma/Z}^{\text{pl}}(k,\vec{b})$ end up cancelling to a large extent at large values of b. The question then is: what is large enough b? By taking b to be slightly greater than the sum of the nuclear radii seems already to be sufficient but we have chosen $b_{\text{min}} = 30$ fm both for the lead and the oxygen to be extra conservative. With this method, we are still left with an integral from b_{min} to infinity over $N_{\gamma/Z}^{\text{pl}}(k,\vec{b})$ but that result is well known in the literature [147],

$$\begin{aligned} k\frac{N_{\gamma/Z}^{\text{pl}}(k)}{dk}\bigg|_{b_{\text{min}}} &= \int_{b_{\text{min}}}^{\infty} d^2\vec{b}\; N_{\gamma/Z}^{\text{pl}}(k,\vec{b}) \\ &= \frac{2Z^2\alpha_{QED}}{\pi}\left[\zeta_R K_0(\zeta_R)K_1(\zeta_R) - \frac{\zeta_R^2}{2}(K_1^2(\zeta_R) - K_0^2(\zeta_R))\right]_{b=b_{\text{min}}}. \end{aligned} \tag{94}$$

Putting all this together means that the photon flux from a nucleus is calculated as

$$
\begin{aligned}
k\frac{dN_\gamma^A(k)}{dk} &= \int_0^{b_{\min}} d^2\vec{b} N_\gamma^A(k,\vec{b})\Gamma_{AA}(\vec{b}) \\
&+ \int_{b_{\min}}^{\infty} d^2\vec{b}\left[N_\gamma^A(k,\vec{b})\Gamma_{AA}(\vec{b}) - N_{\gamma/Z}^{\mathrm{pl}}(k,\vec{b}) + N_{\gamma/Z}^{\mathrm{pl}}(k,\vec{b})\right] \\
&= k\frac{N_{\gamma/Z}^{\mathrm{pl}}(k)}{dk}\bigg|_{b_{\min}} + \int_0^{b_{\min}} d^2\vec{b} N_\gamma^A(k,\vec{b})\Gamma_{AA}(\vec{b}) \\
&+ \int_{b_{\min}}^{\infty} d^2\vec{b}\left[N_\gamma^A(k,\vec{b})\Gamma_{AA}(\vec{b}) - N_{\gamma/Z}^{\mathrm{pl}}(k,\vec{b})\right] \\
&\approx k\frac{N_{\gamma/Z}^{\mathrm{pl}}(k)}{dk}\bigg|_{b_{\min}} + \int_0^{b_{\min}} d^2\vec{b} N_\gamma^A(k,\vec{b})\Gamma_{AA}(\vec{b}).
\end{aligned}
\tag{95}
$$

We should point out that the factor Γ essentially forces the values of the integral on the last line in equation 95 to be zero in the range $[0, R_1 + R_2]$ where R_i are the radii of the colliding nuclei. For this reason the point-like approximation is a rather good approximation for UPCs and the interested reader may see [116, 148, 149] for studies on the differences between this method and the point-like approximation.

4.2 Numerical implementation

In the numerical implementation of the presented results, the most difficult part is the implementation of the integral $I(\xi, t = 0)$ as given in equation 65. To do this, one might proceed as in [98] by carefully taking the analytical limits as $\epsilon \to 0$ and then write the code to match the analytical expression. Another way of doing this is to simply have the complex integrals as they are given in equation 65 with a finite ϵ present in the code. This finite-epsilon method is the way the results of this thesis have been obtained.

Nothing out of the ordinary happens when one does complex integrals numerically since any complex function $f(z)$ can always be written as

$$
f(z) = u(z) + iv(z), \tag{96}
$$

where $u(z) = \mathrm{Re}(f(z))$ and $v(z) = \mathrm{Im}(f(z))$ are real valued functions. This means that any integral of the function $f(z)$ can be written as

$$
\int dz\, f(z) = \int dz\, u(z) + i\int dz\, v(z). \tag{97}
$$

The implementation of this is done in C++ with the help of the standard libraries such as `<cmath>` and `<complex>`, the GSL - GNU scientific library [150] and the

LHAPDF6 library [151]. The question then arises: at what values of ϵ can we start to trust our results?

If we take a large ϵ, we should not be surprised if our results are not valid. In the leading-order calculation we know that the final result is essentially determined by the value of the gluon distribution at $x = \xi$. This motivates us to make the educated guess that we should somehow tie the value of ϵ to ξ. The full integral can be thought to comprise of the LO gluon, the NLO gluon and the NLO quark contributions. Out of the three the LO one is naturally numerically the most stable one. For all of the integrals we use the symmetry properties, as described in previous chapters, of the hard-scattering functions T_g and T_q and of the GPDs $F^g(x,\xi,t)$ and $F^q(x,\xi,t)$ to write the full integral as

$$I(\xi,t) = \int_0^1 dx \left[2F^g(x,\xi,t)T_g(x,\xi) + T_q(x,\xi)\left(F^{q,S}(x,\xi,t) - F^{q,S}(-x,\xi,t)\right)\right]. \tag{98}$$

The numerical NLO quark integral has a particularly poor convergence close to $x \to 0$ due to the fact that the amplitude is proportional to the fastly diverging $q(x) + \bar{q}(x)$. This means that for the NLO quark contribution we have to go to smaller values of ϵ than for the NLO gluon contribution when the integration routine approaches the lower end of the $[0,1]$ interval. But on the other hand we cannot decrease ϵ too small either because of numerical limitations and the fact that at some point we will start to see numerical noise in our results. Additionally, the expressions for $f_q(z)$ and $f_g(z)$, as given in equations 68 and 72, respectively, multiplied by the appropriate PDFs do not converge individually term by term. For example one cannot blindly take from $f_g(z)$ a term proportional to x^{-4}, multiply it by $xg(x)$ and expect the result to converge on the interval $[0,1]$. All this is to say that the hard scattering functions have a delicate structure in which divergences cancel each other when multiplied by the PDFs and integrated over $[0,1]$.

The choice of exact values of ϵ is decided by testing the numerical stability of the results and we have checked that the results converge towards a specific value over few orders of magnitude in ϵ. Eventually, the exact choices were $\epsilon = \xi \cdot 10^{-8}$ for the LO gluon and the NLO quark and $\epsilon = \xi \cdot 10^{-5}$ for the NLO gluon. We have cross checked these finite ϵ results against the analytically continued ones as given in [98] and they are the same up to the numerical integration accuracy of one permille. This gives us confidence to think that the finite epsilon method is a useful way to evaluate numerically QFT expressions in the complex s-plane.

In addition to the hard scattering amplitude we need to implement numerically the photon flux and the form factor calculations. The latter is simple enough through the expressions given in the previous section but the photon flux requires slightly more attention as explained in the previous section. In addition to coding the required analytical expressions, the numerical implementation was done with the help of the integration routines as provided by the GSL - GNU scientific library [150]. The photon flux calculation ended up being one of the more computationally heavy ones so to streamline the full nucleon-nucleon calculation we created a look-up table for the photon flux values as a function of the rapidity and called these values from

a file in the main production code. The main production code then simply tied everything together to produce the final result.

5 RESULTS AND DISCUSSION

One of the early motivations for studying the coherent exclusive photoproduction of vector mesons was to find a new class of processes which could be used to experimentally constrain the low-x behaviour of the gluon PDFs as originally proposed in [91]. The extension of this to the nuclear case was one of the main motivations behind our work as well. The previous chapters summarized the theoretical background – connection between the PDFs, GPDs and their nuclear counterparts and the pQCD calculation of the photoproduction process – and the necessary modeling – implementation of the form factor and of the photon fluxes – before we could start to investigate this possibility. In any case, the framework produced a lot of interesting results, as reported in the papers [PI, PII, PIII], even if we cannot yet claim definitely how useful this process will be in constraining the gluon PDFs. In this chapter we will present a short summary of the main results of this work with some additional analysis which was left out of the original papers.

5.1 Exclusive photoproduction of J/ψ

The first results which we obtained with our framework were reported in [PI]. Out of these results the most surprising one was the clear dominance of the quark channel in the rapidity-differential cross section at central rapidity as shown in Fig. 3. In the figure we see the decomposition of the cross section to only quarks (dotted green), only gluons (dashed red) and their interference (dashdotted red) at the Run2 energy of $\sqrt{s_{NN}} = 5.02$ TeV computed with the EPPS16 nPDF set at the corresponding "optimal" scale of $\mu = \mu_R = \mu_F = 2.37$ GeV. The optimal scale is the best rough fit to the available Run1 and Run2 LHC data and it should be emphasized that there is nothing special about the optimal scale per se. Nevertheless the factor of four difference in the magnitude at central rapidity between the quark and gluon channels was something unexpected.

This big difference can be traced to originate from the fact that the LO and the NLO contributions have opposite signs, i.e., the LO amplitude is negative and

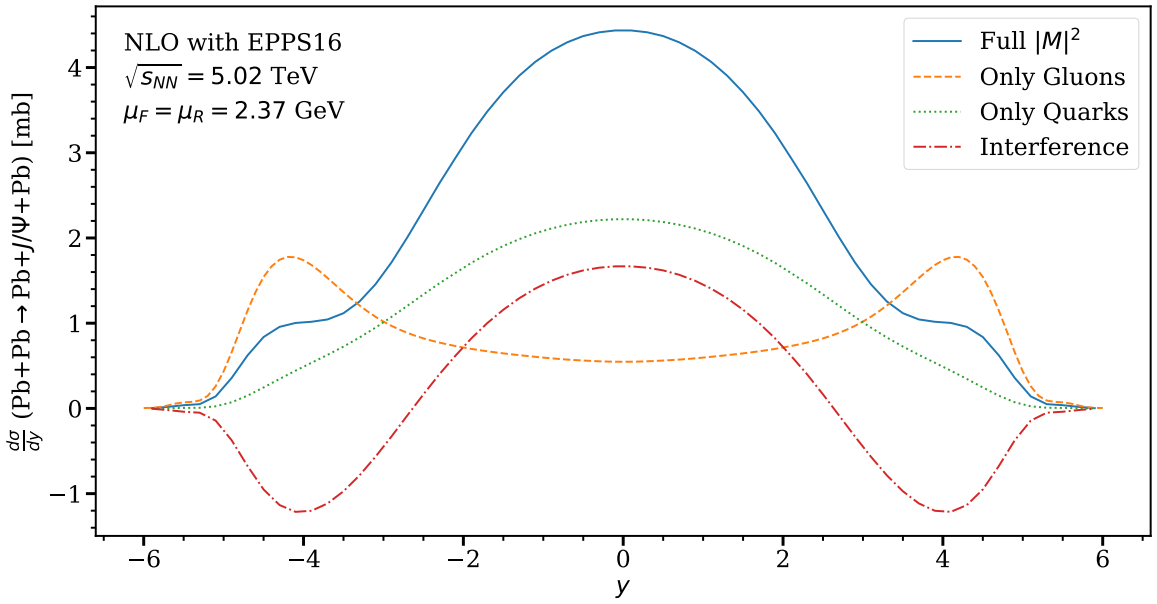

FIGURE 3 The breakdown to only gluons (dashed orange), only quarks (dotted green) and their interference (dashdotted red) of the full result (solid blue) of rapidity-differential cross section of coherent exclusive J/ψ photoproduction in Pb+Pb UPCs. The calculation was done with the scale choice $\mu_R = \mu_F = 2.37$ GeV at the Run2 c.m.s. energy of 5.02 TeV. Figure from [PI].

the NLO contributions to the amplitude are positive. When one then sums together the LO and the NLO contributions to get the gluon channel the value ends up being less than that of the quark channel alone. Interestingly this behaviour holds true for all scale values of μ in the range $[m_c, M_{J/\psi}]$. This then casts some shadows of doubt as to how useful the process will be in determining the low x behaviour of the gluon PDFs.

However, we see that at forward and backward rapidities, in the so called shoulder region of $y \approx \pm 4$, the gluon channel dominates the differential cross section with a similar factor of about 4. So even if the cross section at central rapidity cannot be used to constrain the gluon PDF, maybe the shoulder regions might offer us a handle here. One should also not underestimate the significance of the interference term whose absolute magnitude is greater than that of the gluon in the central rapidity and greater than that of the quarks at backward and forward rapidities. This, in addition to the significant scale dependence of the results as discussed in [PI] (Figs. 1, 2 and 3 and the discussion around them), means that it remains to be seen how useful this process will be in constraining the gluon PDFs.

The quark dominance at central rapidity does not mean that much in itself unless one takes into account the theoretical uncertainties of the calculation. If we disregard all uncertainties related to the scale dependence, or the modeling of the GPDs, form factors and photon fluxes and take our optimal scale prediction to be spot on, what is the size of the PDF related uncertainties? This is shown in figure 4 with the EPPS16 [73] (solid blue) and nCTEQ15 [72] (dashed red) PDF sets for Run1

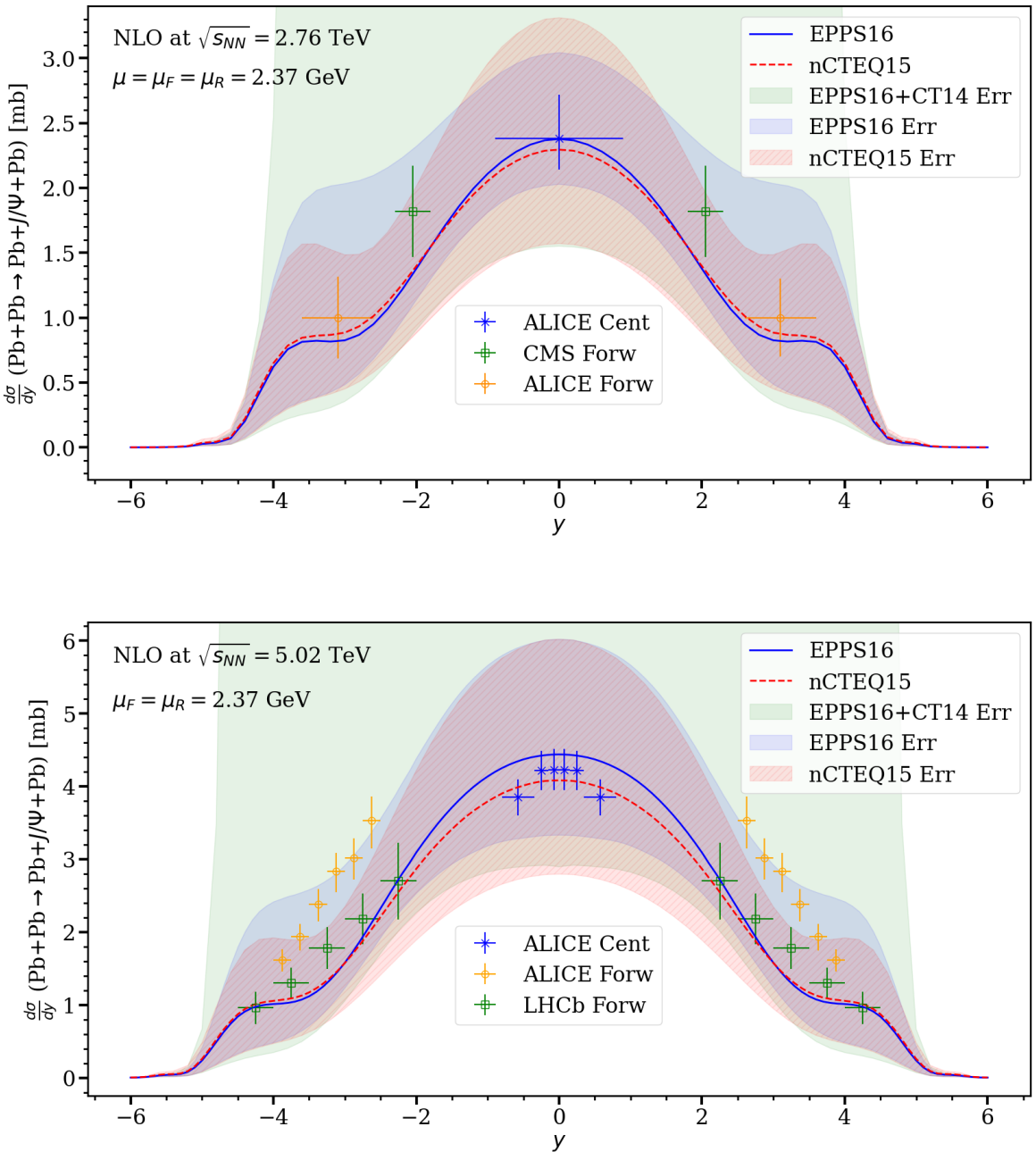

FIGURE 4 The nPDF/PDF uncertainties in the rapidity-differential exclusive J/ψ photoproduction NLO cross sections at the c.m.s. energy of 2.76 TeV (upper panel) and at 5.02 TeV (lower panel) Pb+Pb UPCs, computed at our "optimal" scale $\mu = 2.37$ GeV using the EPPS16+CT14NLO [73, 152] and nCTEQ15 [72] error sets and compared to the Run1 data [128, 153, 154] and Run2 data [126, 127, 129]. The solid (dashed) line shows the EPPS16+CT14NLO (nCTEQ15) central-set results and the corresponding uncertainty bands are explained in the text. Figure from [PI].

and Run2 energies. The uncertainties have been calculated using the asymmetrical EPPS16 convention [73],

$$\delta\mathcal{O}^{\pm} = \sqrt{\sum_i \left[\begin{matrix}\max\\ \min\end{matrix}\{\mathcal{O}(S_i^+) - \mathcal{O}(S_0), \mathcal{O}(S_i^-) - \mathcal{O}(S_0), 0\}\right]^2}, \tag{99}$$

where S_0 is the central PDF set and $S_i^{\pm}$ labels the error PDF sets. The EPPS16 related nuclear uncertainties are shown by the blue band, the CT14NLO [152] related free proton uncertainties with the green band and the nCTEQ15 nuclear uncertainties with the hashed red band. One should note that unlike the EPPS16 error set parametrization, the nCTEQ15 error sets contain only the uncertainties arising from nuclear modeling.

The nuclear uncertainties for these two sets are in the range of twenty to fifty percent at mid-rapidity, increasing slightly upwards when moving to backward and forward rapidities. Interestingly, the free-proton uncertainties originating from the CT14NLO set are orders of magnitude bigger than the nuclear uncertainties but mostly through one single error set which in the EPPS16 error parametrization is the "Set93". This error set grows much faster at small values of x than the rest of the sets and it ends up contributing sizeably to the real part of the LO gluon amplitude [PI]. One should therefore always keep in mind the free proton uncertainties even if considering only nuclear prosesses.

Our results also confirmed the strong scale dependence of the studied J/ψ process as pointed out already in [25]. For us the dependence was quantified by considering the ratio of the results at $\mu = M_{J/\psi}$ and at $\mu = M_{J/\psi}/2$ which at central rapidity for the full NLO result for the rapidity differential cross section was a factor of 50 for EPPS16 (see Fig. 3 in [PI]). This dependence gets slitgthly weaker as one moves away from the central rapidity to backward and forward rapidities both in LO and NLO (see Fig. 4 in [PI]). Furthermore, at LO we found that the cross section is dominated by the imaginary part of the amplitude but that at NLO the situation changes so that at backward and forward rapidities the real part actually dominates the cross section and that at central rapidity it has a non-negligible effect (see Fig. 6 in [PI]). Finally, we also studied the effect of turning on and off the nuclear corrections on the underlying gluon and quark PDFs and found that at central rapidity the effect of the nuclear corrections is not as quadratic as thought before; see Figs. 7, 8 and 9, and the surrounding discussion in [PI], for further details.

The results of paper [PI] were obtained just before the publication of the new, state-of-the-art nPDF sets EPPS21 [76] and nNNPDF3.0 [77] so as one of the first tasks for the second paper [PII], we updated the results for the Pb+Pb collisions with the EPPS21, nNNPDF3.0 and the corresponding state-of-the-art nCTEQ15WZSIH [155] nPDF set from the CTEQ collaboration. The strong scale dependence of the results did not disappear, as was expected, but what was rather surprising was that the nCTEQ15WZSIH set, with the enhanced strangeness quark distribution, was able to better describe simultaneously the central rapidity and the forward/backward rapidity data both at Run1 and Run2 energies.

These updated results are shown in figure 5 for the c.m.s. energies of 2.76 TeV (upper panel) and 5.02 TeV (lower panel) at the optimal scales $\mu = 2.39$ GeV

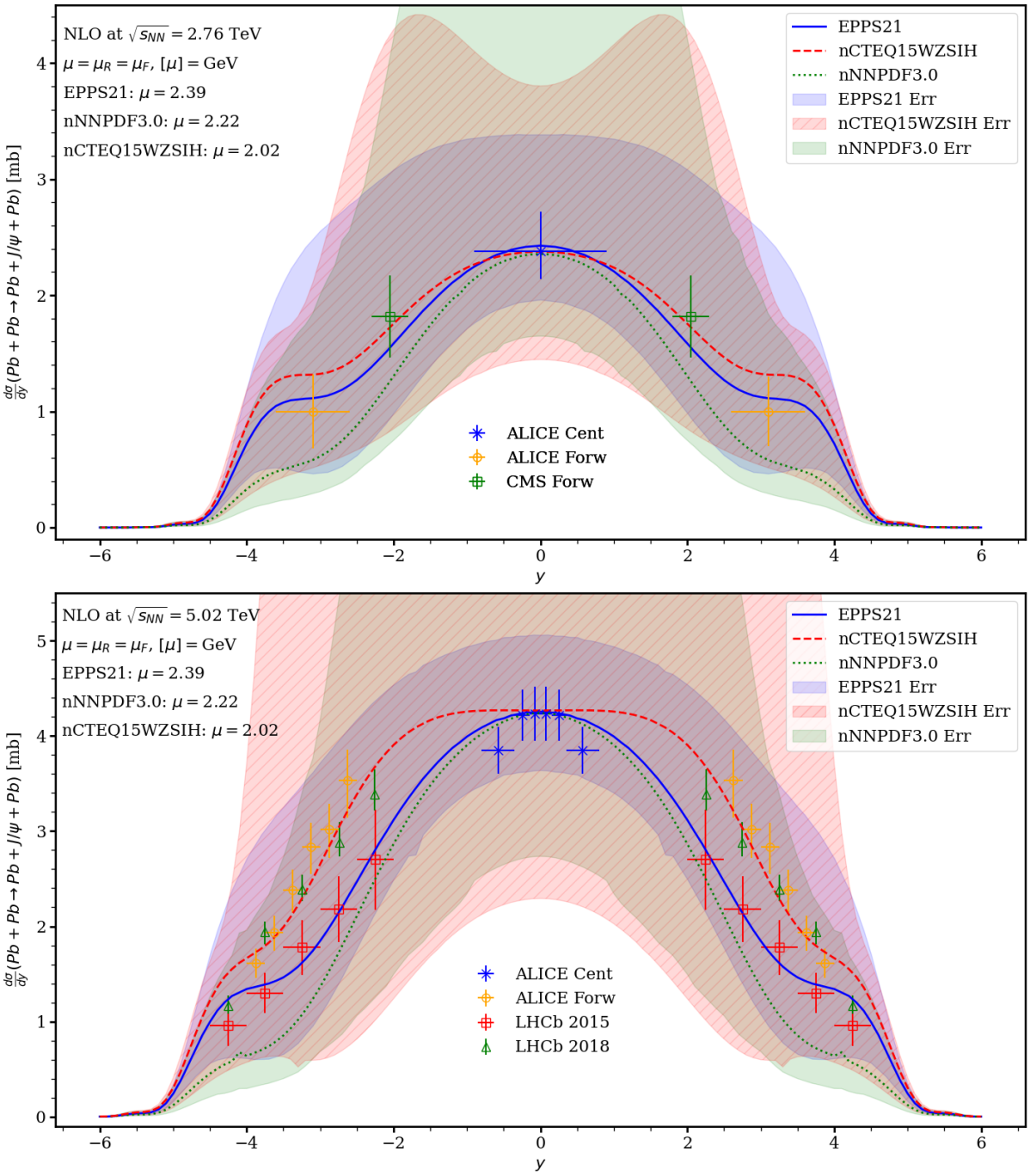

FIGURE 5 The nPDF/PDF uncertainties of the rapidity-differential exclusive J/ψ photoproduction NLO cross sections at the $\sqrt{s_{NN}}$ energies of 2.76 TeV (upper panel) and 5.02 TeV (lower panel) for Pb+Pb UPCs with three different nPDF sets EPPS21 [76] (solid blue), nNNPDF3.0 [77] (dotted green) and nCTEQ15WZSIH [155] (dashed red) at their optimal scales $\mu = 2.39$ GeV, 2.22 GeV and 2.02 GeV, respectively. The error bands are explained in the text and the experimental data points are as in figure 4. Figure from [PII].

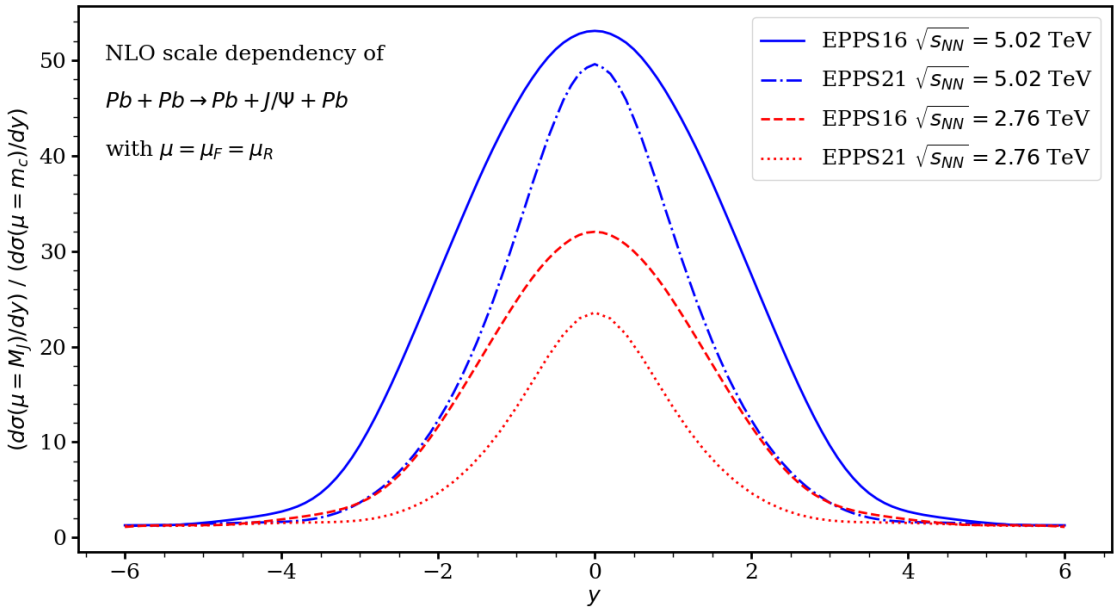

FIGURE 6 The EPPS16 [73] and EPPS21 [76] scale dependencies of the rapidity-differential exclusive J/ψ photoproduction NLO cross sections at the c.m.s. energies of 5.02 TeV (blue) and at 2.76 TeV (red) for Pb+Pb UPCs.

(EPPS21), 2.22 GeV (nNNPDF3.0) and 2.02 GeV (nCTEQ15WZSIH) which, again, carry no special meaning other than that they give the best possible rough fit to the Run1 and Run2 rapidity differential cross section data for each set at $y = 0$. The EPPS21 and nCTEQ15WZSIH uncertainties are calculated using the asymmetrical EPPS21 convention [76] and for the nNNPDF3.0 we used the 90% CL prescription [77]. We see that the full EPPS21 uncertainties are much better constrained than the corresponding EPPS16 uncertainties because EPPS21 no longer contains the fast growing gluon PDF error set which was present in EPPS16. The nNNPDF3.0 and nCTEQ15WZSIH rapidity-differential cross section uncertainties are bigger simply because the underlying error sets are not as tightly constrained as the EPPS21 ones. One should note that the EPPS21 and nNNPDF3.0 uncertainties contain both the nuclear and the free proton uncertainties whereas the nCTEQ15WZSIH contains only the nuclear ones. Finally, because of the strong scale dependence, the usefulness of these data as a constraint for the nPDFs is not clear.

The above mentioned scale dependencies of the NLO results for rapidity-differential cross sections are presented as a function of rapidity y for the EPPS16 and EPPS21 nPDF sets presented in Fig. 6. The results for the Run2 energy of 5.02 TeV is shown with the solid blue curve for EPPS16 and with the dashdotted blue curve for EPPS21. Similarly, the results for the Run1 energy of 2.76 TeV is shown as dashed red for EPPS16 and as dotted red for EPPS21. In addition to the observations we made above, we can make three additional remarks from this figure: (1) At the higher Run2 energy, we see that for both EPPS16 and EPPS21 the scale dependence is greater than at the lower Run1 energy, (2) The scale dependence weakens for all energies and sets the higher we move in the absolute value of the rapidity i.e. $|y|$ and (3) Overall the newer set EPPS21 has a smaller scale dependence than EPPS16.

As discussed above, the scale dependence of the photoproduction cross section in our framework ends up being rather sizeable. This fact was originally pointed out already some twenty years ago in [25] even though in that work the authors modeled the GPDs, basing them on the CTEQ6 PDF parametrization [156], differently in the ERBL-region than what we have done here. The central-set predictions of the CTEQ collaboration for the quark singlet PDFs have stayed more or less the same, i.e. corrections are of the order of some tens of percents in the range $x \in [10^{-7}, 10^{-1}]$ and $\mu \in [m_c, M_{J/\psi}]$, ever since CTEQ61 [157] was published going through the CT10NLO [158], the CT14NLO [152] and the CT18ANLO [159] PDF sets. For the gluons the situation is similar for the exception that there is more variation between the sets since the CTEQ61 PDF set. In this way the qualitative comparison with the results given in [25] are reasonable but a more detailed analysis would obviously require the implementation of the GPD modeling in the ERBL region. Running the photoproduction baseline calculation for the $\gamma + p$ case, see figure 7, with any of the aforementioned sets produces essentially the same result: charm mass scale result stays constant as a function of W at about few nanobarns, increasing the scale to e.g. $3M_{J/\psi}/4$ increases the cross section so that it grows linearly from around zero at $W = 13$ GeV to about 0.7 microbarns at $W = 2000$ GeV and increasing the scale further results in a bigger slope of the cross section.

Keeping in mind the above, there are a few observations which are worth mentioning when applying the photoproduction results to nucleus-nucleus collisions. Firstly: if the gluon distribution differs from any of the above mentioned sets noticeably starting from around $x \approx 10^{-3}$, as is the case with CTEQ6L1 [156] or nNNPDF2.0 [75], then the cross section ends up growing much faster than before due to the real part of the LO gluon amplitude from the ERBL region. Secondly: if the strange quark distribution is strongly enchanced, like is the case with nCTEQ15WZSIH [155], the cross section again grows faster as a function of W. As was noted in [PI], the few very first datapoints – i.e. data in the range $W \in [10, 100]$ GeV – in the free proton photoproduction calculation are undershot with all scales and the increase in the cross section means that these data are captured by the prediction. But if we do this, it means that we overshoot the high W data – i.e. data in the range $W \in [500, 2000]$ GeV – considerably at the "optimal scale".

Focusing a bit more on the small-energy region of $W \in [10, 200]$ GeV, as shown in figure 7 (close up of Fig. 2 in [PI]), we see how the scale uncertainty band is clearly left below the data points. This is particularly important when one keeps in mind the upcoming American based Electron-Ion-Collider (EIC) with the $e + A$ c.m.s. energy range of $[20, 90]$ GeV [95]. In the figure, the solid red line gives us the "optimal" scale result which bears no other special meaning except that it matches with the rapidity differential cross section of the J/ψ photoproduction in nucleus-nucleus collisions (see [PI] for further details). The dashed red line gives us the upper limit of the scale uncertainty ($\mu = M_{J/\psi}$) and the dotted red line gives us the lower limit of the scale uncertainty ($\mu = m_c$). Note that we have a similar type of problem arising in the case of Υ production where we do not match the energy dependence of the photoproduction cross section in the conservative, physical mass scale range of $[m_b, M_\Upsilon]$; see figure 9 below.

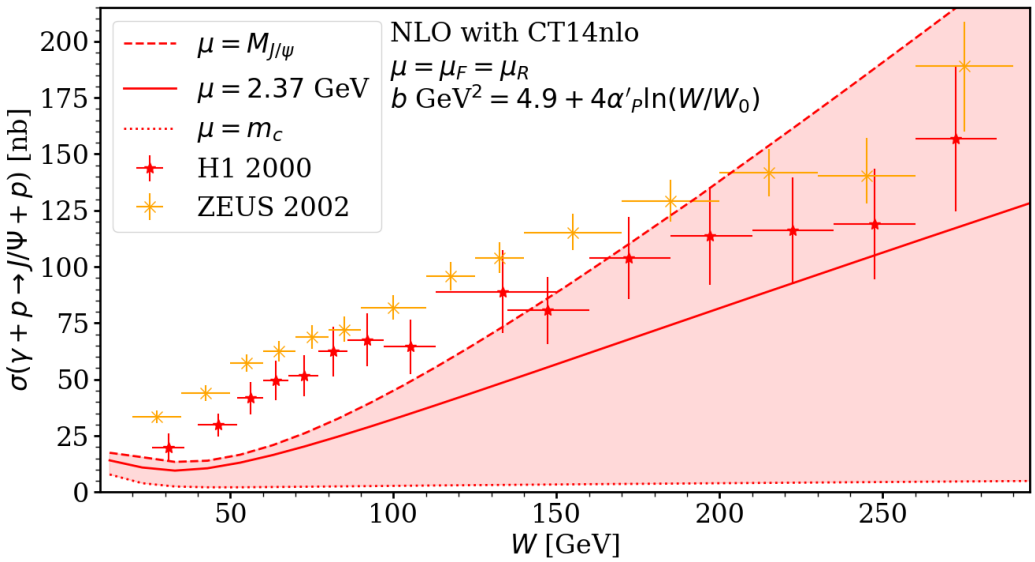

FIGURE 7 The NLO scale-choice uncertainty-envelope of the cross section of the exclusive photoproduction process $\gamma + p \to J/\psi + p$ as a function of the photon-proton c.m.s. energy W in the low energy range juxtaposed with the H1 [162] and ZEUS [163] collaboration results. All of the three lines shown in the figure are calculated with the CT14NLO [152] PDFs where the solid (red) line is the optimal scale as explained in the text. Close up of Fig. (2) in [PI].

All of this is to say that there is clearly a demand to study more in detail how to mitigate the scale dependence. In addition to the obvious task of looking into the NNLO corrections (and the resummation of higher order effects) one might first want to systematically study the effect of the GPD modeling for example through the DGLAP region specific skewness correction and the ERBL region specific meson amplitude corrections. In particular it would be interesting to see if the discrepancy between nNNPDF2.0 and EPPS16 nPDF sets could be mitigated by a more realistic ERBL-region modeling for example as done in Ref. [88] and what exactly is the leading source of discrepancy between our photoproduction baseline and the experimental data. A similar test could then naturally be done for the nCTEQ15WZSIH PDF set as well which might shed some light as to the relative importance between the gluon and the quark distributions. One should also systematically look into the NRQCD corrections [160, 161] to see if that would improve the match between the pQCD prediction and the baseline photoproduction data.

Finally, we should point out that in a future work, if the scale and the nPDF uncertainties have been constrained reasonably well, one might also want to consider the uncertainties arising from the form factor and the photon flux. The 2pF and 3pF distributions are widely used parametrizations for the underlying nuclear density and we have applied the form of Ref. [140] without showing the uncertainties arising from the experimental determination of the free parameters [137, 138]. These density distributions go into both the form factor and the photon flux calculations, and in particular, the application of the density distributions for the form factor might require a more in depth look as discussed in Refs. [125, 164].

5.2 Taming the scale dependence of J/ψ production

The Pb-Pb results are interesting in themselves but the main hope of the second paper [PII] was to constrain the strong scale dependence of the cross section by considering a suitable ratio between two different UPC processes. There is a plan moving forward at the LHC that a short oxygen-oxygen (O-O) run would be performed during Run3 [165–167] which opens up the possibility to consider the scaled ratio

$$R^{\mathrm{O/Pb}} = \left(\frac{A_{\mathrm{Pb}} Z_{\mathrm{Pb}}}{A_{\mathrm{O}} Z_{\mathrm{O}}}\right)^2 \frac{\frac{d\sigma^{\mathrm{O+O\to O+V+O}}}{dy}}{\frac{d\sigma^{\mathrm{Pb+Pb\to Pb+V+Pb}}}{dy}}, \tag{100}$$

where $A_{\mathrm{Pb}} = 208$ is the mass number of lead, $Z_{\mathrm{Pb}} = 82$ is the atomic number of lead, $A_{\mathrm{O}} = 16$ is the mass number of oxygen and $Z_{\mathrm{O}} = 8$ is the atomic number of oxygen.

Before considering the ratio of equation 100 we naturally had to implement the oxygen form factor and photon flux which were relatively easy to do as the only difference – in addition to the obvious differences in the mass number and the atomic number – was that the underlying oxygen nuclear density distribution is described by a three-parameter-Fermi (3pF) instead of the two-parameter-Fermi (2pF) of the lead [PII]. We found that in the ratio $R^{\mathrm{O/Pb}}$ at midrapidity with the same collision energies (If there were no differences the ratio would naturally be equal to 1) we should expect to see a factor of about 4.6 from the ratio of the integrals of the form factors and a factor of about 1.3 from the ratio of the photon fluxes (see Figs. 1 and 2 in [PII]). The rest should then come from the differences in the nuclear corrections.

The results for the production of J/ψ in oxygen-oxygen collisions were very similar to the ones for lead-lead: scale dependence is considerable, real part of the scattering amplitude cannot be neglected and the quarks dominate at central rapidity (see Figs. 5, 7 and 8 in [PII]). For the ratio shown in equation 100 it turned out, as was the hope, that the scale dependencies cancelled out to a large extent, i.e., by a factor of ten for all three nPDF sets under consideration. In addition to the scale uncertainties, we considered the PDF uncertainties in this ratio which are superimposed over each other in figure 8. The figure shows the scaled ratio at central rapidity for the three different nPDF sets EPPS21 (left), nNNPDF3.0 (center) and nCTEQ15WZSIH (right) each on their optimal scale such that in the left panel the Pb-Pb cross section is taken at Run1 energy and in the right panel the Pb-Pb cross section is taken at Run2 energy. The capped blue (green) thin bars show the PDF uncertainties when O-O cross section is taken at the c.m.s. energy of 6.37 TeV (7.00 TeV) and the orange (red) thick bars show the scale uncertainties when the O-O cross section is taken at the c.m.s. energy of 6.37 TeV (7.00 TeV).

The figure shows both the systematics of the results and the lack of them quite nicely. As to the systematics: if we increase the energy of Pb-Pb collisions, the ratio gets smaller and vice versa if we increase the energy of O-O collisions, the ratio gets bigger. And then to the lack of systematic behaviour of the uncertainties: at Run1 energy the PDF uncertainties dominate over the scale uncertainties for EPPS21 but for nNNPDF3.0 the PDF uncertainties dominate upwards and the scale uncertainties downwards whereas for nCTEQ15WZSIH they seem to be of the same order. Then

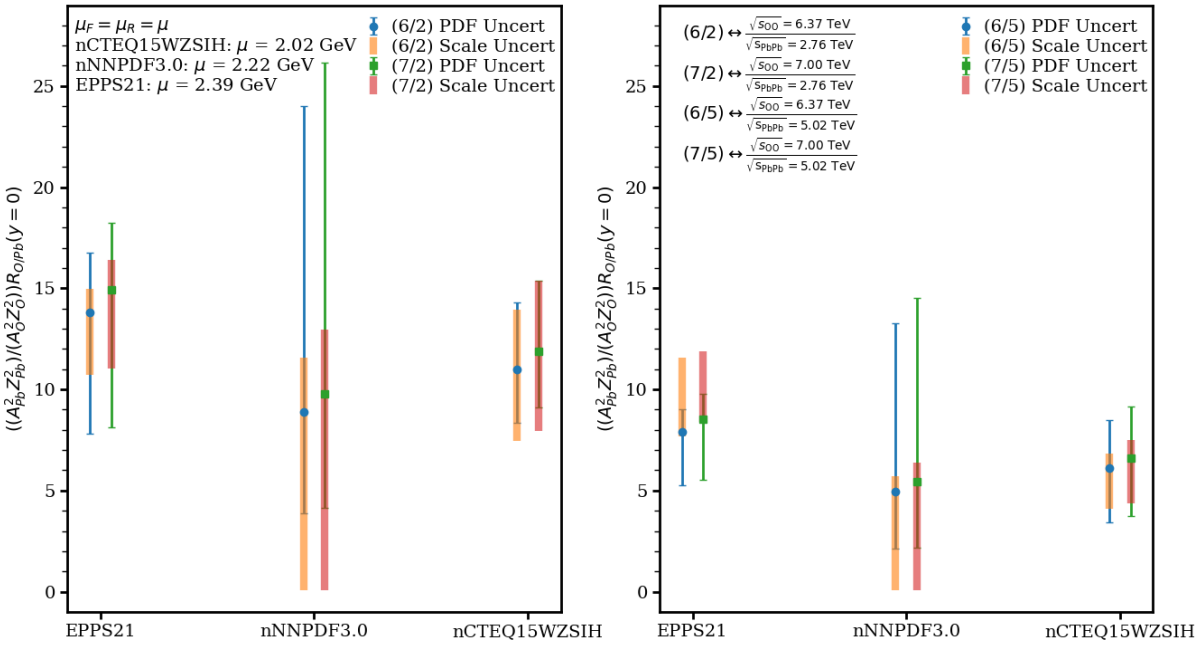

FIGURE 8 The scaled ratio of rapidity differential cross sections of oxygen-oxygen to lead-lead with EPPS21, nNNPDF3.0 and nCTEQ15WZSIH nPDFs at their optimal scales at midrapidity such that the cross sections are taken at different energies. On the left panel Pb-Pb is taken at Run1 energy and on the right panel it is taken at Run2 energy. Figure is from [PII].

at Run2 energy the scale uncertainties dominate upwards and PDF uncertainties downwards for EPPS21 – vice versa for nNNPDF3.0 – and for nCTEQ15WZSIH the scale uncertainties are smaller than the PDF uncertainties. In any case, the figure shows that there is clearly some hope that the ratio could be used to constrain the PDF uncertainties.

5.3 Exclusive photoproduction of Υ

Working still within the forward limit, in addition to J/ψ production, one can consider the photoproduction of Υ mesons with the hope that the scale dependence might be reduced because of the higher scale of the process. Unfortunately at the scale interval of $\mu \in [m_b, M_\Upsilon]$, where m_b is the mass of the bottom quark and M_Υ is the mass of the Upsilon meson, we always seem to undershoot the available photoproduction data from e-p and p-p collisions; see figure 9. We have to drop down to scales of around $m_b/2 \approx 2.37$ GeV in order to get the central prediction to go nicely through the data at high values of W. Moreover still, if one wants the scale uncertainty to better cover all available experimental data, one has to drop down to the scales of the charm mass $m_c \approx 1.55$ GeV.

It was partly for this reason why in [PIII] we ventured further from our forward model and implemented the so called skewness correction through the Shuvaev transform [168, 169] which is a well known way to solve the LO Q^2 evolution of the

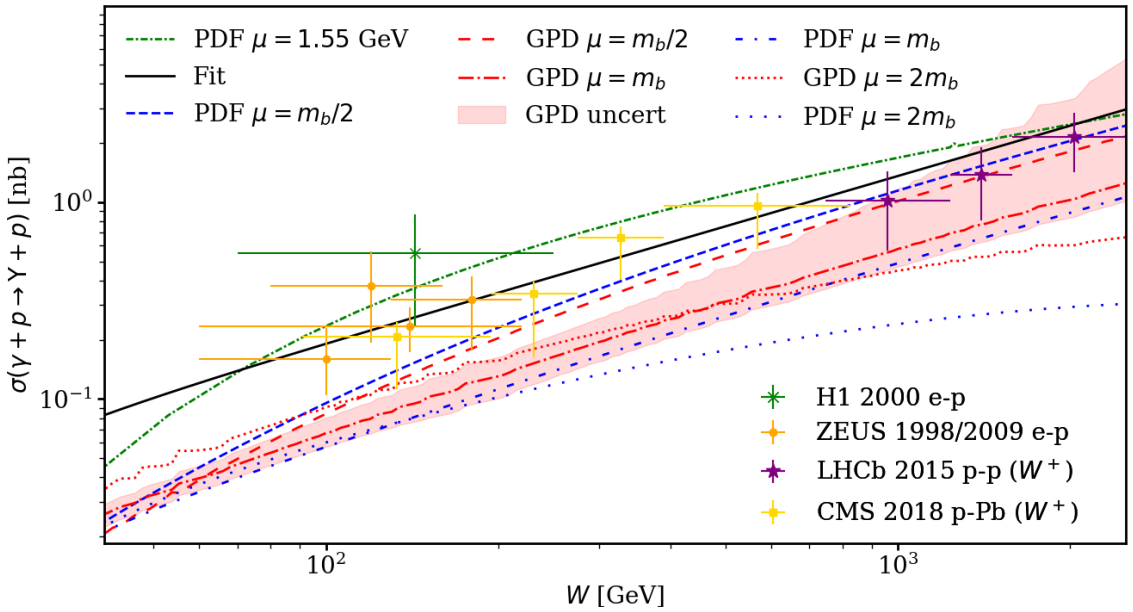

FIGURE 9 The exclusive Υ photoproduction NLO cross sections with CT18ANLO based GPDs and PDFs as a function of the c.m.s energy W compared with the data from ZEUS [170], H1 [162], LHCb [171] and CMS [172] collaborations. The figure is the same as Fig. (2) in [PIII] but with the additional $\mu = 1.55$ GeV PDF curve.

GPDs in the DGLAP region with appropriately chosen input PDFs[1]. For further details of the transform, see [PIII] and references therein. The Shuvaev transform does improve the situation slightly but we still seem to somewhat underestimate the experimental data in the conservative range of $\mu \in [m_b/2, 2m_b]$. Nevertheless, one might be able to exploit the available data by using an *ad hoc* parametrization to describe the W dependence of the cross section. This is exactly what was done with the baseline photoproduction cross section in paper [PIII]. The CT18ANLO based PDF and GPD curves, and the data driven result, are shown in figure 9 along with comparison with the available data from the ZEUS [170], H1 [162], LHCb [171] and CMS [172] collaborations. For the slope parameter b we used the Υ specific parametrization with $\alpha'_P = 0.06$ and $W_0 = 90$ GeV [PIII].

The Shuvaev transform does bring about a 20 percent increase to the photoproduction cross section at $W \approx 200$ GeV when compared to the strict forward case with $\mu = m_b$ but otherwise the skewing of the PDFs to the GPDs does not affect the qualitative results of the Υ production:

(1.) The imaginary part clearly dominates the scattering amplitude in the interval $\mu \in [m_b, M_\Upsilon]$.

(2.) The cross section is hugely dominated by the gluon distribution in the same interval of $\mu \in [m_b, M_\Upsilon]$.

(3.) The NLO scale dependence is opposite to that of the J/ψ case and slightly more moderate.

[1] The modeling of the GPDs does not belong to the scope of this thesis.

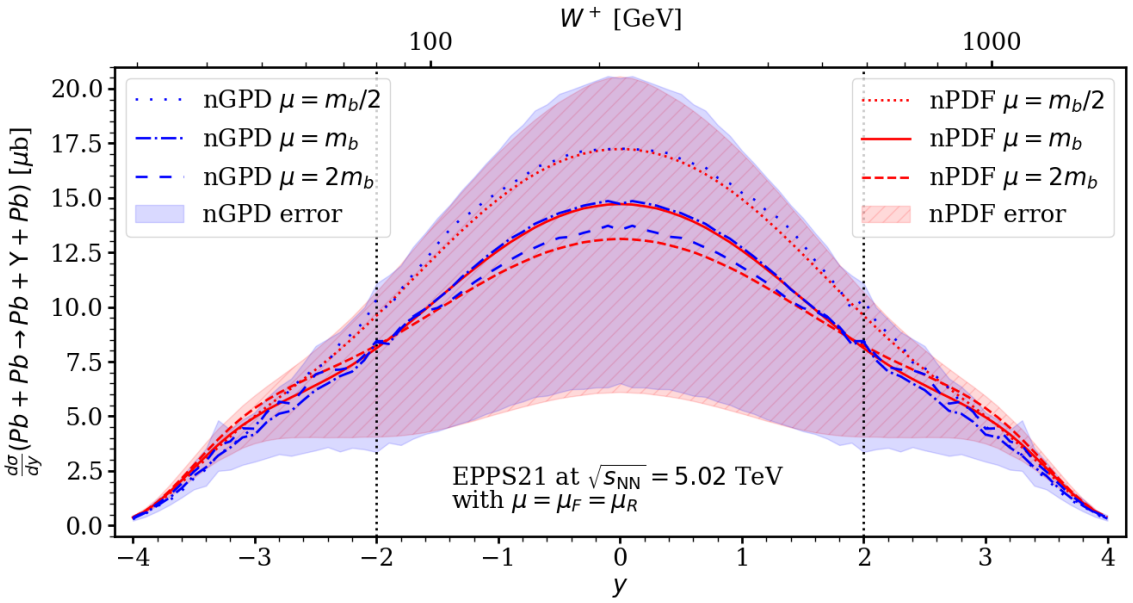

FIGURE 10 The data-driven exclusive rapidity-differetial NLO cross section of Y photoproduction in Pb+Pb UPCs at $\sqrt{s_{NN}} = 5.02$ TeV with EPPS21 based nGPDs (blue) and EPPS21 nPDFs (red). The dotted curves show $\mu = m_b/2$, dashed curves show $\mu = 2m_b$ and dashdotted (solid) show $\mu = m_b$ nGPD (nPDF) results. The blue (hashed red) area shows the nGPD (nPDF) error. The area between the vertical lines at $|y| = 2$ indicate the region in which we can trust the fit $\sigma_{\mathrm{fit}}^{\gamma p \to \mathrm{Y}p}$. Figure is from [PIII].

It should be stressed that the observations (1.) and (2.) are in line with what has been previously thought in the literature in the context of exclusive J/ψ photoproduction [91, 95, 135].

The general behaviour of the cross section as a function of the scale arises from the fact that the NLO corrections have a different sign to that of the LO, see [PI] for an in depth analysis for this in the case of J/ψ, when working in the scale range of $\mu \in [m_Q, 2m_Q]$. But in short the difference between the Y and the J/ψ results can be summarized as follows: Y is probed at a higher scale and thus $\alpha(\mu_R)$ is always smaller leading to smaller NLO corrections, and the skewness variable ξ is about a factor of 10 bigger in Y production than in J/ψ production. The bigger value of ξ means that the effective values at which the PDFs (or the GPDs) are probed are bigger which in turn leads to a more moderate scale evolution (this was already argued in [25]). Finally, the jump from the $\mu = m_b/2$ (dashed blue) curve to $\mu = 1.55$ GeV (densely dashdotted green) curve in figure 9, is in part explained by the fact that the NLO corrections change sign and become negative when we drop down to scales of $\mu \approx 3$ GeV and lower.

The results of the baseline Y photoproduction are interesting in themselves but our desire was to predict how the results would translate to the nuclear case of $\mathrm{Pb} + \mathrm{Pb} \to \mathrm{Pb} + \mathrm{Y} + \mathrm{Pb}$. The above three observations hold also for the nuclear case, see Figs. 2, 3, 4 and 6 in [PIII], but maybe slightly surprisingly the effect of the skewing of the nPDFs is very weak as shown in figure 10. In order to get these results, we used the data driven baseline photoproduction result to better parametrize the

W dependence of the photoproduction cross section:

$$\sigma^{\gamma+\mathrm{Pb}\to\mathrm{Y}+\mathrm{Pb}} = \left(\frac{\sigma^{\gamma+\mathrm{Pb}\to\mathrm{Y}+\mathrm{Pb}}}{\sigma^{\gamma+\mathrm{p}\to\mathrm{Y}+\mathrm{p}}}\right)_{\mathrm{pQCD}} \sigma_{\mathrm{fit}}^{\gamma+\mathrm{p}\to\mathrm{Y}+\mathrm{p}}, \tag{101}$$

where $\sigma^{\gamma+\mathrm{Pb}\to\mathrm{Y}+\mathrm{Pb}}$ and $\sigma^{\gamma+\mathrm{p}\to\mathrm{Y}+\mathrm{p}}$ are standard NLO pQCD predictions and $\sigma_{\mathrm{fit}}^{\gamma+\mathrm{p}\to\mathrm{Y}+\mathrm{p}}$ is a fit to the available $e+p$ data. This fit is based on data for W approximately between 100 GeV to 2000 GeV which in terms of the rapidity translates to roughly $|y| \leq 2$. The data-driven rapidity differential photoproduction cross sections in $\mathrm{Pb}+\mathrm{Pb}$ UPCs were then obtained by folding the data-corrected pQCD cross sections, i.e. equation 101, with the photon fluxes and form factors of the colliding nuclei. For more details on the data driven method, see [PIII].

At $y = 0$ the agreement between nGPD and nPDF results for scale choices $\mu = m_b$ and $\mu = m_b/2$ is of the order of numerical integration accuracy of 10^{-3}. At this central rapidity, only with the scale $\mu = 2m_b$, do we see a difference of around 4 percents. The difference increases the higher we go in rapidity so that the the biggest difference is seen with $\mu = m_b/2$ raising up to around 20 percents at $|y| = 4$. The biggest difference of the data driven approach to the standard pQCD one is that the latter is about a factor of 2-2.5 smaller than the former. Moreover, the shapes of the distribution for the standard NLO pQCD result and the data driven result are roughly the same. As expected, in taking the Pb-to-p ratios of pQCD cross sections (equation 101), the scale dependence indeed reduces significantly [PIII]. This is a promising result for the eventual goal to use the exclusive heavy vector meson photoproduction processes as a possible data constraint in global nPDF analysis.

6 CONCLUSIONS

We have presented a systematic summary of our pQCD framework for calculating predictions for coherent exclusive photoproduction of heavy-vector mesons in UPCs. We started chapter 1 by defining the theories with which we work – QCD and QED – and segued to give a short account of how our inability to completely solve these theories is parametrized and quantified in terms of the experimentally determinable parton distributions in chapter 2. Chapter 3 sketched the calculation of the well known photoproduction amplitude at leading order pQCD which was then applied in chapter 4 to the actual process of interest i.e. $A + A \to A + V + A$.

All of this development first lead to the results presented in article [PI] where the main conclusions were that the $\mathrm{Pb} + \mathrm{Pb} \to \mathrm{Pb} + J/\psi + \mathrm{Pb}$ process is surprinsingly sensitive to the quark distributions and that the scale dependence of the cross section is considerable. Moreover, we found that the predictions are also very sensitive to the underlying nPDF sets, most notably the discrepancy between the EPPS16 and the nNNPDF2.0 results. The difference was traced to originate from the rapidly growing real part of the LO gluon contribution in the case where one encounters very steeply rising small-x gluon PDFs. The conclusion of the study was that the process might not be as good a probe of the gluon distributions or of their nuclear corrections as previously thought.

The scale dependence can be mitigated by considering appropriate ratios of cross sections and this is exactly what was done in article [PII] for the case of J/ψ production where we considered two initial states: lead-lead collisions and oxygen-oxygen collisions. In our framework the switch from one initial state to another is rather easy as it essentially boils down to switching the underlying nPDFs which we take from the LHAPDF-interface [151]. That is, in addition to making sure that one uses the correct form factor and the photon flux. We found the reduction in the scale dependence to always be an order of magnitude regardless of the nPDF set which we used.

Then finally in article [PIII] we applied our framework to the production of the Υ meson and found out that the scale dependence is sligthly milder in this case due to the fact that we probe the process at a higher scale. Moreover, the scale dependence for Υ production is not as straightforward as in the J/ψ case. That

is, for J/ψ increasing the scale meant that we increase the absolute cross section prediction but for Υ the cross section either increases or decreases depending on the exact values of W and μ. Since for the photoproduction cross section of Υ, with the forward limit approximation of papers [PI, PII], we are always below the experimental data of $\gamma + p \to V + p$, we applied the well known Shuvaev transform to take into account skewness corrections. In addition to this, we introduced a data driven procedure where the baseline NLO pQCD cross sections were fitted to the $e + p$ data. Along with the reduction in the scale dependence, we learned that the rapidity differential cross section for producing Υ mesons is dominated by the gluon distributions and the imaginary part of the scattering amplitude. The difference between the final data driven predictions, computed with the nGPDs and the nPDFs, of the rapidity-differential cross section of $\mathrm{Pb} + \mathrm{Pb} \to \mathrm{Pb} + \Upsilon + \mathrm{Pb}$ was discovered to be negligible.

This work then presents the very first steps in systematic studies that should be done when investigating the usefulness of exclusive heavy vector meson photoproduction processes as data constraints for the nPDFs. Even though the scale dependence is considerable, one can find an optimal scale which descibes the Run1 and Run2 data for J/ψ production in lead-lead collisions, as shown in [PI, PII], creating some hope that the data could possibly be used in future as constraints. Also the usefulness of the Υ production remains to be seen in the future as discussed in [PIII]. The next obvious steps to do would be to update the results of the papers [PI, PII] with the "off-forwardness" property of the GPDs for example through the Shuvaev transform and to consider how the modeling of the ERBL region affects the results presented in all three articles [PI, PII, PIII]. These corrections apply already on the free proton level but one should also keep in mind the interesting question of whether the nuclear corrections to GPDs propagate in a different manner than to the nPDFs. That is, how do nuclear corrections on GPDs depend on ξ and t? How does the scale evolution change if the generalized GPD evolution equations are used to evolve the distributions? Are there any non-trivial nuclear corrections to GPDs that are different from nuclear corrections to PDFs? Questions like these related to the GPDs, in addition to the ones relating to our pQCD framework, such as the role of the NRQCD corrections, need to be answered in future studies.

BIBLIOGRAPHY

[PI] Kari J. Eskola, Christopher A. Flett, Vadim Guzey, Topi Löytäinen and Hannu Paukkunen, Exclusive J/ψ photoproduction in ultraperipheral Pb+Pb collisions at the CERN Large Hadron Collider calculated at next-to-leading order perturbative QCD, *Phys. Rev. C* 106, no.3 (2022) 035202, arXiv: 2203.11613 [hep-ph].

[PII] Kari J. Eskola, Christopher A. Flett, Vadim Guzey, Topi Löytäinen and Hannu Paukkunen, Next-to-leading order perturbative QCD predictions for exclusive J/ψ photoproduction in oxygen-oxygen and lead-lead collisions at energies available at the CERN Large Hadron Collider, *Phys. Rev. C* 107, no.4 (2023) 044912, arXiv: 2210.16048 [hep-ph].

[PIII] Kari J. Eskola, Christopher A. Flett, Vadim Guzey, Topi Löytäinen and Hannu Paukkunen, Predictions for exclusive Υ photoproduction in ultraperipheral Pb+Pb collisions at the LHC at next-to-leading order in perturbative QCD (Mar. 2023), submitted to Eur. Phys. J. C., arXiv: 2303.03007 [hep-ph].

[1] N. N. Bogolubov, A. A. Logunov and I. T. Todorov, *Introduction to Axiomatic Quantum Field Theory*, W. A. Benjamin Inc., 1975.

[2] C. Itzykson and J. B. Zuber, *Quantum Field Theory*, International Series In Pure and Applied Physics, New York: McGraw-Hill, 1980, ISBN: 978-0-486-44568-7.

[3] L. D. Faddeev and A. A. Slavnov, *Gauge Fields: Introduction to Quantum Theory*, The Benjamin/Cummings Publishing Company Inc, 1982, ISBN: 0-80539016-2.

[4] George Sterman, *An Introduction to Quantum Field Theory*, Cambridge University press, 1994, ISBN: 0-521-31132-2.

[5] Michael E. Peskin and Daniel V. Schroeder, *Quantum Field Theory*, Perseus Books Publishing, 1995, ISBN: 0-201-50397-2.

[6] Steven Weinberg, *The Quantum Theory of Fields*, Cambridge University press, 1995, ISBN: 0-521-55001-7.

[7] Mark Srednicki, *Quantum Field Theory*, Cambridge University press, 2007, ISBN: 978-0-521-86449-7.

[8] C. P. Burgess and Guy D. Moore, *The Standard Model: A Primer*, Cambridge University press, 2007, ISBN: 978-0-521-86036-9.

[9] Matthew D. Schwartz, *Quantum Field Theory and the Standard Model*, Cambridge University press, 2014, ISBN: 978-1-107-03473-0.

[10] Tom Lancaster and Stephen J. Blundell, *Quantum Field Theory for the Gifted Amateur*, Oxford University Press, 2014, ISBN: 978-0-19-969933-9.

[11] Paul Langacker, *The Standard Model and Beyond*, CRC press, 2010, ISBN: 978-1-4200-7906-7.

[12] R. D. Field, *Applications of Perturbative QCD*, volume 77, 1989.

[13] Raymond Brock et al., Handbook of perturbative QCD: Version 1.0, *Rev. Mod. Phys.* 67 (1995) 157–248.

[14] R. Keith Ellis, W. James Stirling and B. R. Webber, *QCD and collider physics*, volume 8, Cambridge University Press, Feb. 2011, ISBN: 978-0-511-82328-2.

[15] Taizo Muta, *Foundations of Quantum Chromodynamics: An Introduction to Perturbative Methods in Gauge Theories, (3rd ed.)* 3rd, volume 78, World scientific Lecture Notes in Physics, Hackensack, N.J.: World Scientific, 2010, ISBN: 978-981-279-353-9.

[16] John Collins, *Foundations of perturbative QCD*, volume 32, Cambridge University Press, Nov. 2013, ISBN: 978-1-107-64525-7.

[17] Peter Skands, Introduction to QCD, *Theoretical Advanced Study Institute in Elementary Particle Physics: Searching for New Physics at Small and Large Scales* 341–420, arXiv: 1207.2389 [hep-ph].

[18] Ben Ruijl, Takahiro Ueda and Jos Vermaseren, FORM version 4.2 (July 2017), arXiv: 1707.06453 [hep-ph].

[19] Paulo Nogueira, Automatic Feynman graph generation, *J. Comput. Phys.* 105 (1993) 279–289.

[20] C. Studerus, Reduze-Feynman Integral Reduction in C++, *Comput. Phys. Commun.* 181 (2010) 1293–1300, arXiv: 0912.2546.

[21] Wolfram Research Inc., *Mathematica*, version 13.0.0, URL: https://www.wolfram.com/mathematica.

[22] Vladyslav Shtabovenko, Rolf Mertig and Frederik Orellana, FeynCalc 9.3: New features and improvements, *Comput. Phys. Commun.* 256 (2020) 107478, arXiv: 2001.04407 [hep-ph].

[23] ISO/IEC, *ISO International Standard ISO/IEC TS 19570:2018 – Programming Language C++*, URL: https://isocpp.org/std/the-standard.

[24] Python Software Foundation, *Python Language Reference, version 3.6.9*, URL: http://www.python.org.

[25] D. Yu. Ivanov, A. Schafer, L. Szymanowski and G. Krasnikov, Exclusive photoproduction of a heavy vector meson in QCD, *Eur. Phys. J. C* 34, no.3 (2004), [Erratum: Eur.Phys.J.C 75, 75 (2015)] 297–316, arXiv: hep-ph/0401131.

[26] John C. Collins, Intrinsic transverse momentum: Nongauge theories, *Phys. Rev. D* 21 (1980) 2962.

[27] John C. Collins and Davison E. Soper, Parton Distribution and Decay Functions, *Nucl. Phys. B* 194 (1982) 445–492.

[28] John C. Collins, Davison E. Soper and George F. Sterman, Factorization of Hard Processes in QCD, *Adv. Ser. Direct. High Energy Phys.* 5 (1989) 1–91, arXiv: hep-ph/0409313.

[29] A. V. Radyushkin, Nonforward parton distributions, *Phys. Rev. D* 56 (1997) 5524–5557, arXiv: hep-ph/9704207.

[30] John C. Collins and Andreas Freund, Proof of factorization for deeply virtual Compton scattering in QCD, *Phys. Rev. D* 59 (1999) 074009, arXiv: hep-ph/9801262.

[31] M. Diehl, Generalized parton distributions, *Phys. Rept.* 388 (2003) 41–277, arXiv: hep-ph/0307382.

[32] S. Mandelstam, Determination of the pion - nucleon scattering amplitude from dispersion relations and unitarity. General theory, *Phys. Rev.* 112 (1958) 1344–1360.

[33] John C. Collins, Leonid Frankfurt and Mark Strikman, Factorization for hard exclusive electroproduction of mesons in QCD, *Phys. Rev. D* 56 (1997) 2982–3006, arXiv: hep-ph/9611433.

[34] Geoffrey T. Bodwin, Eric Braaten and G. Peter Lepage, Rigorous QCD analysis of inclusive annihilation and production of heavy quarkonium, *Phys. Rev. D* 51 (1995), [Erratum: Phys.Rev.D 55, 5853 (1997)] 1125–1171, arXiv: hep-ph/9407339.

[35] Stanley J. Brodsky, L. Frankfurt, J. F. Gunion, Alfred H. Mueller and M. Strikman, Diffractive leptoproduction of vector mesons in QCD, *Phys. Rev. D* 50 (1994) 3134–3144, arXiv: hep-ph/9402283.

[36] R. P. Feynman, The behavior of hadron collisions at extreme energies, *Conf. Proc. C* 690905 (1969) 237–258.

[37] J. D. Bjorken and Emmanuel A. Paschos, Inelastic Electron Proton and gamma Proton Scattering, and the Structure of the Nucleon, *Phys. Rev.* 185 (1969) 1975–1982.

[38] Xiang-Dong Ji, Off forward parton distributions, *J. Phys. G* 24 (1998) 1181–1205, arXiv: hep-ph/9807358.

[39] A. V. Radyushkin, Generalized parton distributions (Oct. 2000), arXiv: hep-ph/0101225.

[40] K. Goeke, Maxim V. Polyakov and M. Vanderhaeghen, Hard exclusive reactions and the structure of hadrons, *Prog. Part. Nucl. Phys.* 47 (2001) 401–515, arXiv: hep-ph/0106012.

[41] A. V. Belitsky and A. V. Radyushkin, Unraveling hadron structure with generalized parton distributions, *Phys. Rept.* 418 (2005) 1–387, arXiv: hep-ph/0504030.

[42] Sigfrido Boffi and Barbara Pasquini, Generalized parton distributions and the structure of the nucleon, *Riv. Nuovo Cim.* 30, no.9 (2007) 387–448, arXiv: 0711.2625 [hep-ph].

[43] Michel Guidal, Hervé Moutarde and Marc Vanderhaeghen, Generalized Parton Distributions in the valence region from Deeply Virtual Compton Scattering, *Rept. Prog. Phys.* 76 (2013) 066202, arXiv: 1303.6600 [hep-ph].

[44] V. Guzey, Generalized parton distributions and exclusive processes, *Nuovo Cim. C* 036, no.05 (2013) 43–48.

[45] P. Kroll, M. Schurmann and Pierre A. M. Guichon, Virtual Compton scattering off protons at moderately large momentum transfer, *Nucl. Phys. A* 598 (1996) 435–461, arXiv: hep-ph/9507298.

[46] Pierre A. M. Guichon and M. Vanderhaeghen, Virtual Compton scattering off the nucleon, *Prog. Part. Nucl. Phys.* 41 (1998) 125–190, arXiv: hep-ph/9806305.

[47] Xiang-Dong Ji, Deeply virtual Compton scattering, *Phys. Rev. D* 55 (1997) 7114–7125, arXiv: hep-ph/9609381.

[48] A. V. Radyushkin, Asymmetric gluon distributions and hard diffractive electroproduction, *Phys. Lett. B* 385 (1996) 333–342, arXiv: hep-ph/9605431.

[49] Xiang-Dong Ji, Gauge-Invariant Decomposition of Nucleon Spin, *Phys. Rev. Lett.* 78 (1997) 610–613, arXiv: hep-ph/9603249.

[50] A. V. Radyushkin, Scaling limit of deeply virtual Compton scattering, *Phys. Lett. B* 380 (1996) 417–425, arXiv: hep-ph/9604317.

[51] John C. Collins, *Renormalization: An Introduction to Renormalization, The Renormalization Group, and the Operator Product Expansion*, volume 26, Cambridge Monographs on Mathematical Physics, Cambridge: Cambridge University Press, 1986, ISBN: 978-0-521-31177-9.

[52] F. Halzen and Alan D. Martin, *Quarks and leptons: an introductory course in modern particle physics*, 1984, ISBN: 978-0-471-88741-6.

[53] Vincenzo Barone and Enrico Predazzi, *High-Energy Particle Diffraction*, Texts and Monographs in Physics, Springer-Verlag, 2002, ISBN: 3-540-42107-6.

[54] C. P. Burgess and G. D. Moore, *The standard model: A primer*, Cambridge University Press, Dec. 2006, ISBN: 978-0-511-25485-7.

[55] Yuri V. Kovchegov and Eugene Levin, *Quantum chromodynamics at high energy*, volume 33, Cambridge University Press, Aug. 2012, ISBN: 978-0-521-11257-4.

[56] M. Kaku, *Quantum field theory: A Modern introduction*, Oxford University Press, 1993, ISBN: 0-19-507652-4.

[57] Dieter Müller, D. Robaschik, B. Geyer, F. M. Dittes and J. Hořejši, Wave functions, evolution equations and evolution kernels from light ray operators of QCD, *Fortsch. Phys.* 42 (1994) 101–141, arXiv: hep-ph/9812448.

[58] Daniel Boer et al., Gluons and the quark sea at high energies: Distributions, polarization, tomography (Aug. 2011), arXiv: 1108.1713 [nucl-th].

[59] P. Kroll, Status of DVMP, DVCS and GPDs, *EPJ Web Conf.* 85 (2015), edited by Umberto D'Alesio and Francesco Murgia 01005, arXiv: 1410.4450 [hep-ph].

[60] V. Guzey, A. W. Thomas and K. Tsushima, Medium modifications of the bound nucleon GPDs and incoherent DVCS on nuclear targets, *Phys. Lett. B* 673 (2009) 9–14, arXiv: 0806.3288 [hep-ph].

[61] L. Frankfurt, V. Guzey and M. Strikman, Leading Twist Nuclear Shadowing Phenomena in Hard Processes with Nuclei, *Phys. Rept.* 512 (2012) 255–393, arXiv: 1106.2091 [hep-ph].

[62] M. Vanttinen, G. Piller, L. Mankiewicz, W. Weise and K. J. Eskola, Nuclear quark and gluon distributions in coordinate space, *Eur. Phys. J. A* 3 (1998) 351–359, arXiv: hep-ph/9808330.

[63] K. J. Eskola, Shadowing effects on quark and gluon production in ultrarelativistic heavy ion collisions, *Z. Phys. C* 51 (1991) 633–642.

[64] V. Emel'yanov, A. Khodinov, S. R. Klein and R. Vogt, The Effect of shadowing on initial conditions, transverse energy and hard probes in ultrarelativistic heavy ion collisions, *Phys. Rev. C* 61 (2000) 044904, arXiv: hep-ph/9909427.

[65] S. R. Klein and R. Vogt, Inhomogeneous shadowing effects on J/ψ production in dA collisions, *Phys. Rev. Lett.* 91 (2003) 142301, arXiv: nucl-th/0305046.

[66] Ilkka Helenius, Spatially dependent parton distribution functions and hard processes in nuclear collisions, PhD thesis, Jyvaskyla U., 2014, arXiv: 1408.6660 [hep-ph].

[67] K. J. Eskola, V. J. Kolhinen and P. V. Ruuskanen, Scale evolution of nuclear parton distributions, *Nucl. Phys. B* 535 (1998) 351–371, arXiv: hep-ph/9802350.

[68] K. J. Eskola, V. J. Kolhinen and C. A. Salgado, The Scale dependent nuclear effects in parton distributions for practical applications, *Eur. Phys. J. C* 9 (1999) 61–68, arXiv: hep-ph/9807297.

[69] D. de Florian and R. Sassot, Nuclear parton distributions at next-to-leading order, *Phys. Rev. D* 69 (2004) 074028, arXiv: hep-ph/0311227.

[70] M. Hirai, S. Kumano and T. H. Nagai, Determination of nuclear parton distribution functions and their uncertainties in next-to-leading order, *Phys. Rev. C* 76 (2007) 065207, arXiv: 0709.3038 [hep-ph].

[71] K. J. Eskola, H. Paukkunen and C. A. Salgado, EPS09: A New Generation of NLO and LO Nuclear Parton Distribution Functions, *JHEP* 04 (2009) 065, arXiv: 0902.4154 [hep-ph].

[72] K. Kovarik et al., nCTEQ15 - Global analysis of nuclear parton distributions with uncertainties in the CTEQ framework, *Phys. Rev. D* 93, no.8 (2016) 085037, arXiv: 1509.00792 [hep-ph].

[73] Kari J. Eskola, Petja Paakkinen, Hannu Paukkunen and Carlos A. Salgado, EPPS16: Nuclear parton distributions with LHC data, *Eur. Phys. J. C* 77, no.3 (2017) 163, arXiv: 1612.05741 [hep-ph].

[74] Rabah Abdul Khalek, Jacob J. Ethier and Juan Rojo, Nuclear parton distributions from lepton-nucleus scattering and the impact of an electron-ion collider, *Eur. Phys. J. C* 79, no.6 (2019) 471, arXiv: 1904.00018 [hep-ph].

[75] Rabah Abdul Khalek, Jacob J. Ethier, Juan Rojo and Gijs van Weelden, nNNPDF2.0: quark flavor separation in nuclei from LHC data, *JHEP* 09 (2020) 183, arXiv: 2006.14629 [hep-ph].

[76] Kari J. Eskola, Petja Paakkinen, Hannu Paukkunen and Carlos A. Salgado, EPPS21: A global QCD analysis of nuclear PDFs (Dec. 2021), arXiv: 2112.12462 [hep-ph].

[77] Rabah Abdul Khalek et al., nNNPDF3.0: evidence for a modified partonic structure in heavy nuclei, *Eur. Phys. J. C* 82, no.6 (2022) 507, arXiv: 2201.12363 [hep-ph].

[78] Yuri L. Dokshitzer, Calculation of the Structure Functions for Deep Inelastic Scattering and e+ e- Annihilation by Perturbation Theory in Quantum Chromodynamics., *Sov. Phys. JETP* 46 (1977) 641–653.

[79] V. N. Gribov and L. N. Lipatov, Deep inelastic e p scattering in perturbation theory, *Sov. J. Nucl. Phys.* 15 (1972) 438–450.

[80] L. N. Lipatov, The parton model and perturbation theory, *Yad. Fiz.* 20 (1974) 181–198.

[81] Guido Altarelli and G. Parisi, Asymptotic Freedom in Parton Language, *Nucl. Phys. B* 126 (1977) 298–318.

[82] Petja Paakkinen, New constraints for nuclear parton distribution functions from hadron–nucleus collision processes, PhD thesis, Jyvaskyla U., 2019, arXiv: 1912.08156 [hep-ph].

[83] M. Burkardt, C. A. Miller and W. D. Nowak, Spin-polarized high-energy scattering of charged leptons on nucleons, *Rept. Prog. Phys.* 73 (2010) 016201, arXiv: 0812.2208 [hep-ph].

[84] John Koempel, Peter Kroll, Andreas Metz and Jian Zhou, Exclusive production of quarkonia as a probe of the GPD E for gluons, *Phys. Rev. D* 85 (2012) 051502, arXiv: 1112.1334 [hep-ph].

[85] M. Rinaldi and S. Scopetta, Extracting generalized neutron parton distributions from ^3He data, *Phys. Rev. C* 87, no.3 (2013) 035208, arXiv: 1208.2831 [nucl-th].

[86] Ivan Schmidt and M. Siddikov, Nuclear effects in neutrino production of pions, *Phys. Rev. D* 91, no.7 (2015) 073002, arXiv: 1501.04306 [hep-ph].

[87] James Daniel Brandenburg et al., Exploring gluon tomography with polarization dependent diffractive J/ψ production (July 2022), arXiv: 2207.02478 [hep-ph].

[88] A. Freund, M. McDermott and M. Strikman, Modeling generalized parton distributions to describe deeply virtual Compton scattering data, *Phys. Rev. D* 67 (2003) 036001, arXiv: hep-ph/0208160.

[89] C. Mezrag, H. Moutarde and F. Sabatié, Test of two new parametrizations of the generalized parton distribution H, *Phys. Rev. D* 88, no.1 (2013) 014001, arXiv: 1304.7645 [hep-ph].

[90] A. V. Radyushkin, Modeling Nucleon Generalized Parton Distributions, *Phys. Rev. D* 87, no.9 (2013) 096017, arXiv: 1304.2682 [hep-ph].

[91] M.G. Ryskin, Diffractive J/ψ electroproduction in LLA QCD, *Z. Phys. C* 57 (1993) 89–92.

[92] Topi Löytäinen, Lowest Order Perturbative Quantum Field Theory Calculations of Bound State Decay Widths, Master's thesis, University of Jyväskylä, 2017.

[93] A. V. Efremov and A. V. Radyushkin, Factorization and Asymptotical Behavior of Pion Form-Factor in QCD, *Phys. Lett. B* 94 (1980) 245–250.

[94] G. Peter Lepage and Stanley J. Brodsky, Exclusive Processes in Quantum Chromodynamics: Evolution Equations for Hadronic Wave Functions and the Form-Factors of Mesons, *Phys. Lett. B* 87 (1979) 359–365.

[95] A. Accardi et al., Electron Ion Collider: The Next QCD Frontier: Understanding the glue that binds us all, *Eur. Phys. J. A* 52, no.9 (2016), edited by A. Deshpande, Z. E. Meziani and J. W. Qiu 268, arXiv: 1212.1701 [nucl-ex].

[96] Alexandre Deur, Stanley J. Brodsky and Guy F. De Téramond, The Spin Structure of the Nucleon (July 2018), arXiv: 1807.05250 [hep-ph].

[97] Stephen Jones, A study of exclusive processes to NLO and Small-x PDFs from LHC Data, Private communication, PhD thesis, 2015.

[98] Christopher Alexander Flett, Exclusive Observables to NLO and Low x PDF Phenomenology at the LHC, PhD thesis, U. Liverpool (main), 2021.

[99] Zi-Qiang Chen and Cong-Feng Qiao, NLO QCD corrections to exclusive electroproduction of quarkonium, *Phys. Lett. B* 797 (2019), [Erratum: Phys.Lett. B, 135759 (2020)] 134816, arXiv: 1903.00171 [hep-ph].

[100] John B. Kogut and Davison E. Soper, Quantum Electrodynamics in the Infinite Momentum Frame, *Phys. Rev. D* 1 (1970) 2901–2913.

[101] J. D. Bjorken, John B. Kogut and Davison E. Soper, Quantum Electrodynamics at Infinite Momentum: Scattering from an External Field, *Phys. Rev. D* 3 (1971) 1382.

[102] John B. Kogut and Leonard Susskind, The Parton picture of elementary particles, *Phys. Rept.* 8 (1973) 75–172.

[103] Stanley J. Brodsky, Hans-Christian Pauli and Stephen S. Pinsky, Quantum chromodynamics and other field theories on the light cone, *Phys. Rept.* 301 (1998) 299–486, arXiv: hep-ph/9705477.

[104] G. C. Wick, The Evaluation of the Collision Matrix, *Phys. Rev.* 80 (1950) 268–272.

[105] Andrea Petrelli, Matteo Cacciari, Mario Greco, Fabio Maltoni and Michelangelo L. Mangano, NLO production and decay of quarkonium, *Nucl. Phys. B* 514 (1998) 245–309, arXiv: hep-ph/9707223.

[106] Geoffrey T. Bodwin and Andrea Petrelli, Order-v^4 corrections to S-wave quarkonium decay, *Phys. Rev. D* 66 (2002), [Erratum: Phys.Rev.D 87, 039902 (2013)] 094011, arXiv: hep-ph/0205210.

[107] Eric Braaten and Jungil Lee, Exclusive Double Charmonium Production from e^+e^- Annihilation into a Virtual Photon, *Phys. Rev. D* 67 (2003), [Erratum: Phys.Rev.D 72, 099901 (2005)] 054007, arXiv: hep-ph/0211085.

[108] R. Van Royen and V. F. Weisskopf, Hadron Decay Processes and the Quark Model, *Nuovo Cim. A* 50 (1967), [Erratum: Nuovo Cim.A 51, 583 (1967)] 617–645.

[109] Riccardo Barbieri, Raoul Gatto, R. Kogerler and Z. Kunszt, Meson hyperfine splittings and leptonic decays, *Phys. Lett. B* 57 (1975) 455–459.

[110] Pervez Hoodbhoy, Wave function corrections and off forward gluon distributions in diffractive J/ψ electroproduction, *Phys. Rev. D* 56 (1997) 388–393, arXiv: hep-ph/9611207.

[111] M. Vanttinen and L. Mankiewicz, Hard exclusive J/ψ leptoproduction on polarized targets, *Phys. Lett. B* 434 (1998) 141–146, arXiv: hep-ph/9805338.

[112] S. V. Ivanov, G. P. Korchemsky and A. V. Radyushkin, Infrared Asymptotics of Perturbative QCD: Contour Gauges, *Yad. Fiz.* 44 (1986) 230–240.

[113] A. D. Martin, W. J. Stirling and R. S. Thorne, MRST partons generated in a fixed-flavor scheme, *Phys. Lett. B* 636 (2006) 259–264, arXiv: hep-ph/0603143.

[114] A. D. Martin, W. J. Stirling, R. S. Thorne and G. Watt, Parton distributions for the LHC, *Eur. Phys. J. C* 63 (2009) 189–285, arXiv: 0901.0002 [hep-ph].

[115] M. Beneke, A. Signer and Vladimir A. Smirnov, Two loop correction to the leptonic decay of quarkonium, *Phys. Rev. Lett.* 80 (1998) 2535–2538, arXiv: hep-ph/9712302.

[116] A. J. Baltz, The Physics of Ultraperipheral Collisions at the LHC, *Phys. Rept.* 458 (2008), edited by G. Baur et al. 1–171, arXiv: 0706.3356 [nucl-ex].

[117] P. Bosted et al., Search for Sub-threshold Photoproduction of J/ψ Mesons, *Phys. Rev. C* 79 (2009) 015209, arXiv: 0809.2284 [nucl-ex].

[118] P. Bartalini et al., Multi-Parton Interactions at the LHC, arXiv: 1111.0469 [hep-ph].

[119] C. F. von Weizsacker, Radiation emitted in collisions of very fast electrons, *Z. Phys.* 88 (1934) 612–625.

[120] E. J. Williams, Nature of the high-energy particles of penetrating radiation and status of ionization and radiation formulae, *Phys. Rev.* 45 (1934) 729–730.

[121] Manuel Drees and D. Zeppenfeld, Production of Supersymmetric Particles in Elastic *ep* Collisions, *Phys. Rev. D* 39 (1989) 2536.

[122] Carlos A. Bertulani, Spencer R. Klein and Joakim Nystrand, Physics of ultra-peripheral nuclear collisions, *Ann. Rev. Nucl. Part. Sci.* 55 (2005) 271–310, arXiv: nucl-ex/0502005.

[123] Spencer R. Klein and Joakim Nystrand, Interference in exclusive vector meson production in heavy ion collisions, *Phys. Rev. Lett.* 84 (2000) 2330–2333, arXiv: hep-ph/9909237.

[124] W. Schafer and A. Szczurek, Exclusive photoproduction of J/ψ in proton-proton and proton-antiproton scattering, *Phys. Rev. D* 76 (2007) 094014, arXiv: 0705.2887 [hep-ph].

[125] Shreyasi Acharya et al., First measurement of the $|t|$-dependence of coherent J/ψ photonuclear production, *Phys. Lett. B* 817 (2021) 136280, arXiv: 2101.04623 [nucl-ex].

[126] Shreyasi Acharya et al., Coherent J/ψ and ϕ' photoproduction at midrapidity in ultra-peripheral Pb–Pb collisions at $\sqrt{s_{NN}} = 5.02$ TeV, *Eur. Phys. J. C* 81, no.8 (2021) 712, arXiv: 2101.04577 [nucl-ex].

[127] Shreyasi Acharya et al., Coherent J/ψ photoproduction at forward rapidity in ultra-peripheral Pb-Pb collisions at $\sqrt{s_{\rm NN}} = 5.02$ TeV, *Phys. Lett. B* 798 (2019) 134926, arXiv: 1904.06272 [nucl-ex].

[128] Vardan Khachatryan et al., Coherent J/ψ photoproduction in ultra-peripheral PbPb collisions at $\sqrt{s_{NN}} = 2.76$ TeV with the CMS experiment, *Phys. Lett. B* 772 (2017) 489–511, arXiv: 1605.06966 [nucl-ex].

[129] Roel Aaij et al., Study of coherent J/ψ production in lead-lead collisions at $\sqrt{s_{NN}} = 5TeV$ (July 2021), arXiv: 2107.03223 [hep-ex].

[130] Spencer Klein and Joakim Nystrand, Exclusive vector meson production in relativistic heavy ion collisions, *Phys. Rev. C* 60 (1999) 014903, arXiv: hep-ph/9902259.

[131] Eero Byckling and K. Kajantie, *Particle Kinematics: (Chapters I-VI, X)*, Jyvaskyla, Finland: University of Jyvaskyla, 1971.

[132] G. Wolf, Review of High Energy Diffraction in Real and Virtual Photon Proton scattering at HERA, *Rept. Prog. Phys.* 73 (2010) 116202, arXiv: 0907.1217 [hep-ex].

[133] V. A. Khoze, A. D. Martin and M. G. Ryskin, Diffraction at the LHC, *Eur. Phys. J. C* 73 (2013) 2503, arXiv: 1306.2149 [hep-ph].

[134] V. P. Goncalves and C. A. Bertulani, Peripheral heavy ion collisions as a probe of the nuclear gluon distribution, *Phys. Rev. C* 65 (2002) 054905, arXiv: hep-ph/0110370.

[135] Adeola Adeluyi and Carlos Bertulani, Gluon distributions in nuclei probed at the CERN Large Hadron Collider, *Phys. Rev. C* 84 (2011) 024916, arXiv: 1104.4287 [nucl-th].

[136] V. Guzey, E. Kryshen, M. Strikman and M. Zhalov, Nuclear suppression from coherent J/ψ photoproduction at the Large Hadron Collider, *Phys. Lett. B* 816 (2021) 136202, arXiv: 2008.10891 [hep-ph].

[137] C. W. De Jager, H. De Vries and C. De Vries, Nuclear charge and magnetization density distribution parameters from elastic electron scattering, *Atom. Data Nucl. Data Tabl.* 14 (1974), [Erratum: Atom.Data Nucl.Data Tabl. 16, 580–580 (1975)] 479–508.

[138] H. De Vries, C. W. De Jager and C. De Vries, Nuclear charge and magnetization density distribution parameters from elastic electron scattering, *Atom. Data Nucl. Data Tabl.* 36 (1987) 495–536.

[139] Roger D. Woods and David S. Saxon, Diffuse Surface Optical Model for Nucleon-Nuclei Scattering, *Phys. Rev.* 95 (1954) 577–578.

[140] K. J. Eskola, K. Kajantie and J. Lindfors, Quark and Gluon Production in High-Energy Nucleus-Nucleus Collisions, *Nucl. Phys. B* 323 (1989) 37–52.

[141] Spencer R. Klein, Joakim Nystrand, Janet Seger, Yuri Gorbunov and Joey Butterworth, STARlight: A Monte Carlo simulation program for ultra-peripheral collisions of relativistic ions, *Comput. Phys. Commun.* 212 (2017) 258–268, arXiv: 1607.03838 [hep-ph].

[142] M. Vidovic, M. Greiner, C. Best and G. Soff, Impact parameter dependence of the electromagnetic particle production in ultrarelativistic heavy ion collisions, *Phys. Rev. C* 47 (1993) 2308–2319.

[143] V. Guzey and M. Zhalov, Rapidity and momentum transfer distributions of coherent J/ψ photoproduction in ultraperipheral pPb collisions at the LHC, *JHEP* 02 (2014) 046, arXiv: 1307.6689 [hep-ph].

[144] Wojciech Florkowski, *Phenomenology of Ultra-Relativistic Heavy-Ion Collisions*, Mar. 2010, ISBN: 978-981-4280-66-2.

[145] C. Patrignani et al., Review of Particle Physics, *Chin. Phys. C* 40, no.10 (2016) 100001.

[146] Adeola Adeluyi and C. A. Bertulani, Constraining Gluon Shadowing Using Photoproduction in Ultraperipheral pA and AA Collisions, *Phys. Rev. C* 85 (2012) 044904, arXiv: 1201.0146 [nucl-th].

[147] John David Jackson, *Classical Electrodynamics*, Wiley, 1998, ISBN: 978-0-471-30932-1.

[148] V. Guzey and M. Klasen, Diffractive dijet photoproduction in ultraperipheral collisions at the LHC in next-to-leading order QCD, *JHEP* 04 (2016) 158, arXiv: 1603.06055 [hep-ph].

[149] W. Zha, L. Ruan, Z. Tang, Z. Xu and S. Yang, Coherent lepton pair production in hadronic heavy ion collisions, *Phys. Lett. B* 781 (2018) 182–186, arXiv: 1804.01813 [hep-ph].

[150] Mark Galassi, Jim Davies, James Theiler, Brian Gough and Gerard Jungman, *GNU Scientific Library - Reference Manual, Third Edition, for GSL Version 1.12 (3. ed.)*. Jan. 2009, ISBN: 978-0-9546120-7-8.

[151] Andy Buckley et al., LHAPDF6: parton density access in the LHC precision era, *Eur. Phys. J. C* 75 (2015) 132, arXiv: 1412.7420 [hep-ph].

[152] Sayipjamal Dulat et al., New parton distribution functions from a global analysis of quantum chromodynamics, *Phys. Rev. D* 93, no.3 (2016) 033006, arXiv: 1506.07443 [hep-ph].

[153] E. Abbas et al., Charmonium and e^+e^- pair photoproduction at mid-rapidity in ultra-peripheral Pb-Pb collisions at $\sqrt{s_{\rm NN}}$=2.76 TeV, *Eur. Phys. J. C* 73, no.11 (2013) 2617, arXiv: 1305.1467 [nucl-ex].

[154] Betty Abelev et al., Coherent J/ψ photoproduction in ultra-peripheral Pb-Pb collisions at $\sqrt{s_{NN}} = 2.76$ TeV, *Phys. Lett. B* 718 (2013) 1273–1283, arXiv: 1209.3715 [nucl-ex].

[155] A. Kusina et al., Impact of LHC vector boson production in heavy ion collisions on strange PDFs, *Eur. Phys. J. C* 80, no.10 (2020) 968, arXiv: 2007.09100 [hep-ph].

[156] J. Pumplin et al., New generation of parton distributions with uncertainties from global QCD analysis, *JHEP* 07 (2002) 012, arXiv: hep-ph/0201195.

[157] Daniel Stump et al., Inclusive jet production, parton distributions, and the search for new physics, *JHEP* 10 (2003) 046, arXiv: hep-ph/0303013.

[158] Hung-Liang Lai et al., New parton distributions for collider physics, *Phys. Rev. D* 82 (2010) 074024, arXiv: 1007.2241 [hep-ph].

[159] Tie-Jiun Hou et al., Progress in the CTEQ-TEA NNLO global QCD analysis (Aug. 2019), arXiv: 1908.11394 [hep-ph].

[160] Tuomas Lappi, Heikki Mäntysaari and Jani Penttala, Relativistic corrections to the vector meson light front wave function, *Phys. Rev. D* 102, no.5 (2020) 054020, arXiv: 2006.02830 [hep-ph].

[161] Heikki Mäntysaari and Jani Penttala, Exclusive production of light vector mesons at next-to-leading order in the dipole picture, *Phys. Rev. D* 105, no.11 (2022) 114038, arXiv: 2203.16911 [hep-ph].

[162] C. Adloff et al., Elastic photoproduction of J/ψ and Υ mesons at HERA, *Phys. Lett. B* 483 (2000) 23–35, arXiv: hep-ex/0003020.

[163] S. Chekanov et al., Exclusive photoproduction of J/ψ mesons at HERA, *Eur. Phys. J. C* 24 (2002) 345–360, arXiv: hep-ex/0201043.

[164] V. Guzey, M. Strikman and M. Zhalov, Accessing transverse nucleon and gluon distributions in heavy nuclei using coherent vector meson photoproduction at high energies in ion ultraperipheral collisions, *Phys. Rev. C* 95, no.2 (2017) 025204, arXiv: 1611.05471 [hep-ph].

[165] Z. Citron et al., Report from Working Group 5: Future physics opportunities for high-density QCD at the LHC with heavy-ion and proton beams, *CERN Yellow Rep. Monogr.* 7 (2019), edited by Andrea Dainese et al. 1159–1410, arXiv: 1812.06772 [hep-ph].

[166] Jasmine Brewer, Aleksas Mazeliauskas and Wilke van der Schee, Opportunities of OO and pO collisions at the LHC, *Opportunities of OO and pO collisions at the LHC*, arXiv: 2103.01939 [hep-ph].

[167] Jasmine Brewer, Alexander Huss, Aleksas Mazeliauskas and Wilke van der Schee, Ratios of jet and hadron spectra at LHC energies: Measuring high-pT suppression without a pp reference, *Phys. Rev. D* 105, no.7 (2022) 074040, arXiv: 2108.13434 [hep-ph].

[168] A. G. Shuvaev, Krzysztof J. Golec-Biernat, Alan D. Martin and M. G. Ryskin, Off diagonal distributions fixed by diagonal partons at small x and xi, *Phys. Rev. D* 60 (1999) 014015, arXiv: hep-ph/9902410.

[169] A. Shuvaev, Solution of the off forward leading logarithmic evolution equation based on the Gegenbauer moments inversion, *Phys. Rev. D* 60 (1999) 116005, arXiv: hep-ph/9902318.

[170] J. Breitweg et al., Measurement of elastic Υ photoproduction at HERA, *Phys. Lett. B* 437 (1998) 432–444, arXiv: hep-ex/9807020.

[171] Roel Aaij et al., Measurement of the exclusive Υ production cross-section in pp collisions at $\sqrt{s} = 7$ TeV and 8 TeV, *JHEP* 09 (2015) 084, arXiv: 1505.08139 [hep-ex].

[172] A. M. Sirunyan et al., Measurement of exclusive Υ photoproduction from protons in pPb collisions at $\sqrt{s_{\mathrm{NN}}} = 5.02$ TeV, *Eur. Phys. J. C* 79, no.3 (2019), [Erratum: Eur.Phys.J.C 82, 343 (2022)] 277, arXiv: 1809.11080 [hep-ex].

ORIGINAL PAPERS

[PI]

EXCLUSIVE J/ψ PHOTOPRODUCTION IN ULTRAPERIPHERAL Pb+Pb COLLISIONS AT THE CERN LARGE HADRON COLLIDER CALCULATED AT NEXT-TO-LEADING ORDER PERTURBATIVE QCD

by

Kari J. Eskola, Christopher A. Flett, Vadim Guzey, Topi Löytäinen and Hannu Paukkunen,

Phys. Rev. C. 106 **no.3**, 035202, arXiv: 2203.11613 [hep-ph] (Mar. 2022).

Exclusive J/ψ photoproduction in ultraperipheral Pb+Pb collisions at the CERN Large Hadron Collider calculated at next-to-leading order perturbative QCD

K. J. Eskola, C. A. Flett, V. Guzey, T. Löytäinen,* and H. Paukkunen

University of Jyvaskyla, Department of Physics, P.O. Box 35, FI-40014 University of Jyvaskyla, Finland and Helsinki Institute of Physics, P.O. Box 64, FI-00014 University of Helsinki, Finland

(Received 31 March 2022; accepted 12 August 2022; published 15 September 2022)

We present the first next-to-leading-order (NLO) perturbative QCD (pQCD) study of rapidity-differential cross sections of coherent exclusive photoproduction of J/ψ mesons in heavy-ion ultraperipheral collisions (UPCs) at the CERN Large Hadron Collider (LHC), $d\sigma/dy(\mathrm{Pb}+\mathrm{Pb}\to\mathrm{Pb}+J/\psi+\mathrm{Pb})$. For this, we account for the photon-nucleon NLO cross sections at the forward limit, the t dependence using a standard nuclear form factor, and the photon fluxes of the colliding nuclei. Approximating the generalized parton distributions with their forward-limit parton distribution functions (PDFs), we quantify the NLO contributions in the cross sections, show that the real part of the amplitude and quark-PDF contributions must not be neglected, quantify the uncertainties arising from the scale choice and PDFs, and compare our results with ALICE, CMS, and LHCb J/ψ photoproduction data in Pb + Pb UPCs, exclusive J/ψ photoproduction data from HERA, and LHCb data in $p+p$. The scale dependence in $d\sigma/dy(\mathrm{Pb}+\mathrm{Pb}\to\mathrm{Pb}+J/\psi+\mathrm{Pb})$ is significant, but we can find a scale choice that reproduces the Pb + Pb UPC data at both 2.76 and 5.02 TeV collision energies. This process has traditionally been suggested to be a direct probe of nuclear gluon distributions. We show that the situation changes rather dramatically from LO to NLO: the NLO cross sections reflect the nuclear effects of both gluons and quarks in a complicated manner, where the relative signs of the LO and NLO terms in the amplitude play a significant role.

DOI: 10.1103/PhysRevC.106.035202

I. INTRODUCTION

Ultraperipheral collisions (UPCs) are collisions of hadrons or nuclei which take place at large impact parameters in such a way that only the electromagnetic field of one of the colliding particles interacts with the other particle [1–3]. Coherent photoproduction of J/ψ heavy vector mesons in UPCs of lead nuclei at the CERN Large Hadron Collider (LHC), the exclusive process $\mathrm{Pb}+\mathrm{Pb}\to\mathrm{Pb}+J/\psi+\mathrm{Pb}$, has been suggested to be an efficient direct probe of collinear nuclear gluon distributions, $g_{\mathrm{Pb}}(x,Q^2)$, at factorization scales of the order of the vector-meson mass, $Q^2=\mathcal{O}(M_V^2)$, and small longitudinal-momentum fractions $x=\mathcal{O}(M_V^2/W^2)$, where W is the photon-nucleon center-of-momentum-system (c.m.s.) energy [4–11]. This exciting possibility derives from the fact that in such an exclusive process of no hadronic activity, one of the colliding nuclei serves as a source of equivalent real Weizsäcker-Williams photons which probe a color-singlet gluon- or quark-initiated ladder from the other nucleus via formation of a heavy quark-antiquark pair. As first discussed by Ryskin in Ref. [12] in the context of the free-proton process $\gamma+p\to J/\psi+p$, in the leading order (LO) perturbative QCD (pQCD) only the gluon-ladder processes contribute, and, neglecting the longitudinal-momentum imbalance (skewedness) in the ladder and the subleading real part of the amplitude, the forward scattering amplitude factorizes into a calculable hard part and $g_p(x,Q^2)$. Thus the cross section of J/ψ becomes proportional to $[g_p(x,Q^2)]^2$, making the process a very promising one for probing the gluon distribution. This idea has then been transferred to ultraperipheral nucleus-nucleus collisions (UPCs) in, e.g., Refs. [4,5]. Also Monte Carlo event simulations of this process in the UPCs have been developed, such as STARLIGHT [13] and SUPERCHIC [14]. Exclusive photoproduction of J/ψ has also been widely studied in the dipole picture, especially in the high-energy color-glass-condensate approximation of QCD; see, e.g., Refs. [15–25].

With the experimental data being released from the LHC, the situation is becoming ever more interesting. First, the exclusive coherent J/ψ photoproduction cross sections involving real photons have been measured in electron-proton collisions at the DESY-HERA collider by the H1 [26] and ZEUS [27] Collaborations, and extracted also from the LHCb measurements of the process $p+p\to p+J/\psi+p$ at the LHC [28,29]. For detailed next-to-leading order (NLO) pQCD studies of these, see, e.g., Refs. [30–35]. From the viewpoint of the UPCs, these data sets offer also an importantly

*topi.m.o.loytainen@jyu.fi

long lever arm in the photon-proton c.m.s. energy W for cross-checking the pQCD calculations and understanding the necessary modeling input. Secondly, in Pb + Pb UPCs at the LHC, the ALICE Collaboration has measured the rapidity-differential cross section of Pb + Pb → Pb + J/ψ + Pb both at midrapidity [36,37] and at forward/backward rapidities [38,39] at nucleon-nucleon c.m.s. energies $\sqrt{s_{NN}} =$ 5.02 and 2.76 TeV. The CMS Collaboration has performed the corresponding measurement at $\sqrt{s_{NN}} = 2.76$ TeV in one off-central rapidity bin that lies conveniently just between the ALICE rapidity bins [40]. The LHCb Collaboration recently released their 5.02 TeV data at forward/backward rapidities [41], overlapping with the ALICE rapidity region. Very interestingly, however, the ALICE and LHCb forward/backward-rapidity 5.02 TeV data sets do not seem to be fully compatible with each other, which clearly calls for further analyses.[1]

Until now, exclusive J/ψ photoproduction in ultraperipheral nuclear collisions has been studied only to LO pQCD. Now that the LHC experiments are measuring these cross sections to an increasing accuracy, and hopefully also for other UPC systems than Pb + Pb in the future [43], it is clearly of high priority to extend the theory calculations to NLO pQCD. In particular we wish to study whether/how this process could be included in the global analyses of nuclear PDFs, such as in Refs. [44–48], in the future. These are the main motivations for our present NLO study. Also interestingly, so far the LO pQCD, or dipole picture, calculations have not been able to reproduce simultaneously the midrapidity and forward/backward-rapidity data; see, e.g., [36]. This, together with the mentioned incompatibility between the LHCb and ALICE data, serves also as further motivation for our current NLO pQCD study.

The NLO pQCD calculation of cross sections for exclusive photoproduction of heavy vector mesons V off the free proton, $\sigma(\gamma + p \to V + p)$, using collinear factorization at the amplitude level, was performed first by Ivanov *et al.* in Ref. [30], followed then by other groups in Refs. [31,35,49–51]. To be exact, collinear factorization here refers to the factorization of the amplitude to calculable NLO pQCD pieces and to the generalized parton distributions (GPDs) [52] which at the forward limit relax into the usual PDFs [53]. If such a limit is not assumed, then the GPDs have to be modeled in some way, e.g., as suggested in Refs. [54–61]. As shown already in Ref. [30], the full NLO calculation of coherent exclusive photoproduction of J/ψ mesons in $\gamma + p$ collisions, which includes both the imaginary and real parts of the amplitude precisely as they are, and assumes a certain model for the gluon and quark GPDs [56], depends rather heavily on the choice of the renormalization/factorization scale, $Q = \mathcal{O}(M_{J/\psi})$, while for the photoproduction of Υ mesons, which probes a higher scale $Q = \mathcal{O}(M_\Upsilon)$, the situation improves somewhat. Discussion of a systematic procedure for diminishing the scale dependence in the NLO calculation of exclusive J/ψ photoproduction in $\gamma + p$ collisions can be found in [32–35], but in the present exploratory NLO study for the nuclear UPCs we do not follow this avenue.

In the current paper, we present the first NLO pQCD study of exclusive photoproduction of J/ψ mesons in ultraperipheral Pb + Pb collisions at the LHC, with collinear factorization at the amplitude level. Exploiting the analytic results of the impressive calculation of Ref. [30], we have built a numerical code of our own for the rapidity-differential J/ψ photoproduction UPC cross sections, $d\sigma/dy$(Pb + Pb → Pb + J/ψ + Pb). These consist of a rather nontrivial numerical evaluation of the differential NLO forward photoproduction cross sections $d\sigma/dt(\gamma + \text{Pb} \to J/\psi + \text{Pb})$ at vanishing Mandelstam variable t based on Ref. [30], supplemented with a straightforward computation of the nuclear form factor to account for the t dependence of the cross section, as well as a nontrivial numerical evaluation of the photon fluxes from the colliding lead nuclei based on Refs. [62,63]. In the current exploratory NLO study we adopt the simplest possible, forward-limit, approximation for the GPDs where they become just the usual PDFs. With such a "bare bones" GPD/PDF NLO framework, our goal is to test as transparently as possible, and without any additional normalization factors (which typically appear in LO studies) or modeling, how directly and efficiently the exclusive photoproduction of J/ψ mesons in Pb + Pb UPCs at the LHC actually probes the nuclear gluon distributions.

In what follows, we will first chart the scale dependence of the NLO cross sections, and compare the situation with the LO case, too. Even though the scale dependence of the NLO cross sections is known to be quite strong [30], we will show that, interestingly, a reasonable "optimal" scale choice can be found, with which we can, perhaps contrary to our initial expectations, simultaneously reproduce the 5.02 TeV ALICE midrapidity [36] and the LHCb forward-rapidity [41] data, and also the 2.76 TeV ALICE [37,39] and CMS [40] data. We will also study the corresponding NLO cross sections in photon-proton collisions, as well as their scale dependence, against the HERA and LHCb data.

We will also break down the NLO calculation into the contributions from the imaginary and real parts, as well from the gluon and quark PDFs, and show (in accordance with Ref. [30]) that the real part of the amplitude as well as the quark contributions both have a sizable contribution and hence must not be neglected. This result indicates that, contrary to what is often claimed based on the LO results, exclusive J/ψ photoproduction in UPCs is not as direct a probe of the gluon distributions as perhaps previously thought. We will chart, by comparing the predictions obtained with the EPPS16 [45] nuclear PDFs and CT14NLO free proton PDFs [64], and nCTEQ15 [44] and nNNPDF2.0 [46] nuclear PDFs, how the gluon and quark PDFs manifest themselves in the J/ψ photoproduction UPC cross sections at different rapidities. In particular, using EPPS16, we will show that the manifestation of the nuclear effects is nontrivial and influenced especially by the relative signs of the different contributions in the amplitude. Finally, as one of the main goals of the paper, we will study how the uncertainties of the nuclear and free-proton PDFs propagate into the J/ψ photoproduction UPC cross sections.

[1]New LHCb data [42] have appeared after the completion of the current paper.

The rest of this paper will proceed as follows: To make our study more accessible especially for the heavy-ion community and non-GPD-experts in general, we will recapitulate the theoretical NLO framework with collinear factorization and GPDs/PDFs in Sec. II. Also the calculation of the photon fluxes and evaluation of the necessary nuclear form factors are presented there. The main results of the paper, the numerical evaluation of the coherent exclusive J/ψ photoproduction cross sections in Pb + Pb UPCs at the LHC, their analysis, and comparison with the experimental data, are presented in Sec. III. Finally, a discussion and outlook are given in Sec. IV.

II. THEORETICAL FRAMEWORK

A. Differential cross section

In this section, we recapitulate the theoretical framework we use in our calculations for the exclusive process

$$A_1(p_1) + A_2(p_2) \to A_1(p_1') + V(p_3') + A_2(p_2'),$$

where $A_{1,2}$ denote the colliding nuclei and V is some vector meson (in this paper $V = J/\psi$). The initial-state momenta are labeled by p_i and the final-state momenta by p_i'. Within the equivalent-photon (Weizsäcker-Williams) approximation [3,65,66], the total cross section can be expressed as

$$\sigma^{A_1A_2\to A_1VA_2} = \int dk^+ \frac{dN_\gamma^{A_1}(k^+)}{dk^+}\sigma^{\gamma(k^+)A_2\to VA_2} + \int dk^- \frac{dN_\gamma^{A_2}(k^-)}{dk^-}\sigma^{A_1\gamma(k^-)\to A_1V}, \quad (1)$$

where $dN_\gamma^{A_i}(k)/dk$ is the centrality-integrated distribution (or flux) of photons from the nucleus A_i as a function of photon energy k, and $\sigma^{\gamma(k^+)A_2\to VA_2}$ and $\sigma^{A_1\gamma(k^-)\to VA_1}$ are the cross sections for the photoproduction processes

$$\gamma(k_1) + A_2(p_2) \to V(p_3') + A_2(p_2'),$$
$$A_1(p_1) + \gamma(k_2) \to A_1(p_1') + V(p_3').$$

In the equivalent-photon approximation the photon momenta $k_{1,2}$ are considered to be collinear with colliding nuclei, and $|\boldsymbol{k}_{1,2}| = k^\pm$, where the boldface denotes a three-vector. The experimental data in Pb-Pb collisions [36,38,40,41] are differential with respect to the rapidity y of the vector meson. At fixed rapidity and transverse momentum p_T of produced vector meson, the photon energy can be expressed as

$$k^\pm = \frac{M_V^2 - t}{2M_\mathrm{T}e^{\mp y}}, \quad (2)$$

where t refers to the square of the momentum transferred to the target nucleus, $t = (k_{1,2} - p_3')^2$, and $M_\mathrm{T} = \sqrt{M_V^2 + p_\mathrm{T}^2}$ is the transverse mass. In the typical case $|t| \ll M_V^2$ and $p_\mathrm{T}^2 \ll M_V^2$ (see, e.g., Ref. [67]) so that to a very good approximation

$$k^\pm \approx \frac{M_V e^{\pm y}}{2}. \quad (3)$$

It then follows that

$$\frac{d\sigma^{A_1A_2\to A_1VA_2}}{dy} = \left[k\frac{dN_\gamma^{A_1}(k)}{dk}\sigma^{\gamma(k)A_2\to VA_2}\right]_{k=k^+} + \left[k\frac{dN_\gamma^{A_2}(k)}{dk}\sigma^{A_1\gamma(k)\to A_1V}\right]_{k=k^-}. \quad (4)$$

Finally, we note that Eq. (4) above neglects the interference between the amplitudes where the photons are emitted by different nuclei. As discussed in [68] for heavy-ion collisions and in [69] for $p + p$ and $p + \bar{p}$, however, such interference becomes important only at the very smallest values of t and can thus be safely neglected when considering the t-integrated cross sections as we do here.

B. Photoproduction cross section

We will assume that the invariant matrix element $\mathcal{M}^{\gamma A\to VA}$ for the photoproduction process can be factored into two parts, the matrix element evaluated at $t = 0$ and a nuclear form factor $F_A(t)$ (also called the two-gluon form factor [12]) [70],

$$\mathcal{M}^{\gamma A\to VA}(W, t) = \mathcal{M}_A^{\gamma N\to VN}(W, 0)F_A(t), \quad (5)$$

where N labels a bound nucleon and W is the c.m.s. energy of the photon-nucleon collision. It follows that the photoproduction cross section then becomes

$$\sigma^{\gamma A\to VA}(W) = \left.\frac{d\sigma_A^{\gamma N\to VN}}{dt}\right|_{t=0}\int_{t_\mathrm{min}}^\infty dt'|F_A(-t')|^2, \quad (6)$$

$$\frac{d\sigma_A^{\gamma N\to VN}}{dt} = \frac{\overline{|\mathcal{M}_A^{\gamma N\to VN}|^2}}{16\pi W^4}, \quad (7)$$

where $\overline{|\mathcal{M}_A^{\gamma N\to VN}|^2}$ is the square of the per-nucleon matrix element averaged (summed) over the initial-state (final-state) polarizations. The minimum momentum transfer squared is given by $t_\mathrm{min} = [M_V^2/(4k\gamma_\mathrm{L})]^2$, where γ_L is the Lorentz factor, which is approximately 1500 for Pb + Pb collisions at nucleon-nucleon c.m.s. energy $\sqrt{s_{NN}} = 2.76$ TeV and approximately 2700 for Pb + Pb collisions at nucleon-nucleon c.m.s. energy $\sqrt{s_{NN}} = 5.02$ TeV. We model the form factor as the Fourier transform of the Woods-Saxon distribution [71],

$$F_A(t) = \int d^3r\rho_A(r)e^{i\boldsymbol{q}\cdot\boldsymbol{r}}, \quad (8)$$

$$\rho_A(r) = \frac{\rho_0}{1 + e^{\frac{r-R_A}{d}}}, \quad (9)$$

taking $|\boldsymbol{q}| = \sqrt{|t|}$. We take $d = 0.546$ fm [72] for the skin depth and for the nucleus radius R_A we use the parametrization (see, e.g., [73]),

$$R_A/\mathrm{fm} = 1.12 \times A^{1/3} - 0.86 \times A^{-1/3}. \quad (10)$$

The normalization ρ_0 is fixed by requiring that $F_A(0) = A$.

When considering the $\gamma + p$ collisions we take the photoproduction cross section to be of the form [30]

$$\sigma^{\gamma p\to Vp}(W) = \left.\frac{d\sigma^{\gamma p\to Vp}}{dt}\right|_{t=0}\int_0^\infty dt' e^{-bt'} \quad (11)$$

with [35],

$$b/\mathrm{GeV}^{-2} = 4.9 + 4\alpha'_P \ln\left(\frac{W}{W_0}\right), \tag{12}$$

where $W_0 = 90$ GeV and $\alpha'_P = 0.06$. This parametrization grows more slowly with W than that in Ref. [74], but is still compatible with the HERA data for exclusive J/ψ photoproduction. We have chosen the slope parameter α'_P to be compatible with Model 4 of [75], which fits a wider variety of elastic pp data.

C. Photoproduction amplitude

The NLO expressions for the matrix element $\mathcal{M}_A^{\gamma N\to VN}(W,t)$ for photoproduction are well established in the literature [30,76] and the more recent electroproduction results [35,50,51] coincide with these in the limit of an on-shell photon. In these calculations the vector meson is considered as a composite particle of two heavy quarks in the nonrelativistic approximation with zero relative velocity [77–80]. The invariant matrix element can be written as

$$\begin{aligned}\mathcal{M}_A^{\gamma N\to VN} &= \frac{4\pi\sqrt{4\pi\alpha_{\mathrm{QED}}}e_Q(\varepsilon_V^*\cdot\varepsilon_\gamma)}{3\xi}\sqrt{\frac{\langle O_1\rangle_V}{m_Q^3}}I(\xi,t)\\ &= \frac{C}{\xi}I(\xi,t),\end{aligned} \tag{13}$$

where α_{QED} is the fine-structure constant, m_Q the mass of the heavy quark, e_Q the fractional charge of the heavy quark, ε_V the polarization vector of the produced vector meson, ε_γ the polarization vector of the incoming photon, and $\langle O_1\rangle_V$ is a nonrelativistic QCD matrix element associated with the vector meson. Equation (13) defines the factor C which we will use later. The value of $\langle O_1\rangle_V$ is solved from the NLO expression for the vector-meson leptonic decay width [30,81–83],

$$\Gamma(V\to l^+l^-) = \frac{2e_Q^2\pi\alpha_{\mathrm{QED}}^2}{3}\frac{\langle O_1\rangle_V}{m_Q^2}\left[1-\frac{8\alpha_s(\mu_R)}{3\pi}\right]^2, \tag{14}$$

where $\alpha_s(\mu_R)$ is the QCD coupling at a renormalization scale μ_R. The variable ξ that appears in Ji's parametrization of momenta [84] is the so-called skewedness parameter. In the $t \ll M_V^2$ limit,

$$\xi = \frac{\zeta}{2-\zeta}, \quad \text{where } \zeta = \left(\frac{M_V}{W}\right)^2. \tag{15}$$

The function $I(\xi,t)$ is given by

$$\begin{aligned}I(\xi,t) = \int_{-1}^{1} dx[&T_g(x,\xi)F^g(x,\xi,t,\mu_F)\\ &+ T_q(x,\xi)F^{q,S}(x,\xi,t,\mu_F)],\end{aligned} \tag{16}$$

where $T_g(x,\xi)$ and $T_q(x,\xi)$ are the hard-scattering coefficient functions corresponding to gluon and quark contributions [30],

$$\begin{aligned}T_g(x,\xi) &= \frac{\xi}{(x-\xi+i\epsilon)(x+\xi-i\epsilon)}\\ &\quad\times\left[\alpha_s(\mu_R)+\frac{\alpha_s^2(\mu_R)}{4\pi}f_g\left(\frac{x-\xi+i\epsilon}{2\xi}\right)\right],\\ T_q(x,\xi) &= \frac{2\alpha_s^2(\mu_R)}{3\pi}f_q\left(\frac{x-\xi+i\epsilon}{2\xi}\right).\end{aligned} \tag{17}$$

Here the term proportional to $\alpha_s(\mu_R)$ in T_g is the purely gluonic LO contribution and the rest in T_g and the whole T_q constitute the NLO contributions. The exact forms of the functions f_g and f_q are given in Refs. [30,35,76] and we will be using specifically those of Ref. [30]. The parameter ϵ is positive and the function $I(\xi,t)$ is understood to be evaluated in the limit $\epsilon\to 0$. Finally, $F^g(x,\xi,t,\mu_F)$ is the gluon GPD and $F^{q,S}(x,\xi,t,\mu_F)$ is the quark singlet GPD given by

$$F^{q,S}(x,\xi,t,\mu_F) = \sum_{q=u,d,s,c} F^q(x,\xi,t,\mu_F), \tag{18}$$

where μ_F denotes the factorization scale. As we will consider factorization scales above the charm mass threshold, also the charm quarks are included in the above sum in conjunction with GPDs/PDFs defined in variable-flavor-number schemes. As indicated in Eq. (6), we will calculate the amplitude in the approximation in which $t = 0$. In addition, in the current exploratory study we will approximate the GPDs by their values at $\xi = 0$ so that we effectively replace the GPDs with PDFs,

$$\begin{aligned}F^g(x,0,0,\mu_F) &= F^g(-x,0,0,\mu_F) = xg(x,\mu_F),\\ F^q(x,0,0,\mu_F) &= q(x,\mu_F),\\ F^q(-x,0,0,\mu_F) &= -\bar{q}(x,\mu_F),\end{aligned} \tag{19}$$

where $x\in[0,1]$, and $g(x,\mu_F)$ and $q(x,\mu_F)$ are the gluon and quark PDFs. In the cross sections computed here the scale uncertainties will be much larger than the expected effects from a detailed GPD modeling presented, e.g., in Refs. [54–61]. Therefore, we leave the inclusion of the GPD modeling as future work. As long as the value of ξ remains sufficiently small (as it does here[2]), the DGLAP (Dokshitzer-Gribov-Lipatov-Altarelli-Parisi) region $|x|>\xi$ dominates the x integral of Eq. (16) and the above approximation provides a reasonable baseline. In the ERBL (Efremov-Radyushkin-Brodsky-Lepage) region $|x|<\xi$, which contributes only in the subleading real part of the amplitude, the GPDs can be expected to deviate more from the PDFs especially towards the smallest x [56,61]. The largest contribution in the real part comes, however, from the region near $x=\xi$ where the ERBL-region GPDs connect continuously to the DGLAP-region ones, and hence Eq. (19) again offers a relevant starting point for the present first study.

[2]For example, $\xi(y=0)\approx 3.1\times 10^{-4}$ and $\xi(y=4)\approx 5.6\times 10^{-6}$ (1.7×10^{-2}) for W^+ (W^-) at $\sqrt{s_{NN}} = 5.02$ TeV.

The differential cross section can then be written as

$$\left.\frac{d\sigma^{\gamma N\to VN}}{dt}\right|_{t=0} = \frac{\overline{\left|\mathcal{M}_A^{\gamma N\to VN}\right|^2}}{16\pi W^4} = \frac{1}{W^4}\frac{4\pi^2\alpha_{\rm QED}e_Q^2}{9\xi^2}\left(\frac{\langle O_1\rangle_V}{m_Q^3}\right)|I(\xi,t=0)|^2, \tag{20}$$

where

$$|I(\xi,t=0)|^2 = \left|\int_0^1 dx\left[2xg(x,\mu_F)T_g(x,\xi) + T_q(x,\xi)\sum_q\left[q(x,\mu_F)+\bar{q}(x,\mu_F)\right]\right]\right|^2. \tag{21}$$

We take all constants, such as the mass and the decay width of the J/ψ, from the Particle Data Group listing [85]. The value of $\alpha_s(\mu_R)$ is taken from the LHAPDF interface [86] so that the coupling is taken consistently to be the same as the one used in defining the PDF values. The QED coupling, $\alpha_{\rm QED}$, is evaluated throughout the work up to one loop accuracy. In our framework, following Ref. [30], we explicitly set $M_V = 2m_Q$, which is an inherent assumption in our nonrelativistic approximation of the J/ψ wave function. In the square of the integral $|I|^2$ we consistently include both the real part and the imaginary part in the results. The integrals in Eq. (21) are evaluated numerically by keeping the parameter ϵ finite but small enough so that the results are independent of its exact value. We have cross-checked our numerical implementation against the method used in Ref. [35]. The factorization and renormalization scales are taken to be equal, $\mu = \mu_F = \mu_R$, and we consider scale variation between $\mu \in [m_Q, 2m_Q]$.

D. Photon flux

The number of equivalent photons of energy k at a fixed transverse distance $b = |\vec{b}|$ from the center of a nucleus A with Z protons can be written as [3,13,62,63]

$$N_\gamma^A(k,\vec{b}) = \frac{Z^2\alpha_{\rm QED}}{\pi^2}\left|\int_0^\infty dk_\perp \frac{k_\perp^2 F(k_\perp^2+k^2/\gamma_L^2)}{k_\perp^2+k^2/\gamma_L^2}J_1(bk_\perp)\right|^2, \tag{22}$$

where F is the Fourier transform of the form factor in Eq. (8) normalized to 1, $F(q) = F_A(q)/A$, and J_1 is the cylindrical modified Bessel function of the first kind. To obtain the minimum-bias flux appearing in the expression for the cross sections, e.g., in Eq. (1), we integrate over the entire impact-parameter plane multiplying $N_\gamma^A(k,\vec{b})$ by the Glauber-type probability [87] of having no hadronic interaction,

$$k\frac{dN_\gamma^A(k)}{dk} = \int d^2\vec{b}N_\gamma^A(k,\vec{b})\Gamma_{AA}(\vec{b}), \tag{23}$$

$$\Gamma_{AA}(\vec{b}) = \exp[-\sigma_{NN}(s)T_{AA}(\vec{b})], \tag{24}$$

where $\sigma_{NN}(s)$ is the total (elastic + inelastic) hadronic nucleon-nucleon cross section for which we use 90 (80) mb at $\sqrt{s_{NN}} = 5.02$ (2.76) TeV [85], and $T_{AA}(\vec{b})$ is the nuclear overlap function

$$T_{AA}(\vec{b}) = \int d^2\vec{b}_1 T_A(\vec{b}_1)T_A(\vec{b}-\vec{b}_1), \tag{25}$$

where $T_A(\vec{b})$ is the nuclear thickness function,

$$T_A(\vec{b}) = \int_{-\infty}^{\infty} dz\,\rho_A(r), \tag{26}$$

with $r^2 = z^2 + \vec{b}^2$ and z being the longitudinal coordinate. The integrand in Eq. (23) oscillates very rapidly at large values of b, and to improve the convergence we follow Ref. [88] by making use of the flux of photons from a point-like particle. In this case one takes the nuclear density to be a delta function, $\rho^{\rm pl}(\mathbf{r}) = \delta^3(\mathbf{r})$, which leads to [5,89]

$$N_{\gamma/Z}^{\rm pl}(k,\vec{b}) = \frac{Z^2\alpha_{\rm QED}}{\pi^2}\frac{k^2}{\gamma_L^2}\left(K_1^2(\zeta_R)+\frac{1}{\gamma_L^2}K_0^2(\zeta_R)\right), \tag{27}$$

where K_0 and K_1 are modified Bessel functions of the second kind, and

$$\zeta_R = \frac{kb}{\gamma_L}. \tag{28}$$

The integral over the impact-parameter plane with a condition $|\vec{b}| > b_{\rm min}$ is also well known [90],

$$\left.k\frac{dN_{\gamma/Z}^{\rm pl}(k)}{dk}\right|_{b_{\rm min}} = \int_{b_{\rm min}}^\infty d^2\vec{b}N_{\gamma/Z}^{\rm pl}(k,\vec{b}) = \frac{2Z^2\alpha_{\rm QED}}{\pi}\left[\zeta_R K_0(\zeta_R)K_1(\zeta_R) - \frac{\zeta_R^2}{2}\left[K_1^2(\zeta_R)-K_0^2(\zeta_R)\right]\right]_{b=b_{\rm min}}. \tag{29}$$

We now rewrite Eq. (23) by adding and subtracting the flux of photons from a pointlike particle,

$$\begin{aligned} k\frac{dN_\gamma^A(k)}{dk} &= \int d^2\vec{b}N_\gamma^A(k,\vec{b})\Gamma_{AA}(\vec{b}) + \left.k\frac{dN_{\gamma/Z}^{\rm pl}(k)}{dk}\right|_{b_{\rm min}} - \left.k\frac{dN_{\gamma/Z}^{\rm pl}(k)}{dk}\right|_{b_{\rm min}} \\ &= \left.k\frac{dN_{\gamma/Z}^{\rm pl}(k)}{dk}\right|_{b_{\rm min}} + \int_0^{b_{\rm min}} d^2\vec{b}\,N_\gamma^A(k,\vec{b})\Gamma_{AA}(\vec{b}) + \int_{b_{\rm min}}^\infty d^2\vec{b}\left[N_\gamma^A(k,\vec{b})\Gamma_{AA}(\vec{b}) - N_{\gamma/Z}^{\rm pl}(k,\vec{b})\right]. \end{aligned} \tag{30}$$

By taking $b_{\rm min} = 30$ fm or higher, the last term will be negligible. Differences between this result and the point-like approximation have been studied, e.g., in Refs. [3,88].

III. RESULTS

A. Absolute magnitude and scale sensitivity of cross sections

First, we chart the uncertainty arising from the choice of the factorization/renormalization scale in the exclusive

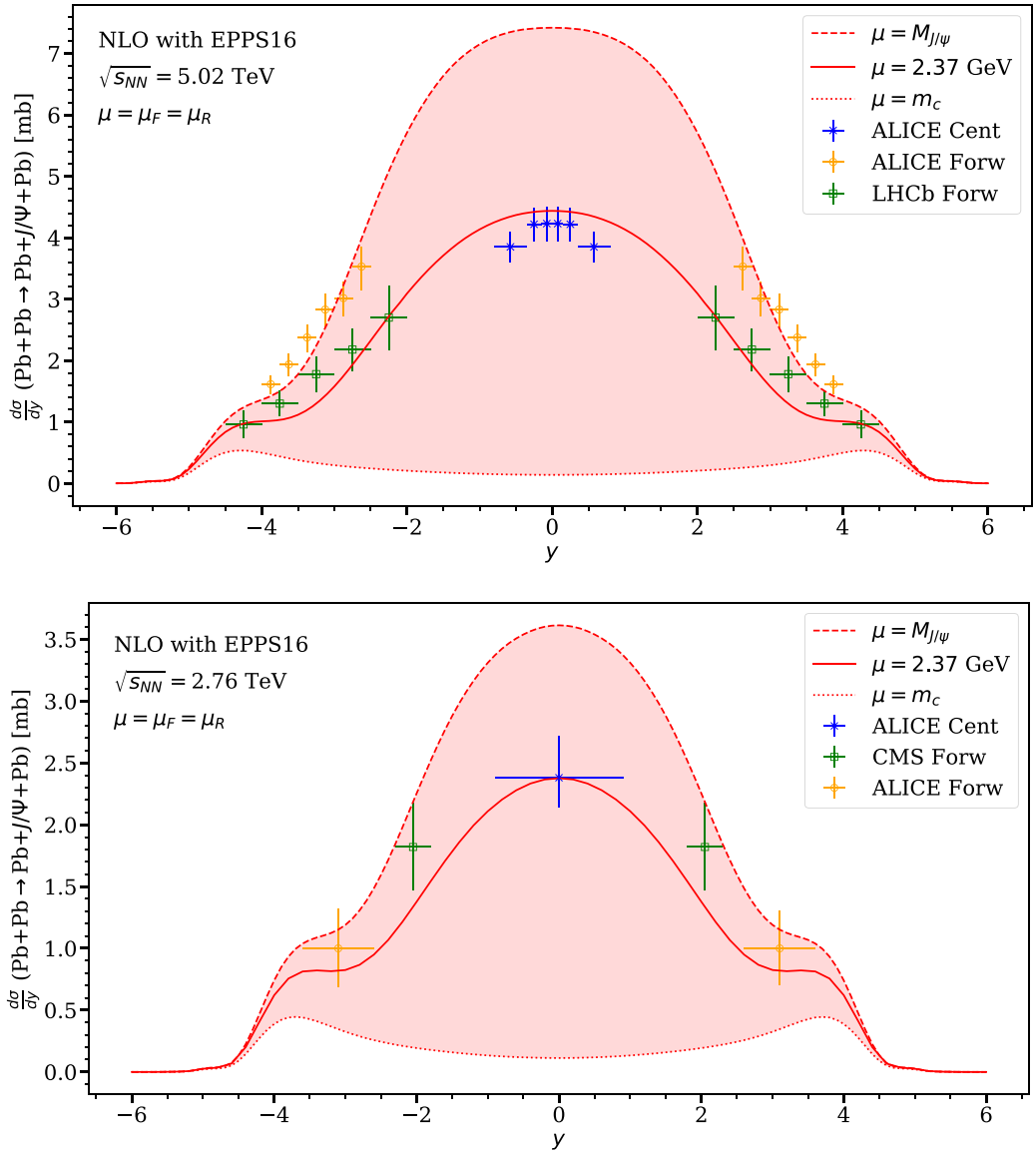

FIG. 1. Upper panel: The scale-choice uncertainty-envelope of the rapidity-differential exclusive J/ψ photoproduction cross section in ultraperipheral Pb + Pb collisions at $\sqrt{s_{NN}} = 5.02$ TeV, as a function of the J/ψ rapidity y, calculated to NLO pQCD with the EPPS16 nPDFs [45] and compared with the experimental data from Refs. [38] (ALICE Forw), [36] (ALICE Cent), and [41] (LHCb Forw). The experimental data points are mirrored with respect to $y = 0$, and their error bars are obtained by adding the statistical and systematic errors in quadrature. The solid (red) curve shows the NLO result with our "optimal" scale explained in the text. Lower panel: The same but at $\sqrt{s_{NN}} = 2.76$ TeV and with experimental data from Refs. [39] (ALICE Forw), [37] (ALICE Cent), and [40] (CMS Cent). For the errorbars of the data, all given errors are added in quadrature.

rapidity-differential J/ψ photoproduction cross sections in ultraperipheral Pb + Pb collisions. Figure 1 shows the uncertainty envelopes that result from varying the scale $\mu = \mu_F = \mu_R$ from $M_{J/\psi}/2$ to $M_{J/\psi}$ at $\sqrt{s_{NN}} = 5.0$ TeV (upper panel) and 2.76 TeV (lower panel), using the central set of the EPPS16 nPDFs [45]. For comparison, the figure also shows the experimental LHC data measured at these energies at forward rapidities by ALICE [38,39], LHCb [41] and CMS [40], and at central rapidities by ALICE [36,37]. The solid (red) lines in the middle parts of the envelopes show the results with $\mu = 0.76 M_{J/\psi} = 2.37$ GeV, a scale we have iteratively obtained by requiring a rough simultaneous fit to the data at both collision energies. In what follows we call this the "optimal" scale, emphasizing, however, that its precise number bears no special significance but it depends, e.g., on the assumed the GPD modeling details and nPDFs in general.

On the one hand, as expected based on Ref. [30], we observe that the scale uncertainty remains quite large also here in the nuclear case. On the other hand then, it is interesting and quite encouraging that already with our current "bare bones" GPD/PDF framework the NLO cross sections with entirely feasible scale choices $\mu = \mathcal{O}(M_{J/\psi})$ not only are of the correct order of magnitude but actually some scale choices can be found with which we can rather well reproduce the data

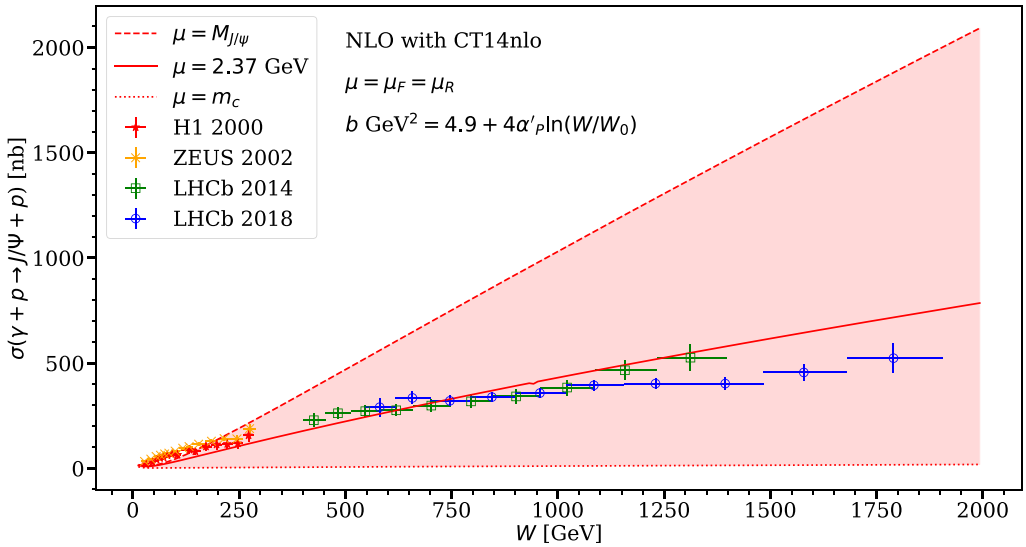

FIG. 2. The scale-choice uncertainty-envelope of exclusive J/ψ photoproduction NLO cross sections in ep and pp collisions as a function of the photon-proton c.m.s. energy W, computed to NLO pQCD with the CT14NLO [64] PDFs and compared against the experimental HERA data from H1 [26] and ZEUS [27], and LHC data from LHCb [28,29]. The solid (red) line corresponds to the "optimal" scale explained in the text.

at all rapidities and both collision energies. Earlier, especially with (*ad hoc* normalized) LO cross sections and the forward ALICE data at 5.02 TeV, this seemed not to be the case [36].

Second, as a further check of our UPC results from the "bare bones" GPD/PDF framework, we study in Fig. 2 to what extent we can reproduce the exclusive J/ψ photoproduction cross sections measured in ep collisions at HERA and in pp collisions at the LHC.[3] The NLO cross sections here are, for consistency, computed with the CT14NLO PDFs [64], which is the free-proton PDF set that the EPPS16 nPDFs are based on. The envelope shows again the uncertainty arising from varying the scale μ between $M_{J/\psi}/2$ and $M_{J/\psi}$. The HERA data in the figure are from H1 [26] and ZEUS [27], and the LHC data from LHCb [28,29]. The solid (red) line in the middle of the envelope is again the NLO cross section computed with our "optimal" scale which reproduced the nuclear data. As expected based on Ref. [30] and other previous NLO studies of this process [31–35], the scale dependence is indeed large, and especially towards larger values of the photon-proton c.m.s. energy W the data easily fall within the envelope. From the point of view of the nuclear UPCs the most relevant c.m.s.-energy region here is $W =$ 10–700 GeV (see the second x axis in Fig. 5 ahead). Interestingly, our framework with the "optimal" scale leads to a rather reasonable overall agreement with the HERA/LHC ep/pp data as well, except perhaps for the very lowest W points. As suggested by earlier work [30–35], there is room for GPD modeling testable against the ep/pp data, but, given the large scale and PDF uncertainties (discussed in Fig. 13 ahead), and also the exploratory nature of the present NLO study for UPCs of nuclei, we leave this as a future improvement.

[3]The photoproduction cross sections are extracted from the LHC pp data through rather minimal modeling [28,29].

With Fig. 2, it is also worth emphasizing that in the previous LO UPC studies one has typically normalized the LO cross sections to the HERA/LHC ep/pp data and carried the obtained normalization factor then over to the UPC study, while in our current NLO study there are *no ad hoc* normalization factors.

Third, we investigate the stability of the rapidity-differential J/ψ photoproduction cross sections in Pb + Pb UPCs, i.e., the changes in the magnitude and shape, and in the scale-dependence of the cross sections, when moving from LO to NLO in pQCD. These questions are answered by Fig. 3, where we show the rapidity-differential cross sections computed with various fixed scales μ between $M_{J/\psi}/2$ and $M_{J/\psi}$ in the LO and NLO cases (upper and lower panels, respectively). To be exact, the LO here refers to the purely gluonic Born-term contribution which enters the full NLO result. For the computation, we again use the EPPS16 nPDFs. We observe that the overall effect of the NLO terms is to reduce the LO cross sections rather significantly, at the "optimal" scale by a factor of 2.3 at midrapidity, and by a factor of 3.3 at $y = \pm 4$. We also see that the studied scale variation causes about a factor of 20 change in the LO case while in the full NLO result the change is about a factor of 50. These results confirm the expectations based on Ref. [30] also now in the nuclear UPC case, that at the low scales of $\mu = \mathcal{O}(M_{J/\psi})$ the NLO contributions do not stabilize the results, yet, but bring the cross sections nevertheless into the right direction. Interestingly, as seen in Fig. 3, also the whole shape of both the LO and the NLO results is quite sensitive to the scale μ, and again perhaps even more so at NLO, in this scale range. In the LO case, the strong scale dependence can be traced back mainly to the rapidly changing gluon distributions, while in the NLO terms the scale μ resides both in the pQCD matrix elements and in the PDFs. In particular, as we will soon see, in the NLO cross sections the rapidly evolving small-x *quark* PDFs start

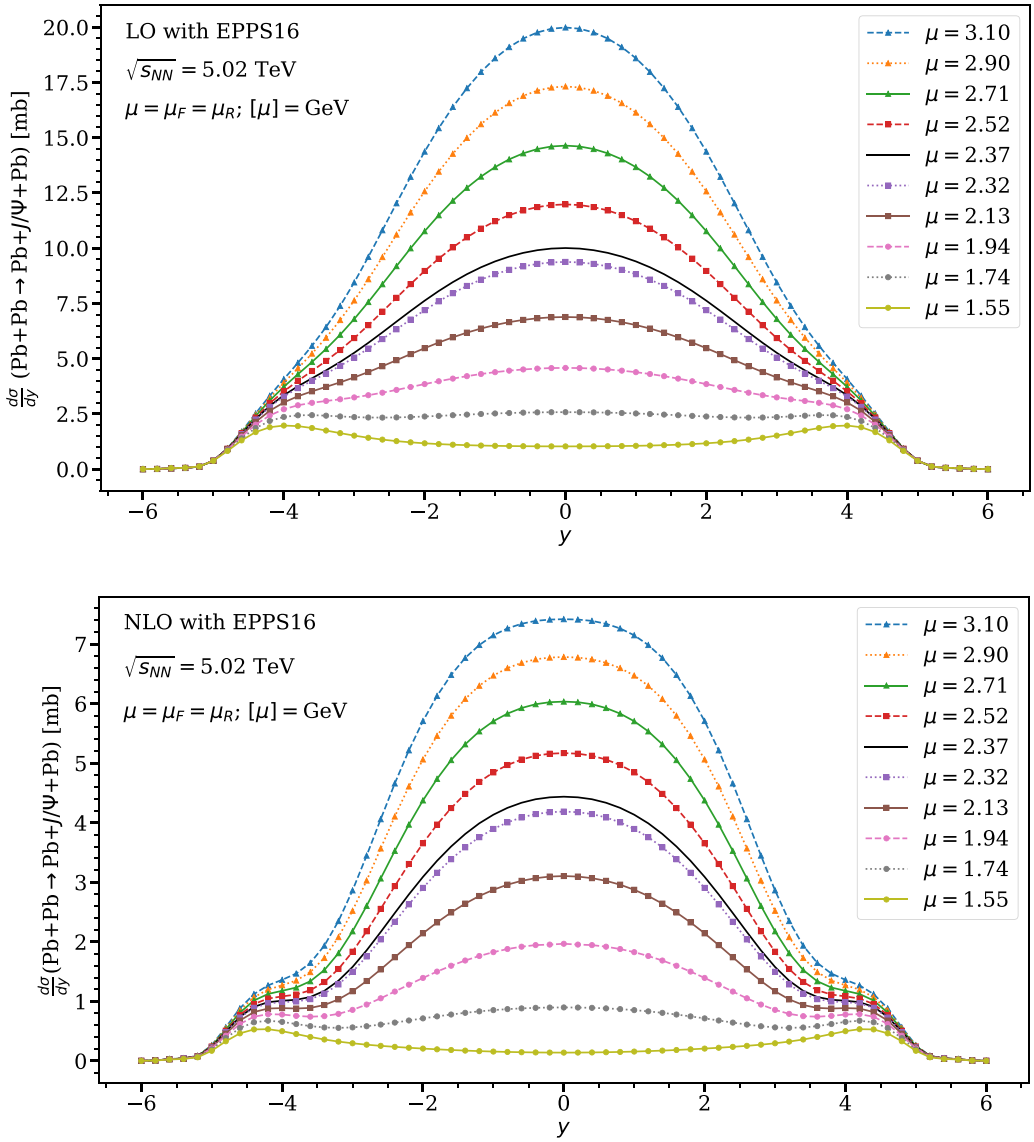

FIG. 3. Upper panel: Rapidity-differential exclusive J/ψ photoproduction cross sections in Pb + Pb UPCs at $\sqrt{s_{NN}} = 5.02$ TeV, as a function of the rapidity y, computed at LO pQCD with the EPPS16 nPDFs at various fixed scales μ. The lowest- and highest-scale results here give the envelope shown in Fig. 1. The result with our "optimal" scale is shown by the solid curve. Lower panel: The same but at NLO pQCD.

to play a surprisingly important role, and at midrapidities even a dominant one.

To analyze the scale dependence of our LO and full NLO results and their interrelation further, we plot in Fig. 4 the computed rapidity-differential cross sections at fixed rapidities $y = 0$ and at $y = \pm 4$ as a function of the scale μ. As we see, at $y = 0$ the scale dependence at low scales is stronger in the NLO than in the LO results, but towards higher scales it actually becomes weaker. At $y = \pm 4$ we see the scale dependence being stronger in NLO at all scales studied. Thus, whether the scale dependence is improved (tamed) when going from LO to NLO depends on the rapidity y and potentially also the scale-choice region. Another interesting observation is that our "optimal" scale $\mu = 2.37$ GeV is right in the region where the scale dependence at $y = 0$ turns from stronger to weaker relative to LO, i.e., where the LO and NLO results are closest to each other. At $y = \pm 4$, however, we do not find a similar taming effect to take place. This figure also shows how the NLO/LO ratio ("K factor") is not a constant as a function of the scale, and certainly not a constant as a function of the J/ψ rapidity.

B. Complex structure of the cross section

Next, we discuss the very interesting consequences of the complex structure of the rapidity-differential J/ψ photoproduction cross sections in 5.02 TeV Pb + Pb UPCs. First, in Fig. 5 we study the $k^{\pm}$ contributions in Eq. (4) to the rapidity-differential J/ψ photoproduction NLO cross section in 5.02 TeV Pb + Pb UPCs, computed with EPPS16 at our "optimal" scale. The photon-proton c.m.s. energy corresponding to the photon energies $k^{\pm}$ in Eq. (4) are denoted by $W^{\pm}$ in what follows. As indicated by the second x axis at the top of Fig. 5, W^+ (W^-) increases to the right (left). As

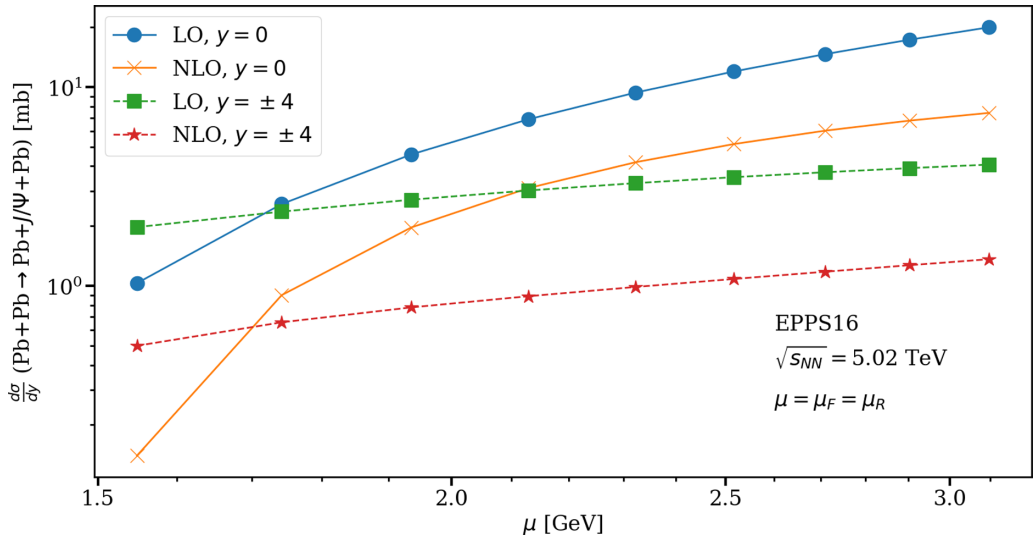

FIG. 4. The NLO (crosses and stars) and LO (filled circles and boxes) rapidity-differential cross sections of Fig. 3 at $y = 0$ (solid lines) and $y = \pm 4$ (dashed lines), as a function of the scale choice μ.

we saw in Fig. 2 above, the photoproduction cross section in the $k^{\pm}$ terms of Eq. (4) increases as a function of $W^{\pm}$, correspondingly. The photon flux, however, decreases rapidly as a function of the energy $W^{\pm}$ (see, e.g., Fig. 3 of [63]), causing the nonmonotonic behavior of the two symmetric contributions, as seen in Fig. 5. Looking at the W^{+} curve (dashed, red) we see that first at backward-most rapidities the photon flux is high enough to produce a noticeable cross section in spite of the smallness of the photoproduction cross section there. Also the t integral of the squared form factor of Eq. (8) reaches non-negligible values by $y \approx -4$, which also contributes to the initial rise of the cross section at backward-most rapidities. Then in the "shoulder" region the decrease of the photon flux wins over the increase of the photoproduction cross section, causing the small dip seen in the figure. Approaching then midrapidities, the increase of the photoproduction cross section now wins over the decrease of the photon flux, until eventually towards forward-most rapidities the photon flux decrease again dominates and the resulting cross section dies out. For the W^{-} component (dotted green curve), the behavior is a mirror image of this, and the final result (solid blue curve) is a combination of the $W^{\pm}$ contributions as seen in the figure.

Second, we quantify the contributions from the imaginary and real parts of the amplitude. The decomposition of the

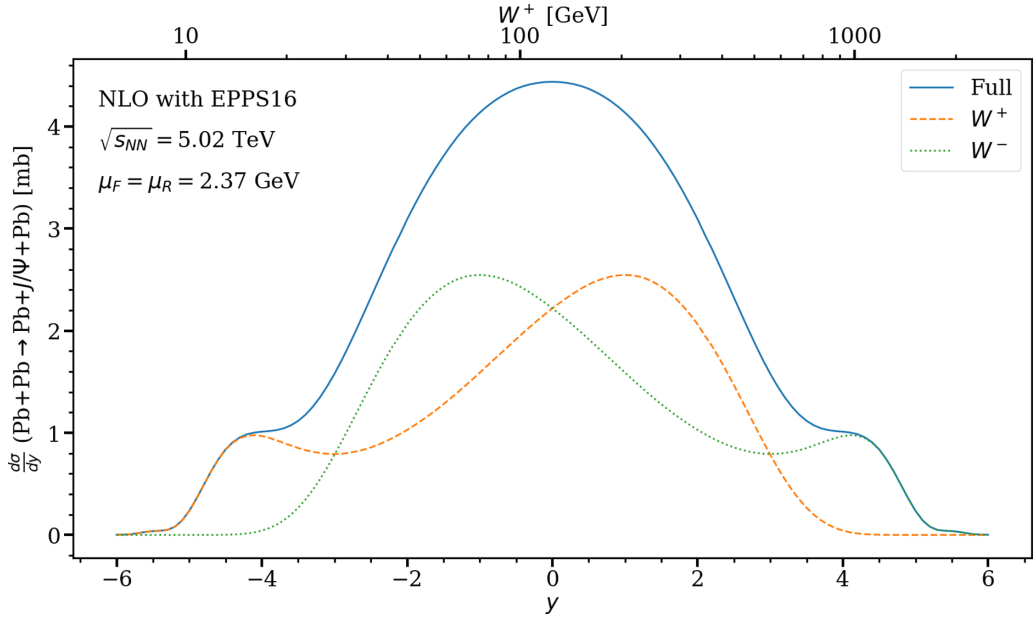

FIG. 5. Contributions from the W^{+} (dashed, red curve) and W^{-} (dotted, green curve) terms in Eq. (4) to the NLO exclusive rapidity-differential J/ψ photoproduction cross section in 5.02 TeV Pb + Pb UPCs as a function of the J/ψ rapidity y, computed using EPPS16 nPDFs and with our "optimal" scale. The second x axis on the top shows the values of W^{+} corresponding to each y.

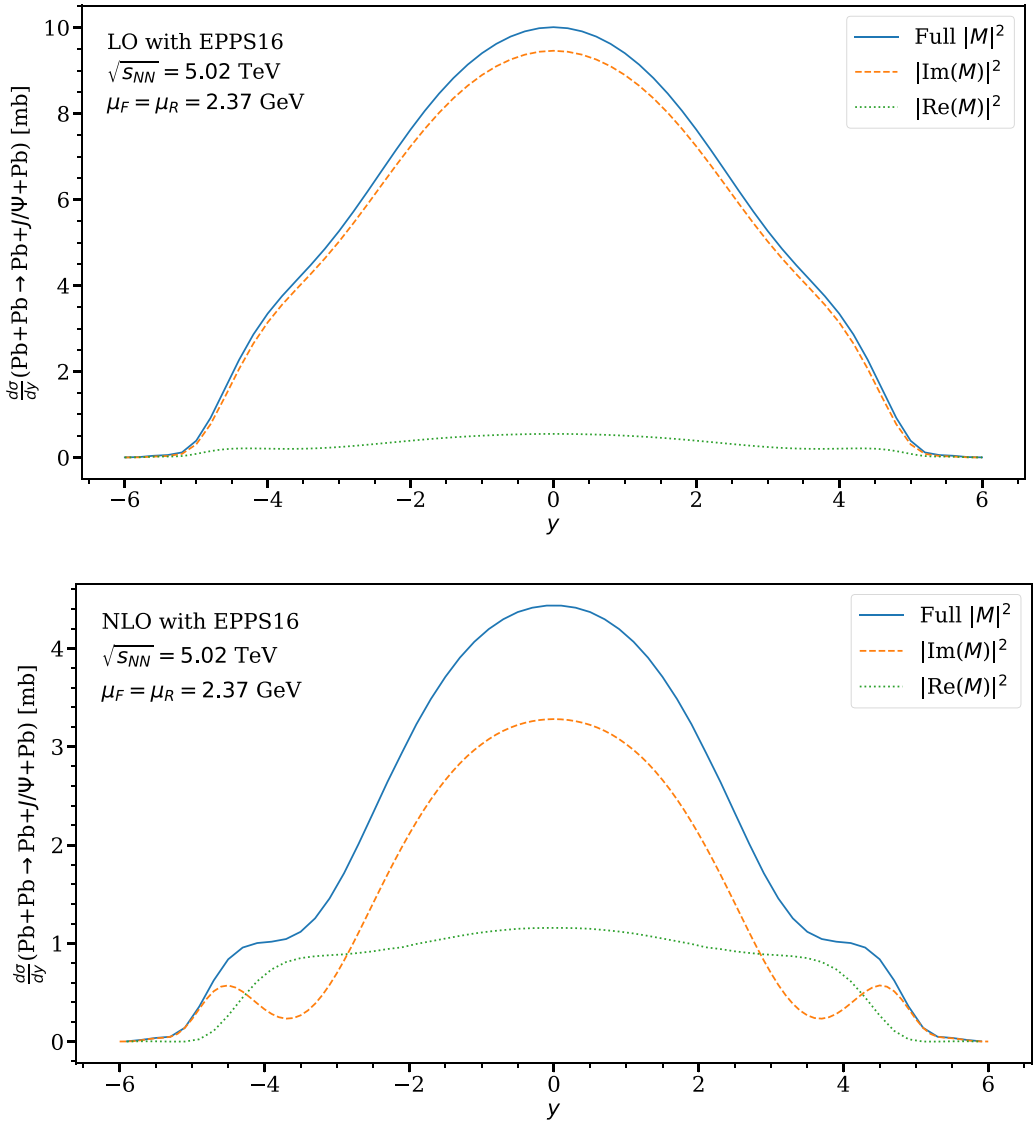

FIG. 6. Upper panel: Contributions from the real part (dotted green curve) and imaginary part (dashed red curve) of the amplitude to the LO exclusive rapidity-differential J/ψ photoproduction cross section in 5.02 TeV Pb + Pb UPCs (solid blue curve) as a function of the rapidity, computed using the EPPS16 nPDFs at our "optimal" scale. Lower panel: The same but in NLO.

full result ($\propto |\mathcal{M}|^2$) into the contributions from the real part ($\propto |\mathrm{Re}(\mathcal{M})|^2$) and the imaginary part ($\propto |\mathrm{Im}(\mathcal{M})|^2$) for both the LO and NLO cross sections is shown in Fig. 6. These results are again obtained with the EPPS16 nPDFs and fixing μ to our "optimal" scale. The LO here again refers to the Born term contributions entering the full NLO result. As the upper panel shows, in the LO case where only gluons contribute, we confirm—at least for gluon PDFs of a modest small-x rise, such as those in EPPS16/CT14NLO—the general claim that the contribution from the imaginary part of the amplitude clearly dominates at all rapidities. However, as the lower panel shows, the situation changes rather dramatically for the NLO cross sections: At midrapidity the contribution from the real part of the amplitude is about a quarter, which clearly is no longer negligible. Towards forward/backward rapidities the real-part contributions become even more important and, as seen in the figure, there is a region at large/small rapidities where they dominate over the imaginary-part contributions. These findings are also consistent with those of Ref. [30]; see Fig. 17 there. The message from Fig. 6 is clear: both the imaginary and real parts of the amplitude must be accounted for in the calculation of these cross sections.

Third, in Fig. 7, we investigate the breakdown of the computed J/ψ photoproduction NLO cross section in 5.02 TeV Pb + Pb UPCs into the quark and gluon contributions, using EPPS16 and our "optimal" scale. The solid (blue) curve labeled "Full $|\mathcal{M}|^2$" is the full NLO cross section of Fig. 6, while the dashed red (dotted green) curve labeled "Only Gluons" ("Only Quarks") is obtained by setting the quark (gluon) distributions to zero. The dashed-dotted curve labeled "Interference" corresponds to the remaining contribution from the cross section pieces that contain both quarks and gluons. As shown by Fig. 7, at midrapidity the quarks-only contribution dominates over the gluons-only by a factor of 4, and

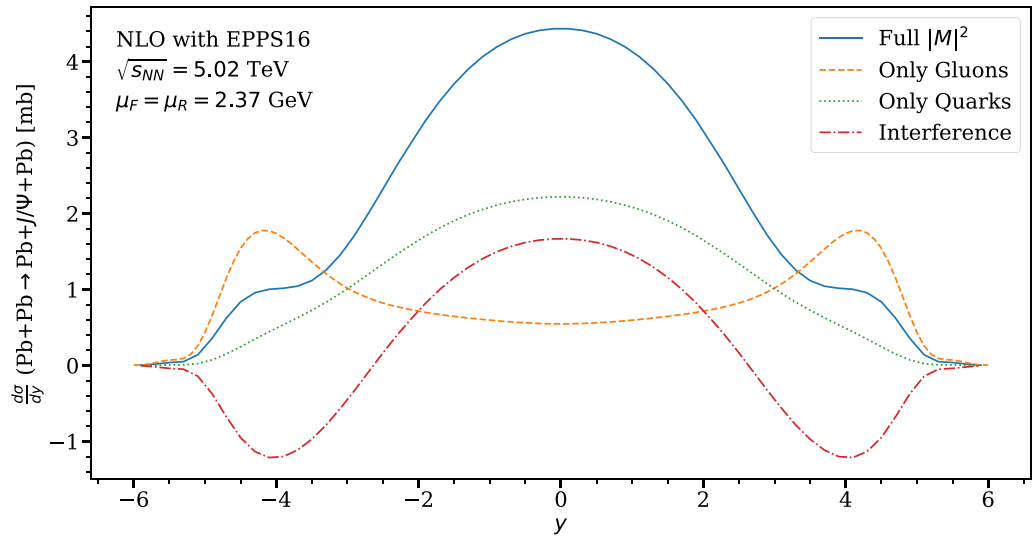

FIG. 7. Decomposition of the exclusive rapidity-differential J/ψ photoproduction cross section, computed with EPPS16 nPDFs at our "optimal" scale, in 5.02 TeV Pb + Pb UPCs (solid blue curve "Full $|\mathcal{M}|^2$") into the contributions with zero quark distributions (dashed orange curve "Only Gluons"), with zero gluon distributions (dotted green curve "Only Quarks") and the one with a mixing of the quark and gluon distributions in the square of the full NLO amplitude (red dashed-dotted curve "Interference").

the quark-gluon term over the gluons-only by a factor of 3. Towards forward/backward-most rapidities the gluons-only contributions become the dominant ones, and we can see that the gluon-quark term also changes its sign when going from midrapidity to forward/backward rapidities.

Recalling the original attraction of the exclusive J/ψ photoproduction in electron-proton collisions and in nuclear UPCs as an exceptionally efficient probe of small-x gluon distributions, the results in Fig. 7 appear at first sight somewhat surprising. Especially the quark dominance at midrapidity seems to be in direct contradiction with the original LO-based gluon-probe suggestion, and in fact also with our expectation that small-x gluons *should* after all dominate also the NLO contributions.

A better understanding of this clearly calls for a more detailed look at the individual contributions in the LO and NLO amplitudes. For this purpose, we write the full NLO amplitude in terms of the LO gluon part $\mathcal{M}_G^{\rm LO}$ and NLO gluon and quark parts $\mathcal{M}_G^{\rm NLO}$ and $\mathcal{M}_Q^{\rm NLO}$,

$$\mathcal{M} = \mathcal{M}_G^{\rm LO} + \mathcal{M}_G^{\rm NLO} + \mathcal{M}_Q^{\rm NLO}, \tag{31}$$

so that the squared amplitude entering the cross section becomes

$$\begin{aligned}|\mathcal{M}|^2 = &\left|\mathcal{M}_G^{\rm LO} + \mathcal{M}_G^{\rm NLO}\right|^2 + \left|\mathcal{M}_Q^{\rm NLO}\right|^2 \\ &+ 2\big[\mathrm{Re}\big(\mathcal{M}_G^{\rm LO} + \mathcal{M}_G^{\rm NLO}\big)\mathrm{Re}\big(\mathcal{M}_Q^{\rm NLO}\big) \\ &+ \mathrm{Im}\big(\mathcal{M}_G^{\rm LO} + \mathcal{M}_G^{\rm NLO}\big)\mathrm{Im}\big(\mathcal{M}_Q^{\rm NLO}\big)\big].\end{aligned} \tag{32}$$

The gluons-only contribution in Fig. 7 comes from the term

$$\begin{aligned}\left|\mathcal{M}_G^{\rm LO} + \mathcal{M}_G^{\rm NLO}\right|^2 = &\left[\mathrm{Re}\big(\mathcal{M}_G^{\rm LO}\big) + \mathrm{Re}\big(\mathcal{M}_G^{\rm NLO}\big)\right]^2 \\ &+ \left[\mathrm{Im}\big(\mathcal{M}_G^{\rm NLO}\big) + \mathrm{Im}\big(\mathcal{M}_G^{\rm NLO}\big)\right]^2\end{aligned} \tag{33}$$

and the quarks-only contribution from

$$\left|\mathcal{M}_Q^{\rm NLO}\right|^2 = \left[\mathrm{Re}\big(\mathcal{M}_Q^{NLO}\big)\right]^2 + \left[\mathrm{Im}\big(\mathcal{M}_Q^{NLO}\big)\right]^2, \tag{34}$$

while the gluon-quark interference contribution corresponds to the third term on the right-hand side of Eq. (32).

Figure 8 shows the above real and imaginary parts of the amplitude, multiplied with the factor ξ/C [(see Eq. (13)], as a function of the rapidity corresponding to W^+.[4] This figure finally reveals exactly what is behind the quark and gluon contributions in Fig. 7: In their *absolute* values, the LO and NLO gluon amplitudes $\mathcal{M}_G^{\rm LO}$ and $\mathcal{M}_G^{\rm NLO}$ indeed *do* clearly dominate over the quark contribution $\mathcal{M}_Q^{\rm NLO}$ both in the real and imaginary parts. However, due to their opposite signs, the LO and NLO gluon amplitudes *cancel* to a large degree in both the real and imaginary parts. The exact efficiency of the cancellation depends on the rapidity (W^+), and $\mathrm{Im}(\mathcal{M}_G^{\rm LO}) + \mathrm{Im}(\mathcal{M}_G^{\rm NLO})$ changes its sign from plus to minus when approaching backward rapidities, which causes the sign change of the quark-gluon mixing term in Fig. 7. Let us look at the following three example-rapidities:

(i) At $y = 0$, where the $W^\pm$ components contribute equally (see Fig. 5), the cancellation of the gluon terms is coincidentally (that is, with these PDFs) almost perfect in the imaginary part, so that

$$\begin{aligned}\big[\mathrm{Im}\big(\mathcal{M}_G^{\rm LO} + \mathcal{M}_G^{\rm NLO}\big)\big]^2 &\lesssim \big[\mathrm{Re}\big(\mathcal{M}_Q^{\rm NLO}\big)\big]^2 \\ &< \big[\mathrm{Re}\big(\mathcal{M}_G^{\rm LO} + \mathcal{M}_G^{\rm NLO}\big)\big]^2 \\ &\ll \big[\mathrm{Im}\big(\mathcal{M}_Q^{\rm NLO}\big)\big]^2,\end{aligned} \tag{35}$$

which makes the imaginary part of the quark amplitude dominate the cross section in Fig. 7. In the

[4]Recall that the photon flux and form factor do not enter here.

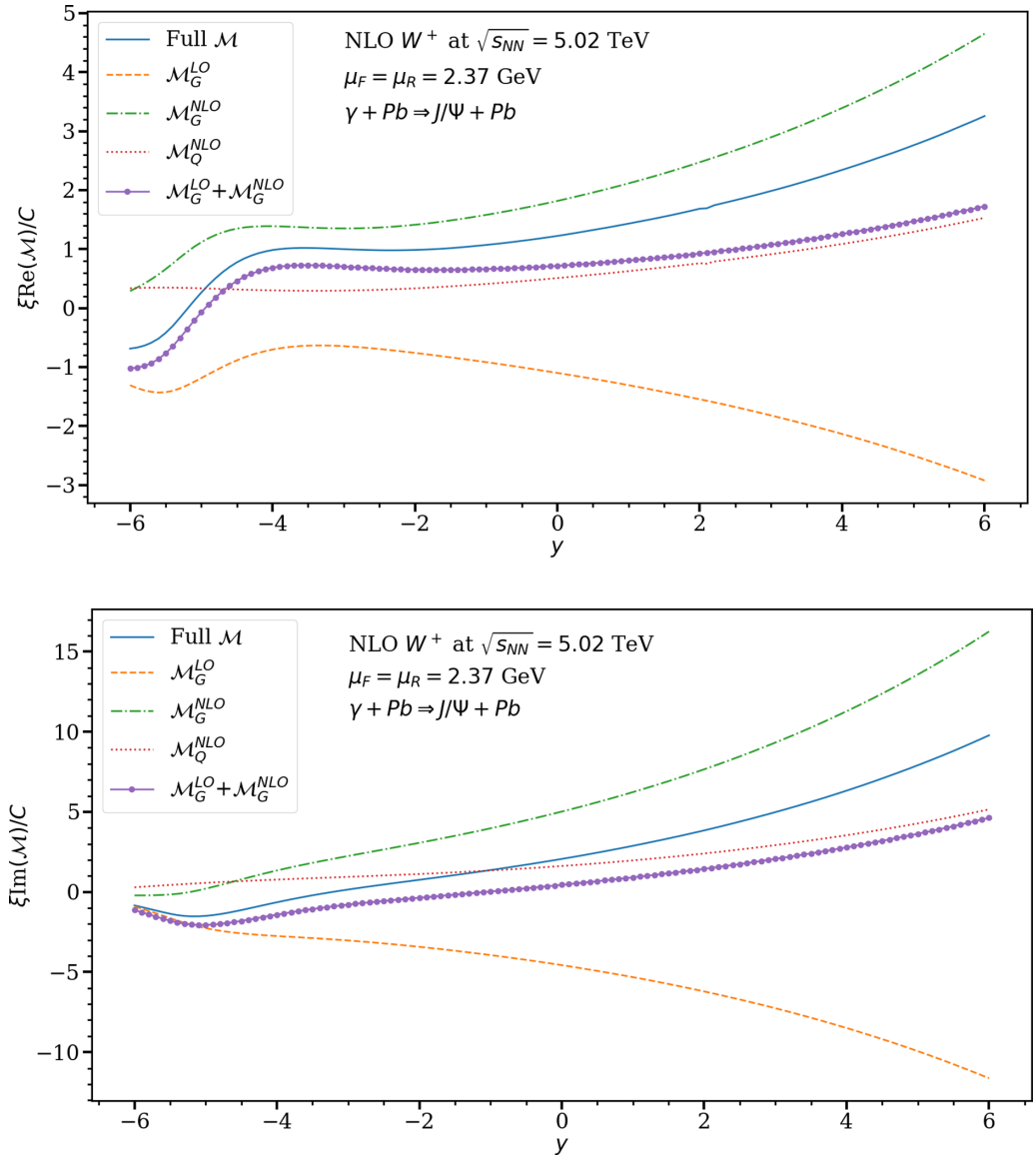

FIG. 8. Upper panel: The ξ/C-scaled real parts of the full amplitude $\mathcal{M}$ (solid blue curve), LO gluon term $\mathcal{M}_G^{\mathrm{LO}}$ (dashed orange), NLO gluon term $\mathcal{M}_G^{\mathrm{NLO}}$ (dashed dotted green), sum of the LO and NLO gluon terms $\mathcal{M}_G^{\mathrm{LO}} + \mathcal{M}_G^{\mathrm{NLO}}$ (solid purple with filled circles), and NLO quark term $\mathcal{M}_Q^{\mathrm{NLO}}$ (dotted red), as a function of the J/ψ rapidity y, for the contribution W^+. For the definition of the scaling factor, see Eq. (13). Lower panel: The same but for the imaginary parts of the amplitudes. Notice the different vertical scale.

quark-gluon mixing term then the product of the imaginary parts dominates over the product of the real parts, and due to the large $\mathrm{Im}(\mathcal{M}_Q^{\mathrm{NLO}})$ the quark-gluon contribution dominates over the gluons-only term.

(ii) At $y \approx -3$, Fig. 5 indicates that the $W^{\pm}$ contributions are equally important, so that Fig. 8 should be read both at $y \approx -3$ and $y \approx +3$. The squared amplitude is larger for $y = 3$ but the rapid decrease of the W^--component's photon flux and nuclear form factor towards negative rapidities now suppresses the W^- component so that it becomes of the same magnitude as the W^+ component whose squared amplitude is smaller but whose photon flux is correspondingly larger. As seen in Figs. 6 and 7, as a result of these competing effects the real and imaginary parts of the amplitude, as well as quarks and gluons, then contribute equally to the rapidity-differential cross section at $y \approx -3$.

(iii) At $y \approx -4$, where the cross section is dominated by the W^+ component as seen in Fig. 5, the LO and NLO gluon terms cancel to a much smaller degree both in the real and imaginary parts, and the hierarchy becomes

$$\begin{aligned}\left[\mathrm{Re}\left(\mathcal{M}_Q^{\mathrm{NLO}}\right)\right]^2 &\ll \left[\mathrm{Re}\left(\mathcal{M}_G^{\mathrm{LO}} + \mathcal{M}_G^{\mathrm{NLO}}\right)\right]^2 \\ &\lesssim \left[\mathrm{Im}\left(\mathcal{M}_Q^{\mathrm{NLO}}\right)\right]^2 \\ &\ll \left[\mathrm{Im}\left(\mathcal{M}_G^{\mathrm{LO}} + \mathcal{M}_G^{\mathrm{NLO}}\right)\right]^2, \end{aligned} \quad (36)$$

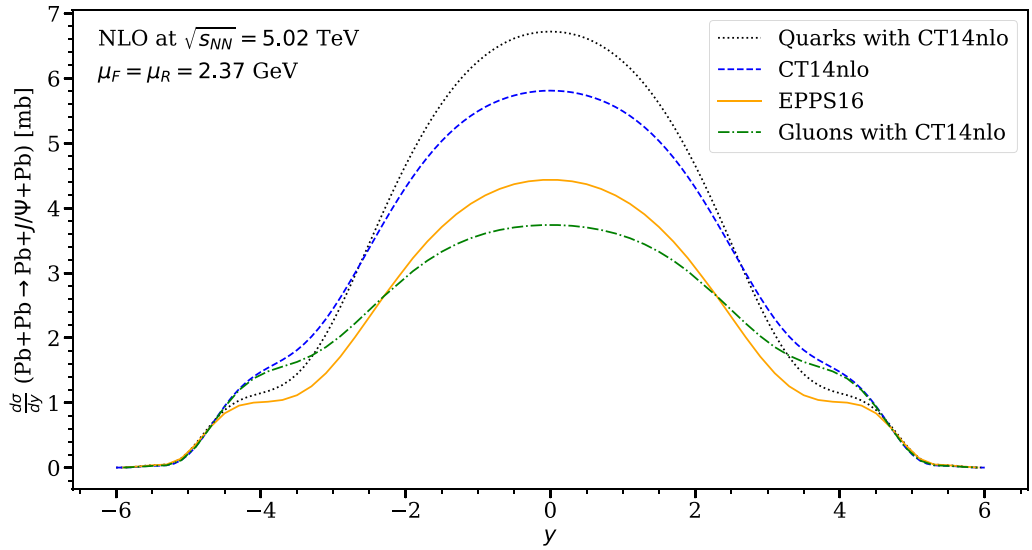

FIG. 9. Rapidity-differential exclusive J/ψ photoproduction cross section in 5.02 TeV Pb + Pb UPCs, computed with the EPPS16 nPDFs (solid orange curve), with CT14NLO PDFs (dashed blue curve), with CT14NLO gluons and EPPS16 quarks (dotted-dashed green curve), and with CT14NLO quarks and EPPS16 gluons. Notice that turning off the nuclear effects in gluons reduces the cross section at $y = 0$; for explanation, see the text.

causing the gluons-only terms to dominate over the quarks-only by almost a factor of 4. In this case, the sizable quark-gluon mixing term is deeply negative because of the large negative term $\mathrm{Im}(\mathcal{M}_G^{\mathrm{LO}}) + \mathrm{Im}(\mathcal{M}_G^{\mathrm{NLO}})$. It is again the negative sign of this term that in the full amplitude causes $[\mathrm{Re}(\mathcal{M})]^2 \gtrsim [\mathrm{Im}(\mathcal{M})]^2$, seen in Fig. 8 and in the lower panel of Fig. 6 at $y = -4$ to -3.

As shown by Figs. 5–8, the full NLO cross section thus has a very detailed complex structure with interplays between the photoproduction cross section, the photon flux, and the nuclear form factor, between the $W^{\pm}$ components, and especially between the various contributions from the real and imaginary parts of the amplitude. The key to understand the obtained rapidity-differential cross sections is the degree of cancellation of the LO and NLO gluon contributions of opposite signs. We have also checked that the situation is qualitatively the same for the 2.76 TeV collision energy, and that the real part contributions become slightly more important for all values of y than for the 5.02 TeV case. We have also checked that, in the case of no nuclear effects, the situation remains qualitatively the same.

C. Nuclear effects and PDF uncertainties in the cross section

Next, we analyze how the nuclear modifications of the PDFs as well as the uncertainties of the nuclear and free-proton PDFs propagate into the exclusive rapidity-differential J/ψ photoproduction cross sections.

Figure 9 compares the rapidity-differential cross sections at 5.02 TeV obtained at our "optimal" scale with the EPPS16 nPDFs (solid orange curve) and the one obtained with the CT14NLO free-proton PDFs (dashed blue) which are the baseline for EPPS16. As seen in the figure, at midrapidity, where the $W^{\pm}$ terms contribute equally, the cross sections show a reduction of a factor of 0.76 from CT14NLO to EPPS16. Towards backward/forward rapidites, i.e., in the regions where the $W^{\pm}$ terms contribute significantly and probe the nuclear effects in different x regions, the net nuclear effects are slightly increasing. Finally at the backward-most (forward-most) rapidities, where the single W^+ (W^-) contribution dominates and one enters the antishadowing region, the nuclear effects essentially die out.

The general behavior and magnitude of the nuclear effects here can be understood as follows:

(i) First, we recall from Figs. 7 and 8 that it is the imaginary part of the quark amplitude that dominates the cross section at $y = 0$. Recalling that $\xi(y) = \zeta(y)/[2 - \zeta(y)]$, where $\zeta(y) = M_{J/\psi}^2/W^2$ and $W^2 = M_{J/\psi} e^y \sqrt{s_{NN}}$, we have $\xi(y = 0) \approx 3 \times 10^{-4}$. This is deep in the shadowing region of nPDFs, and in EPPS16 at this x and our "optimal" scale the average nuclear sea-quark (gluon) modification is about 0.68 (0.74). The fact that there seems to be a weaker than quadratic dependence on the PDF's nuclear modification factor follows, to our understanding, from two reasons: First, in the NLO amplitudes one integrates the parton distributions over x from zero to one: At $x \lesssim \xi$ shadowing is about a constant factor (in EPPS16) while at $x \gtrsim \xi$ shadowing diminishes, so that the net effect of the x integration is a taming of the nuclear effect from that at $x = \xi$. Second, and most importantly, as discussed in detail below, it is again the surprisingly complicated interplay of the different parts of the amplitude and in particular the mutual cancellation of the LO and NLO gluon amplitudes that causes the quark-gluon mixing term to actually cancel some of the nuclear effects.

(ii) Towards backward rapidities there are competing nuclear effects as W^+ decreases, the probed values of ξ increase and the nuclear modifications thereby decrease, and, as simultaneously W^- increases, the probed values of ξ decrease and the nuclear modifications thereby increase (and towards forward rapidities conversely). And, as seen in Fig. 7 also quarks and gluons compete over the dominance of cross section, the quark dominance turning into a gluon one towards backward/forward rapidities.

(iii) At the backward rapidity $y = -4$ then, we recall that the W^+ contribution (Fig. 5) and the NLO real part of the full amplitude (Figs. 6 and 8) dominate the cross section, and from Fig. 7 we again see that both quarks and gluons contribute here. Now $\xi(y = -4) \approx 1.7 \times 10^{-2}$ and the EPPS16 gluon (quark) modification is a factor of 0.88 (0.86) while the net nuclear effect is about a factor of 0.68, i.e., surprisingly large. In this region the integration over x does not tame the nuclear effects to the same degree as at small values of x, and in particular the large and negative quark-gluon mixing term drives the efficiency of nuclear effects up here.

Given the complex intertwined structure of the cross section, it is also useful to analyze what happens if we start from the EPPS16 result and separately turn off the nuclear effects from gluons and quarks, one at the time.

(iv) First turning off the nuclear effects (suppression) in the gluon PDFs results in the dashed-dotted (green) curve labeled "Gluons with CT14NLO" in Fig. 9, which shows a *reduction* in the cross section relative to the EPPS16 result (solid orange curve) at midrapidity. This seems again quite counterintuitive, as we would naively expect a removal of suppression to cause an *increase* instead. Such a behavior can, however, be again understood by studying the real and imaginary parts of the amplitude: In their absolute values, $\mathrm{Re}(\mathcal{M}_G^{\mathrm{LO}})$, $\mathrm{Re}(\mathcal{M}_G^{\mathrm{NLO}})$, $\mathrm{Im}(\mathcal{M}_G^{\mathrm{LO}})$, and $\mathrm{Re}(\mathcal{M}_G^{\mathrm{NLO}})$ all behave as expected, i.e., their absolute values indeed *grow* when the nuclear shadowing (suppression) is removed. However, nuclear modifications of the PDFs affect the LO and NLO amplitudes in a slightly different manner. Hence, the degree of the cancellation of $\mathrm{Re}(\mathcal{M}_G^{\mathrm{LO}})$ against $\mathrm{Re}(\mathcal{M}_G^{\mathrm{NLO}})$ and of $\mathrm{Im}(\mathcal{M}_G^{\mathrm{LO}})$ against $\mathrm{Im}(\mathcal{M}_G^{\mathrm{NLO}})$ changes when switching the PDFs from EPPS16 to CT14NLO. With the CT14NLO gluons at this scale, the cancellation of $\mathrm{Im}(\mathcal{M}_G^{\mathrm{LO}})$ against $\mathrm{Im}(\mathcal{M}_G^{\mathrm{NLO}})$ happens to be practically perfect. This in turn eliminates the previously large contribution $2[\mathrm{Im}(\mathcal{M}_G^{\mathrm{LO}}) + \mathrm{Im}(\mathcal{M}_G^{\mathrm{NLO}})]\mathrm{Im}(\mathcal{M}_Q^{\mathrm{NLO}})$ in the quark-gluon mixing term, causing the *suppression* that we see in Fig. 9 at midrapidity.

(v) Then, turning off the nuclear effects in the quark distributions but leaving them on in the gluon contribution results in the dotted black curve, which lies rather close to the pure CT14NLO case of no nuclear PDF effects at all. This time this is an obvious result, as at midrapidity the quark part $\mathrm{Im}(\mathcal{M}_Q^{\mathrm{NLO}})$ dominates the cross section and removing the suppression in the PDFs just increases the cross section as expected. Figure 9 thus underlines the quark dominance demonstrated earlier in Fig. 7.

Because of the rather counterintuitive results above, and since there is the integration over x from zero to one in the NLO amplitude, we would like to confirm that NLO exclusive photoproduction of J/ψ in Pb + Pb UPCs at the LHC indeed probes the small-x shadowing region ($x \lesssim 0.03$–0.04 in EPPS16), and not the antishadowing region (0.03–$0.04 \lesssim x \lesssim 0.3$ in EPPS16) in the nPDFs. If the process indeed probes the quark and gluon distributions at $x = \mathcal{O}(\xi)$, and $\xi(y = 0) \approx 3 \times 10^{-4}$, then the biggest effect to the final result (relative to the CT14NLO result above) should be attained by turning on only the nuclear corrections in the shadowing region. We have checked that this is indeed the case: Running the code with *ad hoc* modified nPDFs that coincide with EPPS16 in the shadowing region and with CT14NLO elsewhere, the results are essentially (within 6%) the same as the EPPS16 results.

Next, we investigate how sensitive the studied cross sections are to the choice of the nPDFs. Figure 10 shows the rapidity-differential cross sections obtained with the central sets of the EPPS16 (solid orange curve), nCTEQ15 (dashed green), and nNNPDF2.0 (dotted blue) nPDFs. The nCTEQ15 set gives essentially the same result as EPPS16 but there seems to be a huge difference in the nNNPDF2.0 set. The shape of the nNNPDF2.0 result is very different from EPPS16/nCTEQ15, and the magnitude at forward and backward rapidities is off by about a factor of 15. We have traced the very fast growth of the cross section down to the rapidly growing real part of the LO gluon amplitude, which includes again the integration over x from 0 to 1 where the small-x gluons (in the ERBL region $x \lesssim \xi$ but near $x \sim \xi$) start to play a significant role with nNNPDF2.0. The real part of the LO gluon amplitude is not as well numerically canceling against the real part of the NLO gluon amplitude with nNNPDF2.0 as with EPPS16/nCTEQ15, which in turn makes the forward/backward-y cross section again more sensitive to the small-x gluon distributions, and this is what we see in Fig. 10.

We plot in Fig. 11 the gluon distributions $xg(x, \mu)$ and the quark singlet distributions $F^{q,S} = \sum_q [q(x, \mu) + \bar{q}(x, \mu)]$ from EPPS16, nCTEQ15, and nNNPDF2.0 nPDFs as they enter our computation at the "optimal" scale. The figure confirms the similarity of the EPPS16 and nCTEQ15 PDFs and shows that the nNNPDF2.0 quarks differ systematically from these at $x \lesssim 10^{-5}$ and the gluons at $x \lesssim 10^{-4}$. In Fig. 10, the increased small-x gluons of nNNPDF2.0 make the W^- component of the cross section the dominant one at $y = -3$. For the W^- contribution $\xi(y = -3) = \mathcal{O}(10^{-5})$, and at these values of x, Fig. 11 indicates already a factor of three difference between the nNNPDF2.0 and EPPS16/nCTEQ15 gluons.[5] The square of this difference then explains the order

[5] With the nNNPDF3.0 set [48], published recently, this is no longer the case.

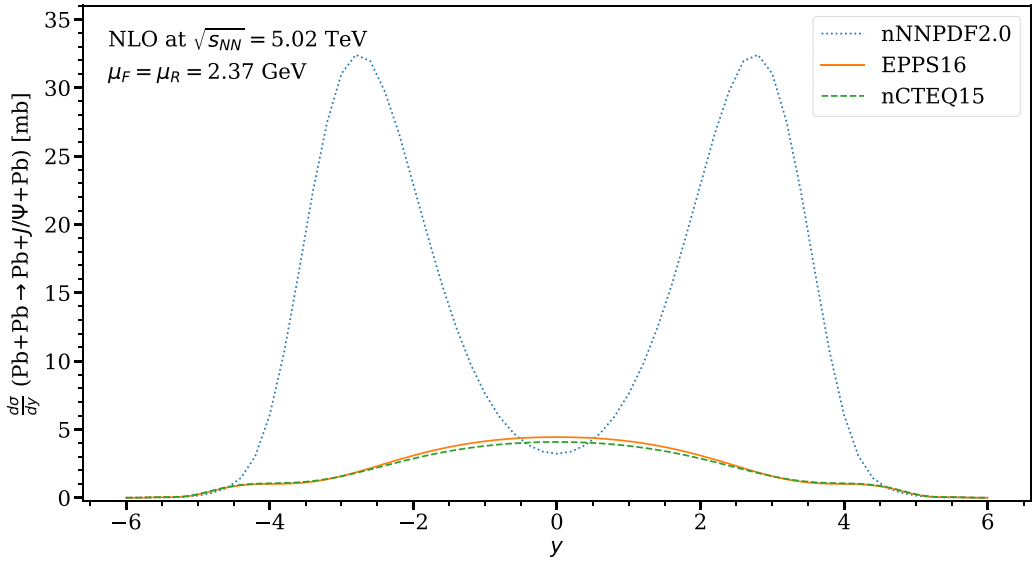

FIG. 10. Rapidity-differential exclusive photoproduction of J/ψ in 5.02 TeV Pb + Pb UPCs, computed at our "optimal" scale using the EPPS16 [45] (solid orange curve), nCTEQ15 [44] (dashed green), and nNNPDF2.0 [46] (dotted blue) nPDFs.

of magnitude of the difference between the nNNPDF and EPPS16/nCTEQ15 results seen in Fig. 10.

Next, we investigate the PDF uncertainties in the computed rapidity-differential cross sections and compare them with the existing data. We propagate the PDF/nPDF uncertainties to the computed cross sections using the asymmetric form [45]

$$\delta\mathcal{O}^{\pm} = \sqrt{\sum_i \left[{}^{\max}_{\min}\{\mathcal{O}(S_i^+) - \mathcal{O}(S_0), \mathcal{O}(S_i^-) - \mathcal{O}(S_0), 0\}\right]^2}, \tag{37}$$

where $S_i^{\pm}$ labels the error sets for the given PDF. We plot the error sets of EPPS16 + CT14NLO in Fig. 12 for the gluon distributions $xg(x, \mu)$, and for the quark singlet distributions $F^{q,S}$, again at our "optimal" scale. As the figure shows, one CT14-related error set, Set93, of the EPPS16 implementation in LHAPDF [86] (error set 53 in CT14NLO), stands clearly out at smallest values of x, and even more strongly than the nNNPF2.0 PDFs did in Fig. 11, while the rest of the EPPS16-related and CT14-related error sets show only rather moderate variations with respect to the central sets. Similarly to the case with the nNNPDF2.0 nPDFs above, the rapid growth of the small-x gluon distributions in this error set induces again a rapid growth of the real part of the LO gluon amplitude, and hence the cross sections.

Figure 13 shows the uncertainties that are induced to the rapidity-differential exclusive J/ψ photoproduction cross sections in 5.02 TeV (upper panel) and 2.76 TeV (lower panel)

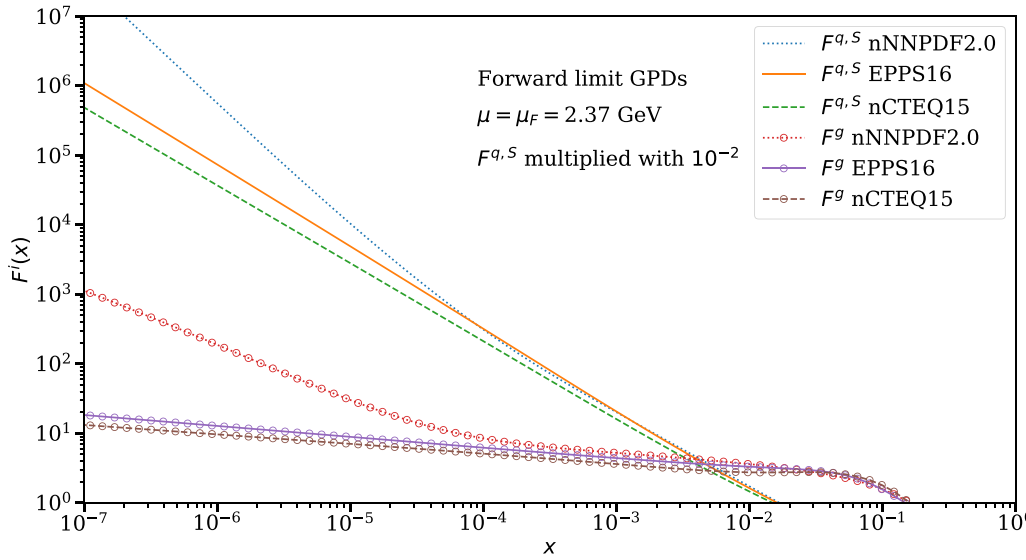

FIG. 11. The nPDF gluon distributions $xg(x, \mu)$ and the quark singlet distributions $F^{q,S} = \sum_q [q(x, \mu) + \bar{q}(x, \mu)]$ as given by EPPS16 (solid lines), nCTEQ15 (dashed), and nNNPDF2.0 (dotted) nPDFs at the "optimal" scale.

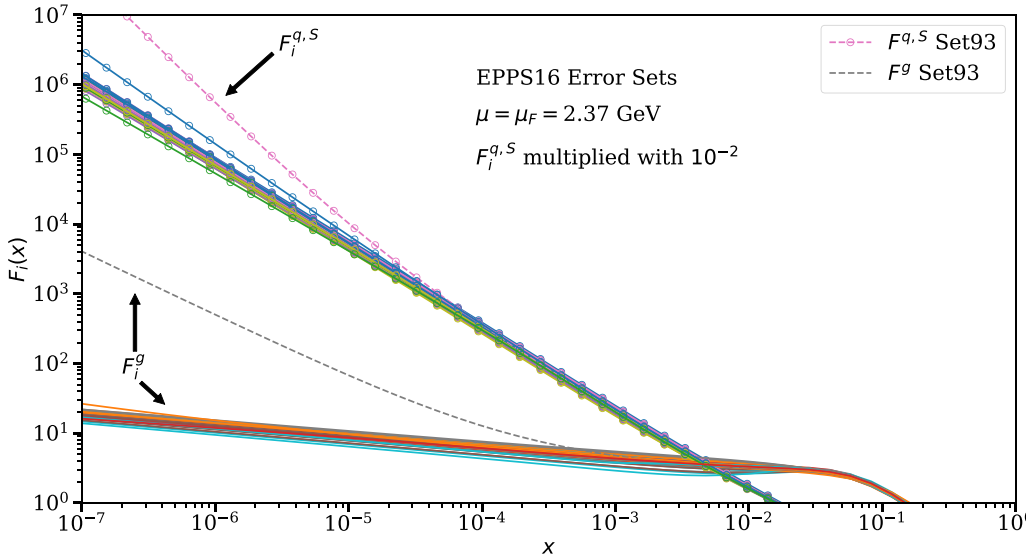

FIG. 12. The error sets of EPPS16 and CT14NLO nPDFs and PDFs for the gluon (lower set of curves) and quark-singlet distributions (upper set) as functions of x, at our "optimal" scale. Altogether 96 error sets are plotted, of which the numbers 1–40 in the LHAPDF setup [86] of EPPS16 are for the nuclear effects and 41–96 for the CT14NLO free-proton PDFs. The CT14NLO-related Set93 is the one clearly standing out from the rest at $x \lesssim 10^{-4}$.

Pb + Pb UPCs by the PDF/nPDF uncertainties. The uncertainties arising from the EPPS16 nuclear effects alone are shown by the dark (blue) bands, while the full EPPS16 + CT14NLO error bands (green) contain uncertainties from both the nuclear effects and the free-proton baseline PDFs. The results with EPPS16 and CT14NLO central sets are shown by the solid (blue) curves. As expected based on Fig. 12, "Set93" above entirely dictates the green error bands. The EPPS16 + CT14NLO full uncertainty band at mid-rapidity (not shown in the figure) goes up to some 150 (37) mb and at $y \approx \pm 2.2$ as high as 1500 (170) mb for the 5.02 (2.76) TeV collision energy. We also have checked that without Set93 the CT14NLO uncertainties become of the same order and slightly smaller than those for EPPS16. For comparison with the EPPS16 results, we also plot the uncertainty bands (hatched) arising from the nCTEQ15 error sets. These now account for the uncertainties in the nuclear effects only, and not in the free-proton PDFs. The central-set results with nCTEQ15 are shown by the dashed (red) line. We should also emphasize that the nCTEQ15 results here have been obtained at our "optimal" scale, without further tuning of the scale.

As we have already seen, the EPPS16 results produce a relatively good fit to the experimental Run1 and Run2 data at our "optimal" scale, and as seen in Fig. 13, so do the nCTEQ15 ones, too. The uncertainties arising from the nuclear effects in EPPS16 and nCTEQ15 are of the same order of magnitude mutually, and typically somewhat larger than the error bars of the data. As the figure indicates, one must not forget the free-proton PDF uncertainties when considering absolute cross sections. Finally, regarding the tension between the ALICE and LHCb data in the forward/backward direction, we can see that at least at our "optimal" scale both the EPPS16 and nCTEQ15 results (but obviously not the nNNPDF2.0) seem to reproduce the LHCb data points better but that both data sets can still be accommodated within the larger EPPS16 uncertainties.

IV. SUMMARY

We have presented the very first implementation of exclusive rapidity-differential J/ψ photoproduction cross sections in ultraperipheral nucleus-nucleus collisions in the framework of collinear factorization and NLO perturbative QCD. We have developed our numerical code for the ultraperipheral nuclear collisions based on the analytical NLO results of Ref. [30], utilizing the experience obtained also in [35,49], and following earlier literature in accounting for the photon fluxes of the colliding nuclei [3,5,13,62,63,88–90] and for the t dependence of the cross section with a standard nuclear form factor. In this exploratory NLO study for the UPCs, we approximate the GPDs involved in the process with their forward-limit nuclear PDFs. Our default choice for the nPDFs and their error sets is EPPS16 [45] but we also study the nPDF sensitivity of our results by using nCTEQ15 [44] and nNNPDF2.0 [46].

We have shown that, as expected based on Ref. [30], the computed rapidity-differential NLO cross sections of J/ψ photoproduction in 5.02 and 2.76 TeV Pb + Pb UPCs at the LHC, as well as the corresponding photoproduction cross sections in ep collisions at HERA, are both in their magnitude and in their shape quite sensitive to the scale choice. As the scale sensitivity is much larger than the error bars of the experimental data at the LHC, it makes it difficult to make solid NLO predictions of the corresponding J/ψ cross section for UPCs at other energies. Quite encouragingly, however, we have found that a scale choice $\mu \approx 0.76 M_{J/\psi}$, which lies in the physically reasonable range $\mu = \mathcal{O}(M_{J/\psi})$, can actually be determined, with which we can well reproduce the ALICE [36–39], LHCb [41], and CMS [40] UPC data

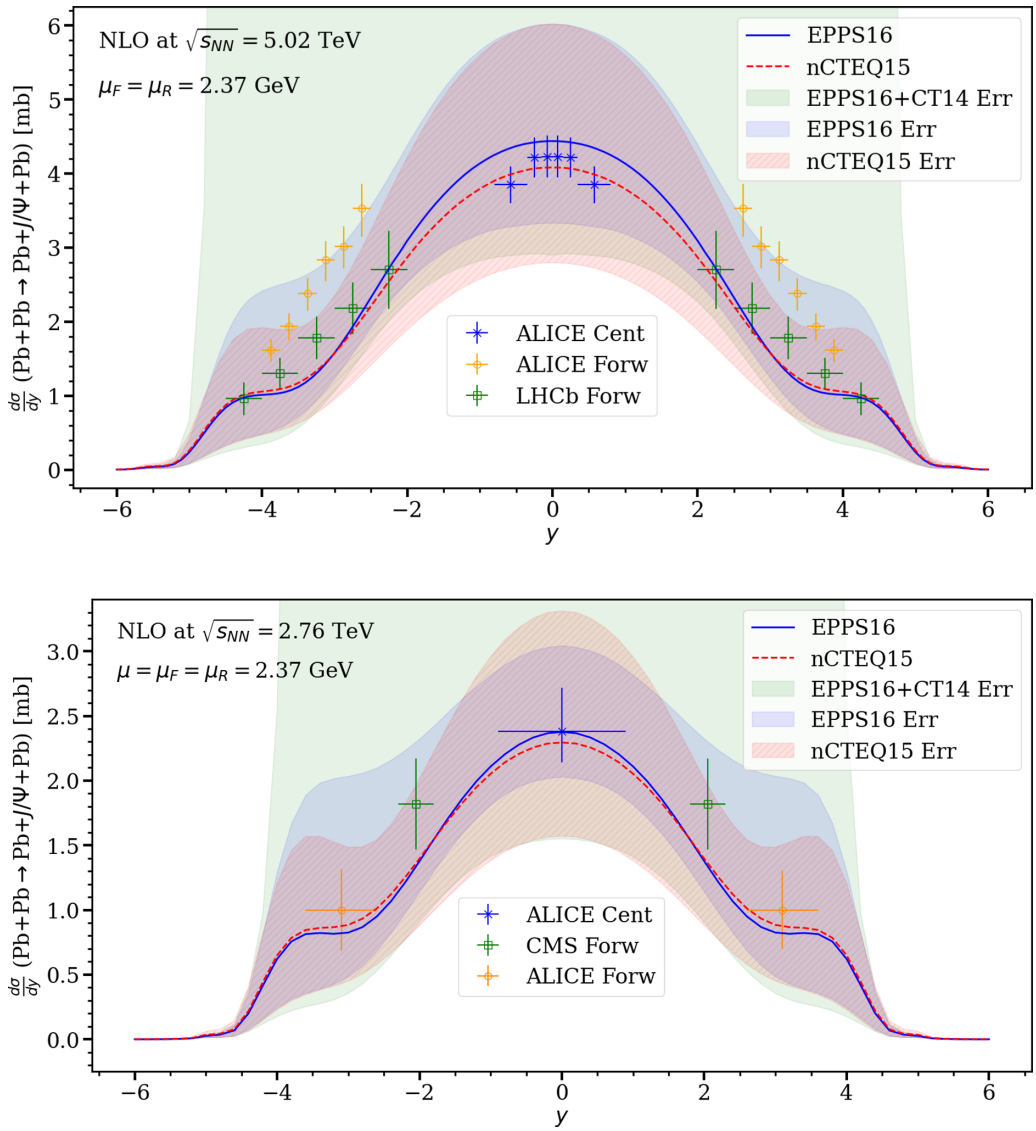

FIG. 13. Upper panel: Uncertainties originating from the nPDFs/PDFs in the rapidity-differential exclusive J/ψ photoproduction NLO cross sections in 5.02 TeV Pb + Pb UPCs, computed at our "optimal" scale $\mu = 2.37$ GeV using the EPPS16 + CT14NLO and nCTEQ15 error sets. The solid (dashed) line shows the EPPS16 + CT14NLO (nCTEQ15) central-set result, and the corresponding uncertainty bands are explained in the text. The experimental data points are from Run2 and the same as in the upper panel of Fig. 1. Lower panel: The same but for $\sqrt{s_{NN}} = 2.76$ TeV and with the same Run1 data as in the lower panel of Fig. 1.

at these energies. We have also tested that the same scale choice, called here the "optimal" scale, works well also with the nCTEQ15 nPDFs. Interestingly, in studying the scale sensitivity at a fixed value of $y = 0$, we noticed that towards the upper end of the scales studied here the scale sensitivity of the full NLO result becomes actually weaker than that of the LO result, but towards the lower end of scales it becomes stronger than in LO. Also interestingly, at midrapidity the "optimal" scale becomes fixed right in the scale region where the NLO contributions are the smallest relative to LO. In the future, it will be interesting to see whether this "minimal-sensitivity" feature remains there also after further modeling of the GPDs.

We have made an effort to analyze in sufficient detail the surprisingly complex structure of the exclusive rapidity-differential J/ψ photoproduction NLO cross sections in Pb + Pb UPCs at 5.02 and 2.76 TeV. In particular, we have shown how the computed NLO cross sections form under various competing and intertwining effects: There are competing contributions from the photon-nucleon c.m.s. energy $W^{\pm}$ components, from the real and imaginary parts of the full amplitude, from the quark and gluon GPD/PDF contributions which also mix in a nontrivial way in the squared amplitude, and most importantly of all, from the gluonic LO and NLO amplitudes which come with opposite signs and cancel each other to a degree that nontrivially depends on the $W^{\pm}$. All these competing contributions need to be taken into account in the full NLO study, as is done in the current paper.

The main result of our NLO study with the EPPS16 nPDFs, similar to the findings in Ref. [30] but now for UPCs, is that due to the canceling LO and NLO gluon amplitudes it

is predominantly the small-x *quark* GPDs/PDFs that exclusive J/ψ photoproduction is probing in UPCs at midrapidity, and not the gluon distributions as has been traditionally suggested before based on LO. This is an important result not addressed before, to our knowledge, in the UPC context. We have also checked that this result is robust against the scale variation studied here. We have also shown that towards the forward/backward rapidities the gluon dominance is eventually recovered but because of the folding with the photon flux (which kills one of the $W^{\pm}$ contributions) the nuclear gluon GPDs/PDFs become probed at larger values of x (where shadowing effects become smaller) than at midrapidity. Thus, our conclusion is—at least in our current "bare bones" GPD/PDF framework and with the EPPS16 and nCTEQ15 nPDFs—that the exclusive rapidity-differential J/ψ photoproduction cross sections at the LHC are not as a direct and efficient probe of the small-x nuclear gluon PDFs as thought before, but that they are primarily probed (at midrapidity at least) through the DGLAP evolution of the quark GPDs/PDFs. Another important observation is that at midrapidity the dependence of the computed NLO cross sections on the nuclear effects in PDFs is not as quadratic as thought before in the LO gluon context. The taming of the net nuclear effects follows partly from the x integration in the NLO amplitude but predominantly from the behavior of the interference term in the squared amplitude, which mixes the quark and gluon contributions in a nontrivial way.

We have also investigated the dependence of our results on the uncertainties of the PDFs. The nCTEQ15 central-set results are essentially the same as those with the central set of EPPS16. At midrapidity, where the quark contributions dominate, these two sets show very similar error bands when the uncertainties of the nuclear effects in the PDFs are propagated into the NLO cross sections. Towards forward/backward rapidities where gluons dominate, the EPPS16 uncertainties become slightly larger, which follows from the more realistic (due to having more freedom in the gluon PDF shape there) estimates of the gluon nPDF uncertainties than in nCTEQ15. In any case, in the current "bare bones" GPD/PDF framework, we observe that both the forward ALICE [38] and LHCb [41] data can be accommodated within the nuclear PDF error bands, while the results with the central sets of EPPS16 and nCTEQ15 agree better with the LHCb data.

Finally, we have observed that if there is a very rapid rise in the small-x gluon distributions, such as in the nNNPDF2.0 central set and the error set 53 in the CT14NLO free-proton PDFs [64] (93 in EPPS16 at LHAPDF), then the smallest-x contribution to the real part of the gluon LO amplitude starts to dominate the cross sections. Concretely, in our results when the EPPS16 nuclear errors and the CT14NLO errors are appropriately combined, the CT14NLO error set 53 (93 in EPPS16 at LHAPDF) dictates the upper boundaries of the very large uncertainty band on our central result. In our "bare bones" GPD/PDF framework, such a growth seems to be ruled out by the UPC data considered here. However, before we can make any further conclusions on this point, uncertainties arising from the modeling of GPDs should be quantified.

The current paper is meant as a baseline for systematic further studies of exclusive photoproduction of vector mesons in ultraperipheral nucleus-nucleus collisions, in collinear factorization and NLO pQCD. An obvious next task is to repeat the NLO study for the photoproduction cross sections of Υ mesons, to investigate in particular how much the scale dependence changes and check exactly what happens with all the intertwined effects at the higher scales $\mu = \mathcal{O}(M_\Upsilon)$. On the basis of Ref. [30], we would expect to see a reduced scale sensitivity and a stronger dependence on the gluon PDFs also in the UPC case.

There are also several ways the current framework could and should be improved. Our strategy for the current exploratory study is that, as the scale- and PDF-related uncertainties are so large, we may leave the GPD modeling (such as in Ref. [56]) as a future challenge. Next, given the studied "bare bones" GPD/PDF baseline, it will be interesting to study how the nPDF uncertainties propagate to the GPDs and via them to the NLO cross sections. As far as we can see, based, e.g., on Refs. [54,91], the skewedness corrections to the GPD quark distributions in the DGLAP region can be expected to be larger for quarks than for gluons, which would further strengthen our conclusion of the quark dominance at midrapidity. Towards forward/backward rapidities, the gluon dominance would then correspondingly kick in more slowly. Particularly interesting here would be to study the role of the nuclear effects in the ERBL region, where the PDFs are known not to be an optimal approximation but which in the current study turned out to be important essentially only with PDF sets that have rapidly growing small-x distributions. Future improvements would also include nonrelativistic QCD corrections into the vector meson wave function [92–94].

ACKNOWLEDGMENTS

We acknowledge the helpful discussions with I. Helenius and H. Mäntysaari. We acknowledge the financial support from the Magnus Ehrnrooth foundation (T.L.), the Academy of Finland Projects No. 297058 (K.J.E.), No. 308301 (H.P.) and No. 330448 (K.J.E.). This research was funded as a part of the Center of Excellence in Quark Matter of the Academy of Finland (Projects No. 346325 and No. 346326). This research is part of the European Research Council Project No. ERC-2018-ADG-835105 YoctoLHC.

[1] C. A. Bertulani and G. Baur, Electromagnetic processes in relativistic heavy ion collisions, Phys. Rep. **163**, 299 (1988).

[2] J. Nystrand, Ultra-peripheral collisions of heavy ions at RHIC and the LHC, Nucl. Phys. A **787**, 29 (2007).

[3] A. J. Baltz, The physics of ultraperipheral collisions at the LHC, Phys. Rep. **458**, 1 (2008).

[4] A. Adeluyi and C. Bertulani, Gluon distributions in nuclei probed at the CERN Large Hadron Collider, Phys. Rev. C **84**, 024916 (2011).

[5] A. Adeluyi and C. A. Bertulani, Constraining gluon shadowing using photoproduction in ultraperipheral *pA* and *AA* Collisions, Phys. Rev. C **85**, 044904 (2012).

[6] V. Guzey, E. Kryshen, and M. Zhalov, Coherent photoproduction of vector mesons in ultraperipheral heavy ion collisions: Update for run 2 at the CERN Large Hadron Collider, Phys. Rev. C **93**, 055206 (2016).

[7] V. Guzey, E. Kryshen, M. Strikman, and M. Zhalov, Nuclear suppression from coherent J/ψ photoproduction at the Large Hadron Collider, Phys. Lett. B **816**, 136202 (2021).

[8] V. Guzey, E. Kryshen, M. Strikman, and M. Zhalov, Evidence for nuclear gluon shadowing from the ALICE measurements of PbPb ultraperipheral exclusive J/ψ production, Phys. Lett. B **726**, 290 (2013).

[9] V. Guzey and M. Zhalov, Exclusive J/ψ production in ultraperipheral collisions at the LHC: Constraints on the gluon distributions in the proton and nuclei, J. High Energy Phys. 10 (2013) 207.

[10] V. Guzey, M. Strikman, and M. Zhalov, Accessing transverse nucleon and gluon distributions in heavy nuclei using coherent vector meson photoproduction at high energies in ion ultraperipheral collisions, Phys. Rev. C **95**, 025204 (2017).

[11] S. P. Jones, A. D. Martin, M. G. Ryskin, and T. Teubner, The exclusive J/ψ process at the LHC tamed to probe the low x gluon, Eur. Phys. J. C **76**, 633 (2016).

[12] M. Ryskin, Diffractive J/ψ electroproduction in LLA QCD, Z. Phys. C **57**, 89 (1993).

[13] S. R. Klein, J. Nystrand, J. Seger, Y. Gorbunov, and J. Butterworth, STARlight: A Monte Carlo simulation program for ultra-peripheral collisions of relativistic ions, Comput. Phys. Commun. **212**, 258 (2017).

[14] L. A. Harland-Lang, M. Tasevsky, V. A. Khoze, and M. G. Ryskin, A new approach to modelling elastic and inelastic photon-initiated production at the LHC: SuperChic 4, Eur. Phys. J. C **80**, 925 (2020).

[15] V. P. Gonçalves and M. V. T. Machado, The QCD pomeron in ultraperipheral heavy ion collisions IV. Photonuclear production of vector mesons, Eur. Phys. J. C **40**, 519 (2005).

[16] T. Lappi and H. Mantysaari, J/ψ production in ultraperipheral Pb+Pb and p+Pb collisions at energies available at the CERN Large Hadron Collider, Phys. Rev. C **87**, 032201 (2013).

[17] H. Mäntysaari and B. Schenke, Probing subnucleon scale fluctuations in ultraperipheral heavy ion collisions, Phys. Lett. B **772**, 832 (2017).

[18] H. Mäntysaari and R. Venugopalan, Systematics of strong nuclear amplification of gluon saturation from exclusive vector meson production in high energy electron–nucleus collisions, Phys. Lett. B **781**, 664 (2018).

[19] J. Cepila, J. G. Contreras, and M. Krelina, Coherent and incoherent J/ψ photonuclear production in an energy-dependent hot-spot model, Phys. Rev. C **97**, 024901 (2018).

[20] H. Mäntysaari and B. Schenke, Accessing the gluonic structure of light nuclei at a future electron-ion collider, Phys. Rev. C **101**, 015203 (2020).

[21] B. Sambasivam, T. Toll, and T. Ullrich, Investigating saturation effects in ultraperipheral collisions at the LHC with the color dipole model, Phys. Lett. B **803**, 135277 (2020).

[22] S. R. Klein and H. Mäntysaari, Imaging the nucleus with high-energy photons, Nat. Rev. Phys. **1**, 662 (2019).

[23] A. Caldwell and H. Kowalski, Investigating the gluonic structure of nuclei via J/ψ scattering, Phys. Rev. C **81**, 025203 (2010).

[24] D. Bendova, J. Cepila, J. G. Contreras and M. Matas, Photonuclear J/ψ production at the LHC: Proton-based versus nuclear dipole scattering amplitudes, Phys. Lett. B **817**, 136306 (2021).

[25] H. Mäntysaari and J. Penttala, Exclusive heavy vector meson production at next-to-leading order in the dipole picture, Phys. Lett. B **823**, 136723 (2021).

[26] C. Adloff *et al.* (H1 Collaboration), Elastic photoproduction of J/ψ and Υ mesons at HERA, Phys. Lett. B **483**, 23 (2000).

[27] S. Chekanov *et al.* (ZEUS Collaboration), Exclusive photoproduction of J/ψ mesons at HERA, Eur. Phys. J. C **24**, 345 (2002).

[28] R. Aaij *et al.* (LHCb Collaboration), Updated measurements of exclusive J/ψ and $\psi(2S)$ production cross-sections in pp collisions at $\sqrt{s} = 7$ TeV, J. Phys. G: Nucl. Part. Phys. **41**, 055002 (2014).

[29] R. Aaij *et al.* (LHCb Collaboration), Central exclusive production of J/ψ and $\psi(2S)$ mesons in pp collisions at $\sqrt{s} = 13$ TeV, J. High Energy Phys. 10 (2018) 167.

[30] D. Y. Ivanov, A. Schafer, L. Szymanowski, and G. Krasnikov, Exclusive photoproduction of a heavy vector meson in QCD, Eur. Phys. J. C **34**, 297 (2004); Erratum to: Exclusive photoproduction of a heavy vector meson in QCD, **75**, 75(E) (2015).

[31] S. P. Jones, A. D. Martin, M. G. Ryskin, and T. Teubner, Exclusive J/ψ and Υ photoproduction and the low x gluon, J. Phys. G: Nucl. Part. Phys. **43**, 035002 (2016).

[32] C. A. Flett, S. P. Jones, A. D. Martin, M. G. Ryskin, and T. Teubner, Towards a determination of the low x gluon via exclusive J/ψ production, PoS **DIS2019**, 053 (2019).

[33] C. A. Flett, S. P. Jones, A. D. Martin, M. G. Ryskin, and T. Teubner, How to include exclusive J/ψ production data in global PDF analyses, Phys. Rev. D **101**, 094011 (2020).

[34] C. A. Flett, A. D. Martin, M. G. Ryskin and T. Teubner, Very low x gluon density determined by LHCb exclusive J/ψ data, Phys. Rev. D **102**, 114021 (2020).

[35] C. A. Flett, Exclusive Observables to NLO and low x PDF phenomenology at the LHC, Ph.D. thesis, University of Liverpool, 2021.

[36] S. Acharya *et al.* (ALICE Collaboration), Coherent J/ψ and ψ' photoproduction at midrapidity in ultra-peripheral Pb–Pb collisions at $\sqrt{s_{NN}} = 5.02$ TeV, Eur. Phys. J. C **81**, 712 (2021).

[37] E. Abbas *et al.* (ALICE Collaboration), Charmonium and e^+e^- pair photoproduction at mid-rapidity in ultra-peripheral Pb-Pb collisions at $\sqrt{s_{NN}} = 2.76$ TeV, Eur. Phys. J. C **73**, 2617 (2013).

[38] S. Acharya *et al.* (ALICE Collaboration), Coherent J/ψ photoproduction at forward rapidity in ultra-peripheral Pb-Pb collisions at $\sqrt{s_{\rm NN}} = 5.02$ TeV, Phys. Lett. B **798**, 134926 (2019).

[39] B. Abelev *et al.* (ALICE Collaboration), Coherent J/ψ photoproduction in ultra-peripheral Pb-Pb collisions at $\sqrt{s_{NN}} = 2.76$ TeV, Phys. Lett. B **718**, 1273 (2013).

[40] V. Khachatryan *et al.* (CMS Collaboration), Coherent J/ψ photoproduction in ultra-peripheral PbPb collisions at $\sqrt{s_{NN}} = 2.76$ TeV with the CMS experiment, Phys. Lett. B **772**, 489 (2017).

[41] R. Aaij *et al.* (LHCb Collaboration), Study of coherent J/ψ production in lead-lead collisions at $\sqrt{s_{NN}} = 5$ TeV, JHEP 07 (2022) 117.

[42] LHCb Collaboration, Study of coherent charmonium production in ultra-peripheral lead-lead collisions, arXiv:2206.08221.

[43] J. Brewer, A. Mazeliauskas, and W. van der Schee, Opportunities of OO and pO collisions at the LHC, arXiv:2103.01939.

[44] K. Kovařík *et al.*, nCTEQ15: Global analysis of nuclear parton distributions with uncertainties in the CTEQ framework, Phys. Rev. D **93**, 085037 (2016).

[45] K. J. Eskola, P. Paakkinen, H. Paukkunen, and C. A. Salgado, EPPS16: Nuclear parton distributions with LHC data, Eur. Phys. J. C **77**, 163 (2017).

[46] R. Abdul Khalek, J. J. Ethier, J. Rojo, and G. van Weelden, nNNPDF2.0: Quark flavor separation in nuclei from LHC data, J. High Energy Phys. 09 (2020) 183.

[47] K. J. Eskola, P. Paakkinen, H. Paukkunen, and C. A. Salgado, EPPS21: A global QCD analysis of nuclear PDFs, Eur. Phys. J. C **82**, 413 (2022).

[48] R. A. Khalek, R. Gauld, T. Giani, E. R. Nocera, T. R. Rabemananjara, and J. Rojo, nNNPDF3.0: Evidence for a modified partonic structure in heavy nuclei, Eur. Phys. J. C **82**, 507 (2022).

[49] S. P. Jones, A. D. Martin, M. G. Ryskin and T. Teubner, Probes of the small x gluon via exclusive J/ψ and Υ production at HERA and the LHC, J. High Energy Phys. 11 (2013) 085.

[50] Z.-Q. Chen and C.-F. Qiao, NLO QCD corrections to exclusive electroproduction of quarkonium, Phys. Lett. B **797**, 134816 (2019); Erratum to "NLO QCD corrections to exclusive electroproduction of quarkonium" [Phys. Lett. B **797**, 134816 (2019)] **809**, 135759(E) (2020).

[51] C. A. Flett, J. A. Gracey, S. P. Jones, and T. Teubner, Exclusive heavy vector meson electroproduction to NLO in collinear factorisation, J. High Energy Phys. 08 (2021) 150.

[52] J. C. Collins, L. Frankfurt, and M. Strikman, Factorization for hard exclusive electroproduction of mesons in QCD, Phys. Rev. D **56**, 2982 (1997).

[53] M. Diehl, Generalized parton distributions, Phys. Rep. **388**, 41 (2003).

[54] A. G. Shuvaev, K. J. Golec-Biernat, A. D. Martin, and M. G. Ryskin, Off diagonal distributions fixed by diagonal partons at small x and ξ, Phys. Rev. D **60**, 014015 (1999).

[55] A. Shuvaev, Solution of the off-forward leading logarithmic evolution equation based on the Gegenbauer moments inversion, Phys. Rev. D **60**, 116005 (1999).

[56] A. Freund, M. McDermott, and M. Strikman, Modeling generalized parton distributions to describe deeply virtual Compton scattering data, Phys. Rev. D **67**, 036001 (2003).

[57] A. D. Martin, C. Nockles, M. G. Ryskin, A. G. Shuvaev, and T. Teubner, Generalised parton distributions at small x, Eur. Phys. J. C **63**, 57 (2009).

[58] K. Kumerički and D. Mueller, Deeply virtual Compton scattering at small x_B and the access to the GPD H, Nucl. Phys. B **841**, 1 (2010).

[59] L. A. Harland-Lang, Simple form for the low-x generalized parton distributions in the skewed regime, Phys. Rev. D **88**034029 (2013).

[60] M. Constantinou *et al.*, Parton distributions and lattice-QCD calculations: Toward 3D structure, Prog. Part. Nucl. Phys. **121**, 103908 (2021).

[61] V. Bertone, H. Dutrieux, C. Mezrag, J. M. Morgado, and H. Moutarde, Revisiting evolution equations for generalised parton distributions, arXiv:2206.01412.

[62] M. Vidovic, M. Greiner, C. Best, and G. Soff, Impact parameter dependence of the electromagnetic particle production in ultrarelativistic heavy ion collisions, Phys. Rev. C **47**, 2308 (1993).

[63] V. Guzey and M. Zhalov, Rapidity and momentum transfer distributions of coherent J/ψ photoproduction in ultraperipheral pPb collisions at the LHC, J. High Energy Phys. 02 (2014) 046.

[64] S. Dulat, T.-J. Hou, J. Gao, M. Guzzi, J. Huston, P. Nadolsky, J. Pumplin, C. Schmidt, D. Stump, and C. P. Yuan, New parton distribution functions from a global analysis of quantum chromodynamics, Phys. Rev. D **93**, 033006 (2016).

[65] M. Drees and D. Zeppenfeld, Production of supersymmetric particles in elastic ep collisions, Phys. Rev. D **39**, 2536 (1989).

[66] C. A. Bertulani, S. R. Klein, and J. Nystrand, Physics of ultraperipheral nuclear collisions, Annu. Rev. Nucl. Part. Sci. **55**, 271 (2005).

[67] S. Acharya *et al.* (ALICE Collaboration), First measurement of the $|t|$-dependence of coherent J/ψ photonuclear production, Phys. Lett. B **817**, 136280 (2021).

[68] S. R. Klein and J. Nystrand, Interference in Exclusive Vector Meson Production in Heavy-Ion Collisions, Phys. Rev. Lett. **84**, 2330 (2000).

[69] W. Schäfer and A. Szczurek, Exclusive photoproduction of J/ψ in proton-proton and proton-antiproton scattering, Phys. Rev. D **76**, 094014 (2007).

[70] S. Klein and J. Nystrand, Exclusive vector meson production in relativistic heavy ion collisions, Phys. Rev. C **60**, 014903 (1999).

[71] R. D. Woods and D. S. Saxon, Diffuse Surface Optical Model for Nucleon-Nuclei Scattering, Phys. Rev. **95**, 577 (1954).

[72] H. De Vries, C. W. De Jager, and C. De Vries, Nuclear charge and magnetization density distribution parameters from elastic electron scattering, At. Data Nucl. Data Tables **36**, 495 (1987).

[73] I. Helenius, K. J. Eskola, H. Honkanen, and C. A. Salgado, Impact-parameter dependent nuclear parton distribution functions: EPS09s and EKS98s and their applications in nuclear hard processes, J. High Energy Phys. 07 (2012) 073.

[74] C. Alexa *et al.* (H1 Collaboration), Elastic and proton-dissociative photoproduction of J/ψ mesons at HERA, Eur. Phys. J. C **73**, 2466 (2013).

[75] V. A. Khoze, A. D. Martin, and M. G. Ryskin, Diffraction at the LHC, Eur. Phys. J. C **73**, 2503 (2013).

[76] S. Jones, A study of exclusive processes to NLO and small-x PDFs from LHC data, Ph.D. thesis, University of Liverpool, 2015 (unpublished); and private communication.

[77] E. L. Berger and D. L. Jones, Inelastic photoproduction of J/ψ and Υ by gluons, Phys. Rev. D **23**, 1521 (1981).

[78] A. Petrelli, M. Cacciari, M. Greco, F. Maltoni, and M. L. Mangano, NLO production and decay of quarkonium, Nucl. Phys. B **514**, 245 (1998).

[79] G. T. Bodwin and A. Petrelli, Order-v^4 corrections to S-wave quarkonium decay, Phys. Rev. D **66**, 094011 (2002); Erratum: Order-v^4 corrections to S-wave quarkonium decay [Phys. Rev. D **66**, 094011 (2002)] **87**, 039902(E) (2013).

[80] E. Braaten and J. Lee, Exclusive double charmonium production from e^+e^- annihilation into a virtual photon, Phys. Rev. D **67**, 054007 (2003); Erratum: Exclusive double-charmonium production from e^+e^- annihilation into a virtual photon [Phys. Rev. D **67**, 054007 (2003)] **72**, 099901(E) (2005)

[81] R. Barbieri, R. Gatto, R. Kogerler, and Z. Kunszt, Meson hyperfine splittings and leptonic decays, Phys. Lett. B **57**, 455 (1975).

[82] G. T. Bodwin, E. Braaten, and G. P. Lepage, Rigorous QCD analysis of inclusive annihilation and production of heavy quarkonium, Phys. Rev. D **51**, 1125 (1995); Erratum: Rigorous QCD analysis of inclusive annihilation and production of heavy quarkonium [Phys. Rev. D **51**, 1125 (1995)] **55**, 5853(E) (1997).

[83] M. Beneke, A. Signer, and V. A. Smirnov, Two-Loop Corrections to the Leptonic Decays of Quarkonium, Phys. Rev. Lett. **80**, 2535 (1998).

[84] X.-D. Ji, Deeply virtual Compton scattering, Phys. Rev. D **55**, 7114 (1997).

[85] P. Zyla *et al.* (Particle Data Group), Review of particle physics, Prog. Theor. Exp. Phys. **2020**, 083C01 (2020).

[86] A. Buckley, J. Ferrando, S. Lloyd, K. Nordström, B. Page, M. Rüfenacht, M. Schönherr, and G. Watt, LHAPDF6: Parton density access in the LHC precision era, Eur. Phys. J. C **75**, 132 (2015).

[87] W. Florkowski, *Phenomenology of Ultra-Relativistic Heavy-Ion Collisions* (World Scientific, Singapore, 2012).

[88] W. Zha, L. Ruan, Z. Tang, Z. Xu, and S. Yang, Coherent lepton pair production in hadronic heavy ion collisions, Phys. Lett. B **781**, 182 (2018).

[89] C. F. V. Weizsäcker, Radiation emitted in collisions of very fast electrons, Z. Phys. **88**, 612 (1934).

[90] J. D. Jackson, *Classical Electrodynamics* (Wiley, New York, 1998).

[91] A. D. Martin and M. G. Ryskin, The effect of off diagonal parton distributions in diffractive vector meson electroproduction, Phys. Rev. D **57**, 6692 (1998).

[92] P. Hoodbhoy, Wave function corrections and off forward gluon distributions in diffractive J/ψ electroproduction, Phys. Rev. D **56**, 388 (1997).

[93] L. Frankfurt, W. Koepf, and M. Strikman, Diffractive heavy quarkonium photoproduction and electroproduction in QCD, Phys. Rev. D **57**, 512 (1998).

[94] T. Lappi, H. Mäntysaari, and J. Penttala, Relativistic corrections to the vector meson light front wave function, Phys. Rev. D **102**, 054020 (2020).

[PII]

NEXT-TO-LEADING ORDER PERTURBATIVE QCD PREDICTIONS FOR EXCLUSIVE J/ψ PHOTOPRODUCTION IN OXYGEN-OXYGEN AND LEAD-LEAD COLLISIONS AT THE LHC

by

Kari J. Eskola, Christopher A. Flett, Vadim Guzey, Topi Löytäinen and Hannu Paukkunen,

Phys. Rev. C. 107 **no.4**, 044912, arXiv: 2210.16048 [hep-ph] (Oct. 2022).

Next-to-leading order perturbative QCD predictions for exclusive J/ψ photoproduction in oxygen-oxygen and lead-lead collisions at energies available at the CERN Large Hadron Collider

K. J. Eskola,* C. A. Flett,† V. Guzey,‡ T. Löytäinen,§ and H. Paukkunen‖
Department of Physics, University of Jyvaskyla, P.O. Box 35, FI-40014 Jyvaskyla, Finland
and Helsinki Institute of Physics, University of Helsinki, P.O. Box 64, FI-00014 Helsinki, Finland

(Received 3 November 2022; accepted 5 April 2023; published 28 April 2023)

We present predictions for the cross sections of coherent J/ψ photoproduction in lead-lead and oxygen-oxygen ultraperipheral collisions (UPCs) as a function of the J/ψ rapidity at the LHC in the framework of collinear factorization at next-to-leading order (NLO) in perturbative QCD. Taking generalized parton distribution functions in their forward limit and using the EPPS21, nNNPDF3.0, and nCTEQ15WZSIH nuclear parton distribution functions, we update our recent results for Pb-Pb collisions, make detailed predictions for O-O collisions for several beam energy configurations, and examine the ratio of O-O and Pb-Pb UPC cross sections. We show that the latter observable allows one to significantly reduce the scale uncertainty of NLO predictions for this process.

DOI: 10.1103/PhysRevC.107.044912

I. INTRODUCTION

Traditionally, parton distribution functions (PDFs) and their nuclear counterparts, nuclear PDFs (nPDFs), have been determined from inclusive processes such as lepton-hadron deep inelastic scattering (DIS) and the production of leptons pairs (Drell-Yan process), light and heavy mesons, dijets, and gauge bosons in hadron-hadron scattering, see Refs. [1–4] for recent reviews. The determination of proton and nuclear PDFs has become an active branch of phenomenological applications of quantum chromodynamics (QCD), for recent examples of global fits of PDFs and nPDFs, see Refs. [5–13]. However, despite the dramatic progress in the methodology of PDF extraction from the available data, including an account of higher-order (up to next-to-next-to-leading order, NNLO) perturbative QCD corrections, effects of heavy (charm and bottom) quark masses and small-x resummation and the reliance on sophisticated statistical and computational methods (Bayesian and Hessian error estimates and neural networks), the resulting PDFs and nPDFs still suffer from significant uncertainties.

As a consequence, there is a continuing interest to explore novel kinematics, processes, and observables, which would allow one to obtain additional constraints on the PDFs. In particular, it has been discussed that the exclusive photoproduction of J/ψ mesons on the proton and nuclear targets in the so-called ultraperipheral collisions (UPCs) allows one to probe the gluon density of the target at small momentum fractions $x \sim 10^{-5}$–10^{-3} and resolution scales $\mu^2 \approx 3\ \mathrm{GeV}^2$ [14–19] (photoproduction of other quarkonium states, ψ' and Υ, has also been considered). This is based on the early observation that in the leading logarithmic approximation, i.e., to the leading order (LO) of perturbative QCD (pQCD), the cross section of this process is directly proportional to the gluon density squared [20]. However, it was later found that the next-to-leading order (NLO) QCD corrections involving both gluon and quark distributions are very large [15,21], which questions the common interpretation in terms of the gluon density. While several methods to stabilize the NLO results have been proposed [16,22,23], further theoretical and phenomenological studies are still required.

We recently performed a detailed study of the cross section of exclusive photoproduction of J/ψ mesons in Pb-Pb UPCs at the Large Hadron Collider (LHC) as a function of the J/ψ rapidity y in the framework of collinear factorization and NLO pQCD, and confirmed the dramatic role of the NLO effects [24]. In particular, we found that at central rapidities the cross section is dominated by the quark contribution since the gluon one largely cancels in the sum of the LO and the NLO terms. Additionally, even though the scale dependence of our results turned out to be, as expected, rather sizable, we determined an optimal scale allowing for a simultaneous reasonable description of the available Run 1 and Run 2 LHC data on this process. In addition, we observed that the amplitude for this process is predominantly imaginary in a broad range of rapidities with a small window at forward and backward rapidities, where the real part gives the dominant contribution.

*kari.eskola@jyu.fi
†chris.a.flett@jyu.fi
‡vadim.a.guzey@jyu.fi
§topi.m.o.loytainen@jyu.fi
‖hannu.paukkunen@jyu.fi

The purpose of this work is to extend the analysis of Ref. [24] by (i) updating our previous results for Pb-Pb collisions with three different state-of-the-art nPDF sets, namely, EPPS21 [11], nNNPDF3.0 [12], and nCTEQ15WZSIH [8], (ii) making detailed predictions for the $\mathrm{O}+\mathrm{O}\to\mathrm{O}+J/\psi+\mathrm{O}$ rapidity differential cross section for the planned oxygen run at the LHC [25,26], and (iii) presenting predictions for the ratio of the J/ψ rapidity distributions in Pb-Pb and O-O UPCs. This allows us not only to better control the theoretical uncertainties associated with the nPDFs, but also to tame (reduce) the scale dependence of our NLO results by considering the ratio of J/ψ production with different nuclear collision systems. For the recent predictions of J/ψ photoproduction in O-O UPCs at the LHC in the color dipole framework, see Ref. [27].

The rest of the paper is organized as follows. In Sec. II, we recapitulate the framework of NLO pQCD coherent exclusive photoproduction of J/ψ in nucleus-nucleus UPCs, pointing out specific extensions to the oxygen beams. Section III contains our results, which include updated predictions for $d\sigma(\mathrm{Pb}+\mathrm{Pb}\to\mathrm{Pb}+J/\psi+\mathrm{Pb})/dy$ with the most recent sets of nPDFs and their comparison to all available LHC data on this process, detailed predictions for $d\sigma(\mathrm{O}+\mathrm{O}\to\mathrm{O}+J/\psi+\mathrm{O})/dy$ for the oxygen run with an analysis of the scale dependence and the decomposition into the imaginary and real parts as well as into the gluon and quark contributions, and, finally, predictions for the ratios of the J/ψ rapidity distributions in O-O and Pb-Pb UPCs with an exhaustive analysis of the scale and energy dependence. We discuss and summarize our findings in Sec. IV.

II. COHERENT J/ψ PHOTOPRODUCTION IN NUCLEUS-NUCLEUS UPCS IN NLO PQCD

In the equivalent photon approximation the cross section of coherent J/ψ photoproduction in UPCs of nuclei (ions) A_1 and A_2, as a function of the J/ψ rapidity y, reads [28]

$$\frac{d\sigma^{A_1A_2\to A_1J/\psi A_2}}{dy}=\left[k\frac{dN_\gamma^{A_1}(k)}{dk}\right]_{k=k^+}\sigma^{\gamma A_2\to J/\psi A_2}(W^+)+\left[k\frac{dN_\gamma^{A_2}(k)}{dk}\right]_{k=k^-}\sigma^{A_1\gamma\to A_1J/\psi}(W^-), \tag{1}$$

where $kdN_\gamma^A(k)/dk$ is the flux of equivalent quasireal photons emitted by ions A_1 and A_2, k is the photon energy and $\sigma^{\gamma A\to VA}(W)$ is the cross section of coherent (without nuclear breakup) J/ψ photoproduction on a nuclear target with W being the collision energy of the photon-nucleon system. The two terms in Eq. (1) represent two possibilities to arrive at the same final state corresponding either to ion A_1 emitting a photon interacting then with ion A_2 or ion A_2 being a source of photons interacting with ion A_1. We define the positive rapidity y in the direction of the ion A_1, from which one obtains that the relation between the photon energies $k^\pm$ and the rapidity y is $k^\pm=(M_{J/\psi}/2)e^{\pm y}$, where k^+ and k^- refer to ions A_1 (positive longitudinal momentum) and A_2 (negative longitudinal momentum), respectively, and $M_{J/\psi}$ is the mass of J/ψ. The corresponding photon-nucleon system energies are $W^+=\sqrt{2M_{J/\psi}e^yE_2}$ and $W^-=\sqrt{2M_{J/\psi}e^{-y}E_1}$, where E_2 and E_1 are the per nucleon energies of beams A_2 and A_1, respectively. For symmetric UPCs, we have $E_2=E_1=\sqrt{s_{NN}}/2$, where $\sqrt{s_{NN}}$ is the nucleon-nucleon center-of-mass system (c.m.s.) energy. The interference between the amplitudes, where the photons are emitted by different nuclei, is important only at very small values of the momentum transfer t (very small values of the J/ψ transverse momentum) [29] and hence can be safely neglected in the case of the UPC cross section integrated over t, which we consider.

The flux of equivalent photons emitted by a relativistic ion in UPCs is given by a convolution of the impact parameter dependent photon flux $N_\gamma^A(k,\vec{b})$ and the nuclear suppression factor $\Gamma_{AA}(\vec{b})$,

$$k\frac{dN_\gamma^A(k)}{dk}=\int d^2\vec{b}\,N_\gamma^A(k,\vec{b})\Gamma_{AA}(\vec{b}), \tag{2}$$

where $\vec{b}$ is a two-dimensional impact parameter vector denoting the distance between the centers of colliding nuclei in the transverse plane. Furthermore, the impact parameter dependent photon flux $N_\gamma^A(k,\vec{b})$ of a relativistic nucleus A with Z protons can be readily calculated in QED [30],

$$N_\gamma^A(k,\vec{b})=\frac{Z^2\alpha_{\mathrm{e.m.}}}{\pi^2}\left|\int_0^\infty dk_\perp\frac{k_\perp^2\tilde{F}_A\left(k_\perp^2+k^2/\gamma_L^2\right)}{k_\perp^2+k^2/\gamma_L^2}J_1(|\vec{b}|k_\perp)\right|^2, \tag{3}$$

where $\alpha_{\mathrm{e.m.}}$ is the fine-structure constant, γ_L is the nucleus Lorentz factor, J_1 is the cylindrical modified Bessel function of the first kind, and $\tilde{F}_A(t)$ is the nucleus form factor normalized to one, i.e., $\tilde{F}_A(t)=F_A(t)/A$. The nuclear form factor $F_A(t)$, accompanied with the normalization condition $F_A(0)=A$, is in turn given by the standard Fourier transform of the nuclear density $\rho_A(r)$,

$$F_A(t)=\int d^3\boldsymbol{r}\,e^{i\boldsymbol{q}\cdot\boldsymbol{r}}\rho_A(r), \tag{4}$$

where $t=-|\boldsymbol{q}|^2$.

The nuclear density is well known from measurements of elastic electron-nucleus scattering and is usually parameterized in the form of two-parameter Fermi model (also called Woods-Saxon model) and three-parameter Fermi model (3pF) [31]. The former is typical for heavy nuclei, for lead, see Ref. [24], and latter is usually employed for medium-heavy nuclei. In particular, in this work we use the 3pF parametrization for oxygen

$$\rho_O(r)=\frac{\rho_0\left(1+w\left(\frac{r}{R_A}\right)^2\right)}{1+e^{(r-R_A)/d}}, \tag{5}$$

with the free parameters determined from nuclear charge-density measurements [31],

$$d=0.513\ \mathrm{fm}\ \text{and}\ w=-0.051. \tag{6}$$

For lead we use $d=0.546$ fm and $w=0$. The effective nuclear radii are here taken from the following empirical

parametrization (see, e.g., Ref. [32])[1]

$$R_A/\text{fm} = 1.12\,A^{1/3} – 0.86\,A^{-1/3}. \quad (7)$$

Further, in Eq. (2), the nuclear suppression factor $\Gamma_{AA}(\vec{b})$ represents the probability of having no hadronic interactions at impact parameter $\vec{b}$, which can be evaluated using the Glauber model for nucleus-nucleus scattering

$$\Gamma_{AA}(\vec{b}) = \exp[-\sigma_{NN}(s_{NN})T_{AA}(\vec{b})], \quad (8)$$

where $\sigma_{NN}(s_{NN})$ is the total nucleon-nucleon cross section [33] and $T_{AA}(\vec{b}) = \int d^2\vec{b}' T_A(\vec{b}')T_A(\vec{b}-\vec{b}')$ is the nuclear overlap function with $T_A(\vec{b}) = \int dz \rho_A(\vec{r})$. In Eq. (2), the effect of $\Gamma_{AA}(b)$ is to suppress the contribution of the $|\vec{b}| < 2R_A$ region.

For the cross section of coherent J/ψ photoproduction on nuclei A we use the form where the t dependence governed by the nuclear form factor squared $|F_A(t)|^2$, is factorized from the cross section of J/ψ production on bound nucleons N of the nuclear target, i.e., $d\sigma_A^{\gamma N\to J/\psi N}/dt$ (this is indicated by the subscript),

$$\sigma^{\gamma A\to J/\psi A}(W) = \left.\frac{d\sigma_A^{\gamma N\to J/\psi N}}{dt}\right|_{t=0} \int_{|t_{\min}|}^{\infty} dt' |F_A(-t')|^2, \quad (9)$$

where $|t_{\min}| = [M_{J/\psi}^2/(4k\gamma_L)]^2$. In the case of the t-integrated cross section, the factorized form of Eq. (9) approximates with a several-percent precision a more accurate expression that takes into account the correlation between t and x, i.e., the correlation between the momentum transfer and the magnitude of nuclear effects (nuclear shadowing) affecting $d\sigma_A^{\gamma N\to J/\psi N}/dt$, see the discussion in Refs. [34,35].

The QCD dynamics of the process is contained in the $d\sigma_A^{\gamma N\to J/\psi N}/dt(t=0)$ cross section. In the framework of collinear factorization for exclusive processes in NLO perturbative QCD and using the nonrelativistic (static) approximation for the charmonium wave function, the cross section reads (see Refs. [21,24] for details and references)

$$\left.\frac{d\sigma_A^{\gamma N\to J/\psi N}}{dt}\right|_{t=0} = \frac{1}{W^4}\frac{4\pi^2\alpha_{\text{e.m.}}e_c^2\langle O_1\rangle_V}{9\xi^2 m_c^3}|I(\xi, t=0)|^2, \quad (10)$$

where the reduced scattering amplitude is given by a convolution of the gluon and quark hard scattering coefficient functions $T_g(x,\xi,\mu_R,\mu_F)$ and $T_q(x,\xi,\mu_R,\mu_F)$ with the corresponding gluon and quark generalized parton distribution functions (GPDs) $F^g(x,\xi,t,\mu_F)$ and $F^{q,S}(x,\xi,t,\mu_F)$ of the bound nucleons,

$$I(\xi,t=0) = \int_{-1}^{1} dx [T_g(x,\xi,\mu_R,\mu_F)F^g(x,\xi,t=0,\mu_F) + T_q(x,\xi,\mu_R,\mu_F)F^{q,S}(x,\xi,t=0,\mu_F)]. \quad (11)$$

[1]For the oxygen case this means that the radius, as given in Eq. (7), is taken in the approximation $w=0$ with the same parameter values as for lead.

In Eq. (10), $e_c = 2/3$ and $m_c = M_{J/\psi}/2$ is the charm quark mass in the nonrelativistic limit, $\langle O_1\rangle_V$ is the nonrelativistic QCD matrix element associated with the $J/\psi\to l^+l^-$ leptonic decay, $\xi = \zeta/(2-\zeta)$ is the so-called skewness parameter with $\zeta = M_{J/\psi}^2/W^2$ being an analog of Bjorken x in inclusive DIS. Note that the quark contribution in Eq. (11) contains a singlet combination of quark GPDs of four active flavors, $F^{q,S}(x,\xi,t=0,\mu_F) = \sum_{q=u,d,s,c} F^q(x,\xi,t=0,\mu_F)$. In our analysis we take the factorization and renormalization scales to be equal, i.e., $\mu = \mu_F = \mu_R$, which sets the term $\sim\beta_0 \ln(\mu_R^2/\mu_F^2)$ in the NLO gluon contribution to zero, see Eq. (3.72) in Ref. [21]. This choice corresponds to the BLM scale setting prescription [36]. We quantify the dependence of our results on the scale choice by varying the scale in the $m_c \leqslant \mu \leqslant 2m_c$ interval.

In general, GPDs are complicated nonperturbative distributions depending on two light-cone momentum fractions x and ξ and the momentum transfer t as well as the factorization scale μ_F. However, in the high-energy limit the skewness parameter is very small ($\xi \ll 1$) and its effect on GPDs is expected to be rather moderate. In particular, in the calculation of the $d\sigma_A^{\gamma N\to J/\psi N}/dt(t=0)$ cross section, theoretical uncertainties associated with detailed modeling of GPDs are expected to be much smaller than the scale and nPDF uncertainties. Therefore, as a first approximation, we neglect the skewness effect and take GPDs in the forward limit, where they can be identified with the usual PDFs,

$$\begin{aligned} &F^g(x,\xi,t=0,\mu_F) = F^g(-x,\xi,t=0,\mu_F) \to x g_A(x,\mu_F),\\ &F^q(x,\xi,t=0,\mu_F) \to q_A(x,\mu_F),\\ &F^q(-x,\xi,t=0,\mu_F) \to -\bar{q}_A(x,\mu_F), \end{aligned} \quad (12)$$

where now $0 \leqslant x \leqslant 1$. The distributions $g_A(x,\mu_F)$, $q_A(x,\mu_F)$ and $\bar{q}_A(x,\mu_F)$ are the usual gluon, quark, and antiquark nPDFs per nucleon. They encode nuclear modifications of bound nucleon PDFs, the most relevant being small-x nuclear shadowing and antishadowing. In our analysis, we use the recent nPDF sets EPPS21 [11], nNNPDF3.0 [12], and nCTEQ15WZSIH [37].

III. RESULTS

A plan is moving forward that an oxygen-oxygen (O-O) run would be performed at the LHC in Run 3 [25,26,38]. In addition to shedding light on the soft QCD dynamics and studying hard scattering with small nuclear systems, it might help to address open questions relating to forward scattering physics. From the point of view of UPC studies, as we pointed out in Sec. I, an analysis of coherent J/ψ photoproduction in O-O UPCs and a comparison to the case of Pb-Pb UPCs can be used to constrain theoretical uncertainties of our NLO pQCD predictions for this process. At the time of writing of this paper, it is not yet completely clear at which nucleon-nucleon c.m.s. energy $\sqrt{s_{NN}}$ the O-O run will be completed. Therefore, we will consider four scenarios with $\sqrt{s_{NN}} = 2.76$, 5.02, 6.37 [38], and 7 TeV [25], which will help us to better understand the energy dependence of our results.

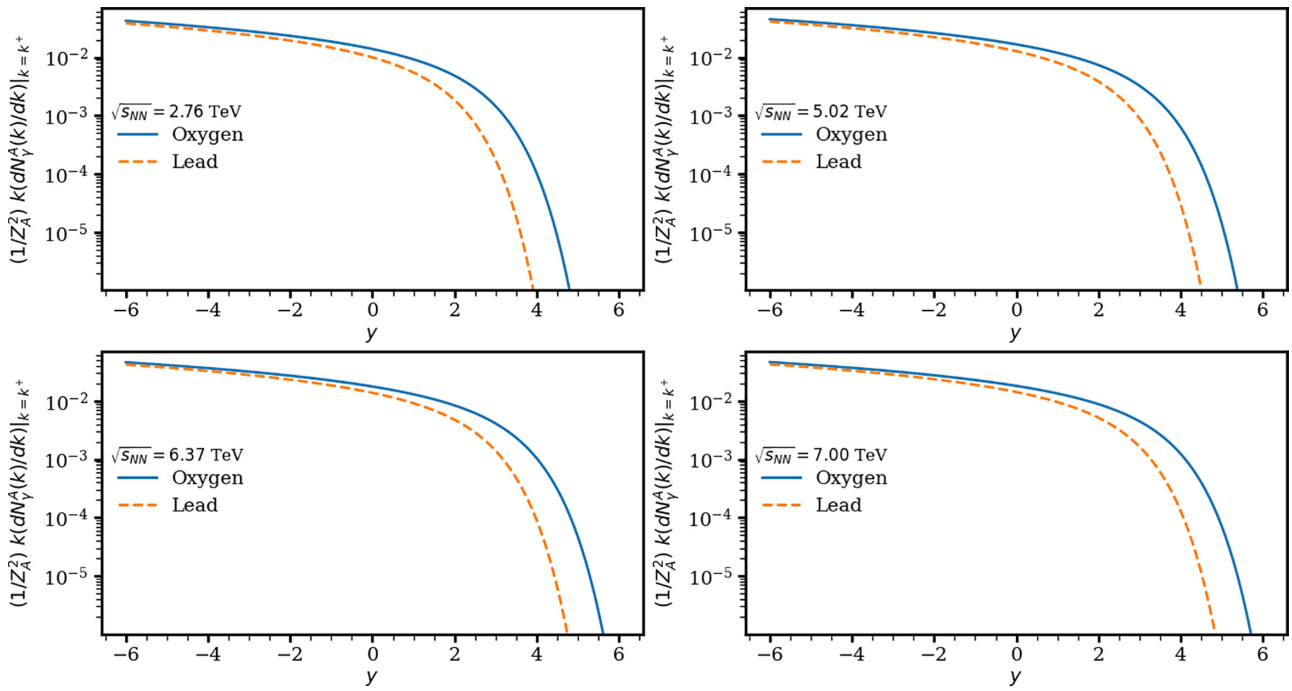

FIG. 1. The scaled photon flux $(1/Z^2)kdN_\gamma^A(k)/dk$ as a function of the rapidity y in the plus direction for the oxygen and lead beams for four different values of the c.m.s. energy $\sqrt{s_{NN}} = 2.76$, 5.02, 6.37, and 7 TeV.

A. Photon fluxes and nuclear form factors

The results for the $kdN_\gamma^A(k)/dk$ photon flux obtained through Eq. (2), where $k = (M_{J/\psi}/2)e^y$, i.e., positive rapidity y corresponds to large photon energies k, for oxygen and lead beams for four different values of the invariant collision energy $\sqrt{s_{NN}}$ are presented in Fig. 1. In the figure, the blue solid curves correspond to the oxygen case and the orange dashed curves to the lead case. In order to conveniently compare the two cases, we normalized the fluxes by the factor of $1/Z^2$ with $Z_O = 8$ for oxygen and $Z_{Pb} = 82$ for lead.

One can see from the figure that at negative rapidities (small photon momenta) the photon flux of the lead beam is much larger than that for the oxygen beam, $[kdN_\gamma^{Pb}(k)/dk]/[kdN_\gamma^{O}(k)/dk] \approx Z_{Pb}^2/Z_O^2 \approx 100$. At the same time, since the effective nuclear radius of lead is almost three times as large as that of oxygen, the spectrum of equivalent photons of lead falls off more rapidly when y is increased (corresponding to an increase in k) than that of oxygen. Eventually, for large values of rapidity $y \geqslant 4.4$ corresponding to $k \geqslant 120$ GeV, the photon flux for oxygen becomes bigger than that of lead.

We have numerically checked that setting $w = 0$ in Eq. (5), i.e., assuming the two-parameter Fermi (2pF) model for oxygen with the same d and R_A parameters, leads to a relative difference of under four percent in the photon flux for the photon energies up to $k \approx 50$ GeV corresponding to the J/ψ rapidities $|y| \leqslant 3.5$. In addition, we have checked that the photon flux is not sensitive to the exact value of σ_{NN} used in $\Gamma_{AA}(\vec{b})$, see Eq. (8). For example, at $\sqrt{s_{NN}} = 6.37$ and 7 TeV, calculations for the photon flux with $\sigma_{NN} = 95$ mb and $\sigma_{NN} = 100$ mb differ by less than 1% all the way up to $|y| = 4$. Thus, we conclude that the major difference between the scaled photon fluxes of the oxygen and lead ions originates from the different effective radii R_A of these nuclei.

In the left panel of Fig. 2 we show the results for the oxygen and lead form factors scaled by the corresponding mass number A as they are given by Eq. (4). The values of the scaled form factors approach one due to our normalization constraint $F_A(0) = A$ but, as we move to higher values of t, we see that the scaled oxygen form factor is the dominant one except for the oscillations at very high values of t. But again, since $A_{Pb} \gg A_O$, the absolute magnitude of the form factor of lead is the bigger one. Then, in the photoproduction cross section $\sigma^{\gamma A \to VA}$, we have an integral over the square of the absolute value of the form factor. The right panel of Fig. 2 shows the values of this integral scaled by the square of the mass number A for both the oxygen (solid blue) and the lead (dashed orange) cases. Similarly to the photon flux, this ratio gets intertwined in the ratios of the cross sections, but at central rapidities $y = 0$ corresponding to $|t_{min}| \approx 10^{-6}$ GeV^2, we should expect to see a factor of 4.6 from the ratio of the integrals.

B. Rapidity-dependent cross sections in Pb-Pb UPCs and comparison with the LHC data

Based on the NLO pQCD theoretical framework outlined in Sec. II, we present below our predictions for the $d\sigma(\mathrm{Pb} + \mathrm{Pb} \to \mathrm{Pb} + J/\psi + \mathrm{Pb})/dy$ cross section of coherent J/ψ photoproduction in Pb-Pb UPCs as a function of the J/ψ rapidity y at $\sqrt{s_{NN}} = 2.76$ TeV (Run 1) and $\sqrt{s_{NN}} = 5.02$ TeV (Run 2) at the LHC and compare them with all available LHC data on this process. We performed our

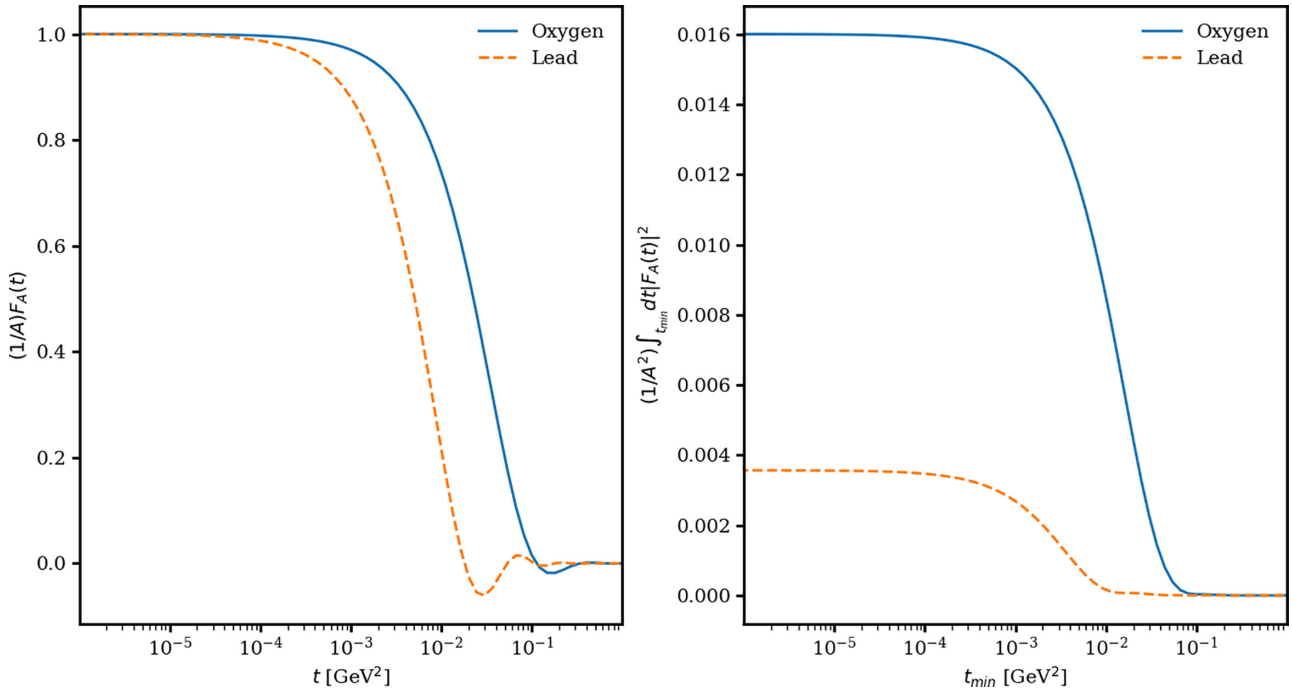

FIG. 2. Left: Form factors scaled by the corresponding mass number A for oxygen and lead as a function of t. The scaled oxygen form factor reaches out farther in t than the corresponding lead one. Right: The values of the integral of the absolute value of the form factor squared scaled by the square of the corresponding mass number A given as a function of the lower limit $t_{\rm min}$ of the integral. At small enough values of $t_{\rm min}$, the ratio between the oxygen and the lead results is about 4.6.

calculations using the most recent EPPS21 [11], nNNPDF3.0 [12], and nCTEQ15WZSIH [37] sets of nPDFs, which updates our predictions in Ref. [24].

Figure 3 demonstrates the variation of our predictions due to the choice of the scale μ, which is allowed to vary in the $m_c \leqslant \mu \leqslant 2m_c$ interval ($m_c = M_{J/\psi}/2 = 1.55$ GeV in the nonrelativistic limit that we use): the top dashed curves correspond to $\mu = 3.1$ GeV, while the bottom dotted curves are for $\mu = 1.55$ GeV. The solid curve in each panel corresponds to an optimal scale, which is chosen to simultaneously describe the central rapidity data available from Run 1 (left panels) and Run 2 (right panels) at the LHC. The Run 1 data at $\sqrt{s_{NN}} = 2.76$ TeV include the ALICE data at the central rapidity $|y| < 0.9$ [39] (labeled "ALICE Cent") and at the forward rapidity $2.6 < |y| < 3.6$ [40] labeled "ALICE Forw") as well as the CMS data in the rapidity interval $1.8 < |y| < 2.3$ [41] (labeled "CMS Forw"). The Run 2 data taken at $\sqrt{s_{NN}} = 5.02$ TeV are the ALICE data at midrapidity $|y| < 0.8$ [42] (labeled "ALICE Cent"), the ALICE data at forward rapidities $2.5 < |y| < 4$ [43] (labeled "ALICE Forw"), the LHCb data at forward rapidities $2 < |y| < 4.5$ [44] (labeled "LHCb 2015") and their recent update [45] (labeled "LHCb 2018"). The three rows of panels correspond to the results of our calculations using three different sets of nPDFs: EPPS21 [11] (top row), nNNPDF3.0 [12] (middle row), and nCTEQ15WZSIH [37] (bottom row). Our analysis shows that the resulting optimal scales μ slightly differ for different nPDF sets: $\mu = 2.39$ GeV for EPPS21, $\mu = 2.22$ GeV for nNNPDF3.0, and $\mu = 2.02$ GeV for nCTEQ15WZSIH.

A comparison of the results presented in Fig. 3 with our results in Ref. [24] shows that the difference between our calculations using EPPS21 and EPPS16 is very small with a very similar value of the optimal scale and the same shape of the y dependence as well as the matching magnitude of the scale dependence and the quality of the data description. To be exact, at central rapidity $y = 0$, for Run 1 there is a factor of about 22 between the highest scale and the lowest scale results and for Run 2 energy this factor is about 55.

The improvement, when moving from nNNPDF2.0 [46] (Fig. 10 of Ref. [24]) to the newer nNNPDF3.0 set, is rather dramatic. We find that the shape of the $d\sigma(\mathrm{Pb}+\mathrm{Pb} \to \mathrm{Pb}+J/\psi+\mathrm{Pb})/dy$ cross section at the optimal scale $\mu = 2.22$ GeV is qualitatively similar to that obtained with EPPS16 or EPPS21. Simultaneously, however, the correspondence with the data is slightly worse: while the data at $y \approx 0$ is reproduced by construction, the solid curve somewhat underestimates the data at $|y| \neq 0$. Note that the good agreement with the data at $y \approx 0$ is important for the comparison of the Pb-Pb and O-O UPC data; see the discussion in Sec. III D. The ratio between the highest scale and the lowest scale at central rapidity is about 17 for Run 1 and about 26 for Run 2.

In contrast to EPPS21 and nNNPDF3.0, we find that the newest nCTEQ15WZSIH nPDF set actually does better on all accounts. The scale dependence at central rapidity is only about a factor of 10 for Run 1 and about a factor of 12 for Run 2. The curve corresponding to the optimal scale of $\mu = 2.02$ GeV goes through the central rapidity data points in addition to the forward/backward data both at Run 1 and Run 2 energies. Moreover, the nCTEQ15WZSIH nPDF set favors the ALICE forward data [43] and the newer LHCb 2018 data [45] over the 2015 LHCb data [44]. We have checked that the better agreement of our calculations using

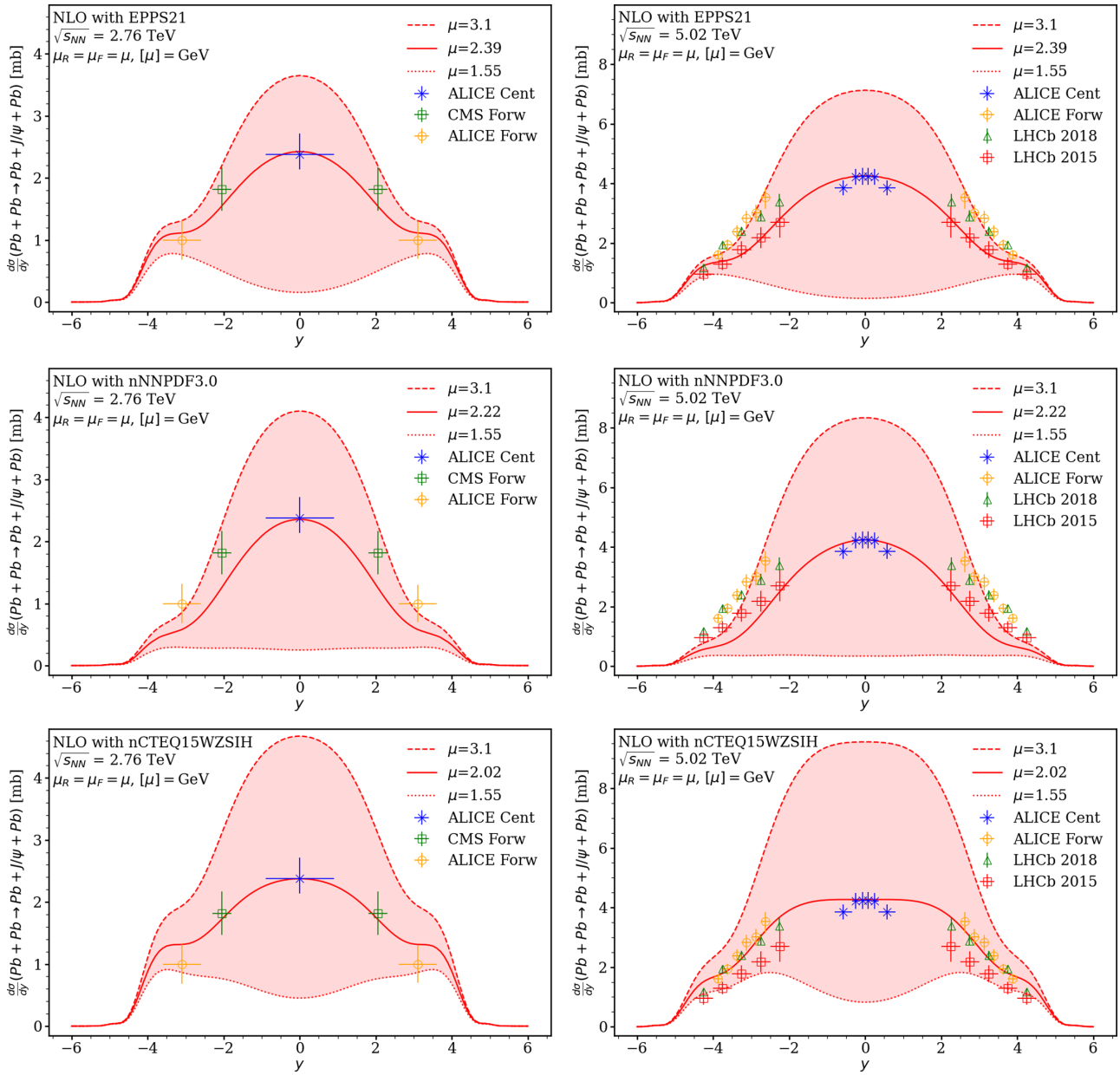

FIG. 3. The scale dependence of the NLO pQCD predictions for the $d\sigma(\mathrm{Pb} + \mathrm{Pb} \to \mathrm{Pb} + J/\psi + \mathrm{Pb})/dy$ cross section as a function of the rapidity y for Run 1 ($\sqrt{s_{NN}} = 2.76$ TeV, left column) and Run 2 ($\sqrt{s_{NN}} = 5.02$ TeV, right column) at the LHC and a comparison with the corresponding Run 1 [39–41] and Run 2 [42–45] data, the statistical and systematic errors added in quadrature. The data have been mirrored with respect to $y = 0$. The scale-dependence envelope spans the results corresponding to $\mu = 3.1$ GeV (top dashed curve) and $\mu = 1.55$ GeV (bottom dotted curve); the solid curve corresponds to the optimal scale. The three rows of panels correspond to EPPS21 (top), nNNPDF3.0 (middle), and nCTEQ15WZSIH (bottom) nPDFs.

the nCTEQ15WZSIH nPDF set with the UPC data is due to the very strongly enhanced strange quark distributions, see Fig. 4 in Ref. [47]. Thus, this process may give an interesting opportunity to obtain new constraints on the elusive strange quark distribution in the proton and nuclei.

For all three sets, when considering the full range of scales $\mu \in [m_c, M_{J/\psi}]$, the scale uncertainty decreases slightly—as was with the earlier EPPS16 set—as we move farther away from the central rapidity towards backward and forward rapidities. This is partly because at very large values of rapidity, i.e., $|y| > 3$, the photoproduction amplitude receives a large contribution from the W-component corresponding to small values of k, which in turn means that we are probing the underlying GPDs at high values of x, where the scale dependence is constrained rather well. In any case, it is interesting to notice that this rapidity dependence seems to be a common property for both the old and the new nPDF sets (see Fig. 4 in Ref. [24]).

To estimate the PDF uncertainty of our predictions due to the EPPS21 and nCTEQ15WZSIH nPDFs, we used the

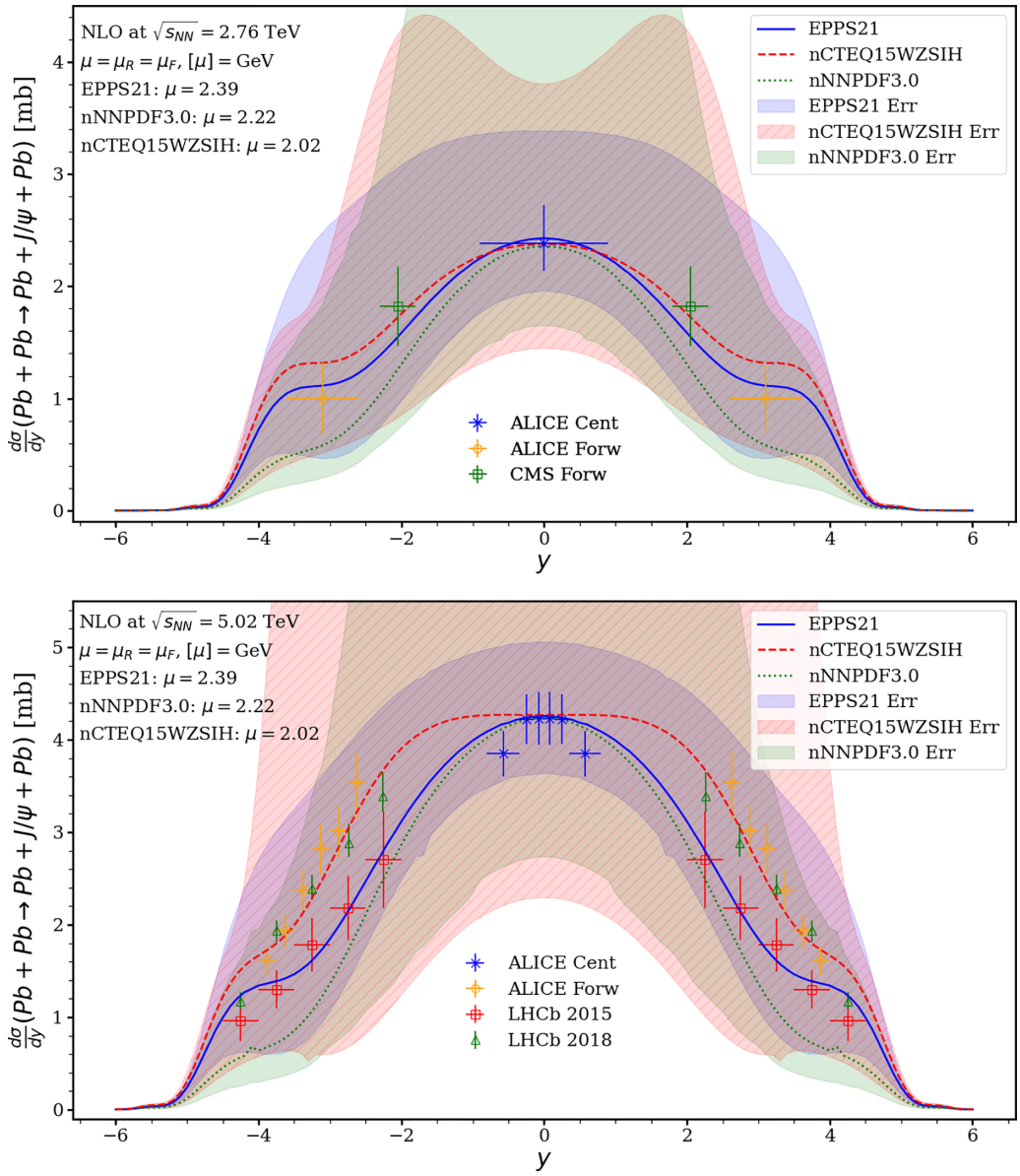

FIG. 4. The PDF uncertainties of the NLO pQCD predictions for the $d\sigma(\mathrm{Pb} + \mathrm{Pb} \to \mathrm{Pb} + J/\psi + \mathrm{Pb})/dy$ cross section as a function of y for Run 1 (top) and Run 2 (bottom) at the LHC, and a comparison with the corresponding Run 1 [39–41] and Run 2 [42–45] data, mirrored with respect to $y = 0$ and with the statistical and systematic errors added in quadrature. The results corresponding to the central sets of nPDFs are shown by the blue solid (EPPS21), red dashed (nCTEQ15WZSIH), and green dotted (nNNPDF3.0) curves, respectively, and the error bands are represented by the corresponding shaded regions. All calculations are performed at the indicated values of the optimal scale μ.

following asymmetric form for the uncertainty $\delta\mathcal{O}^{\pm}$ [9]:

$$\delta\mathcal{O}^{\pm} = \sqrt{\sum_i \left[{}^{\max}_{\min}\{\mathcal{O}(S_i^+) - \mathcal{O}(S_0), \mathcal{O}(S_i^-) - \mathcal{O}(S_0), 0\}\right]^2}, \tag{13}$$

where $\mathcal{O}(S_0)$ denotes the predictions with the central set for the observable $\mathcal{O}$ and $\mathcal{O}(S_i^{\pm})$ correspond to the values calculated with the plus and minus PDF error sets. In the case of nNNPDF3.0, we used the 90% confidence level (CL) interval prescription [12]. All PDF uncertainty calculations are performed at the corresponding values of the optimal scale μ.

Figure 4 illustrates the uncertainty of our predictions for the $d\sigma(\mathrm{Pb} + \mathrm{Pb} \to \mathrm{Pb} + J/\psi + \mathrm{Pb})/dy$ cross section due to errors of nPDFs and compares it with the Run 1 (top panel) and Run 2 (bottom panel) LHC data. The calculations using the central sets of nPDFs are given by the blue solid (EPPS21), red dashed (nCTEQ15WZSIH), and green dotted (nNNPDF3.0) curves and the error bands are represented by the corresponding shaded regions. One can see from the figure that within the PDF uncertainties the framework of NLO pQCD describes the data rather well; the agreement with the data is very good at central rapidity for all three nPDF sets (by construction), continues to be good for nCTEQ15WZSIH in

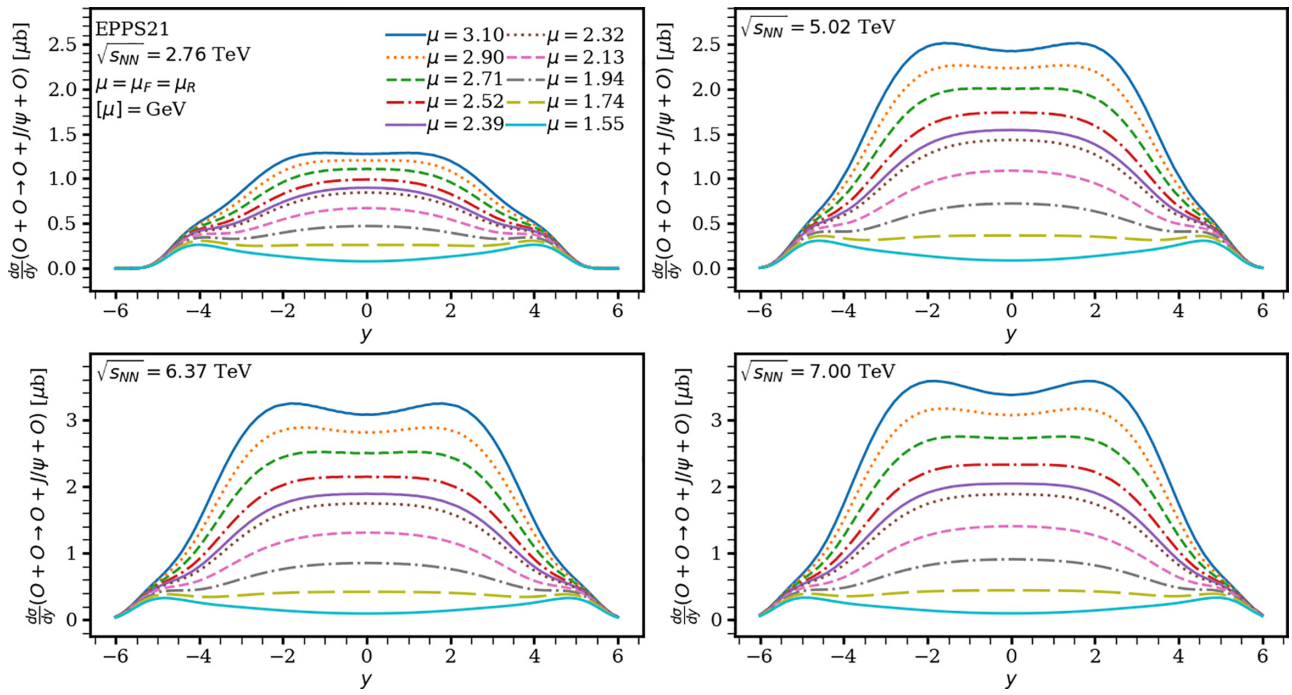

FIG. 5. The NLO pQCD results for the rapidity differential cross section of coherent J/ψ photoproduction in O-O UPCs as a function of the rapidity y, obtained with the EPPS21 nPDFs at $\sqrt{s_{NN}} = 2.76$, 5.02, 6.37, and 7 TeV. The different lines show the results for ten choices of the scale μ ranging from $\mu = m_c$ (lowest curve) to $\mu = M_{J/\psi}$ (highest curve) with a step of $m_c/8$. The $\mu = 2.39$ GeV optimal scale prediction lies in the middle of this scale-uncertainty envelope.

the entire range of measured y, but becomes somewhat worse at higher $|y|$ for EPPS21 and NNPDF3.0.

A comparison of our EPPS21 results with the previous EPP16 ones [24] shows that the full PDF uncertainty band, which receives contributions from varying the parameters of nPDFs and the baseline free proton PDFs, has come down to the order of few millibarns. As we discussed in Ref. [24], the free proton CT14nlo PDFs accompanying the EPPS16 nPDFs contain a particular error set dramatically growing at small x, which results in an abnormally large small-x uncertainty. In the new EPPS21 nPDFs, where the nuclear effects are correlated with the baseline CT18ANLO [5] free proton PDF error sets, this behavior no longer persists.

One can clearly see from Fig. 4 that the EPPS21 nPDFs correspond to significantly smaller uncertainties than nNNPDF3.0 and CTEQ15WZSIH. In particular, the nNNPDF3.0 uncertainties, which also account for the free proton PDF errors, at central rapidity rise up to around 8 mb at Run 1 and up to around 13.5 mb at Run 2. The nCTEQ15WZSIH uncertainties, which account for the nPDF errors only, are smaller both for Run 1 and Run 2 at central rapidities than at $y \approx \pm 2.0$, which leads to a valleylike structure. For instance, for Run 2, the uncertainty rises up to around 8.5 mb at $y = 0$ and then to its maximum of approximately 18 mb at $y \approx \pm 2.5$. As with EPPS21, no single error PDFs set stands out in the nCTEQ15WZSIH and nNNPDF3.0 parametrizations, but the larger uncertainty bands are simply the result of a wider distribution in the underlying error sets.

C. Predictions for rapidity-dependent cross sections in O-O UPCs at the LHC

In this section, we present detailed predictions for the $d\sigma(\mathrm{O}+\mathrm{O}\to\mathrm{O}+J/\psi+\mathrm{O})/dy$ cross section of coherent J/ψ photoproduction in NLO perturbative QCD as a function of the J/ψ rapidity y in oxygen-oxygen UPCs at the LHC. As mentioned above, since the exact energy of O-O collisions is not yet determined, we consider four scenarios with $\sqrt{s_{NN}} =$ 2.76, 5.02, 6.37, and 7 TeV. In addition to studying the energy dependence of our predictions, this choice enables a direct comparison to the case of Pb-Pb UPCs at $\sqrt{s_{NN}} = 2.76$ TeV (Run 1) and $\sqrt{s_{NN}} = 5.02$ TeV (Run 2), see the discussion in Sec. III D.

Figure 5 illustrates the scale dependence of our predictions and shows our results for $d\sigma(\mathrm{O}+\mathrm{O}\to\mathrm{O}+J/\psi+\mathrm{O})/dy$ with the EPPS21 nPDFs at ten different values of the scale μ ranging from $\mu = m_c$ up to $\mu = M_{J/\psi}$ for the four different values of $\sqrt{s_{NN}}$. One can see from the figure that the O-O UPC cross section is approximately 1000 times smaller than that in the Pb-Pb case primarily due to the much smaller photon flux. On the other hand, the shape of the y dependence is similar in the O-O and Pb-Pb cases: it is rather broad at midrapidity with sloping shoulders at forward and backward rapidities; higher scales correspond to larger $d\sigma(\mathrm{O}+\mathrm{O}\to\mathrm{O}+J/\psi+\mathrm{O})/dy$, which also tend to develop a valleylike structure at the highest scales of $\mu \approx M_{J/\psi}$.

To quantify the magnitude of the scale dependence, we consider the ratio between the $\mu = M_{J/\psi}$ and $\mu = m_c$ results at $y = 0$, which we denote by R_{scale}. One can see from Fig. 5

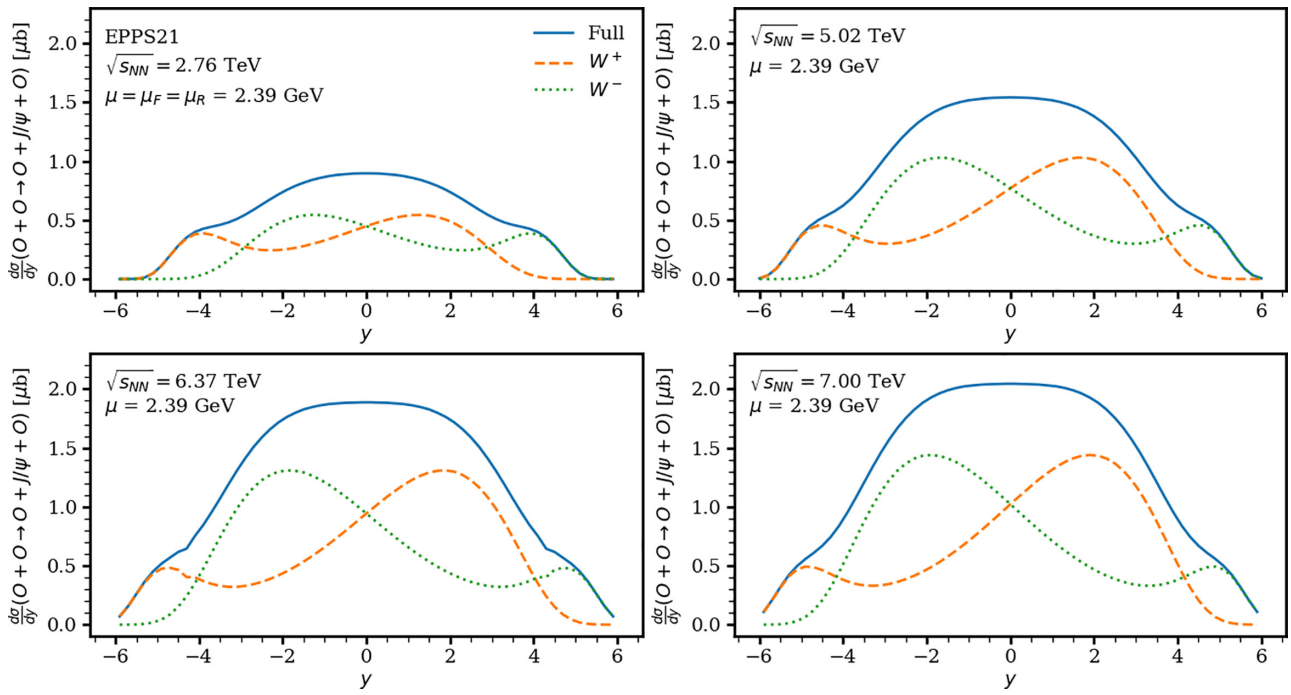

FIG. 6. Separation of the NLO pQCD predictions for the $d\sigma(\mathrm{O}+\mathrm{O}\to\mathrm{O}+J/\psi+\mathrm{O})/dy$ cross section of coherent J/ψ photoproduction in O-O UPCs as a function of the rapidity y into the W^+ (dashed orange curve) and W^- (dotted green curve) components; the solid blue line is their sum. The calculation employs the EPPS21 nPDFs at $\mu = 2.39$ GeV. The different panels correspond to $\sqrt{s_{NN}} = 2.76$, 5.02, 6.37, and 7 TeV.

that R_{scale} is of the same order of magnitude as in Pb-Pb collisions starting at $R_{\mathrm{scale}} \approx 16$ at $\sqrt{s_{NN}} = 2.76$ TeV and rising up to $R_{\mathrm{scale}} \approx 35$ at $\sqrt{s_{NN}} = 7$ TeV. We have checked that with nCTEQ15WZSIH the scale dependence is of the same order as with EPPS21: $R_{\mathrm{scale}} \approx 12$ at $\sqrt{s_{NN}} = 2.76$ TeV and increasing to approximately $R_{\mathrm{scale}} = 20$ at $\sqrt{s_{NN}} = 7$ TeV. At the same time, for nNNPDF3.0 the scale dependence is considerably stronger: $R_{\mathrm{scale}} \approx 800$ at $\sqrt{s_{NN}} = 2.76$ TeV and increases up to $R_{\mathrm{scale}} \approx 2700$ at $\sqrt{s_{NN}} = 7$ TeV. This huge scale dependence is due to the nearly perfect cancellation between the LO and the NLO contributions in both the real and the imaginary parts of the amplitude at the lowest scale of $\mu = m_c$. At forward and backward rapidities over the full range $\mu \in [m_c, M_{J/\psi}]$, the scale dependence is not as strong for all three nPDF sets under consideration.

Figure 6 shows the separate contributions of the two terms to $d\sigma(\mathrm{O}+\mathrm{O}\to\mathrm{O}+J/\psi+\mathrm{O})/dy$ in Eq. (1), labeled "W^+" (dashed orange) and "W^-" (dotted green), along with their sum labeled "Full" (solid blue). The calculation is carried out using the EPPS21 nPDFs at $\mu = 2.39$ GeV, which is the optimal scale in the Pb-Pb case. The results are qualitatively similar to those for the Pb-Pb collision system [24]. Looking only at the W^+ contribution, we observe a small bump at backward rapidities caused by the interplay of the large photon flux with the increasing photoproduction cross section and the integral of the nuclear form factor squared. This increase in the differential cross section is momentarily halted and then decreases as one moves from $y \approx -4$ to $y \approx -2$ (i.e., at Run 1 $\sqrt{s_{NN}}$ and slightly differently for the other energies). Then the growth of the photoproduction cross section forces an increase of the absolute magnitude of the UPC cross section until around $y \approx 2$, when the decrease in the photon flux eventually forces the cross section to zero. One can see that this holds for all four energies and we have checked that the results are qualitatively similar for all the three nPDF sets studied here.

Figure 7 quantifies the contributions of the imaginary and real parts of the $\gamma + A \to J/\psi + A$ amplitude to the $d\sigma(\mathrm{O}+\mathrm{O}\to\mathrm{O}+J/\psi+\mathrm{O})/dy$ UPC cross section: the dashed orange curve gives the result, when only the imaginary part is included, the dotted green curve shows the result, when only the real part is included, and the solid blue curve is their sum. One can see from the figure that with increasing $\sqrt{s_{NN}}$, the imaginary part becomes more important at central rapidity and, when moving from 2.76 to 6.37 TeV, the dip in the imaginary part at around $y \pm 3$ seen at $\sqrt{s_{NN}} = 2.76$ TeV actually rises above the real part, i.e., the imaginary part becomes the dominant contribution at all values of rapidity. Qualitatively, the results are the same for the other two nPDF sets nNNPDF3.0 and nCTEQ15WZSIH.

Finally, in Fig. 8 we show the separate contributions of different parton channels to the UPC cross section. The dashed orange curve gives the gluon contribution, i.e., it corresponds to the situation when the contribution of quarks is neglected, the dotted green line gives the quark contribution, the red dash-dotted curve is the interference term between the gluon and quark contributions, and the solid blue curve is the complete result. The calculation corresponds to the EPPS21 nPDFs and $\mu = 2.39$ GeV. One can see from the figure that at all four considered values of $\sqrt{s_{NN}}$, the UPC cross section at central rapidities is dominated by the quark contribution, while the gluons begin to dominate at forward and backward

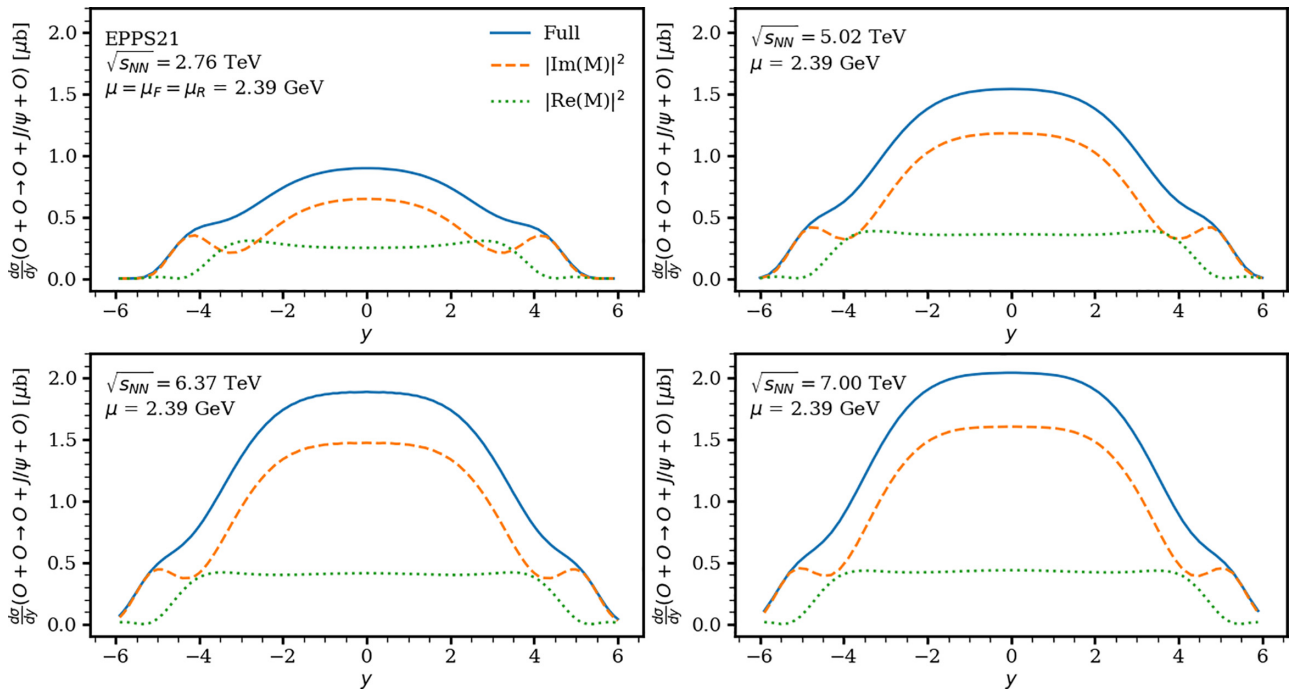

FIG. 7. The contributions of the imaginary (dashed orange curve) and real (green dotted curve) parts of the $\gamma + A \to J/\psi + A$ amplitude to the $d\sigma(\mathrm{O} + \mathrm{O} \to \mathrm{O} + J/\psi + \mathrm{O})/dy$ cross section of coherent J/ψ photoproduction in O-O UPCs as a function of the rapidity y; the solid blue curve is the full result. The calculation uses the EPPS21 nPDFs at $\mu = 2.39$ GeV. The different panels correspond to $\sqrt{s_{NN}} = 2.76$, 5.02, 6.37, and 7 TeV.

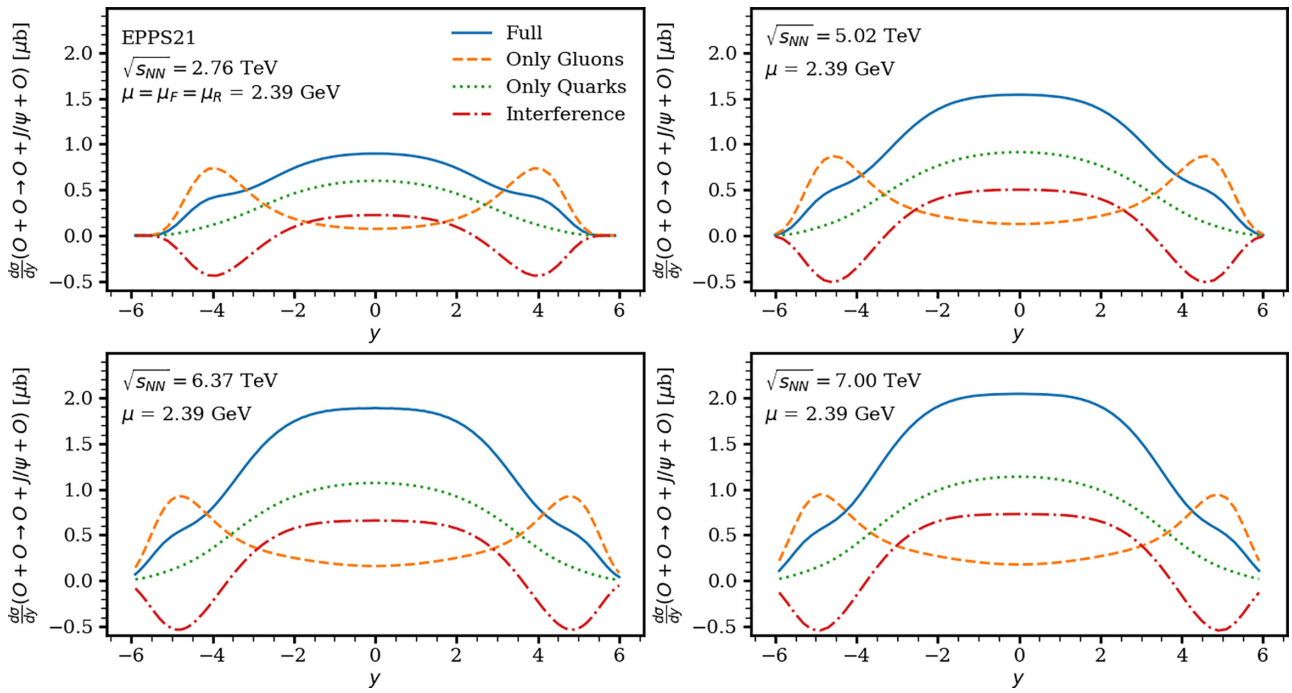

FIG. 8. The breakdown of the NLO pQCD predictions for the $d\sigma(\mathrm{O} + \mathrm{O} \to \mathrm{O} + J/\psi + \mathrm{O})/dy$ cross section of coherent J/ψ photoproduction in O-O UPCs as a function of the rapidity y into the contribution of different parton channels: gluon (dashed orange curve), quark (green dotted curve), and their interference (red dash-dot curve); the solid blue curve is the full result. The calculation uses the EPPS21 nPDFs at $\mu = 2.39$ GeV. The different panels correspond to $\sqrt{s_{NN}} = 2.76$, 5.02, 6.37, and 7 TeV.

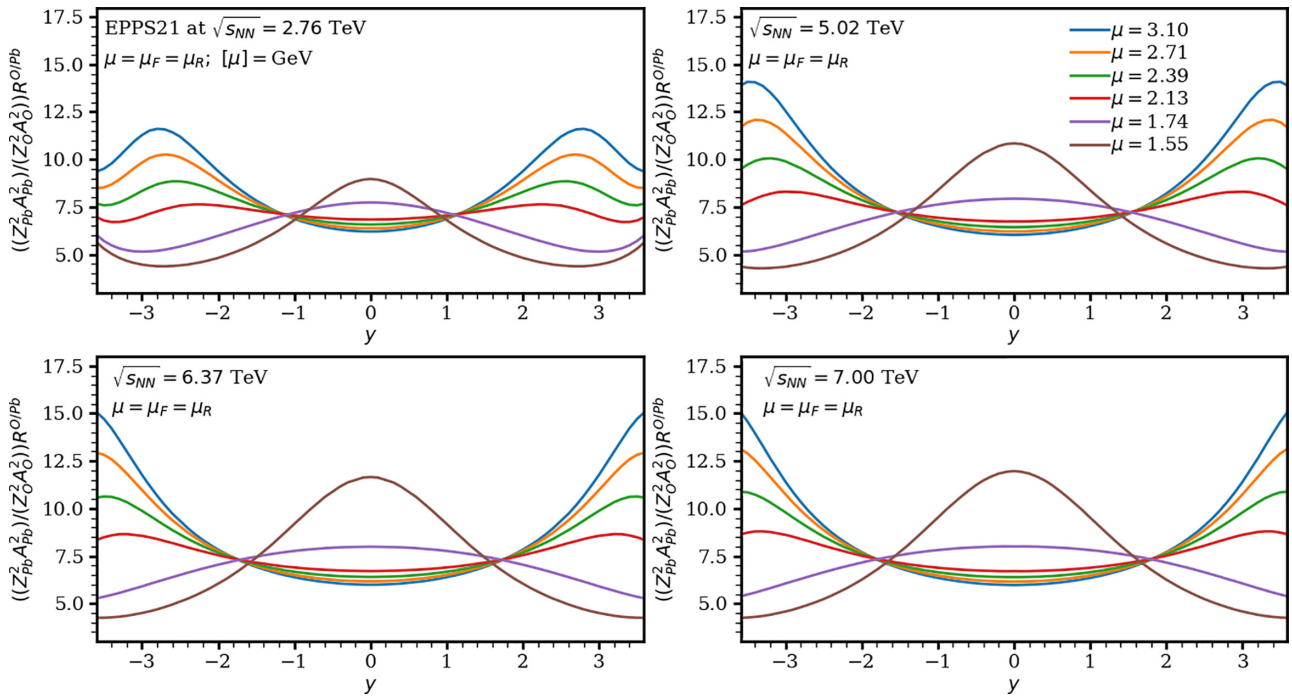

FIG. 9. The NLO pQCD predictions using the EPPS21 nPDFs for the scaled ratio of cross sections of J/ψ photoproduction in O-O and Pb-Pb UPCs as a function of the rapidity y for six different values of the scale μ at four different values of $\sqrt{s_{NN}}$.

rapidities. We have checked that this trend also persists for the nNNPDF3.0 and nCTEQ15WZSIH nPDFs.

Lastly, a few words about the feasibility of measurements of this process in O-O UPCs. Experimentally the $d\sigma^{\rm coh}_{J/\psi}/dy$ rapidity differential cross section for the coherent photoproduction of J/ψ in the lepton channel l^+l^- is given by [39]

$$\frac{d\sigma^{\rm coh}_{J/\psi}}{dy} = \frac{N^{\rm coh}_{J/\psi}}{\mathcal{E}\Gamma_{l^+l^-}\mathcal{L}_{\rm int}\Delta y}, \tag{14}$$

where $N^{\rm coh}_{J/\psi}$ is the yield, i.e., the number of observed J/ψ particles, $\mathcal{E}$ is the combined acceptance and efficiency of the detector, $\Gamma_{l^+l^-}$ is the branching ratio to the desired final state l^+l^-, $\mathcal{L}_{\rm int}$ is the integrated luminosity, and Δy is the width of the rapidity interval under consideration. By considering only the central rapidity and the muon channel with $\Gamma_{l^+l^-} = 5.961\%$ [48] and taking the values given in Ref. [39], $\mathcal{E} = 4.57\%$, $\Delta y = 1.8$, and $N^{\rm coh}_{J/\psi} = 250$, together with $d\sigma^{\rm coh}_{J/\psi}/dy = 2\,\mu$b from Fig. 6, we can estimate the required integrated luminosity $\mathcal{L}_{\rm int}$ to be

$$\mathcal{L}_{\rm int} \approx 25.5 \times 10^3 \frac{1}{\mu b}. \tag{15}$$

It was discussed in Ref. [25] that in the high luminosity O-O run at the LHC, the average luminosity would be $\langle \mathcal{L}_{AA} \rangle = 8.99 \times 10^{30}$ cm^{-2}s^{-1}. This means that in a specialized 24-hour O-O run at ALICE, the integrated luminosity would be approximately $7.8 \times 10^5\ \mu$b^{-1} resulting in approximately 7.5×10^3 J/ψ's making the experimental data acquisition more than feasible. Unfortunately, at the proposed short data acquisition during Run 3, one would most likely acquire only the integrated luminosity of $500\,\mu$b^{-1}, which means that one expects to see only five events [25].

D. Ratios of O-O and Pb-Pb UPC cross sections

Our results presented above indicate that the scale dependence is considerable for both O-O and Pb-Pb collision systems. To reduce it, we examine the following scaled ratio of the O-O and Pb-Pb UPC cross section,

$$R^{\rm O/Pb} = \left(\frac{208Z_{\rm Pb}}{16Z_{\rm O}}\right)^2 \frac{d\sigma({\rm O+O \to O + }J/\psi {\rm + O})/dy}{d\sigma({\rm Pb+Pb \to Pb + }J/\psi {\rm + Pb})/dy}, \tag{16}$$

where the factor of $[(208Z_{\rm Pb}/(16Z_{\rm O})]^2$ is introduced to remove the effects of the Z^2 scaling of the photon flux and the A^2 scaling of the nuclear form factor squared. Since the hard scattering part is the same for both O-O and Pb-Pb scatterings, the scale dependence, which we expect to see in this ratio, comes from the underlying nPDF sets and the different weights of the photon fluxes and the form factors, when we consider both processes at the same $\sqrt{s_{NN}}$. From a practical point of view, the O-O run will most likely be done at a different $\sqrt{s_{NN}}$, which generates an additional scale uncertainty due to the fact that the O-O process will be probed at a smaller x value due to the skewness parameter ξ becoming smaller.

Figures 9–11 present our NLO pQCD predictions for $R^{\rm O/Pb}$ evaluated at six different values of the scale μ ranging from $\mu = 1.55$ GeV to $\mu = 3.1$ GeV using the EPPS21, nNNPDF3.0 and nCTEQ15WZSIH nPDFs, respectively. One can see from the figures that the relative scale uncertainty seems to be the smallest for EPPS21 and nCTEQ15WZSIH at $y \approx 0$, which then grows slightly towards backward and

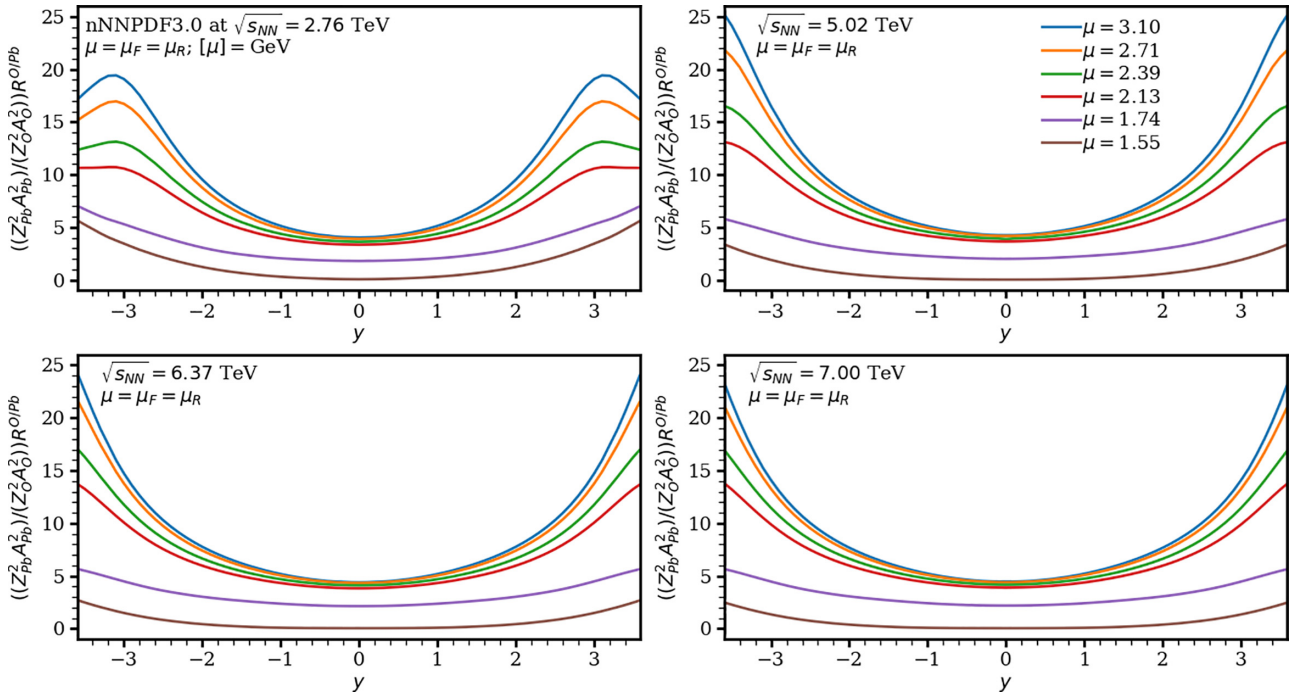

FIG. 10. The same as in Fig. 9, but with the nNNPDF3.0 nPDFs.

forward rapidities. However, in the nNNPDF3.0 case the situation is reversed due to the almost exact cancellation of the photoproduction amplitude for the O-O process at central rapidity. Moreover, depending on the energy, the EPPS21 nPDF set produces a node at $y \approx \pm 1.1$ or $y \approx \pm 1.8$, where all the scales except for the lowest $\mu = m_c$ seem to agree with each other. Such a node is missing in the results given by nNNPDF3.0 or nCTEQ15WZSIH. In addition, we would like to point out that our predictions for $R^{\mathrm{O/Pb}}$ for each nPDF set separately tend to cluster together at higher values of μ.

To quantify the magnitude of the relative scale dependence, we consider the super-ratio of ratios $R^{\mathrm{O/Pb}}$ at $y = 0$, which are

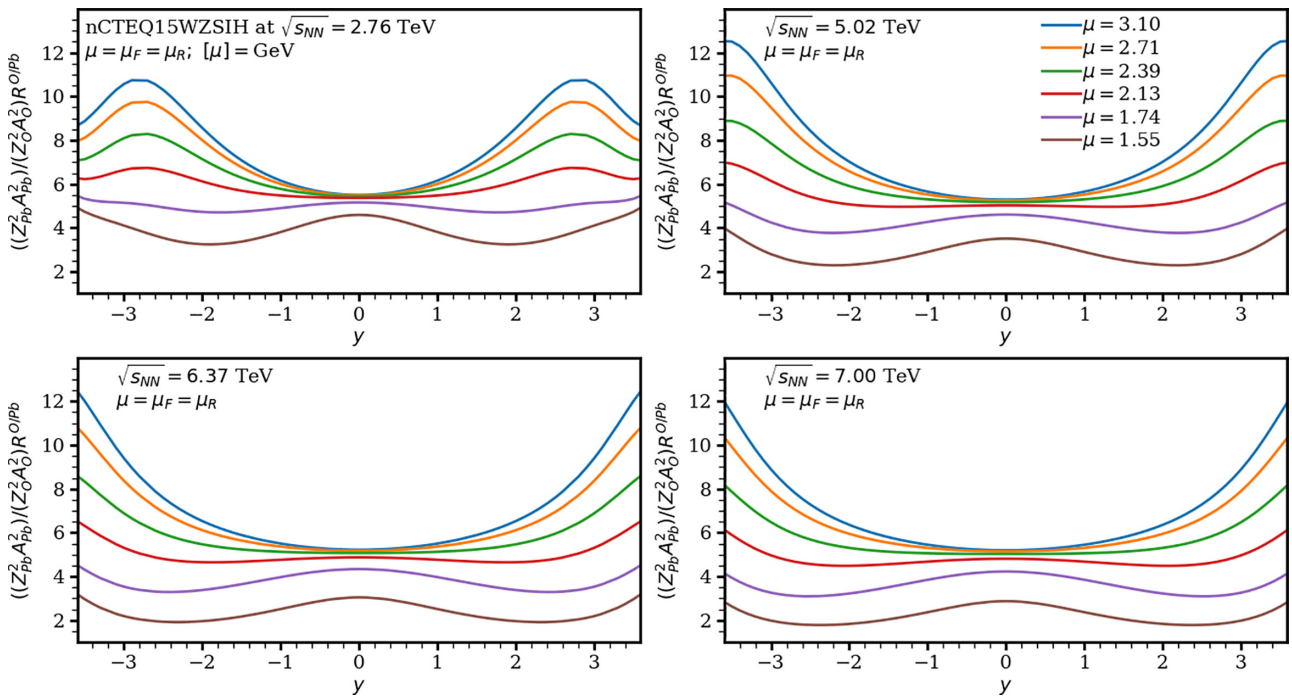

FIG. 11. The same as in Fig. 9, but with the nCTEQ15WZSIH nPDFs.

TABLE I. The ratios $R^{\mathrm{O/Pb}}(\mu = M_{J/\psi})/R^{\mathrm{O/Pb}}(\mu = m_c)$ at $y = 0$ for EPPS21, nNNPDF3.0, and nCTEQ15WZSIH nPDFs for four values of the collision energy $\sqrt{s_{NN}}$, which is taken to be the same for O-O and Pb-Pb runs.

$\sqrt{s_{NN}}$	EPPS21	nNNPDF3.0	nCTEQ15WZSIH
2.76 TeV	0.7	51.5	1.2
5.02 TeV	0.6	86.1	1.5
6.37 TeV	0.5	90.6	1.7
7.00 TeV	0.5	91.4	1.8

evaluated at $\mu = M_{J/\psi}$ and $\mu = m_c$,

$$R^{\mathrm{O/Pb}}_{\mathrm{scale}} = \frac{R^{\mathrm{O/Pb}}(\mu = M_{J/\psi})}{R^{\mathrm{O/Pb}}(\mu = m_c)}. \tag{17}$$

The results for $R^{\mathrm{O/Pb}}_{\mathrm{scale}}$ are presented in Table I. One can see from the table that for all three sets of nPDFs, the scale uncertainty of $R^{\mathrm{O/Pb}}_{\mathrm{scale}}$ is smaller by approximately a factor of 10 than that of the predictions for the individual Pb-Pb and O-O UPC cross sections (the exact size of the reduction in the scale dependence depends on the particular nPDF set and $\sqrt{s_{NN}}$). The scale uncertainty also increases, when $\sqrt{s_{NN}}$ is increased, since at higher energies one probes the nPDFs at progressively smaller x, where the scale evolution of the nPDFs is faster.

One can see from the table that the scale uncertainty characterized by the ratio $R^{\mathrm{O/Pb}}_{\mathrm{scale}}$ of Eq. (17) turns out to be very large in the case of nNNPDF3.0 nPDFs. This is an artifact of the cancellation between LO and NLO contributions to the scattering amplitude at $\mu = m_c$ that we discussed above. If instead of $\mu = m_c = 1.55$ GeV, one selects, e.g., $\mu = 1.74$ GeV in the denominator of Eq. (17), the scale uncertainty becomes dramatically reduced with $R^{\mathrm{O/Pb}}_{\mathrm{scale}} \leqslant 2.3$ for all four considered values of $\sqrt{s_{NN}}$, while only moderately affecting the EPPS21 and nCTEQ15WZSIH results.

To better understand the scale and energy dependence of the ratio of the O-O and Pb-Pb UPC cross sections, we consider the ratio $R^{\mathrm{O/Pb}}$, when the numerator of Eq. (16), the $d\sigma(\mathrm{O} + \mathrm{O} \to \mathrm{O} + J/\psi + \mathrm{O})/dy$ cross section, is evaluated at $\sqrt{s_{NN}} = 6.37$ and 7 TeV, and the denominator of Eq. (16), the $d\sigma(\mathrm{Pb} + \mathrm{Pb} \to \mathrm{Pb} + J/\psi + \mathrm{Pb})/dy$ cross section, is evaluated at $\sqrt{s_{NN}} = 2.76$ TeV (Run 1) and 5.02 TeV (Run 2). Our results for the EPPS21, nNNPDF3.0, and nCTEQ15WZSIH nPDF sets are presented in Figs. 12–14, respectively. One can see from the figures that qualitatively the scale dependence is similar for nNNPDF3.0 and nCTEQ15WZSIH, but in the case of EPPS21 for Pb-Pb UPCs at $\sqrt{s_{NN}} = 2.76$ TeV the node disappears and the systematics of the scale dependence becomes similar for all three nPDF sets.

The general effect of taking $R^{\mathrm{O/Pb}}_{\mathrm{scale}}$ at different energies means that the scale dependence is increased as given in Table II. As we take O-O consistently at a higher energy, $d\sigma/dy$ increases scale by scale, as was shown in Fig. 5. For EPPS21 the situation is more involved since for the first two entries the scale dependence is flipped, but the magnitude of the dependence stays the same. For the last two entries, i.e., Pb-Pb taken at $\sqrt{s_{NN}} = 5.02$ TeV, the dependence actually gets smaller. For nNNPDF3.0 the situation is the worst: taking the ratio at different energies means that we increase the scale dependence by a factor of three at worst.

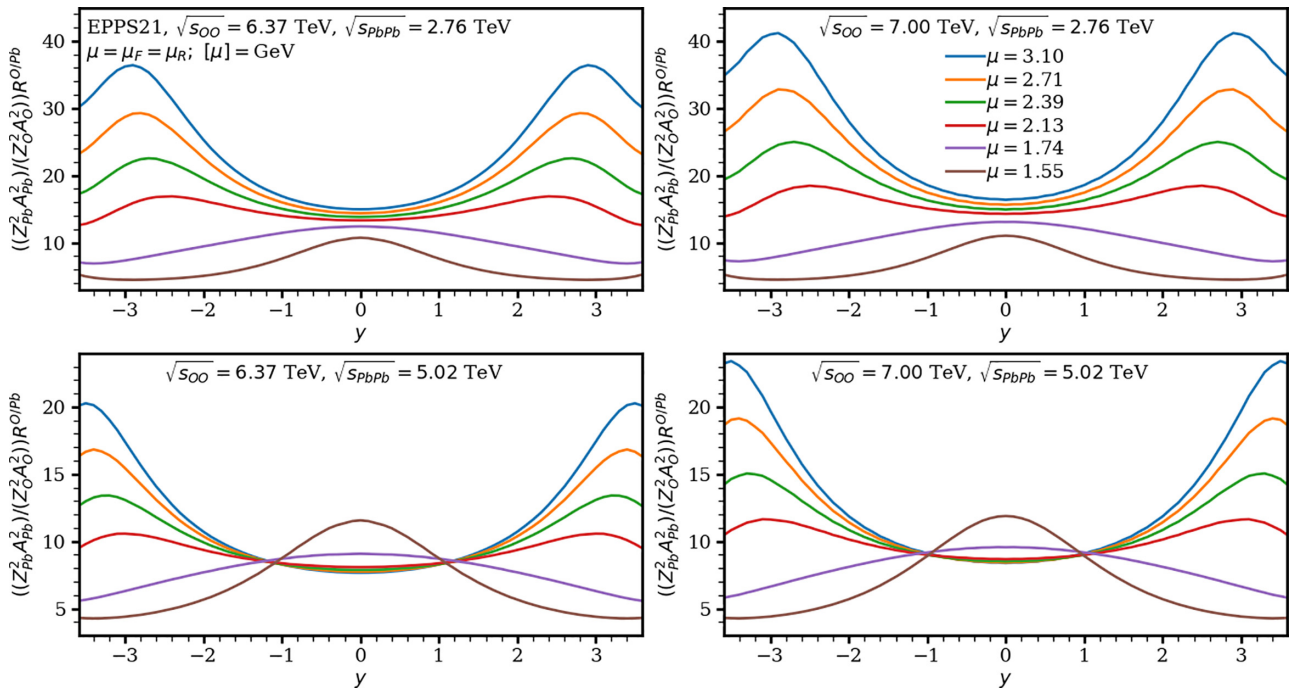

FIG. 12. The scaled ratio of the NLO pQCD cross sections of J/ψ photoproduction in O-O and Pb-Pb UPCs as a function of the rapidity y for six different values of the scale μ at nonequal values of O-O and Pb-Pb collision energies. The results are obtained with the EPPS21 nPDFs.

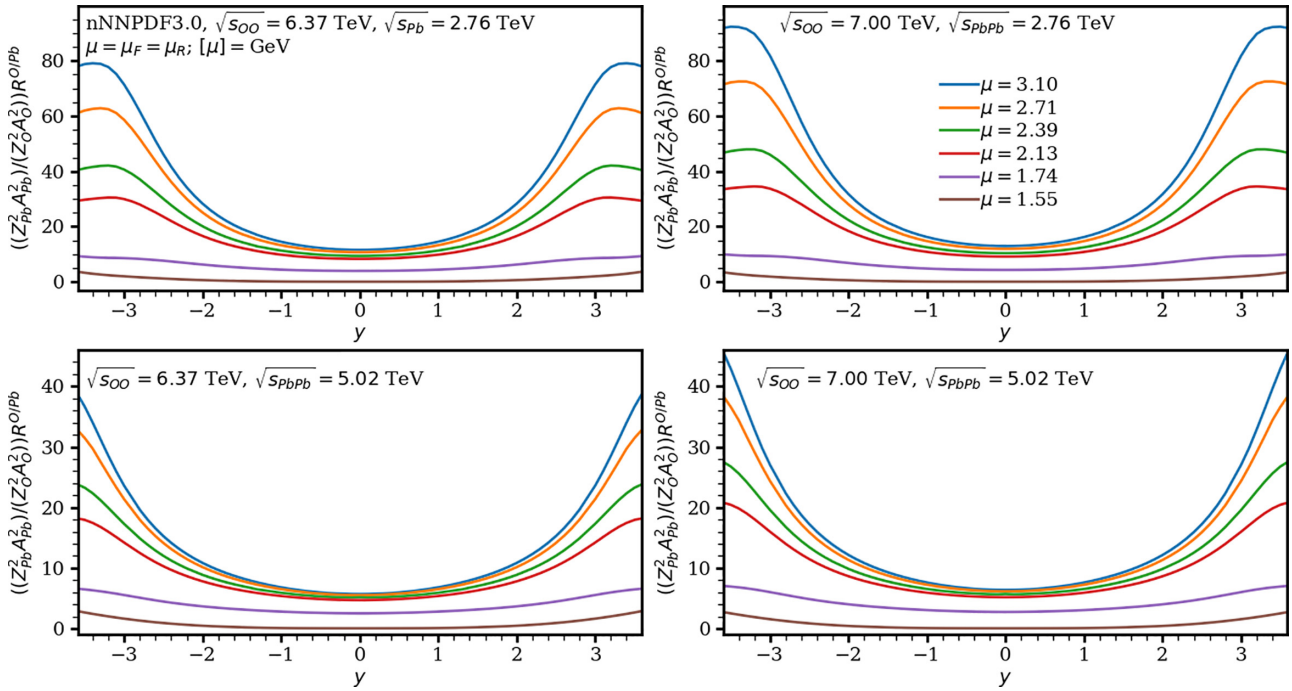

FIG. 13. The same as in Fig. 12, but with the nNNPDF3.0 nPDFs.

For nCTEQ15WZSIH the factor is only about 1.6. However, if we disregard the lowest scale and take $\mu = 1.74$ GeV instead, the scale dependence becomes smaller for all three sets. For nNNPDF3.0 the drop is quite sizable again: at all energies the scale dependence drops to less than a factor of 3.

Figure 15 illustrates the PDF uncertainties of our NLO pQCD predictions for $R^{\mathrm{O/Pb}}$ as a function of y for EPPS21, nNNPDF3.0, and nCTEQ15WZSIH nPDFs. The calculations using the central sets of the nPDFs at their corresponding optimal scales are given by the blue solid (EPPS21), green dotted (nNNPDF3.0), and red dashed (nCTEQ15WZSIH) curves. The corresponding uncertainties are given by the shaded bands. They are calculated by first finding the ratio $R^{\mathrm{O/Pb}}$ for each error set and then using the asymmetric form [see

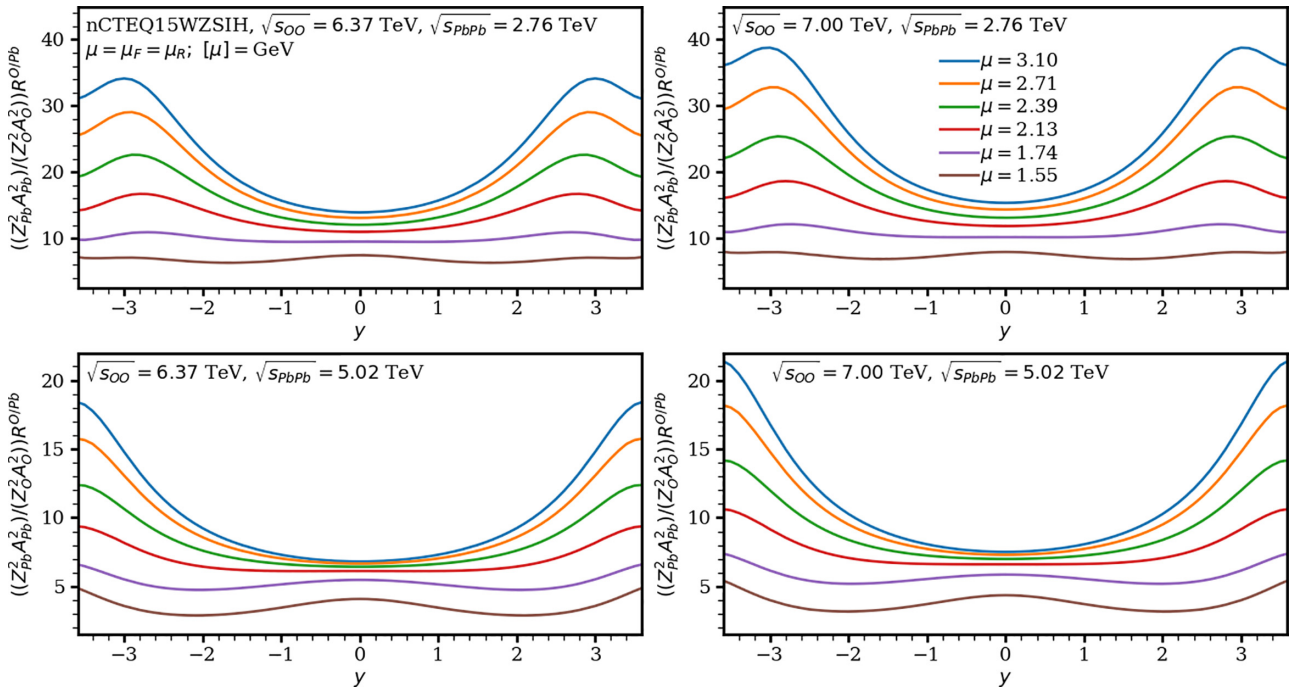

FIG. 14. The same as in Fig. 12, but with the nCTEQ15WZSIH nPDFs.

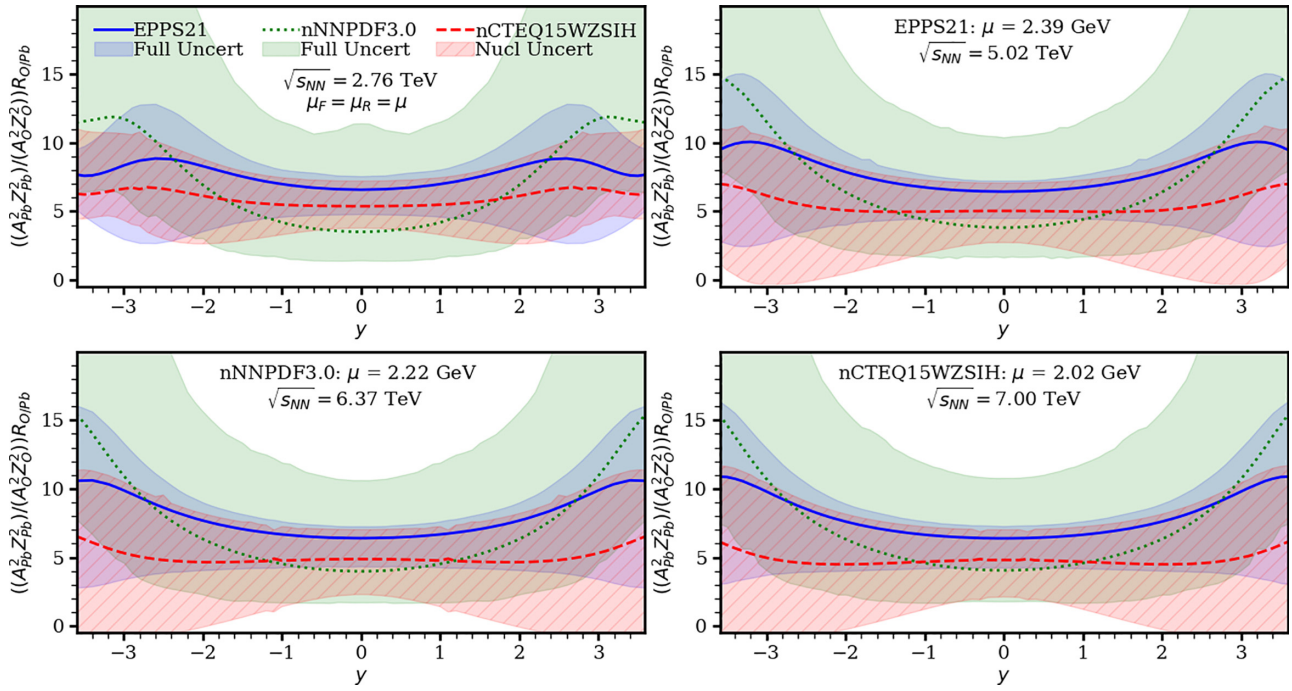

FIG. 15. The PDF uncertainties of NLO pQCD predictions for $R^{\mathrm{O/Pb}}$ as a function of the rapidity y. The results corresponding to the central nPDF sets at the optimal scales are shown by the blue solid (EPPS21), green dotted (nNNPDF3.0), and red dashed (nCTEQ15WZSIH) curves, respectively. The corresponding uncertainties are shown by the shaded bands, see text for details. Different panels correspond to different $\sqrt{s_{NN}}$.

Eq. (13)] for EPPS21 and nCTEQ15WZSIH and the CL prescription for nNNPDF3.0. Thus, the blue and green bands give the full (free proton + nuclear) uncertainty of EPPS21 and nNNPDF3.0 nPDFs, respectively, while the hashed red band gives the nuclear uncertainty of the nCTEQ15WZSIH set. We see that the predictions agree within the PDF uncertainty bands.

One can see from the figure that as $|y|$ is increased, the uncertainty bands grow bigger for all three sets. It can be understood by noticing that at higher positive rapidities, the W^+ component gets probed at smaller and smaller values of x (similarly for the W^- component at negative rapidities). For the EPPS21 and nNNPDF3.0 sets, the band stays always at positive values, but for nCTEQ15WZSIH, the uncertainty band reaches negative values starting from $\sqrt{s_{NN}} = 5.02$ TeV at large enough $|y|$. Interestingly the uncertainties in nNNPDF3.0 are upward dominated and in nCTEQ15WZSIH they are downward dominated.

TABLE II. The ratios $R^{\mathrm{O/Pb}}(\mu = M_{J/\psi})/R^{\mathrm{O/Pb}}(\mu = m_c)$ at $y = 0$ for the EPPS21, nNNPDF3.0, and nCTEQ15WZSIH nPDFs for different values of $\sqrt{s_{NN}}$ in the numerator and denominator.

$\sqrt{s_{\mathrm{OO}}}/\sqrt{s_{\mathrm{PbPb}}}$	EPPS21	nNNPDF3.0	nCTEQ15WZSIH
6.37/2.76	1.4	156.1	1.9
7.00/2.76	1.5	166.5	1.9
6.37/5.02	0.7	104.6	1.7
7.00/5.02	0.7	111.7	1.7

A comparison of the PDF and scale uncertainties in $R^{\mathrm{O/Pb}}$ at $y = 0$ as a function of $\sqrt{s_{NN}}$ is shown in Fig. 16. The PDF uncertainties are calculated at the corresponding optimal scales for the EPPS21 (left), nNNPDF3.0 (middle), and nCTEQ15WZSIH (right) nuclear PDFs. The scale uncertainty represents the range between the scales $\mu = m_c$ and $\mu = M_{J/\psi}$. In absolute terms the EPPS21 PDF uncertainty is typically smaller than the scale uncertainty, while for nNNPDF3.0 and nCTEQ15WZSIH the scale uncertainty is smaller than the PDF uncertainty. The figure also shows the lack of uniformity between the uncertainties between different sets. For instance, in the EPPS21 case, the scale uncertainty dominates upward, whereas the PDF uncertainties dominate downward. For nNNPDF3.0, the situation is reversed: PDF uncertainties dominate the upward uncertainty and scale uncertainties the downward uncertainty. Then interestingly for nCTEQ15WZSIH, the set with the enhanced strange quark contribution, the scale uncertainties are smaller than the PDF uncertainties at all energies. The value of the ratio stays approximately constant as a function of $\sqrt{s_{NN}}$ for all three sets.

Figure 17 presents the nPDF uncertainties of the ratio $R^{\mathrm{O/Pb}}$ as a function of y, when the O-O and Pb-Pb UPC cross sections are evaluated at different collision energies (see our discussion above). The notation of the curves and shaded bands is the same as in Fig. 15. A comparison with Fig. 15 shows that the results in the two figures are similar. In particular, at central rapidity for EPPS21 the ratio between the upper bound and the lower bound for the PDF uncertainties is about 2.2 for Pb-Pb taken at Run 1 energy and 1.8 for Pb-Pb taken at Run 2 energy, which means that the PDF

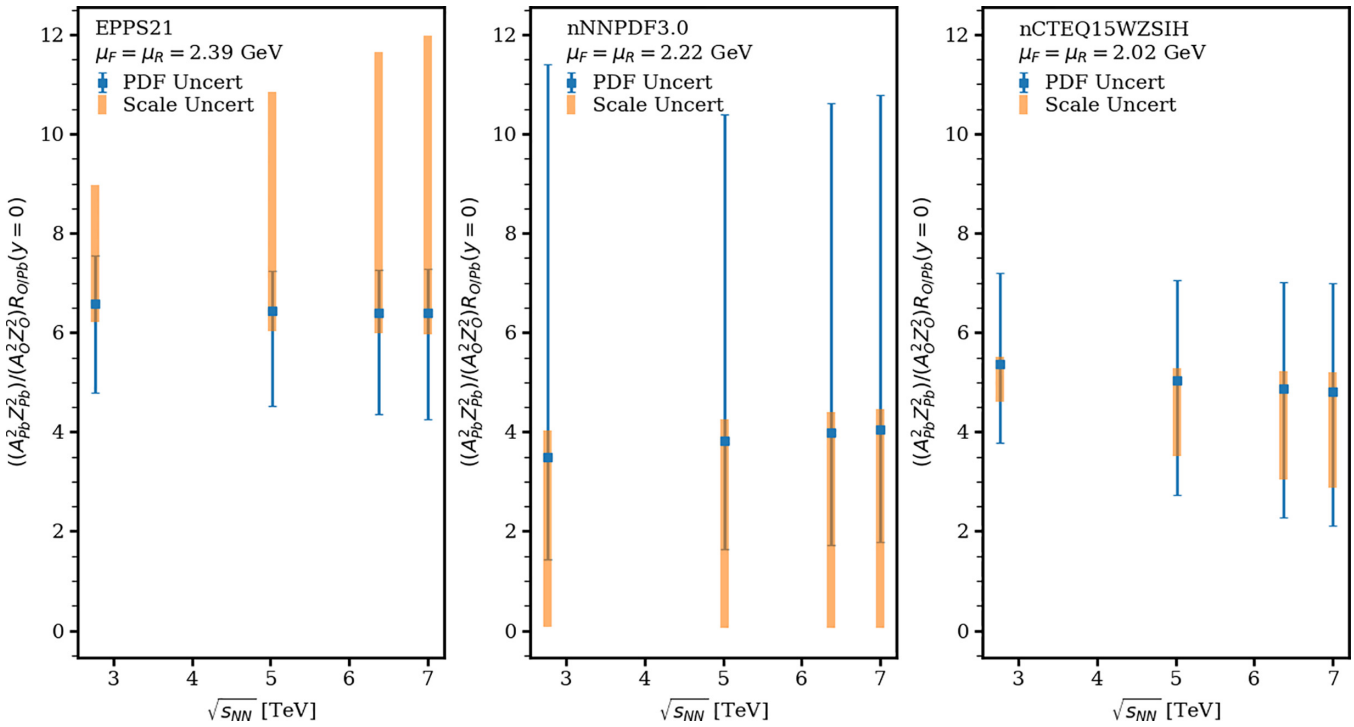

FIG. 16. Comparison of the PDF (thin blue) and scale (wide orange) uncertainties in the ratio of the NLO pQCD calculation of O-O to Pb-Pb rapidity differential cross section at central rapidity, $y = 0$, for three different nPDF sets: EPPS21 (left), nNNPDF3.0 (center), and nCTEQ15WZSIH (right). Here O-O and Pb-Pb are taken at same energy and all sets at their corresponding optimal scales.

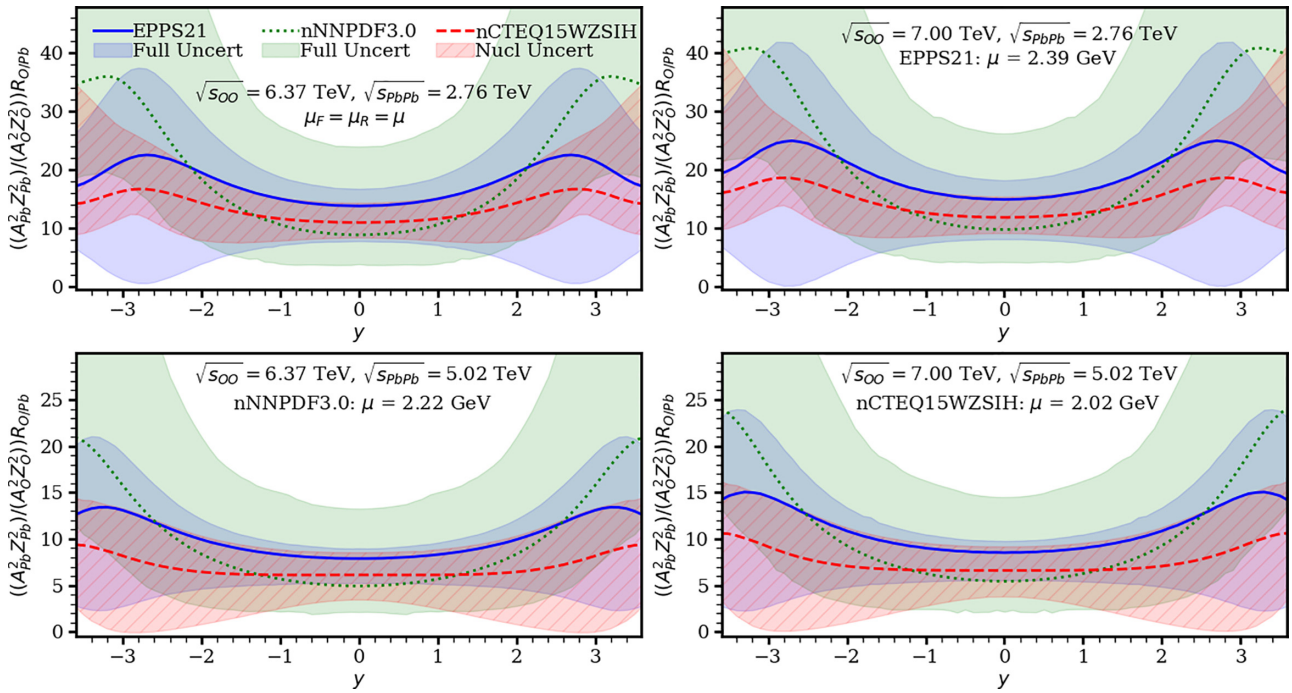

FIG. 17. The scaled ratios for EPPS21 (solid blue), nNNPDF3.0 (dotted green), and nCTEQ15WZSIH (dashed red) at their optimal scales as a function of the J/ψ rapidity. The blue band gives the EPPS21 uncertainty, the green band gives the nNNPDF3.0 90% CL uncertainty, and the hatched red band gives the nCTEQ15WZSIH nuclear uncertainty. In the first row Pb-Pb has been taken at Run 1 energy and in the second row at Run 2 energy. The O-O energies correspond to the two proposed energies of 6.37 TeV (left column) and 7 TeV (right column).

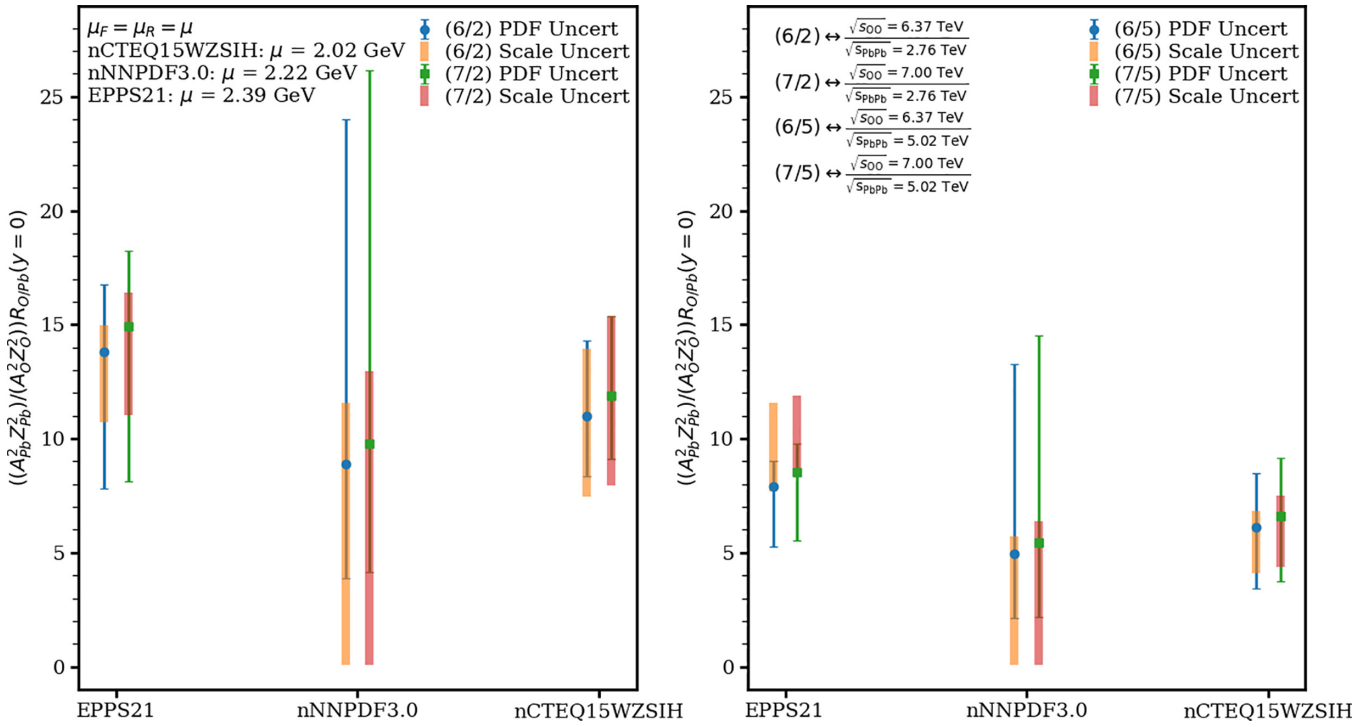

FIG. 18. The scaled ratios of O-O to Pb-Pb rapidity differential cross sections for EPPS21, nNNPDF3.0, and nCTEQ15WZSIH at their corresponding optimal scales at central rapidity, $y = 0$, where O-O and Pb-Pb have been taken at different $\sqrt{s_{NN}}$ energies. In the left panel the Pb-Pb collision is taken at Run 1 energy and in the right panel at Run 2 energy.

uncertainty is slightly larger at all energies under consideration than the scale uncertainty (see Table II). For nNNPDF3.0 the same ratio is around 6.7 for all energies and again the scale uncertainty is clearly the dominating one, when considering $\mu \in [m_c, M_{J/\psi}]$. If we ignore the lowest scale $\mu = m_c$, we find that the PDF uncertainty is again the larger one. For nCTEQ15WZSIH the corresponding ratios are about 1.7 and 2.5 for Run 1 and Run 2 energies, respectively.

These results are summarized in Fig. 18, which shows the $R^{\mathrm{O/Pb}}$ ratio at $y = 0$ for EPPS21, nNNPDF3.0, and nCTEQ15WZSIH for different configurations of collision energies as discussed above. The color-coded bars give the scale (wide error bars) and PDF (thin error bars with caps) uncertainties; the former are calculated using the central sets of the respective nPDF fits and the latter are evaluated at the respective values of the optimal scale μ. The left and right panels correspond to the Run 1 and Run 2 energies of Pb-Pb collisions, respectively. One can see from the figure that $R^{\mathrm{O/Pb}}$ at $y = 0$ and its uncertainties decrease as the Pb-Pb c.m.s. energy is increased and that $R^{\mathrm{O/Pb}}$ at $y = 0$ and its uncertainties increase as the O-O c.m.s. energy is increased. One can also see that the different nPDF set predictions agree within the PDF uncertainties.

Note that the issue of large NLO pQCD scale uncertainties of the heavy quarkonium photoproduction cross section in UPCs in the LHC kinematics has been identified to be related to the parametrically large corrections proportional to $\log(1/\xi)$. Possible ways to tame them by means of effective small-x resummation have been investigated in the literature [15,22,49].

IV. CONCLUSIONS

This work continues our studies of J/ψ photoproduction in nucleus-nucleus UPCs at the LHC within the framework of collinear factorization and NLO perturbative QCD. In particular, we update our results for this process in Pb-Pb UPCs and make predictions for the $d\sigma(\mathrm{Pb} + \mathrm{Pb} \to \mathrm{Pb} + J/\psi + \mathrm{Pb})/dy$ cross section as a function of the J/ψ rapidity y using the state-of-the-art EPPS21, nNNPDF3.0, and nCTEQ15WZSIH nPDF sets. Taking nuclear generalized parton distribution functions in their forward limit, where they reduce to the nPDFs, we obtain a good description of Run 1 and Run 2 LHC data on $d\sigma(\mathrm{Pb} + \mathrm{Pb} \to \mathrm{Pb} + J/\psi + \mathrm{Pb})/dy$. This is achieved by choosing an optimal scale for each set of nPDFs: $\mu = 2.39$ GeV for EPPS21, $\mu = 2.22$ GeV for nNNPDF3.0, and $\mu = 2.02$ GeV for nCTEQ15WZSIH.

Compared to our earlier calculations using EPPS16, nNNPDF2.0, and nCTEQ15 nPDFs [24], we can make the following observations. The results employing the central set of the EPPS21 nPDFs are found to be similar to those with the EPPS16 nPDFs with the corresponding optimal scale $\mu = 2.37$ GeV. In addition, with the EPPS21 set, the PDF uncertainties have reduced significantly. At the same time, our results with the nNNPDF3.0 nPDFs exhibit a much more regular behavior than those corresponding to the nNNPDF2.0 nPDFs and, as a result, better reproduce the data. This is due to the fact that the gluon distribution in nNNPDF3.0 grows at small x much slower than that in nNNPDF2.0 nPDFs. The best description of the data at both central and forward/backward rapidities at Run 1 and Run 2 energies is achieved with

the nCTEQ15WZSIH, which also performs better than the nCTEQ15 set. This is due to the strongly enhanced strange quark content at small x. Thus, at least at NLO pQCD, this process is a potential probe of the elusive strange quark PDFs. It should be kept in mind that, because the scale dependence is significant, the situation may still change at NNLO.

We also made detailed predictions for the $\mathrm{O}+\mathrm{O}\to\mathrm{O}+J/\psi+\mathrm{O}$ rapidity differential UPC cross section in anticipation of the planned oxygen run at the LHC. Comparing with Pb-Pb UPCs, we observe that the shape of the rapidity distribution in the O-O case is qualitatively similar to that in Pb-Pb, but the former begins to develop a valleylike structure around $y=0$ at high enough scales $\mu\approx M_{J/\psi}$. At central rapidity, the scale dependence of our results for O-O corresponding to the EPPS21 and nCTEQ15WZSIH nPDFs is slightly smaller than that for Pb-Pb collisions, but it is still of the same order of magnitude. For nNNPDF3.0, the situation is worse: the scale uncertainty grows to the order of 10^3 due to the nearly perfect cancellation of the sum of the LO and the NLO contributions both in the real part and the imaginary parts of the amplitude at the smallest scale of $\mu=m_c$.

The decomposition of the O-O results into the $W^{\pm}$ components, the imaginary and the real parts, and the gluon and quark contributions did not differ significantly from the results in the Pb-Pb case [24]. Namely, the $W^{\pm}$ contributions exhibit a two-bump structure; the imaginary part gives the dominant contribution over a larger range of y, while the real part cannot be neglected, especially for large values of $|y|$; the quark contribution dominates at central rapidity, but the gluons become important at backward or forward rapidities. Furthermore, the interplay between the gluon and the quark contributions plays an important role.

In order to reduce the significant scale and nPDF uncertainties, we have studied the ratio of the J/ψ rapidity distributions in O-O and Pb-Pb UPCs at different collision energies $\sqrt{s_{NN}}$. We found that for EPPS21 and nCTEQ15WZSIH, the scale uncertainties in the ratio indeed became significantly smaller. The reduction in the scale dependence is largest at central rapidities and slightly smaller toward backward and forward rapidities both when the ratio is taken at the same value of $\sqrt{s_{NN}}$ and when taken at different values. For nNNPDF3.0, the situation is the same at central rapidity, i.e., the ratio has a smaller scale dependence when compared to the O-O case. Interestingly, and contrary to EPPS21 and nCTEQ15WZSIH, the scale dependence of the nNNPDF3.0 ratio at forward and backward rapidities becomes even smaller since the LO and NLO contributions in the O-O results no longer cancel to such an exact degree.

The PDF uncertainties for the ratios of the rapidity distribution in O-O to Pb-Pb UPCs were found to be the smallest for EPPS21, then for nCTEQ15WZSIH, and lastly for nNNPDF3.0. This is a direct consequence of the tightly constrained error sets in EPPS21, whereas in nCTEQ15WZSIH and nNNPDF3.0, there is more variation. The comparison of the PDF and scale uncertainties for the ratios taken at the same energy shows that the scale uncertainty is the dominant one for the EPPS21 and nNNPDF3.0 sets, while for nCTEQ15WZSIH the situation is reversed. For the ratios taken at different energies, the PDF uncertainties are of the same magnitude for EPPS21 and nCTEQ15WZSIH, but for nNNPDF3.0 the scale uncertainty still dominates because of the cancellation at scale $\mu=m_c$.

Our analysis demonstrates that the large-scale uncertainty of our NLO pQCD results can be tamed through suitably considered ratios of rapidity differential cross sections. In future work, it would be instructive to extend our analysis to J/ψ photoproduction in p-Pb and p-O asymmetric UPCs and also to photoproduction of Υ mesons in nucleus-nucleus UPCs. In addition, our framework could be improved through a more detailed GPD modeling [50] and the inclusion of the nonrelativistic QCD corrections to the charmonium wave function [51–54].

ACKNOWLEDGMENTS

We acknowledge the helpful discussions with I. Helenius, H. Mäntysaari, and J. Penttala. We acknowledge the financial support from the Magnus Ehrnrooth foundation (T.L.), the Academy of Finland Projects No. 308301 (H.P.) and No. 330448 (K.J.E.). This research was funded as a part of the Center of Excellence in Quark Matter of the Academy of Finland (Projects No. 346325 and No. 346326). This research is part of the European Research Council Project No. ERC-2018-ADG-835105 YoctoLHC.

[1] J. Gao, L. Harland-Lang, and J. Rojo, The Structure of the Proton in the LHC Precision Era, Phys. Rep. **742**, 1 (2018).
[2] J. Rojo, *The Partonic Content of Nucleons and Nuclei* (Oxford Encyclopedia of Physics, Oxford, 2019).
[3] K. Kovařík, P. M. Nadolsky, and D. E. Soper, Hadronic structure in high-energy collisions, Rev. Mod. Phys. **92**, 045003 (2020).
[4] J. J. Ethier and E. R. Nocera, Parton Distributions in Nucleons and Nuclei, Annu. Rev. Nucl. Part. Sci. **70**, 43 (2020).
[5] T.-J. Hou *et al.*, New CTEQ global analysis of quantum chromodynamics with high-precision data from the LHC, Phys. Rev. D **103**, 014013 (2021).
[6] R. D. Ball *et al.* (NNPDF Collaboration), The path to proton structure at 1% accuracy, Eur. Phys. J. C **82**, 428 (2022).
[7] R. D. Ball *et al.* (PDF4LHC Working Group), The PDF4LHC21 combination of global PDF fits for the LHC Run III, J. Phys. G **49**, 080501 (2022).
[8] K. Kovařík *et al.*, nCTEQ15 - Global analysis of nuclear parton distributions with uncertainties in the CTEQ framework, Phys. Rev. D **93**, 085037 (2016).
[9] K. J. Eskola, P. Paakkinen, H. Paukkunen, and C. A. Salgado, EPPS16: Nuclear parton distributions with LHC data, Eur. Phys. J. C **77**, 163 (2017).

[10] H. Khanpour, M. Soleymaninia, S. Atashbar Tehrani, H. Spiesberger, and V. Guzey, Nuclear parton distribution functions with uncertainties in a general mass variable flavor number scheme, Phys. Rev. D **104**, 034010 (2021).

[11] K. J. Eskola, P. Paakkinen, H. Paukkunen, and C. A. Salgado, EPPS21: A global QCD analysis of nuclear PDFs, Eur. Phys. J. C **82**, 413 (2022).

[12] R. Abdul Khalek, R. Gauld, T. Giani, E. R. Nocera, T. R. Rabemananjara, and J. Rojo, nNNPDF3.0: Evidence for a modified partonic structure in heavy nuclei, Eur. Phys. J. C **82**, 507 (2022).

[13] I. Helenius, M. Walt, and W. Vogelsang, NNLO nuclear parton distribution functions with electroweak-boson production data from the LHC, Phys. Rev. D **105**, 094031 (2022).

[14] S. P. Jones, A. D. Martin, M. G. Ryskin, and T. Teubner, Probes of the small x gluon via exclusive J/ψ and Υ production at HERA and the LHC, J. High Energy Phys. 11 (2013) 085.

[15] S. P. Jones, A. D. Martin, M. G. Ryskin, and T. Teubner, Exclusive J/ψ and Υ photoproduction and the low x gluon, J. Phys. G **43**, 035002 (2016).

[16] C. A. Flett, S. P. Jones, A. D. Martin, M. G. Ryskin, and T. Teubner, How to include exclusive J/ψ production data in global PDF analyses, Phys. Rev. D **101**, 094011 (2020).

[17] V. Guzey, E. Kryshen, M. Strikman, and M. Zhalov, Evidence for nuclear gluon shadowing from the ALICE measurements of PbPb ultraperipheral exclusive J/ψ production, Phys. Lett. B **726**, 290 (2013).

[18] V. Guzey and M. Zhalov, Exclusive J/ψ production in ultraperipheral collisions at the LHC: constrains on the gluon distributions in the proton and nuclei, J. High Energy Phys. 10 (2013) 207.

[19] V. Guzey, E. Kryshen, M. Strikman, and M. Zhalov, Nuclear suppression from coherent J/ψ photoproduction at the Large Hadron Collider, Phys. Lett. B **816**, 136202 (2021).

[20] M. Ryskin, Diffractive J/ψ electroproduction in LLA QCD, Z. Phys. C **57**, 89 (1993).

[21] D. Yu. Ivanov, A. Schäfer, L. Szymanowski, and G. Krasnikov, Exclusive photoproduction of a heavy vector meson in QCD, Eur. Phys. J. C **34**, 297 (2004); Erratum: **75**, 75 (2015).

[22] S. P. Jones, A. D. Martin, M. G. Ryskin, and T. Teubner, The exclusive J/ψ process at the LHC tamed to probe the low x gluon, Eur. Phys. J. C **76**, 633 (2016).

[23] C. A. Flett, A. D. Martin, M. G. Ryskin, and T. Teubner, Very low x gluon density determined by LHCb exclusive J/ψ data, Phys. Rev. D **102**, 114021 (2020).

[24] K. J. Eskola, C. A. Flett, V. Guzey, T. Löytäinen, and H. Paukkunen, Exclusive J/ψ photoproduction in ultraperipheral Pb+Pb collisions at the CERN Large Hadron Collider calculated at next-to-leading order perturbative QCD, Phys. Rev. C **106**, 035202 (2022).

[25] Z. Citron *et al.*, Report from Working Group 5: Future physics opportunities for high-density QCD at the LHC with heavy-ion and proton beams, CERN Yellow Rep. Monogr. **7**, 1159 (2019).

[26] J. Brewer, A. Mazeliauskas, and W. van der Schee, Opportunities of OO and pO collisions at the LHC, arXiv:2103.01939 [hep-ph].

[27] V. P. Goncalves, B. D. Moreira, and L. Santana, Exclusive ρ and J/ψ photoproduction in ultraperipheral pO and OO collisions at the Large Hadron Collider, arXiv:2210.11911 [hep-ph].

[28] A. J. Baltz, The physics of ultraperipheral collisions at the LHC, Phys. Rep. **458**, 1 (2008).

[29] S. R. Klein and J. Nystrand, Interference in Exclusive Vector Meson Production in Heavy-Ion Collisions, Phys. Rev. Lett. **84**, 2330 (2000).

[30] M. Vidovic, M. Greiner, C. Best, and G. Soff, Impact parameter dependence of the electromagnetic particle production in ultrarelativistic heavy ion collisions, Phys. Rev. C **47**, 2308 (1993).

[31] H. De Vries, C. W. De Jager, and C. De Vries, Nuclear charge and magnetization density distribution parameters from elastic electron scattering, At. Data Nucl. Data Tables **36**, 495 (1987).

[32] I. Helenius, K. J. Eskola, H. Honkanen and C. A. Salgado, Impact-parameter dependent nuclear parton distribution functions: EPS09s and EKS98s and their applications in nuclear hard processes, J. High Energy Phys. 07 (2012) 073.

[33] C. Patrignani *et al.* (Particle Data Group Collaboration), Review of particle physics, Chin. Phys. C **40**, 100001 (2016).

[34] V. Guzey, M. Strikman, and M. Zhalov, Accessing transverse nucleon and gluon distributions in heavy nuclei using coherent vector meson photoproduction at high energies in ion ultraperipheral collisions, Phys. Rev. C **95**, 025204 (2017).

[35] S. Acharya *et al.* (ALICE Collaboration), First measurement of the $|t|$-dependence of coherent J/ψ photonuclear production, Phys. Lett. B **817**, 136280 (2021).

[36] S. J. Brodsky, G. P. Lepage, and P. B. Mackenzie, On the elimination of scale ambiguities in perturbative quantum chromodynamics, Phys. Rev. D **28**, 228 (1983).

[37] A. Kusina *et al.*, Impact of LHC vector boson production in heavy ion collisions on strange PDFs, Eur. Phys. J. C **80**, 968 (2020).

[38] J. Brewer, A. Huss, A. Mazeliauskas, and W. van der Schee, Ratios of jet and hadron spectra at LHC energies: Measuring high-pT suppression without a pp reference, Phys. Rev. D **105**, 074040 (2022).

[39] E. Abbas *et al.* (ALICE Collaboration), Charmonium and e^+e^- pair photoproduction at mid-rapidity in ultra-peripheral Pb-Pb collisions at $\sqrt{s_{\rm NN}} = 2.76$ TeV, Eur. Phys. J. C **73**, 2617 (2013).

[40] B. Abelev *et al.* (ALICE Collaboration), Coherent J/ψ photoproduction in ultra-peripheral Pb-Pb collisions at $\sqrt{s_{NN}} =$ 2.76 TeV, Phys. Lett. B **718**, 1273 (2013).

[41] V. Khachatryan *et al.* (CMS Collaboration), Coherent J/ψ photoproduction in ultra-peripheral PbPb collisions at $\sqrt{s_{NN}} =$ 2.76 TeV with the CMS experiment, Phys. Lett. B **772**, 489 (2017).

[42] S. Acharya *et al.* (ALICE Collaboration), Coherent J/ψ and ψ' photoproduction at midrapidity in ultra-peripheral Pb–Pb collisions at $\sqrt{s_{NN}} = 5.02$ TeV, Eur. Phys. J. C **81**, 712 (2021).

[43] S. Acharya *et al.* (ALICE Collaboration), Coherent J/ψ photoproduction at forward rapidity in ultra-peripheral Pb-Pb collisions at $\sqrt{s_{\rm NN}} = 5.02$ TeV, Phys. Lett. B **798**, 134926 (2019).

[44] R. Aaij *et al.* (LHCb Collaboration), Study of coherent J/ψ production in lead-lead collisions at $\sqrt{s_{\rm NN}} = 5$ TeV, J. High Energy Phys. 07 (2022) 117.

[45] LHCb Collaboration, Study of coherent charmonium production in ultra-peripheral lead-lead collisions, arXiv:2206.08221 [hep-ex].

[46] R. A. Khalek, J. J. Ethier, J. Rojo, and G. van Weelden, nNNPDF2.0: Quark flavor separation in nuclei from LHC data, J. High Energy Phys. 09 (2020) 183.

[47] P. Duwentäster, T. Ježo, M. Klasen, K. Kovařík, A. Kusina, K. F. Muzakka, F. I. Olness, R. Ruiz, I. Schienbein, and J. Y. Yu,

Impact of heavy quark and quarkonium data on nuclear gluon PDFs, Phys. Rev. D **105**, 114043 (2022).

[48] P. A. Zyla *et al.* (Particle Data Group Collaboration), Review of Particle Physics, PTEP **2020**, 083C01 (2020).

[49] D. Y. Ivanov, B. Pire, L. Szymanowski, and J. Wagner, GPDs in heavy meson production and Compton scattering, EPJ Web Conf. **112**, 01020 (2016).

[50] A. Freund, M. McDermott, and M. Strikman, Modeling generalized parton distributions to describe deeply virtual Compton scattering data, Phys. Rev. D **67**, 036001 (2003).

[51] W. Zha, L. Ruan, Z. Tang, Z. Xu, and S. Yang, Coherent lepton pair production in hadronic heavy ion collisions, Phys. Lett. B **781**, 182 (2018).

[52] C. F. v. Weizsäcker, Radiation emitted in collisions of very fast electrons, Z. Phys. **88**, 612 (1934).

[53] J. D. Jackson, *Classical Electrodynamics* (Wiley, New York, 1998).

[54] H. Mäntysaari and J. Penttala, Exclusive heavy vector meson production at next-to-leading order in the dipole picture, Phys. Lett. B **823**, 136723 (2021).

[PIII]

PREDICTIONS FOR EXCLUSIVE Υ PHOTOPRODUCTION IN ULTRAPERIPHERAL Pb+Pb COLLISIONS AT THE LHC AT NEXT-TO-LEADING ORDER IN PERTURBATIVE QCD

by

Kari J. Eskola, Christopher A. Flett, Vadim Guzey, Topi Löytäinen and Hannu Paukkunen,

submitted to Eur. Phys. J. C, arXiv: 2303.03007 [hep-ph] (Mar. 2023).

Eur. Phys. J. C manuscript No.
(will be inserted by the editor)

Predictions for exclusive Υ photoproduction in ultraperipheral Pb + Pb collisions at the LHC at next-to-leading order in perturbative QCD

Kari J. Eskola[1,2,a], **C. A. Flett**[1,2,3,b], **V. Guzey**[1,2,c], **T. Löytäinen**[1,2,d], **H. Paukkunen**[1,2,e]

[1]University of Jyvaskyla, Department of Physics, P.O. Box 35, FI-40014 University of Jyvaskyla, Finland
[2]Helsinki Institute of Physics, P.O. Box 64, FI-00014 University of Helsinki, Finland
[3]Université Paris-Saclay, CNRS, IJCLab, 91405 Orsay, France

the date of receipt and acceptance should be inserted later

Abstract We present predictions for the rapidity-differential cross sections of exclusive Υ photoproduction in ultraperipheral collisions (UPCs) of lead ions at the Large Hadron Collider (LHC). We work in the framework of collinear factorization at next-to-leading order (NLO) in perturbative QCD, modeling the generalized parton distributions (GPDs) through the Shuvaev transform of nuclear parton distribution functions (nPDFs). While the effects due to the GPD modeling turn out to be small, the direct NLO predictions still carry significant nPDF-originating uncertainties and depend strongly on the choices of the factorization and renormalization scales. To tame the scale dependence and to account for the fact that the NLO calculations generally underpredict the photoproduction measurements on protons, we also present alternative, data-driven predictions. In this approach the underlying photoproduction cross sections on lead are found by combining their nuclear modifications calculated at NLO with the measured photoproduction cross sections on protons. The data-driven strategy reduces the uncertainties associated with the scale choices, and essentially eliminates the effects of GPD modeling thereby leaving the cross sections sensitive mainly to the input nPDFs. Our estimates indicate that the process is measurable in Pb + Pb collisions at the LHC.

[a]e-mail: kari.eskola@jyu.fi
[b]e-mail: christopher.flett@ijclab.in2p3.fr
[c]e-mail: vadim.a.guzey@jyu.fi
[d]e-mail: topi.m.o.loytainen@jyu.fi
[e]e-mail: hannu.paukkunen@jyu.fi

1 Introduction

The exclusive production of heavy vector mesons V in ultraperipheral collisions (UPCs) of heavy nuclei, $A_1 + A_2 \to A_1 + V + A_2$, has for a long time captured the interest of both the theoretical and experimental high-energy physics communities. It allows one to study not only the perturbative aspects of Quantum Chromodynamics (QCD) but to also probe the non-perturbative structure of nuclei [1,2,3,4]. These ultraperipheral events are largely initiated by electromagnetic interactions as the short-range hadronic interactions are strongly suppressed by the exclusivity of the final state. The vector meson production then effectively proceeds through an interaction of a quasi-real photon from one nucleus with the other nucleus such that the colliding nuclei remain intact and the exclusivity of the vector meson production is maintained via a net-colourless production mechanism. At leading order (LO) in perturbative QCD (pQCD) [5], the production is mediated through a two-gluon exchange, while at next-to-leading order (NLO), there is also a quark-pair initiated contribution [6]. The exchanged partons carry different longitudinal momentum fractions depending on an additional off-forward skewness parameter, ξ. This results in a factorization [7] of the scattering amplitude into the perturbatively calculable hard-scattering part and non-perturbative generalized parton distribution functions (GPDs) [8,9,10].

The first UPC measurements of exclusive J/ψ mesons came from the PHENIX collaboration at the Relativistic Heavy Ion Collider (RHIC) in Au+Au collisions at the nucleon-nucleon centre-of-mass system (c.m.s.) energy of $\sqrt{s_{NN}} = 200$ GeV [11]. Subsequently, the ALICE, CMS, and LHCb collaborations at the Large Hadron Collider (LHC) have measured the same pro-

cess in heavier Pb+Pb UPCs at $\sqrt{s_{NN}} = 2.76$ and 5.02 TeV in a wide range of the J/ψ rapidities from $y = 0$ up to $|y| \sim 4.5$ [12,13,14,15,16,17,18]. These data – not forgetting the multitude of statistics anticipated in the heavy-ion programme of the High Luminosity LHC [19] – provide ample grounds for understanding the perturbative structure of QCD and the nuclear shadowing phenomenon encoded e.g. in nuclear parton distribution functions (nPDFs) [20,21,22,23], down to momentum fractions of $x \sim (M_V/\sqrt{s_{NN}})\exp(-|y|) \sim 10^{-5}$ at resolution scales $\mu^2 \sim \mathcal{O}(M_V^2)$, where M_V is the mass of the vector meson.

In our previous works [24,25], we studied the exclusive photoproduction of J/ψ mesons in Pb + Pb and O + O collisions to next-to-leading order (NLO) in pQCD. By approximating the GPDs with PDFs, we demonstrated the complicated interplay of the quark and gluon contributions at NLO over the entire LHC acceptance in rapidity, and showed that our theoretical predictions agree with the experimental data for this process [12,13,14,15,16,17,18] within the large theoretical uncertainties associated with the choice of the factorization/renormalization scales and nPDFs. Valuable and complementary information on nPDFs at small momentum fractions x, in particular, on the scale dependence of nuclear shadowing, can be obtained by studying exclusive photoproduction of heavier vector mesons such as Υ mesons consisting of a bottom quark and its antiquark. To date, while there have been measurements of the exclusive photoproduction of Υ in $e + p$ collisions at Hadron Electron Ring Accelerator (HERA) [26,27,28], as well as in p+p [29] and p+Pb collisions at the LHC [30], there has been no reported measurement of the exclusive production of Υ mesons in heavy-ion collisions.

In the work presented here, we make predictions for the rapidity-differential cross sections of this process at $\sqrt{s_{NN}} = 5.02\,\text{TeV}$ in Pb + Pb collisions, extending our previous framework to incorporate a more careful GPD modeling by relating the nPDF to nuclear GPDs through the so-called Shuvaev integral transform [31, 32,33]. Despite the larger interaction scale in comparison to the J/ψ case, the theoretical uncertainties in the case of Υ production are still sizable and – as was already noticed in the pioneering work of Ref. [6] and as we confirm in this work as well – natural choices of the factorization/renormalization scales $\mu^2 \sim \mathcal{O}(M_\Upsilon^2)$ do not lead to a particularly good description of the HERA data. This would then cast doubts also on our direct NLO predictions in Pb + Pb. As a workaround, we will adopt an alternative method in which we anchor our predictions for the underlying γ+Pb $\to \Upsilon$+Pb cross sections on the HERA data on the $\gamma + p \to \Upsilon + p$ process by using the NLO calculations only for the ratios of cross sections between these two processes. We call this method the data-driven approach. We also analyze the nuclear modifications of the $\gamma + \text{Pb} \to \Upsilon + \text{Pb}$ cross sections due to nuclear effects in PDFs and show that for $\xi < 10^{-3}$, they coincide very closely with the gluon nuclear modification factor squared.

The rest of the paper is organised as follows. In Sec. 2.1, we summarize our theoretical framework for the exclusive photoproduction of Υ in ultraperipheral Pb + Pb collisions within NLO pQCD, and then discuss the modeling of GPDs in Sec. 2.2. The ingredients of our data-driven approach are explained in Sec. 3. In Sec. 4, we then present our results for the cross sections and their nuclear modifications, discussing also how our calculations build up from various components. Finally, we draw our conclusions in Sec. 5, outlining also future directions.

2 Theoretical framework

2.1 Exclusive Υ photoproduction in Pb + Pb UPCs at NLO pQCD

Within the equivalent-photon approximation [1,2], the rapidity-differential cross section for the process Pb + Pb $\to$ Pb + Υ + Pb can be written as

$$\frac{\mathrm{d}\sigma^{\text{Pb+Pb}\to\text{Pb+}\Upsilon\text{+Pb}}}{\mathrm{d}y} = \left(k\frac{dN_\gamma^{\text{Pb}}(k)}{dk}\sigma^{\gamma(k)\text{Pb}\to\Upsilon\text{Pb}}\right)_{k=k^+} + \left(k\frac{dN_\gamma^{\text{Pb}}(k)}{dk}\sigma^{\text{Pb}\gamma(k)\to\text{Pb}\Upsilon}\right)_{k=k^-}, \tag{1}$$

where $kdN_\gamma^{\text{Pb}}(k)/dk$ is the Weizsäcker-Williams (WW) number density or flux of photons from the Pb nucleus as a function of the photon energy $k^\pm = (M_\Upsilon/2)\exp(\pm y)$ with M_Υ being the mass of the Υ meson. The cross sections for the underlying photoproduction subprocesses are labelled by $\sigma^{\text{Pb}\gamma(k^-)\to\text{Pb}\Upsilon}$ and $\sigma^{\gamma(k^+)\text{Pb}\to\Upsilon\text{Pb}}$. The two terms in Eq. (1) correspond to the right-moving and left-moving photon sources, which results in a twofold ambiguity of the photon energy at a given value of $y \neq 0$.

The WW flux is given by a convolution of the impact-parameter dependent photon flux $N_\gamma^A(k,\vec{b})$ calculable in QED [34] and the nuclear suppression factor $\Gamma_{AA}(\vec{b})$,

$$k\frac{dN_\gamma^A(k)}{dk} = \int d^2\vec{b}\, N_\gamma^A(k,\vec{b})\Gamma_{AA}(\vec{b})\,. \tag{2}$$

Here, $\vec{b}$ is the two-dimensional vector between the centres of the two colliding Pb nuclei in the transverse

plane, and $\Gamma_{AA}(\vec{b})$ encodes the Glauber-model probability of having no additional hadronic interaction in the event; for details see [24].

The cross section for the photoproduction process mediating the ultraperipheral Pb + Pb $\to$ Pb + Υ + Pb reaction can be expressed in terms of the exclusive photoproduction cross section per bound nucleon N, $d\sigma_A^{\gamma N\to\Upsilon N}(W)/dt$, and the nuclear form factor $F_A(t)$ as

$$\sigma^{\gamma A\to\Upsilon A}(W) = \left.\frac{\mathrm{d}\sigma_A^{\gamma N\to\Upsilon N}(W)}{\mathrm{d}t}\right|_{t=0} \int_{|t_{\min}|}^{\infty} \mathrm{d}t|F_A(-t)|^2\,, \tag{3}$$

where

$$\left.\frac{\mathrm{d}\sigma_A^{\gamma N\to\Upsilon N}(W)}{\mathrm{d}t}\right|_{t=0} = \frac{|\mathcal{M}_A^{\gamma N\to\Upsilon N}|^2}{16\pi W^4} \tag{4}$$

is the t-differential cross section evaluated at $t = 0$, the variable t being the squared momentum transfer in the process, W is the γ-N c.m.s. energy, and $|t_{\min}| = m_N^2(M_\Upsilon^2/W^2)^2$ is the minimal momentum transfer squared with m_N denoting the nucleon mass.

The nuclear form factor $F_A(t)$ is well known from measurements of elastic electron-nucleus scattering and for heavy nuclei it is typically given by the Fourier transform of the two-parameter Woods-Saxon charge distribution $\rho(r)$ [35],

$$F_A(t) = \int d^3r\, e^{i\mathbf{q}\cdot\mathbf{r}}\rho(r)\,, \tag{5}$$

where

$$\rho(r) = \frac{\rho_0}{1+\exp\left(\frac{r-R_A}{d}\right)}\,, \tag{6}$$

with $|\mathbf{q}| = \sqrt{-t}$. We take $d = 0.546$ fm for the nucleus skin depth and $R_A/\mathrm{fm} = 1.12A^{1/3} - 0.86A^{-1/3}$ for the nuclear radius. The normalization $\rho_0 \approx 0.17$ fm^{-3} is fixed by requiring that $F_A(0) = A = 208$ for Pb.

The hard scattering amplitude for exclusive Υ photoproduction per nucleon N bound in the nucleus A can be described at NLO in collinear factorization by [6],

$$\mathcal{M}_A^{\gamma N\to\Upsilon N}(\xi, t=0) = \frac{4\pi\sqrt{4\pi\alpha}e_b(\epsilon_\Upsilon^*\cdot\epsilon_\gamma)}{N_c}\left(\frac{\langle O_1\rangle_\Upsilon}{m_b^3}\right)^{1/2} \times I(\xi, t=0)\,, \tag{7}$$

where

$$I(\xi,t=0) = \int_{-1}^{1}\mathrm{d}x\Big[T_g(x,\xi,\mu_R,\mu_F)F^g(x,\xi,t=0,\mu_F) + T_q(x,\xi,\mu_R,\mu_F)F^{q,S}(x,\xi,t=0,\mu_F)\Big]\,. \tag{8}$$

In Eq. (7), $e_b = 1/3$ and $m_b = M_\Upsilon/2$ are the electric charge and the mass of the bottom quark, respectively; α is the fine-structure constant; $N_c = 3$ is the number of colors; ϵ_γ and ϵ_Υ^* are the polarization vectors of the initial-state photon and the final-state vector meson, respectively; $\langle O_1\rangle_\Upsilon$ is the non-relativistic QCD (NRQCD) matrix element for the $\Upsilon\to b\bar{b}$ transition, which is proportional to the radial Υ wavefunction at the origin and which is fixed by the experimental value of the Υ decay width to a dilepton pair, see [36]. Note that in this approach, $M_\Upsilon = 2m_b$.

The reduced matrix element $I(\xi, t=0)$ is given by a convolution of the gluon $T_g(x,\xi,\mu_R,\mu_F)$ and quark $T_q(x,\xi,\mu_R,\mu_F)$ NLO coefficient functions with the gluon $F^g(x,\xi,t,\mu_F)$ and quark singlet $F^{q,S}(x,\xi,t,\mu_F)$ matrix elements involving the corresponding GPDs. Note that the coefficient functions depend on the longitudinal momentum fraction x, the skewness $\xi = M_\Upsilon^2/(2W^2 - M_\Upsilon^2)$, the renormalization scale μ_R, and the factorization scale μ_F. In our analysis, we set $\mu = \mu_R = \mu_F$ and vary μ in the $m_b/2 \le \mu \le 2m_b$ interval.

In the leading-twist approximation and neglecting the mass of the nucleons, the factors F^g and $F^{q,S}$ in the $t = 0$ limit can be expressed in terms of the helicity-conserving gluon $H^g(x,\xi,t,\mu_F)$ and quark singlet $H^{q,S}(x,\xi,t,\mu_F)$ GPDs as follows [10],

$$\begin{aligned} F^g(x,\xi,t=0,\mu_F) &= \sqrt{1-\xi^2}H^g(x,\xi,t=0,\mu_F), \\ F^{q,S}(x,\xi,t=0,\mu_F) &= \sqrt{1-\xi^2}H^{q,S}(x,\xi,t=0,\mu_F)\,, \end{aligned} \tag{9}$$

with

$$H^{q,S}(x,\xi,t=0,\mu_F) = \sum_{q=u,d,s,c}\Big[H^q(x,\xi,t=0,\mu_F) - H^q(-x,\xi,t=0,\mu_F)\Big]\,. \tag{10}$$

At $\xi = t = 0$, these GPDs reduce to the usual gluon, quark, and antiquark PDFs of the (bound) nucleons,

$$\begin{aligned} H^g(\pm x,\xi=0,t=0,\mu_F) &= xg(x,\mu_F)\,, \\ H^q(x,\xi=0,t=0,\mu_F) &= q(x,\mu_F)\,, \\ H^q(-x,\xi=0,t=0,\mu_F) &= -\bar{q}(x,\mu_F) \\ H^{q,S}(x,\xi=0,t=0,\mu_F) &= \sum_{q=u,d,s,c}\Big[q(x,\mu_F)+\bar{q}(x,\mu_F)\Big] \\ &\equiv q^S(x,\mu_F)\,. \end{aligned} \tag{11}$$

where $x \in [0,1]$.

In Eq. (8), each value of the skewness parameter ξ entails an integration over the convolution variable x. In the literature, see [10] for review, the $|x| \ge \xi$ interval is called the DGLAP region since GPDs there can be interpreted as parton distribution functions evolving in

$\log(\mu_F^2)$ according to the modified Dokshitzer-Gribov-Lipatov-Altarelli-Parisi (DGLAP) evolution equations. The $|x| < \xi$ interval is called the ERBL region because GPDs there resemble parton distribution amplitudes, whose μ_F evolution is given by the modified Efremov-Radyushkin-Brodsky-Lepage (ERBL) evolution equations. In this work, we employ the Shuvaev transform at NLO to model the ξ dependence of GPDs and to relate the GPDs to PDFs in the DGLAP region, see details in Sec. 2.2. To counteract the possible invalidity of the Shuvaev transform in the time-like ERBL region of $|x| < \xi$, we convolute the GPDs with only the imaginary part of the gluon and quark coefficient functions in Eq. (8), which vanish identically for $|x| < \xi$. We then restore the real part via the high-energy dispersion relation [37]

$$\frac{\Re e\mathcal{M}_A^{\gamma N\to\Upsilon N}(\xi,t=0)}{\Im m\mathcal{M}_A^{\gamma N\to\Upsilon N}(\xi,t=0)} = \tan\left(\frac{\pi}{2}\,\frac{\partial\ln(\Im m\mathcal{M}_A^{\gamma N\to\Upsilon N}(\xi,t=0)/(1/\xi))}{\partial\ln(1/\xi)}\right). \tag{12}$$

We have checked that this relation accurately reproduces the directly computed real part contribution for $W \gtrsim 40$ GeV at a percent level in the case that GPDs are approximated by PDFs. At smaller W the deviation increases but, as will be discussed, our main data-driven predictions will nevertheless be valid only for $W \gtrsim 100\,\text{GeV}$.

To summarize, the standard pQCD approach to the calculation of the $\sigma^{\gamma A\to\Upsilon A}(W)$ cross section is based on Eqs. (3) and (4), where the hard scattering nuclear amplitude per bound nucleon $\mathcal{M}_A^{\gamma N\to\Upsilon N}(\xi,t=0)$ is calculated using the bound nucleon (nucleus) gluon and quark GPDs, see Eqs. (7) and (8). Replacing the bound nucleon by the free proton in these equations, one readily obtains the NLO pQCD predictions for the proton target. The cross section of exclusive Υ photoproduction on the proton reads [compare to Eq. (3)]

$$\sigma^{\gamma p\to\Upsilon p}(W) = \frac{1}{B_\Upsilon(W)}\frac{\mathrm{d}\sigma^{\gamma p\to\Upsilon p}(W)}{\mathrm{d}t}\bigg|_{t=0}, \tag{13}$$

where $B_\Upsilon(W)$ is the energy-dependent slope of the t dependence of the $\gamma + p \to \Upsilon + p$ cross section, which is assumed to be exponential; $\mathrm{d}\sigma^{\gamma p\to\Upsilon p}(W)/\mathrm{d}t(t=0)$ is the differential cross section at $t = 0$, which is calculated using Eqs. (4), (7) and (8) with nuclear GPDs replaced by their free-proton counterparts.

The t dependence of the $\gamma + p \to \Upsilon + p$ cross section has never been measured. Therefore, for the $B_\Upsilon(W)$ slope, we use the following parametrization motivated by Regge phenomenology,

$$B_\Upsilon(W) = B_0 + 4\alpha'_{I\!P}\ln\left(\frac{W}{W_0}\right), \tag{14}$$

where $B_0 = 4.63\ \text{GeV}^{-2}$, $\alpha'_{I\!P} = 0.06\ \text{GeV}^{-2}$, and $W_0 = 90$ GeV. While the value of B_0 is compatible with fits to the t dependence of elastic J/ψ photoproduction on the proton at HERA [26,38], the value of slope of the Pomeron trajectory $\alpha'_{I\!P}$ is fixed by Model 4 of [39], which fits a wide variety of data on diffraction in proton-proton scattering at the LHC.

2.2 GPD modeling

Generalized parton distributions naturally appear in the framework of collinear factorization for hard exclusive processes [7] and combine properties of usual PDFs, distribution amplitudes and elastic form factors [8,9,10]. Since GPDs depend on two light-cone momentum fractions x and ξ, the invariant momentum transfer squared t, and the factorization scale μ_F, their modeling and extraction from the available experimental data has been notoriously challenging, see, e.g. [40]. However, at small values of the skewness ξ, GPDs rather closely resemble usual PDFs in the $|x| \geq \xi$ DGLAP region and the $|x| < \xi$ ERBL region plays typically only a minor role. These facts significantly simplify the modeling of GPD-originating effects even if the experimental constraints for the three-dimensional structure of GPDs are weak.

One of the most widely used models of GPDs at small ξ is based on the so-called Shuvaev transform, which is a method to analytically solve the LO Q^2 evolution equations of GPDs [31,32,33]. It is a generalization of solving the usual DGLAP evolution equations using Mellin moments of PDFs. To briefly summarize the method, one first defines effective PDFs, whose Mellin moments are equal to the Gegenbauer (conformal) moments of GPDs. One then inverts these relations and expresses GPDs as certain integrals of the effective PDFs at any given factorization scale μ_F. Finally, using the condition of polynomiality of the conformal moments (see details in [32,41]), one argues that the effective PDFs can be approximated by the usual PDFs and obtains the desired connection between GPDs at small ξ and PDFs. In other words, the input GPDs at some low scale μ_0 are assumed to be independent of ξ, and the ξ dependence is then generated radiatively during the scale evolution – this warrants to speak about perturbative skewness. Moreover, since the mixing of the conformal moments under the NLO Q^2 evolution is suppressed by powers of ξ, the Shuvaev transform can also be safely used at NLO in the $\xi \ll 1$ limit [31]. As a phenomenological application of the method, it was shown in NLO and next-to-next-to-leading order (NNLO) analyses [42] that a flexible parametrization of quark and gluon GPDs of the proton in terms of their

conformal moments describes well the available HERA data on deeply virtual Compton scattering (DVCS) on the proton. In the case that the condition $\xi \ll 1$ is not met, the Shuvaev transform should be substituted by explicitly solving the GPD evolution equations [43,44].

In our work, we employ the Shuvaev transform at NLO as a means to relate the GPDs to PDFs in the DGLAP region. Thus, the quark and gluon GPDs are obtained as integrals of the corresponding quark and gluon PDFs,

$$
\begin{aligned}
&H^q(x,\xi,t=0,\mu_F) = \\
&\int_{-1}^{1} \mathrm{d}x' \left[\frac{2}{\pi}\Im m \int_0^1 \frac{\mathrm{d}s}{y(s)\sqrt{1-y(s)x'}}\right] \frac{\mathrm{d}}{\mathrm{d}x'} \frac{q(x',\mu_F)}{|x'|}\,, \\
&H^g(x,\xi,t=0,\mu_F) = \\
&\int_{-1}^{1} \mathrm{d}x' \left[\frac{2}{\pi}\Im m \int_0^1 \frac{\mathrm{d}s\ (x+\xi(1-2s))}{y(s)\sqrt{1-y(s)x'}}\right] \frac{\mathrm{d}}{\mathrm{d}x'} \frac{g(x',\mu_F)}{|x'|}\,,
\end{aligned}
\tag{15}
$$

where the kernel of the transform is

$$
y(s) = \frac{4s(1-s)}{x+\xi(1-2s)}\,. \tag{16}
$$

As we explained above, Eq. (15) is used only to calculate the imaginary part of the hard scattering amplitude $\mathcal{M}_A^{\gamma N\to\Upsilon N}(\xi,t=0)$. The real part probing the ERBL region is restored via the high-energy dispersion relation (12). In practice, the Shuvaev integrals in Eqs. (15) involving derivatives of the input PDFs converge rather slowly and have to be precomputed before evaluating Eq. (8). To this end, we have computed the GPDs in a three-dimensional $x, \xi/x, \mu^2$ grid using Eqs. (15). The construction of the GPD grid is optimised such that areas in the parameter space that result in a flat interpolation are not overly populated: having more points around $\xi/x \sim 1$ mitigates edge effects at the boundary of the DGLAP and ERBL regions [41], while the interpolation in μ^2 is relatively smooth and requires fewer points.

In Fig. 1, we illustrate the effect of finite skewness in GPDs by comparing the gluon and quark-singlet GPDs, $F^g(x,\xi)$ and $F^{q,S}(x,\xi)$, obtained through the Shuvaev transform, with their values at $\xi=0$, $xg(x)$ and $q^S(x)$, as a function of x at the scale $\mu_F = m_b$. We have used here the CT18ANLO proton PDFs [45] taken from the LHAPDF library [46]. In these plots, we have fixed $\xi \approx 10^{-3}$, which corresponds to the kinematic value of the skewness parameter probed in Υ photoproduction in Pb + Pb UPCs at 5.02 TeV and $y=0$. The distributions are plotted in a small interval of the DGLAP region, $x \in [\xi, 10^{-2}]$, where the Shuvaev transform is a reliable way to obtain the perturbatively generated skewness of the GPDs. One can see from the figure that the effect of skewness – the deviation between the blue and orange curves – is rather small for most values of x, but grows towards the point $x=\xi$, especially in the case of quarks. At the same time, to compare with the commonly used skewness factor due to the Shuvaev transform [32,47], we also show the gluon and quark singlet PDFs evaluated at the $x+\xi$ point, $(x+\xi)g(x+\xi,\mu_F)$ and $q^S(x+\xi,\mu_F)$. In this case, the effect of skewness is noticeable (the deviation between the blue and green lines is significant). However, in our NLO pQCD analysis the $(x+\xi)g(x+\xi,\mu_F)$ and $q^S(x+\xi,\mu_F)$ PDFs do not play any special role and we find that the numerical effect of the skewness effects induced by the Shuvaev transform in the calculated cross sections of Υ photoproduction on the proton and a heavy nucleus is small.

The effect of the Shuvaev transform is larger at larger scales μ_F, where the effective power growth of the partons becomes steeper and reflects the sensitivity of the Shuvaev transform to the slope of the input PDFs through Eq. (15). The enhancement in the quark singlet GPD is clearly larger than that in the gluon one. However, our analysis shows that the contribution of the quarks is subleading and so the overall effect of incorporating the skewness through the Shuvaev transform is dictated by the gluon GPDs. Our results for the differences between $F^g(x,\xi,\mu_F)$ and $xg(x,\mu_F)$, and $F^{q,S}(x,\xi,\mu_F)$ and $q^S(x,\mu_F)$, are qualitatively similar to those presented in the DGLAP region at LO in Fig. 3 of Ref. [43].

3 Data-driven approach

As discussed in our previous works in the context of exclusive J/ψ photoproduction in Pb + Pb and O+O UPCs [25,24], the photoproduction scattering amplitude $\mathcal{M}_A^{\gamma N\to\Upsilon N}(\xi,t=0)$ introduced above suffers from a large factorization/renormalization scale dependence. While it is milder for the case of Υ photoproduction considered here since the interaction scale is higher than in the J/ψ photoproduction, it is still rather sizeable as we will show later on in Sec. 4. In addition, the NLO results will be shown to somewhat underpredict the HERA and LHC data on the $\gamma+p\to\Upsilon+p$ cross section. An approach to alleviate the strong scale dependence through consideration of additional power corrections $\sim \mathcal{O}(\mu_F^2/Q_0^2)$ arising in the so-called Q_0 subtraction, where Q_0 is the PDF or GPD parametrization scale, was advocated in [48,49,50,51,52] in the context of $p+p$ and $p+\mathrm{Pb}$ collisions. Instead of the Q_0 subtraction, we adopt a data-driven pQCD approach, where the $\gamma + \mathrm{Pb} \to \Upsilon + \mathrm{Pb}$ cross section is given by the product of the ratio between the Υ photoproduction cross sections on the nucleus and the proton calculated

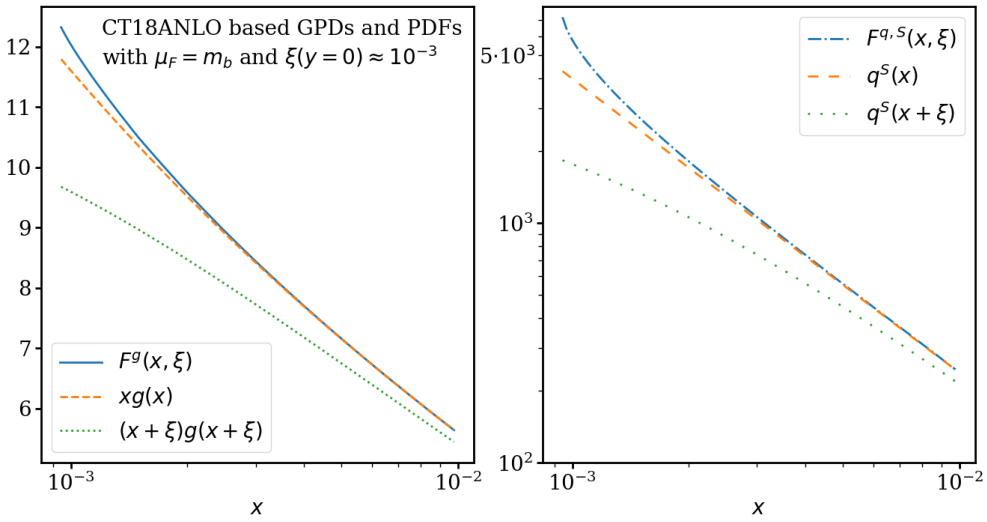

Fig. 1 The gluon (left panel) and quark singlet (right panel) GPDs (blue curves) $F^g(x,\xi)$ and $F^{q,S}(x,\xi)$ with $\xi \approx 10^{-3}$ obtained through the Shuvaev transformation, compared with PDFs $xg(x)$ and $q^S(x)$ (orange dashed curves) at $\mu_F = m_b$ as a function of x. In addition, we also present the distributions $(x+\xi)g(x+\xi)$ and $q^S(x+\xi)$ (green dotted curves).

in NLO in pQCD, and the $\gamma + p \to \Upsilon + p$ cross section fitted to the available HERA [26,27,28] and LHC data [29],

$$\sigma^{\gamma\mathrm{Pb}\to\Upsilon\mathrm{Pb}}(W) = \left[\frac{\sigma^{\gamma\mathrm{Pb}\to\Upsilon\mathrm{Pb}}(W)}{\sigma^{\gamma p\to\Upsilon p}(W)}\right]_{\mathrm{pQCD}} \sigma_{\mathrm{fit}}^{\gamma p\to\Upsilon p}(W)\,. \tag{17}$$

Using a simple power-like ansatz for $\sigma_{\mathrm{fit}}^{\gamma p\to\Upsilon p}(W)$ with an additional factor parametrizing the behavior of the cross section near the kinematic threshold [53], one obtains [54]

$$\sigma_{\mathrm{fit}}^{\gamma p\to\Upsilon p}(W) = \frac{0.902\ \mathrm{nb\,GeV}^{-2}}{B_\Upsilon(W)}\left[1-\frac{(M_\Upsilon+m_N)^2}{W^2}\right]^{1.5} \times \left(\frac{W^2}{\widetilde{W}_0^2}\right)^{0.447}, \tag{18}$$

with $\widetilde{W}_0 = 100$ GeV. Note that while the 2018 CMS data [30] have not been included in the fit, they are nevertheless well reproduced, see Fig. 2 ahead. One way to interpret Eq. (17) is that we supplement the fitted $\gamma + p \to \Upsilon + p$ cross sections by the theoretical nuclear modification $R(W)$,

$$R(W) = \left[\frac{\sigma^{\gamma\mathrm{Pb}\to\Upsilon\mathrm{Pb}}(W)}{\sigma^{\gamma p\to\Upsilon p}(W)}\right]_{\mathrm{pQCD}}, \tag{19}$$

which can be anticipated to carry a reduced dependence on the choice of the factorization scale and on the explicit modeling of GPDs. In the first approximation, these effects cancel in $R(W)$ and it becomes mainly sensitive to the PDFs of protons and nuclei. Alternatively, one can interpret that in Eq. (17) one rescales the calculated $\gamma + \mathrm{Pb} \to \Upsilon + \mathrm{Pb}$ cross sections by a factor that is needed to match the calculated $\gamma + p \to \Upsilon + p$ cross sections with the experimental ones – an effective "K factor". In what follows, we will call the cross sections computed through Eq. (17) the "data-driven" ones, in contrast to the "standard" pQCD predictions calculated without any reference to experimental data. The approach here is similar in spirit to the leading-order pQCD analysis of the nuclear suppression factor for exclusive J/ψ photoproduction in Pb+Pb collisions introduced and discussed in Refs. [53,55,56].

4 Results

In this section, we present and discuss our results for the Υ photoproduction process on the proton, $\gamma + p \to \Upsilon + p$, and the rapidity-differential Υ spectra in Pb+Pb UPCs, $\mathrm{Pb} + \mathrm{Pb} \to \mathrm{Pb} + \Upsilon + \mathrm{Pb}$. To estimate the sensitivity of our predictions to higher-order perturbative corrections, we adopt a standard, conservative prescription and vary the factorization and renormalization scales together in the interval of $\mu_F = \mu_R \in \{1/2, 1, 2\} \times m_b$. As input proton and nuclear PDFs, we use CT18ANLO [45] and EPPS21 [21] PDFs, respectively, from the LHAPDF interface [46]. The corresponding GPDs are obtained using the Shuvaev transform as discussed in Sec. 2.2. Note that we use the version "A" of the CT18NLO analysis since this was the free proton baseline used in the EPPS21 nPDF analysis. It differs from the default CT18NLO mainly in the strange quark distributions. In the first instance we make NLO predictions following the standard pQCD

approach, and then subsequently compare and contrast features of these predictions with those obtained from the data-driven method explained in Sec. 3, as well as with our earlier analyses [24,25] of J/ψ photoproduction in Pb + Pb UPCs.

4.1 Standard pQCD results for $\gamma + p \to \Upsilon + p$ cross section

Figure 2 presents the $\sigma^{\gamma p\to\Upsilon p}(W)$ cross section of exclusive Υ photoproduction on the proton, $\gamma+p \to \Upsilon+p$, as a function of the invariant photon-proton c.m.s. energy W. The dashed, dot-dashed and dotted curves correspond to the NLO pQCD predictions of Eq. (13), which as input use either the proton GPDs obtained via the Shuvaev transform (the curves labeled "GPD") or the usual proton PDFs, i.e., the $\xi = 0$ forward limit of the GPDs (the curves labeled "PDF"). Each pair of predictions is evaluated with three scale settings $\mu = \mu_F = \mu_R \in \{1/2, 1, 2\} \times m_b$. The shaded band represents the propagated uncertainty of the proton PDFs used for the GPD-based predictions at $\mu = m_b$. These results are compared with the available HERA [27,26,28] and the LHC data [29,30] on this process. Note that it is argued in [51] that the extracted values of $\sigma^{\gamma p\to\Upsilon p}(W)$ at the largest W from the LHCb rapidity-differential measurements [29] should be shifted upwards because the collaboration used a less accurate approximation for the photon flux in their analysis. Finally, the black solid line labeled "Fit" is the parametrization of Eq. (18).

One can see from the figure that while our NLO pQCD predictions reproduce the trends of the W dependence of the data, they underestimate the normalization of the cross section, especially at larger values of μ. A reliable description of the normalization would thus require a better theoretical understanding of the perturbative structure of the process including, e.g. the relevance of unknown next-to-NLO corrections, significance of the double logarithmic $\alpha_s \log(\mu_F^2/m_b^2) \log(1/\xi)$ terms present already in the NLO hard coefficient functions T_g and T_q [6,57][1], and the size of the relativistic corrections to the quarkonium wave function [58]. An account of these effects is beyond the scope of this paper and we will work around these issues through the data-driven predictions.

The systematics of the NLO pQCD predictions in Fig. 2 can be summarized as follows. First, as discussed in Sec. 2.2, the effect of skewness is rather mild, i.e., the difference between the GPD-based and PDF-based predictions is small, especially at smaller values of μ. Second, while the GPD-based predictions correspond to higher values of $\sigma^{\gamma p\to\Upsilon p}(W)$ than the corresponding PDF-based ones at $\mu = m_b$ and $\mu = 2m_b$, this hierarchy of predictions is reversed at $\mu = m_b/2$. A detailed examination indicates that this originates from a delicate interplay among the LO gluon and NLO gluon and quark contributions in $\mathcal{M}_A^{\gamma N\to\Upsilon N}(\xi, t = 0)$ whose relative signs vary depending on the scale choices. This is further complicated by the fact that the magnitude of the skewness effect generated by the Shuvaev transform (15) depends on both W (through its dependence on ξ) and μ_F controlling the slope of the x dependence of the gluon and quark PDFs. Third, as a result of scale-dependent sign differences of quark/gluon contributions, the relative ordering of predictions from low to high μ depends on W.

4.2 Standard pQCD results for $\mathrm{Pb} + \mathrm{Pb} \to \mathrm{Pb} + \Upsilon + \mathrm{Pb}$ UPC cross section

In Fig. 3, we show our standard NLO pQCD predictions for $\mathrm{d}\sigma^{\mathrm{Pb+Pb}\to\mathrm{Pb}+\Upsilon+\mathrm{Pb}}/\mathrm{d}y$ as a function of the Υ rapidity y at $\sqrt{s_{NN}} = 5.02$ TeV, see Eqs. (1), (3), (4) and (7). As input, we use the nuclear GPDs constructed using the Shuvaev transform and the EPPS21 nPDFs (central plus error sets). The three curves correspond to the three different choices of the factorization/renormalization scales $\mu = \{m_b/2, m_b, 2m_b\}$. The shaded band gives the propagated uncertainty of the EPPS21 nPDFs in the $\mu = m_b$ case. As a useful reference, the upper x-axis shows the values of W^+ corresponding to each y, that is, $W^+ = (M_\Upsilon \sqrt{s_{NN}} e^y)^{1/2}$.

Two features of the results in Fig. 3 deserve to be mentioned. First, one can see from the figure that apart from the very tails of the rapidity distribution, $|y| > 3$, the central prediction with $\mu = m_b$ does not lie between the other scale choice predictions with $\mu = m_b/2$ and $\mu = 2m_b$. This feature can be readily observed also in the results for the proton cross section in Fig. 2. Indeed, taking, for instance, $y = 0$ corresponding to $W \approx 200$ GeV, one can see that the predictions for $\sigma^{\gamma p\to\Upsilon p}(W)$ with $\mu = m_b$ lie below the corresponding predictions at $\mu_F = m_b/2$ and $\mu_F = 2m_b$. Second, the scale uncertainty is rather large and the prediction with $\mu = m_b/2$ lies outside the nPDF uncertainty band. We will show in Sec. 4.3 that both of these features can be tamed through our data-driven approach.

In Figs. 4, 5 and 6, we show various decompositions of $\mathrm{d}\sigma^{\mathrm{Pb+Pb}\to\mathrm{Pb}+\Upsilon+\mathrm{Pb}}/\mathrm{d}y$ at $\mu = m_b$ as a function of y. Figure 4 presents the breakdown of the full cross section into the quark, gluon and interference contributions. It is clear that over the entire considered rapidity region,

[1] Note that these terms should be more relevant at low ξ i.e. at high W whereas the normalization seems to be an increasingly serious issue towards low values of W.

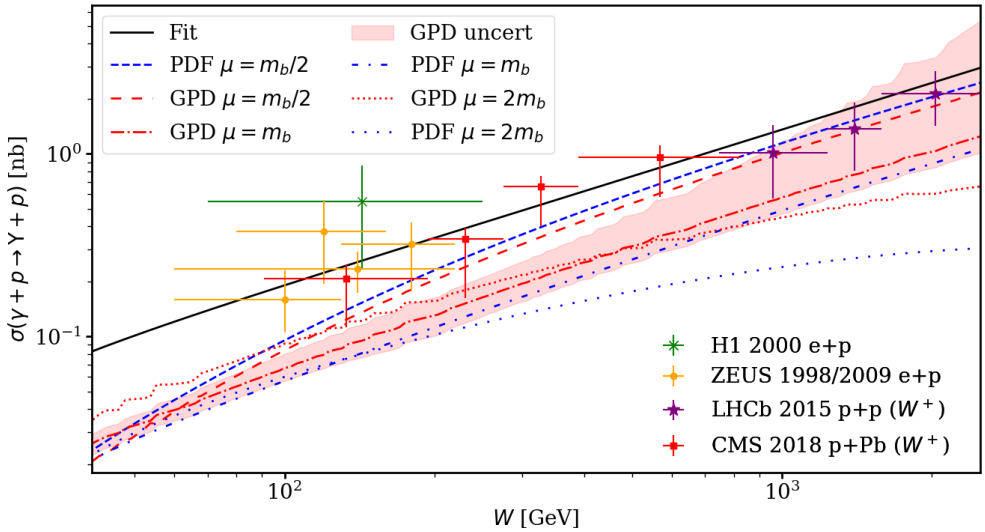

Fig. 2 The $\gamma + p \to \Upsilon + p$ cross section as a function of W. The NLO pQCD GPD-based (red curves) and PDF-based (blue curves) predictions evaluated at $\mu = \{m_b/2, m_b, 2m_b\}$ are presented by the dashed, dot-dashed and dotted lines; the shaded band is the propagated CT18ANLO PDF uncertainty for the GPD-based result at $\mu = m_b$. The HERA [27,26,28] and LHC data [29,30] data on this process are shown as well, together with a fit [Eq. (18)] to the HERA data (the black solid line labeled "Fit").

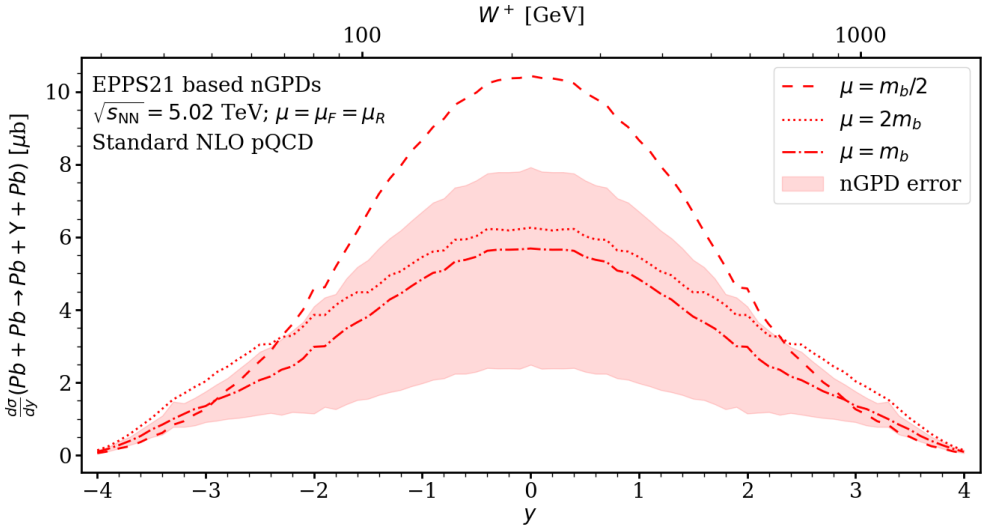

Fig. 3 Standard NLO pQCD prediction for the rapidity-differential cross section for exclusive coherent Υ photoproduction in Pb + Pb UPCs as a function of the Υ rapidity y at $\sqrt{s_{NN}} = 5.02$ TeV. We use nuclear GPDs constructed from the EPPS21 nPDFs via the Shuvaev transform. The dashed-dotted curve represents the prediction with $\mu = m_b$, and the band indicates the nPDF-originating uncertainty evaluated at the same scale. The predictions with $\mu = m_b/2$ (dashed) and $\mu = 2m_b$ (dotted) are also shown. The upper x-axis shows the values of W^+ as a function of y.

the gluon contribution dominates the quark contribution, in dissimilarity to the analogous breakdown for the J/ψ rapidity-differential cross section in Pb + Pb UPCs in NLO pQCD shown in our previous studies [25, 24], where the quark contribution was shown to be the dominant one around mid rapidity. One should note that even if the quark contribution is small, it is not zero or structureless and it leads to a visible contribution in the interference terms. One can speculate that the interaction scale in the Υ photoproduction is already sufficiently large so that NNLO corrections will not change the mutual hierarchy of quark/gluon contributions. The situation could be very different in the case of J/ψ photoproduction where the quark dominance is a consequence of a coincidental cancellation between the LO and NLO gluon contributions.

In Fig. 5, we show the W^+ and W^- decomposition i.e. separately plot the two contributions in Eq. (1). The situation is very similar to that in our J/ψ analysis, see [24,25] for more details. For instance, the W^- con-

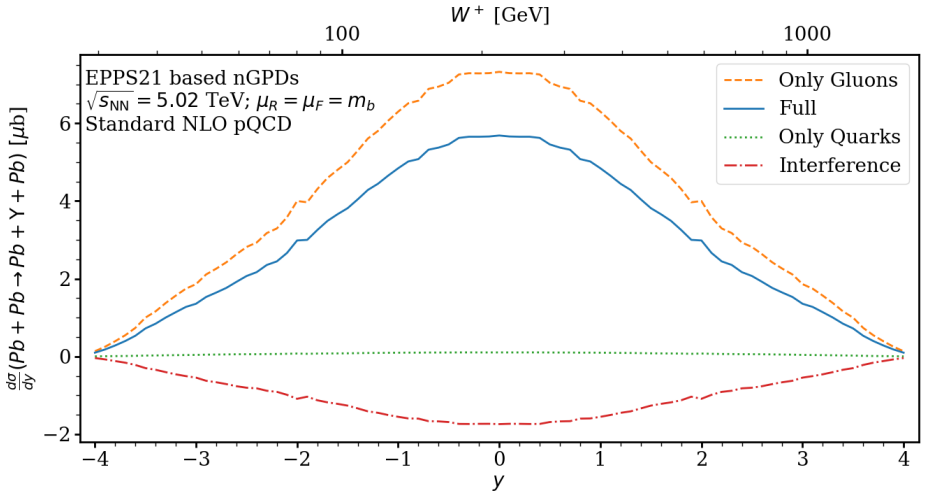

Fig. 4 Decomposition of the rapidity-differential $\mathrm{Pb}+\mathrm{Pb}\to\mathrm{Pb}+\Upsilon+\mathrm{Pb}$ cross section with $\mu=m_b$ into the quark, gluon and quark-gluon interference contributions, in our standard NLO pQCD approach.

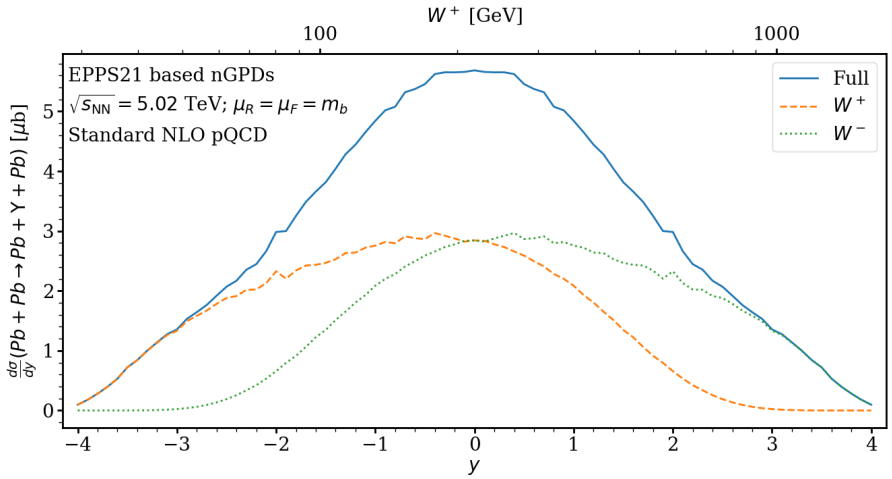

Fig. 5 Decomposition of the rapidity-differential $\mathrm{Pb}+\mathrm{Pb}\to\mathrm{Pb}+\Upsilon+\mathrm{Pb}$ cross section with $\mu=m_b$ into the W^+ and W^- components, in our standard NLO pQCD approach.

tribution dominates at positive forward rapidities (large W^+) because there $(kdN_\gamma^{\mathrm{Pb}}/dk)_{k=k^-}\gg(kdN_\gamma^{\mathrm{Pb}}/dk)_{k=k^+}$. The situation is reversed in the region of backward rapidities corresponding to small W^+. The presence of two terms in Eq. (1) complicates the extraction of the small-x contribution from UPC cross sections at $y\neq 0$. However, it is possible to separate the W^+ and W^- contributions by studying UPCs accompanied by forward neutron emission due to electromagnetic excitation of one or both colliding nuclei [59]. Such an analysis in the case of coherent J/ψ photoproduction in Pb+Pb UPCs at 5.02 TeV was recently performed by the CMS collaboration [60], which allowed one to deepen the small-x reach down to $x\sim 10^{-4}$.

Finally, Fig. 6 presents the decomposition of $\mathrm{d}\sigma^{\mathrm{Pb+Pb}\to\mathrm{Pb}+\Upsilon+\mathrm{Pb}}/\mathrm{d}y$ into the contributions of the real and imaginary parts of $\mathcal{M}_A^{\gamma N\to\Upsilon N}(\xi,t=0)$. The imaginary part clearly dominates over the entire range of rapidity. Again, the situation was much more involved in the case of J/ψ, where the interplay of the two was highly non-trivial [24,25].

4.3 Data-driven pQCD predictions for the $\mathrm{Pb}+\mathrm{Pb}\to\mathrm{Pb}+\Upsilon+\mathrm{Pb}$ UPC cross section

The data-driven pQCD prediction for the UPC cross section $\mathrm{d}\sigma^{\mathrm{Pb+Pb}\to\mathrm{Pb}+\Upsilon+\mathrm{Pb}}/\mathrm{d}y$ is given by Eq. (17), where only the ratio of the nucleus and proton cross sections $R(W)$ of Eq. (19) is calculated using our NLO pQCD framework, while the absolute normalization is given by $\sigma_{\mathrm{fit}}^{\gamma p\to\Upsilon p}(W)$ obtained from a fit to the proton data, see Eq. (18). The results for the differential cross section as a function of the Υ rapidity y are shown in Fig. 7. The numerator and the denominator of the ra-

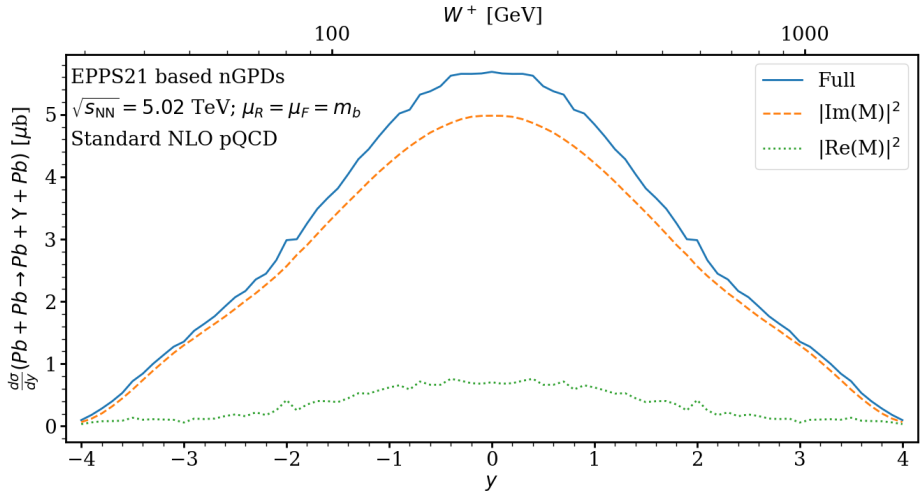

Fig. 6 Decomposition of the rapidity-differential $\mathrm{Pb}+\mathrm{Pb}\to\mathrm{Pb}+\Upsilon+\mathrm{Pb}$ cross section with $\mu = m_b$ into the contributions from the real and imaginary parts, in our standard NLO pQCD approach.

tio $R(W)$ are calculated using the EPPS21-based and the CT18ANLO-based GPDs, respectively; these curves are labeled "nGPD". For comparison, we also show the results of the calculation, where we neglect the effect of skewness and use the forward $\xi \to 0$ limit for nuclear and proton GPDs; these curves are labeled "nPDF". The blue dot-dashed curve represents our central prediction at $\mu = m_b$ with the blue shaded band quantifying the propagation of the EPPS21 nPDF and the CT18ANLO proton PDF uncertainties; their counterparts in the case, where GPDs are taken in the forward limit, are given by the red solid curve and the corresponding red shaded band. The dotted and dashed curves correspond to the ratio $R(W)$ evaluated at $\mu = m_b/2$ and $\mu = 2m_b$, respectively. The uncertainties in $\sigma_{\rm fit}^{\gamma p\to\Upsilon p}(W)$ are not included in our estimates. For reference, we give the values of $W^+ = (M_\Upsilon\sqrt{s_{NN}}\,e^y)^{1/2}$ probed at a given rapidity y on the upper x-axis, and also mark in the figure the points $|y| = 2$, beyond which the $\sigma_{\rm fit}^{\gamma p\to\Upsilon p}(W)$ fit to the $\gamma{+}p\to\Upsilon{+}p$ photoproduction data is an extrapolation: the HERA data are available only for $W \geq 100\,\mathrm{GeV}$ (see Fig. 2), but for $|y| \geq 2$ there is a large contribution from $W < 100\,\mathrm{GeV}$, see Fig. 5.

It is important to contrast our results in Fig. 7 with the standard NLO pQCD predictions shown in Fig. 3. First, while the shapes of the y distribution are very similar, the normalization of the data-driven results is approximately a factor of $2-2.5$ higher. This is a straightforward consequence of the rescaling of the cross section of exclusive Υ photoproduction on the proton to fit the available data. Second, the dependence on the factorization/renormalization scale μ is now more regular in the central rapidities: the central prediction with $\mu = m_b$ lies below the $\mu = m_b/2$ result and above the $\mu = 2m_b$ one. Most importantly, the scale dependence has reduced significantly. Third, the effects of GPD modeling are seen to largely cancel in the ratio $R(W)$. As a result, the data-driven pQCD predictions for $\mathrm{d}\sigma^{\mathrm{Pb+Pb\to Pb+\Upsilon+Pb}}/\mathrm{d}y$ are here mainly sensitive to the input PDFs. Note that for lower W, where the real part restoration via Eq. (12) is less accurate, the behavior of our results is less regular, but this lies in the tails of the y distributions where our predictions anyhow lean on an extrapolation of $\sigma_{\rm fit}^{\gamma p\to\Upsilon p}(W)$ into non-measured values of W.

To quantify the magnitude of nuclear effects probed in exclusive Υ photoproduction in Pb+Pb UPCs at the LHC, it is convenient to consider separately the ratio $R(W)$ in Eq. (19). Indeed, at a given value of the Υ rapidity $y \neq 0$, the Pb + Pb UPC cross section contains two terms leading to a two-fold ambiguity in the photon-nucleon c.m.s. energy $W^\pm$. As a consequence, this mixes the low-x and medium-x contributions to the UPC cross section and makes it challenging to extract the information on small-x physics, which is often thought to be at the heart of the process under consideration. This issue is absent in the case of $R(W)$ although it cannot be experimentally measured in a model-independent way. In the upper panel of Fig. 8, we show the ratio $R(W)$ as a function of W^+. On the x-axis at the top, we also give the corresponding values of the skewness $\xi^+ = M_\Upsilon^2/[2(W^+)^2 - M_\Upsilon^2]$. The curve corresponds to the central prediction at $\mu = m_b$ shown in Fig. 7, where the numerator and the denominator of $R(W)$ are calculated using the EPP21-based nuclear GPDs and the CT18ANLO-based free proton GPDs, respectively. The shaded band is the result of the propagation of the EPPS21 nPDF and the CT18ANLO proton PDF uncertainties. We see that the rescaling factor $R(W)$ depends strongly on W and its value can be

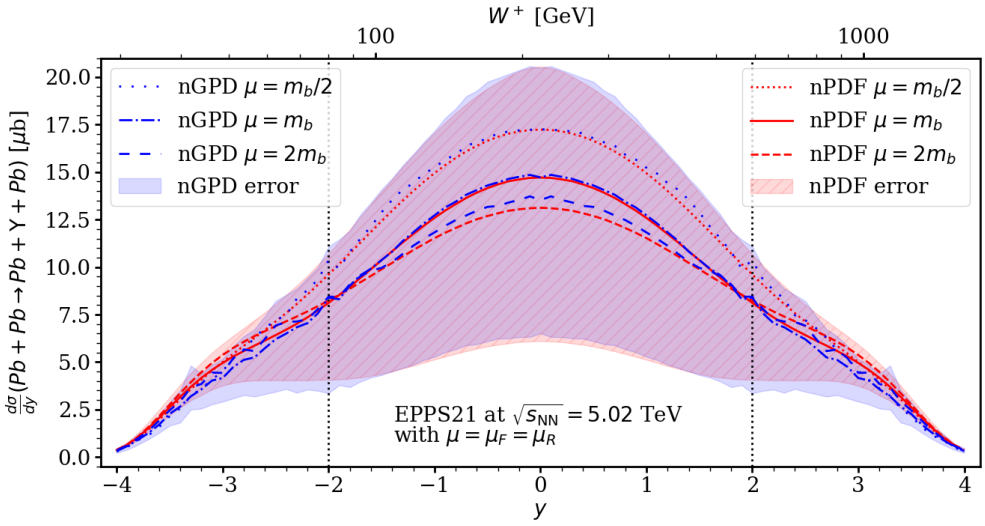

Fig. 7 Data-driven NLO pQCD prediction for the rapidity-differential cross section for exclusive coherent Υ photoproduction in Pb + Pb UPCs as a function of the Υ rapidity y at $\sqrt{s_{NN}} = 5.02$ TeV. We use the nuclear and proton GPDs constructed from the EPPS21 nPDFs and CT18ANLO proton PDFs, respectively, obtained via the Shuvaev transform (the curves labeled "nGPD"). For comparison, we also show the results based on the $\xi = 0$ limit of the used GPDs (the curves labeled "nPDF"). The blue dot-dashed line represents the central prediction with $\mu = m_b$ and the blue band gives the propagated uncertainties of the nuclear and proton PDFs. The predictions for $\mu = m_b/2$ (dotted) and $\mu = 2m_b$ (dashed) are also shown. The upper x-axis shows the values of W^+ for each y. The vertical dashed lines denote the points $|y| = 2$, beyond which the results are sensitive to low W where $\sigma_{\rm fit}^{\gamma p \to \Upsilon p}(W)$ is an extrapolation.

as large as several hundreds. The absolute value can, however, be mostly explained through the proton and nuclear form factors. To see this and to provide a closer comparison with nuclear modifications of nPDFs, one can eliminate the effects of the nuclear and the proton form factors in the $R(W)$ ratio by rescaling it by the factor of $R'(W)$,

$$R'(W) = \frac{1/B_\Upsilon(W)}{\int_{|t_{\rm min}|}^{\infty} {\rm d}t\, |F_A(-t)|^2}\,, \tag{20}$$

where $B_\Upsilon(W)$ is the slope of the t dependence of the $\gamma + p \to \Upsilon + p$ differential cross section in Eq. (14) and $F_A(t)$ is the nuclear form factor in Eq. (5). Note that $R'(W)$ depends on W^+ through $|t_{\rm min}| = m_N^2 (M_\Upsilon/W^+)^4$ and $B_\Upsilon(W^+)$. In the lower panel of Fig. 8, we present the scaled $R(W)$ ratio, i.e., the product $R(W) \times R'(W)$, as a function of W^+ by the red solid curve. The propagated nuclear and free proton PDF uncertainties are given by the red shaded band. One can see from the figure that as a function of ξ^+, $R(W) \times R'(W)$ exhibits significant suppression for small $\xi^+ < 0.05$ and a $\sim 10\%$ enhancement at $\xi^+ \sim 0.1$. This behaviour reflects the characteristic nuclear modifications of nPDFs associated with nuclear shadowing at small x and nuclear anti-shadowing at $x \sim 0.1$. To highlight the latter point, we also show the squared EPPS21 nuclear modification factors for the gluon and quark singlet,

$$R_g^2(\xi, \mu_F) = \left[\frac{g_A(\xi, \mu_F)}{g_p(\xi, \mu_F)}\right]^2\,, \tag{21}$$

$$R_q^2(\xi, \mu_F) = \left[\frac{q_A^S(\xi, \mu_F)}{q_p^S(\xi, \mu_F)}\right]^2\,, \tag{22}$$

as a function of $\xi = \xi^+$, where g_A (q_A^S) and g_p (q_p^S) are the gluon (quark-singlet) distributions per nucleon in the nucleus and the free proton, respectively. The corresponding shaded bands represent the EPPS21 nPDF uncertainties of these ratios. One can see that the shape and normalization of both $R_g^2(\xi)$ and $R_q^2(\xi)$ is similar to those of $R(W) \times R'(W)$. Moreover, because of the dominance of the gluon-initiated contribution over the quark one, see Fig. 4, and the flat shape of the gluon nuclear modifications at small x, the values of $R(W) \times R'(W)$ and $R_g^2(\xi)$ become very close for $\xi^+ \leq 10^{-3}$ ($W^+ > 200$ GeV).

4.4 Feasibility of the measurement of Υ photoproduction in Pb + Pb UPCs at the LHC

Having now obtained an educated estimate for the Υ cross section in Pb + Pb collisions, we will here check to what extent an experimental measurement of the process would be feasible. To this end, we lean on the exclusive Υ p+Pb measurement by the CMS collaboration [30] at $\sqrt{s_{NN}} = 5.02$ TeV. This measurement with

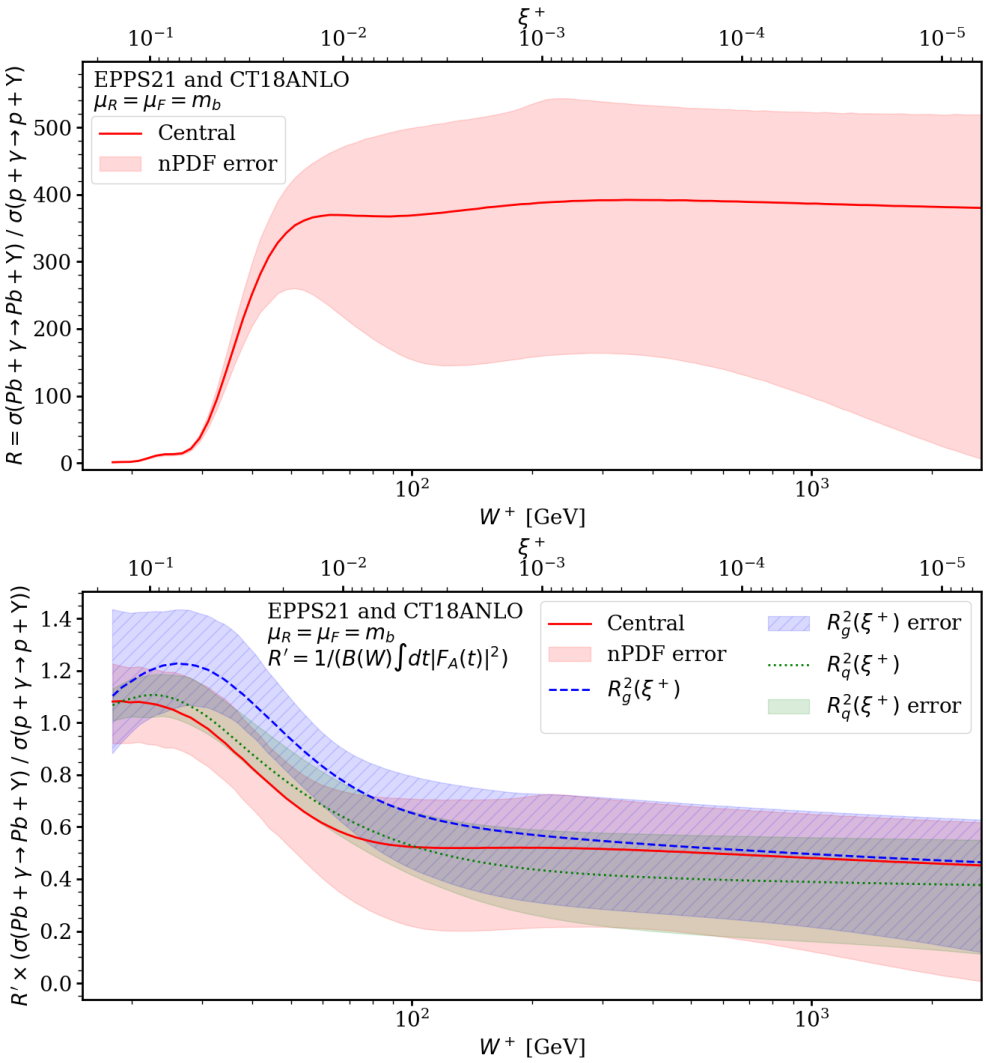

Fig. 8 Upper panel: The ratio $R(W) = \left[\sigma^{\gamma\mathrm{Pb}\to\Upsilon\mathrm{Pb}}(W)/\sigma^{\gamma p\to\Upsilon p}(W)\right]_{\mathrm{pQCD}}$ as a function of the c.m.s. energy W^+ evaluated using the EPPS21 nuclear and CT18ANLO free proton PDFs at $\mu = m_b$. The shaded band corresponds to the EPPS21 and CT18ANLO PDFs uncertainties. The upper x-axis indicates the corresponding values of the skewness ξ^+. Lower panel: the rescaled ratio $R'(W) \times R(W)$ as a function of W^+. For comparison, the EPPS21 gluon and quark-singlet nuclear modifications squared along with their uncertainties are overlaid. The shaded bands show the PDF-originated uncertainties.

an integrated luminosity of $\mathcal{L}(p + \mathrm{Pb}) = 32.6\ \mathrm{nb}^{-1}$ reported ~ 80 identified $\Upsilon(1S)$ particles and yielded a total cross section $\sigma(p + \mathrm{Pb}) = 94.8$ nb in the rapidity interval $|y| < 2.2$. If we desire a Pb + Pb measurement that is as precise as the p+Pb measurement (the same number of events), and assume the same efficiency, the condition is

$$\sigma(p + \mathrm{Pb})\mathcal{L}(p + \mathrm{Pb}) \ = \sigma(\mathrm{Pb} + \mathrm{Pb})\mathcal{L}(\mathrm{Pb} + \mathrm{Pb})\,. \quad (23)$$

From Fig. 7, we find a total cross section $\sigma(\mathrm{Pb}+\mathrm{Pb}) \sim 52\,\mu$b in the same rapidity interval $-2.2 < y < 2.2$. It then follows that the required integrated luminosity should be

$$\mathcal{L}(\mathrm{Pb} + \mathrm{Pb}) = 0.06\,\mathrm{nb}^{-1}\,, \quad (24)$$

to observe ~ 80 events. Given that the recorded luminosity at the 2018 Pb + Pb run for CMS is as high as 1.7 nb^{-1} [61], our counting would thus promise $\sim 80 \times (1.7/0.06) \approx 2300$ events. Moreover, in Run III CMS aims for an integrated luminosity of 13 nb^{-1} [19], so the measurement of exclusive Υ photoproduction in Pb + Pb collisions looks more than feasible to be performed at the CMS experiment.

5 Conclusions and Outlook

We presented the first study of the rapidity-differential cross section of exclusive Υ photoproduction in ultraperipheral lead-lead collisions at the LHC using collinear factorization at NLO pQCD. In addition, we extended

our previous framework in [25,24] by now including explicit GPD modeling through the Shuvaev integral transform. In our standard NLO pQCD approach, we showed that the GPD effects are small, and unlike in the J/ψ case, the imaginary part and gluon contributions dominate the amplitude. The scale uncertainties are significantly reduced from the J/ψ case, but they are still alarmingly large. In the $\gamma + p$ case, the NLO calculation was shown to underpredict the HERA data, which calls for further improvements such as NNLO pQCD and NRQCD corrections.

Using the $\gamma + p \to \Upsilon + p$ cross section from HERA and the LHC as a baseline, we proposed a data-driven pQCD approach to make more constrained predictions for $\mathrm{d}\sigma(\mathrm{Pb} + \mathrm{Pb} \to \mathrm{Pb} + \Upsilon + \mathrm{Pb})/\mathrm{d}y$ and showed that the resulting factorization/renormalization dependence becomes smaller than that in the standard pQCD result for this process. In addition, effects due to the explicit GPD modeling largely cancel and most of the remaining uncertainty is due to PDFs of free and bound nucleons. This serves as a first step towards being able to include heavy quarkonia UPC data in the global analyses of nPDFs to provide constraints on partons inside nuclei at moderate to low x. We also estimated that the production cross sections are high enough for this process to be measured in Pb+Pb collisions at the LHC. While the theoretical situation nevertheless seems a little better for the Υ production, the experimental statistics obtainable may be sparser than that for J/ψ. Future works can therefore include applying our data-driven approach to exclusive J/ψ photoproduction in nucleus-nucleus collisions, where also the statistical quality of the baseline $\gamma + p$ data is greater than for Υ production. In the J/ψ case, the GPD modeling given by the Shuvaev transform is surmised to have an even smaller effect in comparison to the Υ photoproduction considered here, but to what extent the scale dependence can be tamed, calls for a detailed analysis.

Acknowledgments

We acknowledge the financial support from the Magnus Ehrnrooth foundation (T.L.), the Academy of Finland Projects No. 308301 (H.P.) and No. 330448 (K.J.E.). This research was funded as a part of the Center of Excellence in Quark Matter of the Academy of Finland (Projects No. 346325 and No. 346326). This research is part of the European Research Council Project No. ERC-2018-ADG-835105 YoctoLHC.

References

1. C. A. Bertulani, S. R. Klein and J. Nystrand, Ann. Rev. Nucl. Part. Sci. **55** (2005), 271-310 doi:10.1146/annurev.nucl.55.090704.151526 [arXiv:nucl-ex/0502005 [nucl-ex]].
2. A. J. Baltz, G. Baur, D. d'Enterria, L. Frankfurt, F. Gelis, V. Guzey, K. Hencken, Y. Kharlov, M. Klasen and S. R. Klein, *et al.* Phys. Rept. **458** (2008), 1-171 doi:10.1016/j.physrep.2007.12.001 [arXiv:0706.3356 [nucl-ex]].
3. J. G. Contreras and J. D. Tapia Takaki, Int. J. Mod. Phys. A **30** (2015), 1542012 doi:10.1142/S0217751X15420129
4. S. R. Klein and H. Mäntysaari, Nature Rev. Phys. **1** (2019) no.11, 662-674 doi:10.1038/s42254-019-0107-6 [arXiv:1910.10858 [hep-ex]].
5. M. G. Ryskin, Z. Phys. C **57** (1993), 89-92 doi:10.1007/BF01555742
6. D. Y. Ivanov, A. Schafer, L. Szymanowski and G. Krasnikov, Eur. Phys. J. C **34** (2004) no.3, 297-316 [erratum: Eur. Phys. J. C **75** (2015) no.2, 75] doi:10.1140/epjc/s2004-01712-x [arXiv:hep-ph/0401131 [hep-ph]].
7. J. C. Collins, L. Frankfurt and M. Strikman, Phys. Rev. D **56** (1997), 2982-3006 doi:10.1103/PhysRevD.56.2982 [arXiv:hep-ph/9611433 [hep-ph]].
8. X. D. Ji, Phys. Rev. D **55** (1997), 7114-7125 doi:10.1103/PhysRevD.55.7114 [arXiv:hep-ph/9609381 [hep-ph]].
9. A. V. Radyushkin, Phys. Rev. D **56** (1997), 5524-5557 doi:10.1103/PhysRevD.56.5524 [arXiv:hep-ph/9704207 [hep-ph]].
10. M. Diehl, Phys. Rept. **388** (2003), 41-277 doi:10.1016/j.physrep.2003.08.002 [arXiv:hep-ph/0307382 [hep-ph]].
11. S. Afanasiev *et al.* [PHENIX], Phys. Lett. B **679** (2009), 321-329 doi:10.1016/j.physletb.2009.07.061 [arXiv:0903.2041 [nucl-ex]].
12. B. Abelev *et al.* [ALICE], Phys. Lett. B **718** (2013), 1273-1283 doi:10.1016/j.physletb.2012.11.059 [arXiv:1209.3715 [nucl-ex]].
13. E. Abbas *et al.* [ALICE], Eur. Phys. J. C **73** (2013) no.11, 2617 doi:10.1140/epjc/s10052-013-2617-1 [arXiv:1305.1467 [nucl-ex]].
14. V. Khachatryan *et al.* [CMS], Phys. Lett. B **772** (2017), 489-511 doi:10.1016/j.physletb.2017.07.001 [arXiv:1605.06966 [nucl-ex]].
15. S. Acharya *et al.* [ALICE], Phys. Lett. B **798** (2019), 134926 doi:10.1016/j.physletb.2019.134926 [arXiv:1904.06272 [nucl-ex]].
16. S. Acharya *et al.* [ALICE], Eur. Phys. J. C **81** (2021) no.8, 712 doi:10.1140/epjc/s10052-021-09437-6 [arXiv:2101.04577 [nucl-ex]].
17. R. Aaij *et al.* [LHCb], JHEP **07** (2022), 117 doi:10.1007/JHEP07(2022)117 [arXiv:2107.03223 [hep-ex]].
18. LHCb Collaboration, [arXiv:2206.08221 [hep-ex]].
19. Z. Citron, A. Dainese, J. F. Grosse-Oetringhaus, J. M. Jowett, Y. J. Lee, U. A. Wiedemann, M. Winn, A. Andronic, F. Bellini and E. Bruna, *et al.* CERN Yellow Rep. Monogr. **7** (2019), 1159-1410 doi:10.23731/CYRM-2019-007.1159 [arXiv:1812.06772 [hep-ph]].
20. A. Kusina, T. Ježo, D. B. Clark, P. Duwentäster, E. Godat, T. J. Hobbs, J. Kent, M. Klasen, K. Kovařík and F. Lyonnet, *et al.* Eur. Phys. J. C **80** (2020) no.10, 968 doi:10.1140/epjc/s10052-020-08532-4 [arXiv:2007.09100 [hep-ph]].
21. K. J. Eskola, P. Paakkinen, H. Paukkunen and C. A. Salgado, Eur. Phys. J. C **82** (2022) no.5, 413 doi:10.1140/epjc/s10052-022-10359-0 [arXiv:2112.12462 [hep-ph]].

22. I. Helenius, M. Walt and W. Vogelsang, Phys. Rev. D **105** (2022) no.9, 9 doi:10.1103/PhysRevD.105.094031 [arXiv:2112.11904 [hep-ph]].
23. R. Abdul Khalek, R. Gauld, T. Giani, E. R. Nocera, T. R. Rabemananjara and J. Rojo, Eur. Phys. J. C **82** (2022) no.6, 507 doi:10.1140/epjc/s10052-022-10417-7 [arXiv:2201.12363 [hep-ph]].
24. K. J. Eskola, C. A. Flett, V. Guzey, T. Löytäinen and H. Paukkunen, Phys. Rev. C **106** (2022) no.3, 035202 doi:10.1103/PhysRevC.106.035202 [arXiv:2203.11613 [hep-ph]].
25. K. J. Eskola, C. A. Flett, V. Guzey, T. Löytäinen and H. Paukkunen, [arXiv:2210.16048 [hep-ph]].
26. C. Adloff *et al.* [H1], Phys. Lett. B **483** (2000), 23-35 doi:10.1016/S0370-2693(00)00530-X [arXiv:hep-ex/0003020 [hep-ex]].
27. J. Breitweg *et al.* [ZEUS], Phys. Lett. B **437** (1998), 432-444 doi:10.1016/S0370-2693(98)01081-8 [arXiv:hep-ex/9807020 [hep-ex]].
28. S. Chekanov *et al.* [ZEUS], Phys. Lett. B **680** (2009), 4-12 doi:10.1016/j.physletb.2009.07.066 [arXiv:0903.4205 [hep-ex]].
29. R. Aaij *et al.* [LHCb], JHEP **09** (2015), 084 doi:10.1007/JHEP09(2015)084 [arXiv:1505.08139 [hep-ex]].
30. A. M. Sirunyan *et al.* [CMS], Eur. Phys. J. C **79** (2019) no.3, 277 [erratum: Eur. Phys. J. C **82** (2022) no.4, 343] doi:10.1140/epjc/s10052-019-6774-8 [arXiv:1809.11080 [hep-ex]].
31. A. Shuvaev, Phys. Rev. D **60** (1999), 116005 doi:10.1103/PhysRevD.60.116005 [arXiv:hep-ph/9902318 [hep-ph]].
32. A. G. Shuvaev, K. J. Golec-Biernat, A. D. Martin and M. G. Ryskin, Phys. Rev. D **60** (1999), 014015 doi:10.1103/PhysRevD.60.014015 [arXiv:hep-ph/9902410 [hep-ph]].
33. K. J. Golec-Biernat, A. D. Martin and M. G. Ryskin, Phys. Lett. B **456** (1999), 232-239 doi:10.1016/S0370-2693(99)00504-3 [arXiv:hep-ph/9903327 [hep-ph]].
34. M. Vidovic, M. Greiner, C. Best and G. Soff, Phys. Rev. C **47** (1993), 2308-2319 doi:10.1103/PhysRevC.47.2308
35. R. D. Woods and D. S. Saxon, Phys. Rev. **95** (1954), 577-578 doi:10.1103/PhysRev.95.577
36. P. Hoodbhoy, Phys. Rev. D **56** (1997), 388-393 doi:10.1103/PhysRevD.56.388 [arXiv:hep-ph/9611207 [hep-ph]].
37. M. G. Ryskin, R. G. Roberts, A. D. Martin and E. M. Levin, Z. Phys. C **76** (1997), 231-239 doi:10.1007/s002880050547 [arXiv:hep-ph/9511228 [hep-ph]].
38. C. Alexa *et al.* [H1], Eur. Phys. J. C **73** (2013) no.6, 2466 doi:10.1140/epjc/s10052-013-2466-y [arXiv:1304.5162 [hep-ex]].
39. V. A. Khoze, A. D. Martin and M. G. Ryskin, Eur. Phys. J. C **73** (2013), 2503 doi:10.1140/epjc/s10052-013-2503-x [arXiv:1306.2149 [hep-ph]].
40. B. Berthou, D. Binosi, N. Chouika, L. Colaneri, M. Guidal, C. Mezrag, H. Moutarde, J. Rodríguez-Quintero, F. Sabatié and P. Sznajder, *et al.* Eur. Phys. J. C **78** (2018) no.6, 478 doi:10.1140/epjc/s10052-018-5948-0 [arXiv:1512.06174 [hep-ph]].
41. A. D. Martin, C. Nockles, M. G. Ryskin, A. G. Shuvaev and T. Teubner, Eur. Phys. J. C **63** (2009), 57-67 doi:10.1140/epjc/s10052-009-1087-y [arXiv:0812.3558 [hep-ph]].
42. K. Kumerički and D. Mueller, Nucl. Phys. B **841** (2010), 1-58 doi:10.1016/j.nuclphysb.2010.07.015 [arXiv:0904.0458 [hep-ph]].
43. V. Bertone, H. Dutrieux, C. Mezrag, J. M. Morgado and H. Moutarde, Eur. Phys. J. C **82** (2022) no.10, 888 doi:10.1140/epjc/s10052-022-10793-0 [arXiv:2206.01412 [hep-ph]].
44. H. Dutrieux, M. Winn and V. Bertone, [arXiv:2302.07861 [hep-ph]].
45. T. J. Hou, J. Gao, T. J. Hobbs, K. Xie, S. Dulat, M. Guzzi, J. Huston, P. Nadolsky, J. Pumplin and C. Schmidt, *et al.* Phys. Rev. D **103** (2021) no.1, 014013 doi:10.1103/PhysRevD.103.014013 [arXiv:1912.10053 [hep-ph]].
46. A. Buckley, J. Ferrando, S. Lloyd, K. Nordström, B. Page, M. Rüfenacht, M. Schönherr and G. Watt, Eur. Phys. J. C **75** (2015), 132 doi:10.1140/epjc/s10052-015-3318-8 [arXiv:1412.7420 [hep-ph]].
47. M. Diehl and W. Kugler, Phys. Lett. B **660** (2008), 202-211 doi:10.1016/j.physletb.2007.12.047 [arXiv:0711.2184 [hep-ph]].
48. S. P. Jones, A. D. Martin, M. G. Ryskin and T. Teubner, Eur. Phys. J. C **76** (2016) no.11, 633 doi:10.1140/epjc/s10052-016-4493-y [arXiv:1610.02272 [hep-ph]].
49. C. A. Flett, S. P. Jones, A. D. Martin, M. G. Ryskin and T. Teubner, Phys. Rev. D **101** (2020) no.9, 094011 doi:10.1103/PhysRevD.101.094011 [arXiv:1908.08398 [hep-ph]].
50. C. A. Flett, A. D. Martin, M. G. Ryskin and T. Teubner, Phys. Rev. D **102** (2020), 114021 doi:10.1103/PhysRevD.102.114021 [arXiv:2006.13857 [hep-ph]].
51. C. A. Flett, S. P. Jones, A. D. Martin, M. G. Ryskin and T. Teubner, Phys. Rev. D **105** (2022) no.3, 034008 doi:10.1103/PhysRevD.105.034008 [arXiv:2110.15575 [hep-ph]].
52. C. A. Flett, S. P. Jones, A. D. Martin, M. G. Ryskin and T. Teubner, Phys. Rev. D **106** (2022) no.7, 074021 doi:10.1103/PhysRevD.106.074021 [arXiv:2206.10161 [hep-ph]].
53. V. Guzey, E. Kryshen, M. Strikman and M. Zhalov, Phys. Lett. B **726** (2013), 290-295 doi:10.1016/j.physletb.2013.08.043 [arXiv:1305.1724 [hep-ph]].
54. E. Kryshen, private communication, 2016.
55. V. Guzey and M. Zhalov, JHEP **10** (2013), 207 doi:10.1007/JHEP10(2013)207 [arXiv:1307.4526 [hep-ph]].
56. V. Guzey, E. Kryshen, M. Strikman and M. Zhalov, Phys. Lett. B **816** (2021), 136202 doi:10.1016/j.physletb.2021.136202 [arXiv:2008.10891 [hep-ph]].
57. D. Y. Ivanov, B. Pire, L. Szymanowski and J. Wagner, [arXiv:1510.06710 [hep-ph]].
58. T. Lappi, H. Mäntysaari and J. Penttala, Phys. Rev. D **102** (2020) no.5, 054020 doi:10.1103/PhysRevD.102.054020 [arXiv:2006.02830 [hep-ph]].
59. V. Guzey, M. Strikman and M. Zhalov, Eur. Phys. J. C **74** (2014) no.7, 2942 doi:10.1140/epjc/s10052-014-2942-z [arXiv:1312.6486 [hep-ph]].
60. CMS Collaboration, CMS-PAS-HIN-22-002.
61. `https://twiki.cern.ch/twiki/bin/view/CMSPublic/LumiPublicResults`